SONNE-Berichte

Pan-Atlantic connectivity of marine biogeochemical and ecological processes and the impact of anthropogenic pressures

SO287

11.12.2021– 11.01.2022

Las Palmas (Spain) – Guayaquil (Ecuador)

CONNECT

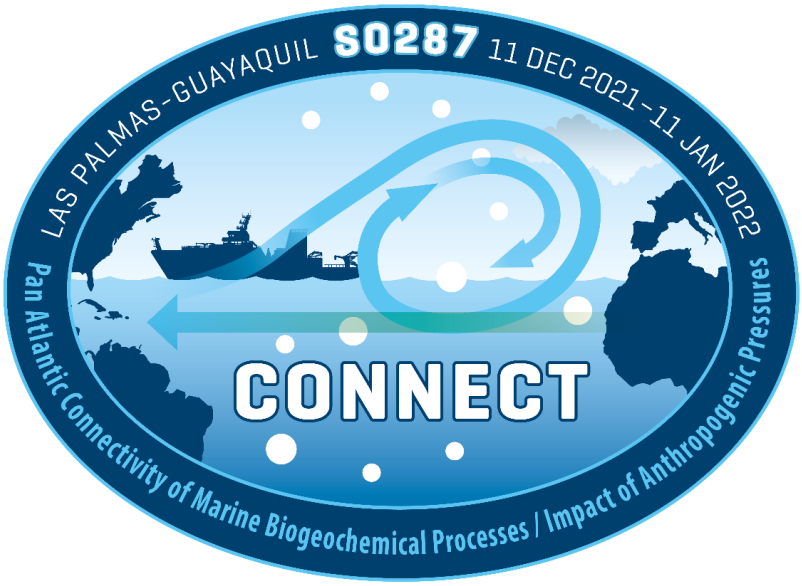

Birgit Quack, Sigrid Auganæs, Tim Bösch, Dennis Booge, Inga Brockmann, Lucy Brown, Claudio Cardoso, Ndague Diogoul, Helmke Hepach, Martin Hieronymi, Riel Ingeniero, Miriam Latsch, Alice Offin, Philippe Potin, Kastriot Qelaj, Alexandra Rosa, Jesus Reis, Rüdiger Röttgers, Lindsay Scheidemann, Gesa Schulz, Hanif Sulaiman, Greta Wunderlich, Peihang Xu, Isabella Zehender

Dr. Birgit Quack

GEOMAR Helmholtz Centre for Ocean Research Kiel

2022

Table of Content

1 Cruise Summary

1.1 Summary in English

The transit of RV SONNE from Las Palmas (departure: 11.12.2021) to Guayaquil, Ecuador (arrival: 11.01.2022) is directly related to the international collaborative project SO287-CONNECT of GEOMAR in cooperation with Hereon and the University of Bremen, supported by the German Federal Ministry of Education and Research (BMBF) between October 15 2021 and January 15 2024. The research expedition was conducted to decipher the coupling of biogeochemical and ecological processes and their influence on atmospheric chemistry along the transport pathway of water from the upwelling zones off Africa into the Sargasso Sea and further to the Caribbean and the equatorial Pacific. Nutrient-rich water rises from the deep and promotes the growth of plant and animal microorganisms, and fish at the ocean surface off West Africa. The North Equatorial Current water carries the water from the upwelling, which contains large amounts of organic material across the Atlantic to the Caribbean, supporting bacterial activity along the way. But how the nutritious remnants of algae and other substances are processed on their long journey, biochemically transformed, decomposed into nutrients and respired to carbon dioxide, has so far only been partially investigated.

Air, seawater and particles were sampled in order to provide new details about the large cycles of carbon and nitrogen, but also of many other elements such as oxygen, iodine, bromine and sulfur. Inorganic and organic bromine and iodine compounds are generally emitted naturally from the ocean into the atmosphere, promote cloud formation and affect climate, and some even reach the stratosphere where they contribute to ozone depletion. We measured how much of these compounds are released from the ocean, and at what locations and how they are transformed in the ocean and in the atmosphere. *Sargassum* algae, which have become a nuisance on beaches in the western and eastern Atlantic, support life and contribute to carbon cycling in the middle of the Atlantic, the Sargasso Sea and in the Caribbean, while their contribution to halogen cycling and marine bromine and iodine emissions was previously unknown. We investigated the influence of various natural parameters such as temperature and solar radiation on the biogeochemical transformation processes in order to understand the influence of climate change on these processes in incubation experiments with seawater and algae. We investigated how anthropogenic signals such as shipping traffic influence the nitrogen and sulphur cycle in the ocean, as well as the impact of nitrogen oxides from ship exhaust and sulphurous, acidic and dirty water from purification systems on organisms and biochemical processes. Plastic debris was sampled from the surface waters to investigate its contribution to global biogeochemical transformation processes. The working hypotheses of the research program were:

- Bioavailability of dissolved organic carbon in surface waters decreases along the productivity gradient and transport pathway from the Eastern to the Western Tropical North Atlantic.
- Nutrient gradients from East to West constrain the microbial utilization of organic matter-contributing to an accumulation of C-rich organic matter due to a) limited mineralization and b) enhanced exudation- also leading to gel-like particles accumulation in the western tropical North Atlantic and Sargasso Sea.
- Tropospheric and stratospheric ozone are strongly impacted by biogeochemical and ecological processes occurring around and in the NA gyre system related to marine iodine and bromine cycles.
- The long-range transport of natural and anthropogenic organic matter in water and of gases and aerosols in the air impact carbon-export, biogeochemical cycles in the water column, and the release of gases and particles from the ocean significantly.

The data and samples obtained specifically target carbon, nutrient and halogen cycling, the composition of phytoplankton, bacteria, the transport and sequestration of macro algae and the air-sea exchange processes of climate relevant gases and aerosols. The influence of ecological and transport processes, as well as anthropogenic impacts on the North Atlantic gyre system, specifically in the Sargasso Sea and the influence of ship emissions throughout the Atlantic towards the west and into the Pacific will be investigated with the data.

1.2 Zusammenfassung

Der Transit der RV SONNE von Las Palmas (Abfahrt: 11.12.2021) nach Guayaquil, Ecuador (Ankunft: 11.01.2022) steht in direktem Zusammenhang mit dem internationalen Verbundprojekt SO287-CONNECT des GEOMAR in Kooperation mit Hereon und der Universität Bremen, das vom Bundesministerium für Bildung und Forschung (BMBF) vom 15. Oktober 2021 bis zum 15. Januar 2024 gefördert wird. Die Forschungsexpedition wurde durchgeführt, um die Kopplung biogeochemischer und ökologischer Prozesse und deren Einfluss auf die Atmosphärenchemie entlang des Transportweges von Wasser aus den Auftriebsgebieten vor Afrika in die Sargassosee und weiter in die Karibik und den äquatorialen Pazifik zu entschlüsseln. Nährstoffreiches Wasser steigt aus der Tiefe auf und fördert das Wachstum von pflanzlichen und tierischen Mikroorganismen sowie von Fischen an der Meeresoberfläche vor Westafrika. Der Nordäquatorialstrom transportiert das Wasser, das große Mengen an organischem Material enthält, aus dem Auftrieb über den Atlantik in die Karibik und unterstützt auf dem Weg dorthin die bakterielle Aktivität. Doch wie die nahrhaften Algenreste und andere Stoffe auf ihrer langen Reise verarbeitet, biochemisch umgewandelt, zu Nährstoffen abgebaut und zu Kohlendioxid veratmet werden, ist bisher nur teilweise untersucht worden.
Luft, Meerwasser und Partikel wurden beprobt, um neue Details über die großen Kreisläufe von Kohlenstoff und Stickstoff, aber auch von vielen anderen Elementen wie Sauerstoff, Jod, Brom und Schwefel zu erfahren. Anorganische und organische Brom- und Jodverbindungen werden in der Regel auf natürliche Weise aus dem Ozean in die Atmosphäre emittiert, fördern die Wolkenbildung und beeinflussen das Klima, und einige erreichen sogar die Stratosphäre, wo sie zum Ozonabbau beitragen. Wir haben gemessen, wie viel von diesen Verbindungen aus dem Meer freigesetzt werden, an welchen Orten und wie sie im Meer und in der Atmosphäre umgewandelt werden. *Sargassum*-Algen, die an den Stränden des West- und Ostatlantiks zu einer Plage geworden sind, unterstützen das Leben und tragen zum Kohlenstoffkreislauf im offenen Atlantik in der Sargassosee und in der Karibik bei, während ihr Beitrag zum Halogenkreislauf und zu den marinen Brom- und Jodemissionen bisher unbekannt war. Wir haben den Einfluss verschiedener natürlicher Parameter wie Temperatur und Sonneneinstrahlung auf die biogeochemischen Umwandlungsprozesse und Algen in Inkubationsexperimenten untersucht, um den Einfluss des Klimawandels auf diese Prozesse mit Meerwasser zu verstehen. Wir untersuchten, wie anthropogene Signale wie der Schiffsverkehr den Stickstoff- und Schwefelkreislauf im Ozean beeinflussen, sowie die Auswirkungen von Stickoxiden aus Schiffsabgasen und schwefelhaltigem, saurem und schmutzigem Wasser aus Abgaswaschanlagen auf Organismen und biochemische Prozesse. Plastikmüll wurde im Oberflächenwasser gesammelt, um seinen Beitrag zu globalen biogeochemischen Umwandlungsprozessen zu untersuchen. Die Arbeitshypothesen des Forschungsprogramms lauteten:

- Die Bioverfügbarkeit von gelöstem organischem Kohlenstoff im Oberflächenwasser nimmt entlang des Produktivitätsgradienten und des Transportweges vom östlichen zum westlichen tropischen Nordatlantik ab.
- Nährstoffgradienten von Ost nach West schränken die mikrobielle Verwertung von organischem Material ein, was zu einer Anreicherung von C-reichem organischem Material

aufgrund von a) begrenzter Mineralisierung und b) verstärkter Exsudation führt, was wiederum zur Anreicherung von gelartigen Partikeln im westlichen tropischen Nordatlantik und der Sargassosee führt.
- Das troposphärische und stratosphärische Ozon wird stark durch biogeochemische und ökologische Prozesse beeinflusst, die um und im NA-Gyre-System stattfinden und mit den marinen Jod- und Bromkreisläufen zusammenhängen.
- Der weiträumige Transport von natürlichen und anthropogenen organischen Stoffen im Wasser sowie von Gasen und Aerosolen in der Luft hat erhebliche Auswirkungen auf den Kohlenstoffexport, die biogeochemischen Kreisläufe in der Wassersäule und die Freisetzung von Gasen und Partikeln aus dem Ozean.

Die gewonnenen Daten und Proben zielen speziell auf den Kohlenstoff-, Nährstoff- und Halogenkreislauf, die Zusammensetzung des Phytoplanktons, die Bakterien, den Transport und die Bindung von Makroalgen und die Luft-Meer-Austauschprozesse von klimarelevanten Gasen und Aerosolen ab. Der Einfluss von ökologischen und Transportprozessen sowie anthropogenen Einflüssen auf das nordatlantische Wirbelsystem, insbesondere in der Sargassosee, und der Einfluss von Schiffsemissionen im gesamten Atlantik nach Westen und in den Pazifik werden anhand der Daten untersucht.

2 Participants

2.1 Principal Investigators

Name	Institution
Quack, Birgit, PhD	GEOMAR, Kiel, Germany
Engel, Anja, Prof.	GEOMAR, Kiel, Germany
Röttgers, Rüdiger, PhD	Hereon, Geesthacht, Germany
Wittrock, Folkard, PhD	IUP, Bremen, Germany
Marandino, Christa, Prof	GEOMAR, Kiel, Germany
Bange, Hermann, Prof	GEOMAR, Kiel, Germany
Löscher, Carolin , Prof	SDU, Odense, Denmark
Weinberger, Florian, PhD	GEOMAR, Kiel, Germany
Potin, Philippe, Prof	CNRS, Roscoff, France
Dähnke, Kirstin, PhD	Hereon Geesthacht
Atlas, Elliot, Prof.	RSMAS, Miami, US
Baker, Alex, PhD	UEA, Norwich, UK
Carpenter, Lucy, Prof.	UoY, York, UK
Ball, Stephen, PhD	ULE, Leicester, UK
Brehmer, Patrice, PhD	IRD-Senegal, Dakar, France
Krüger, Kirstin, Prof	UiO, Oslo, Norway
Kiko, Rainer, PhD	LOV Villefranche-sur-Mer, France
Matthiessen, Birte, PhD	GEOMAR, Kiel, Germany
van Pinxteren, Manuela PhD	TROPOS, Leipzig, Germany
Tegtmeier, Susann, Prof	USASK, Sasketchewan, Saskatoon, Canada

2.2 Scientific Party

Name		Discipline	Institution
Quack	Birgit, PhD	Chief scientist/Halocarbons	GEOMAR
Auganæs	Sigrid	Masterstudent/Ozone sonding	University of Oslo
Boehme	Wanja	Masterstudent/Microphytopl. 16S rRNA, Metatranscript.	GEOMAR
Boesch	Tim, PhD	Scientist/Atmospheric pollution from ships	Universität Bremen,
Brockmann	Inga	Student/ DMS, DMSP, DMSO, incubations	GEOMAR
Brown	Lucy	PhD-student/Ozone uptake coefficients	University of York, GB
Burmester	Henning	Ing/Optical instrumentation	Hereon
Reis	Jesus	Scientist/CTD/ ADCP-ocean currents	ARDITI
Cardoso	Cláudio	Scientist/CTD/ SSH-Eddies	ARDITI
Devresse	Quentin	PhD-student/Microbial respiration, Enzymes.	GEOMAR
Diogoul	Ndague, PhD	Scientist/Echsounding of the water column	IRD-Senegal
Feil	Hendrik	Student/ GC/MS of halocarbons	GEOMAR
Golde	Sandra	Tech/ Bacterial production	GEOMAR
Hepach	Helmke, PhD	Scientist/ UVP, Lipids, CDOM	GEOMAR
Heymann	Kerstin	Tech/Pigments	Hereon
Hieronymi	Martin, PhD	Scientist/Surface reflectance	Hereon
Ingeniero	Riel	PhD-student/NO-production	GEOMAR
Karnatz	Josefine	Masterstudent/ Halocarbons and carbon from *Sargassum*	GEOMAR
Kluever	Tania	Tech/Primary production	GEOMAR
Latsch	Miriam	PhD-student/Atmospheric pollution	Universität Bremen
Loades	David	PhD-studentScientist/Ozone air-sea flux, deposition	University of York, GB
Mickenbecker	Julia	Student/ GC/MS of halocarbons	GEOMAR
Mueller	Tobias	Masterstudent/TEP, CSP	GEOMAR
Offin	Alice	PhD-student/ Iodine from ocean and *Sargassum*	University of Leicester, GB
Potin	Philippe, Prof.	Scientist/ *Sargassum* incubations	CNRS
Qelaj	Kastriot	Tech/Nutrient analysis	GEOMAR
Roa	Jon	Tech/ DOC + TDN, DAA, DC, DOP	GEOMAR
Rosa	Alexandra	Scientist/CTD	ARDITI
Röttgers	Rüdiger, PhD	Scientist/Absorptionspectroscopy	Hereon
Röttgers	Sünje	High-School student/Aerosol and air sampling	GEOMAR
Röttgers	Lucie	Student/ Aerosol and air sampling	GEOMAR
Schartau	Markus, PhD	Scientist/ Bio. part. silica, (POC, PN)	GEOMAR
Scheidemann	Lindsay	PhD-student/ Plastic marine debris , biofilm	GEOMAR
Schulz	Gesa	PhD-student/ Nitrous oxide and methane fluxes	Hereon
Sulaiman	Hanif	Student/ $15NO_3^-$, $15N_2O$, CH_4, N_2O	GEOMAR
Weddell	Katherine	PhD-student/ POM, fatty acids	University of York, GB
Wunderlich	Greta	Student/ DMS, DMSP, DMSO, ship emissions	GEOMAR
Xu	Peihang, PhD	Scientist/ Microbial comm., carbon fix., flow cytometry	Univers. of South. Denmark
Zehender	Isabella	Student/ Dissolved oxygen	GEOMAR

Figure 2.1: The scientific crew of SO287-CONNECT (photo: Riel Ingeniereo).

2.3 Participating Institutions

GEOMAR Helmholtz-Zentrum für Ozeanforschung Kiel
Düsternbrooker Weg 20
24105 Kiel; Germany
www.geomar.de

Hereon
Helmholtz-Zentrum hereon GmbH
Max-Planck-Straße 1
21502 Geesthacht, Germany

IUP
Institut für Umweltphysik
Universität Bremen
Otto-Hahn-Allee 1
28359 Bremen, Germany

ARDITI
Agência Regional para o Desenvolvimento da Investigação, Tecnologia e Inovação
Madeira Tecnopolo, Piso2 Caminho da Penteada
Funchal 9020-105, Portugal

IRD
Institut de Recherche pour le Développement
Campus international Université Cheikh Anta Diop- de Hann IRD,
Route des Pères Maristes
CP 18524 Dakar, Senegal

CRODT
Centre de Recherche Océanographique de Dakar Thiaroye
B.P. 224, Dakar, Senegal

Laboratoire d'Océanographie de Villefranche-sur-mer
Station Zoologique
181 Chemin du Lazaret
06230 Villefranche-sur-mer, France

RSMAS
Rosenstiel School of Marine and Atmospheric Science
4600 Rickenbacker Causeway,
Miami, Florida, USA

SDU
University of Southern Denmark
Campusvej 55
5230 Odense M, Denmark

CNRS: Centre national de la recherche scientifique, Station Biologique de Roscoff
Pl. Georges Teissier,
29680 Roscoff, France

TROPOS
Leibniz-Institut für Troposphärenforschung e.V.
Permoserstraße 15
04318 Leipzig, Germany

UiO
University of Oslo
Blindern
Oslo, Norway

University of East Anglia
Norwich Research Park
Norwich,UK

University of Leicester
University Road
Leicester LE1 7RH, UK

University of York
Heslington
York YO10 5DD
North Yorkshire, UK

USASK
University of Saskatchewan
Room 265 Arts Building
9 Campus Drive
Saskatoon, SK S7N 5A5, Canada

3 Research Program

3.1 Description of the Work Area

The North Atlantic (NA) gyre is confined by the Canary Current (CanC) to the east and the North Equatorial Current (NEC) to the south, connecting the west coast of Northern Africa with the east coast of Central and North America. The CanC feeds the eastern boundary upwelling system at the North African coast, where nutrient-rich deep water fosters high primary production, subsequently fueling the food web. Along with organic matter production, climate active trace gases like bromoform ($CHBr_3$) and dibromomethane (CH_2Br_2) (Quack et al., 2007), dimethylsulfide (DMS) and its derivates DMSP and DMSO are produced as well as other volatile biogenic compounds such as isoprene (Zindler et al., 2012, 2014). Primary production also influences inorganic iodine cycling (Hepach et al., 2020) strongly impacting tropospheric ozone chemistry. The NEC and mesoscale eddies therein transport organic matter and other biogeochemical constituents offshore into the open Atlantic (Lathuilliere et al., 2010). Instabilities generated by velocity shear of the coastal current systems and Ekman circulation favor the generation of eddies in the Eastern Tropical North Atlantic upwelling systems. Eddies can be considered as a continuation of the upwelling system transporting material and properties laterally into the open ocean. By trapping coastal waters of upwelling origin and transporting them offshore, these eddies play an important role in the lateral mixing and transport of physical and biogeochemical properties and thereby modulate biogeochemistry and biological productivity. The importance of eddies in the biogeochemical processes along the lateral flow of the North Equatorial Current transporting the upwelled water, rich in organic material across the Atlantic is insufficiently understood. The fate of the upwelled nutrients and fixed organic carbon and thereby the overall CO_2 source/sink along the transport pathway of the North Equatorial Current is unclear. In the center of the North Atlantic gyre lies the Sargasso Sea, with still waters and constant downwelling conditions that favor accumulation of floating, long-lived matter, such as *Sargassum* seaweed, man-made plastics or refractory organic compounds. Due to the strong circulation pattern, the biogeochemistry and ecology of the NA gyre is characterized by distant component sources. Lateral transport of organic matter originating from highly productive upwelling systems in the ETNA and microbial processes along the path, supplemented by *Sargassum* exudations, may be responsible for net heterotrophic conditions in the central NA and even link to excess organic carbon accumulation in the Sargasso Sea.

The warm NEC, connecting the ETNA with the WTNA, could play a significant role in understanding the dissolved organic carbon (DOC)-enigma, i.e., high DOC concentrations in the WTNA, associated with low concentrations of dissolved organic nitrogen (DON). Trichodesmium, a large colony-forming diazotrophic cyanobacterium is abundant in the NEC and potentially leads to DOC accumulation in the WTNA (Carpenter and Romans, 1991). Trichodesmium takes up iron and DIP, depleting the ocean surface of these important nutrients (Held et al., 2020). Carbon utilizing bacteria can acquire dissolved inorganic phosphorous (DIP) from dissolved organic phosphorous (DOP) using extracellular enzymes such as alkaline phosphatase (APA). However, a recent study demonstrated decreased APA activity with increasing iron limitation (Browning et al., 2017). This supports the hypothesis of less efficient DOC utilization in the WTNA. Since the oligotrophic gyres have been suggested to expand (Polovina et al., 2008) and autotrophic DOC exudation may likely increase (Engel et al., 2011) under global warming and ocean acidification, this DOC-enigma needs to be unraveled to understand how future changes may impact oceanic carbon cycling in the Atlantic Ocean and its contribution to CO2 release to the atmosphere. Trichodesmium blooms and reduced bacterial activity also influence trace gas and iodine cycling. Isoprene, DMSO and DMSP have been associated to Trichodesmium cells (Bucciarelli et al., 2013). Recently, iodine oxidation has been associated to ammonium-oxidizing bacteria (Wadley et al., 2020). Adding missing data

from the central NEC and the WTNA could close important knowledge gaps related to the iodine cycle.

Decoupling of carbon from nitrogen cycling also occurs in the Sargasso Sea. One explanation involves production of organic matter rich in carbon (Fawcett et al., 2018). Transparent exopolymer particles (TEP) and other gel-like particles are enriched in carbon and contribute to the decoupling (Engel et al., 2002). Exudates from *Sargassum* seaweed may foster high gel-like particle formation. In addition, macroalgae contribute to the cycles of halogenated compounds. This includes both the organic and inorganic iodine cycle, potentially releasing I_2 directly (Chance et al., 2009). DOC released from macroalgae transforms into $CHBr_3$ and CH_2Br_2 via bromoperoxidases from the same algae (Lin and Manley, 2012). While tropical *Sargassum* species produce large amounts of brominated trace gases (Mithoo-singh et al., 2017), nothing is known about the production from *Sargassum* in the NA. Other trace gases (e.g., isoprene) are likely to be emitted from these free-floating macroalgae as well. The Sargasso Sea has furthermore been identified as a source region for DMS, with anomalously high DMS compared to chlorophyll a in summer. Light availability and bacterial production of DMS have been suggested as potential reasons for this so-called “summer paradox” (Polimene et al., 2011). As bacterial activity is dependent on carbon utilization, deciphering the organic matter utilization in the Sargasso Sea helps to investigate this phenomenon.

Anthropogenic influences are particularly evident in the NA., where large patches of plastic and human debris accumulate in the Sargasso Sea and trans-Atlantic micro- and macro plastics participate in biogeochemical cycles to a yet unknown extent. Pan-Atlantic trading has resulted in high ship traffic and emissions in the region. The release of highly acidified scrubber water and the deposition of nitrogenous compounds and their influence on ecology, biogeochemistry and trace gas production are largely unknown to date. SO287 was set up to unravel the coupling of biogeochemical and ecological processes and their influence on atmospheric chemistry along the transport pathway of water from the upwelling zones off Africa into the Sargasso Sea. SO287 investigated how changes may affect marine planetary boundary functions, in particular with respect to productivity and climate. Therefore, SO287 specifically targeted carbon and nutrient cycling and the air-sea exchange processes of climate relevant gases and aerosols. The cruise investigated the influence of ecological and transport processes, as well as anthropogenic impacts on the NA gyre system, specifically the transport and accumulation of plastic debris in the Sargasso Sea and the influence of ship emissions.

3.2 Aims of the Cruise

SO287 aimed to unravel the spatial coupling of biogeochemical and ecological processes along the southern branch of the NA gyre system with a comprehensive work program combining continuous underway water and atmospheric sampling and 36 CTD stations along the route in international waters, as well as underway measurements, incubation experiments and intense sample workup on board SO287 in the EEZs of the Caribbean islands. During the cruise the lateral transport of organic matter originating from highly productive upwelling systems in the ETNA was investigated. SO287 followed the transport path of water from the upwelling zones off the coast of Africa, and across the Atlantic into the Sargasso Sea. The findings are of importance to significantly improve our fundamental understanding of the future development and maintenance of marine carbon export especially in view of ongoing environmental changes such as ocean deoxygenation, eutrophication, and oceanic and atmospheric pollution. The interactions of biota and external forcing (e.g., light, dust) within the NA ecosystems and with the marine biogeochemical trace gas cycles of halogenated and sulphurous compounds in water and atmosphere were scrutinized. SO287 investigated the trans-Atlantic micro-plastic and how it contributes to the biogeochemical cycles. The influence of ship emissions, in particular the release of highly acidified scrubber water, deposition of nitrogenous compounds, and elemental

carbon on ecology, biogeochemistry and trace gas production along the southern branch of the NA gyre system, was examined. As the cruise track was through the Equatorial Pacific (EqPac) as well, we took the opportunity to revisit a section at 85.5°W which covers the EqPac OMZ, that has been sampled and investigated on prior cruises.

The work program of the SO287-CONNECT expedition consisted of three work packages with thirteen sub-topics:

WP1: Biogeochemical cycles of organic material, iodine and bromine under the influence of transport and ecological processes

- WP1/1: DOM & POM quantitative and qualitative assessment and microbial activity, phytoplankton (PI: Anja Engel, GEOMAR)
- WP1/2: Nutrient, O_2 and nitrogen cycle (PI: Hermann Bange, GEOMAR, Kirstin Dähnke, Hereon)
- WP1/3: N-cycle, C-fixation, microbial diversity (PI: Carolin Löscher, SDU, Hermann Bange, GEOMAR)
- WP1/4: Iodine cycle in seawater and the release of iodine into the atmosphere (PI: Lucy Carpenter, University of York)
- WP1/5: Production of brominated halogenated hydrocarbons in seawater and their influence on the atmosphere (PI: Birgit Quack, GEOMAR, Elliot Atlas, RSMAS, Philippe Potin, CNRS)

WP2: Natural influences on biogeochemical cycles (ecology, light and dust)

- WP2/1: Physical oceanography and meteorology (PI: Birgit Quack, GEOMAR; Kirstin Krüger, UIO)
- WP2/2: Optical properties and phytoplankton specification (PI: Rüdiger Röttgers, Hereon)
- WP2/3: Marine particle flux, particle and plankton distribution (PI: Anja Engel, GEOMAR, Patrice Brehmer, IRD)
- WP2/4: Aerosols (PI: Manuela van Pinxerten TROPOS, Leipzig)
- WP2/5: The lateral transport of continental algae (PI: Florian Weinberger, GEOMAR)

WP3: Anthropogenic influences on biogeochemical cycles (shipping, large-scale transport and plastic)

- WP3/1: Influence of ship emissions on dissolved trace gases (PI: Christa Marandino, GEOMAR)
- WP3/2: Atmospheric trace gases (PI: Folkard Wittrock, IUP, Bremen)
- WP3/3: Plastic waste (PMD) (PI: Anja Engel, GEOMAR)

3.3 Agenda of the Cruise

When the transit was advertised for July / August 2021 in November 2020, we developed a work program between Las Palmas, Spain and Callao, Peru, which met our scientific goals to to unravel the coupling of biogeochemical and ecological processes and their influence on atmospheric chemistry along the transport pathway of water from the upwelling zones off Africa into the Sargasso Sea and further to the Caribbean and also in the equatorial Pacific. At that time the measurements were restricted to take place in international waters, and it was intended to use the harbour and transit time from Las Palmas to the first station in international waters to set up our instrumentation and dismantle our equipment after the last station in the Pacific. The transit time in the Caribbean Sea and the Panama Canal was intended to be used for incubations and sample workup.

When the cruise proposal was reviewed and the ship time was granted to us in July 2021, the cruise was postponed by five months to December 2021-January 2022, and we were given the opportunity to apply for conducting research in the exclusive economic zones (EEZ) we passed. We notified Spain, Puerto Rico, the Dominican Republic, Haiti, Jamaica, Columbia, and Panama and diplomatic clearances could be achieved for all countries. In these countries surface water and atmospheric sampling and measurements were conducted during transit, hydroaccoustic measurements for a scientific evaluation of the water column and the determination of currents, as well as individual catamaran deployments for the collection of neuston were performed in the EEZs. Continuous underway measurements and samples were taken at regular intervals between 1hz and 12 hours. Atmospheric trace gases where sampled in canisters every 6 hours and aerosols were filtered for 24 hours. On 36 stations (6-8 hr station time per day for 2 stations in international waters), the ship CTD and a biological CTD were deployed as well as the working boat of RV SONNE and the catamaran. An intended submersible pump for continuous measurements of the upper 100m failed after the first operation and the water demand was met by an additional shallow CTD- cast.

Five incubators where placed on the stern to perform nitrogen, halogen, sulfur, and VOC cycling incubation experiments for turnover rate and trace gas production measurements and the influence of natural factors and anthropogenic stressors.

Agenda of measurements during the cruise, which was finally conducted from 11.12.2021 to 11.01.2022 from Las Palmas Spain to Guayaquil in Ecuador (Figure 3.3.1): Analysis of organic compounds: DOC, DON, DOP, DHAA, DCCHO, POC, PON, POP, CDOM, bacterial production and respiration, auto- and heterotrophic pico- and nanoplankton and virus analyzed by flow cytometry, activities of hydrolytic extracellular enzymes (glucosidase, aminopeptidase, phosphatase)was performed form depth profiles. Diss. N_2O underway surface measurements, using off-axis integrated cavity output spectroscopy. Water column distribution of N_2O, CH_4,, DMS/P/O (discrete samples); stable isotope distributions ($\delta^{15}N$, $\delta^{18}O$) in nitrate, nitrite and particulate nitrogen; dissolved nutrients (NO_3^-, NO_2^-, PO_4^{3-}, SiO_2) and oxygen (Winkler titration); potential NO production and consumption processes by measuring NO production in incubation experiments was performed. N_2 and C fixation was constrained quantitatively using on board incubations; microbial diversity and functionality.

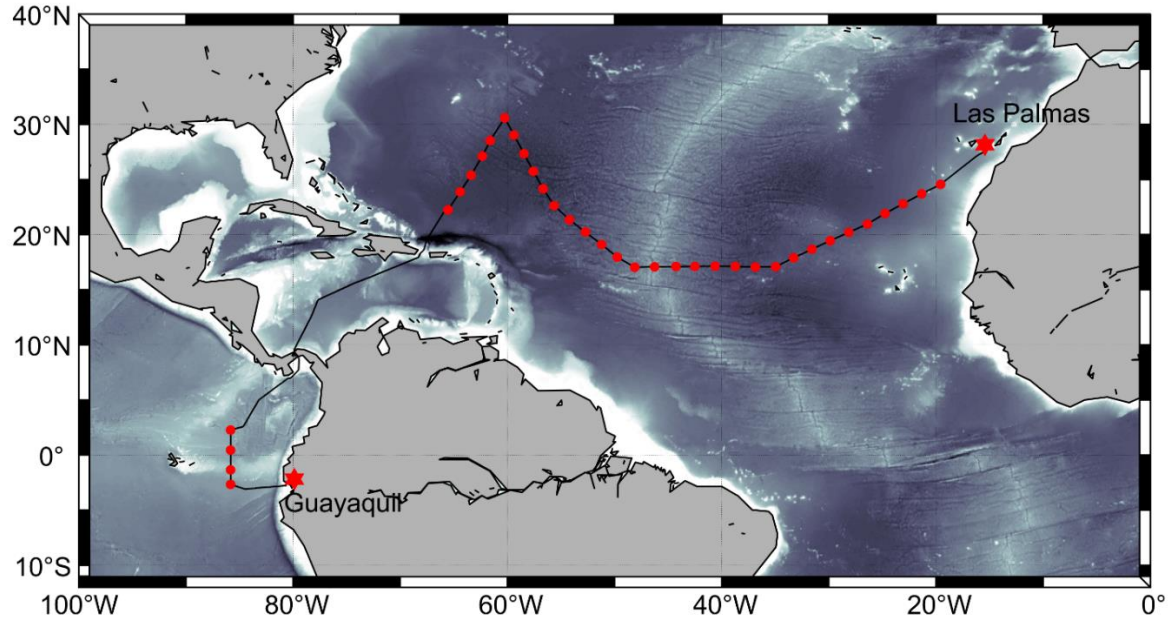

Figure 3.1: Track chart of RV SONNE cruise SO287-CONNECT with stations.

Iodide (I^-) and surfactant activity by voltammetry; Water-soluble marine DOM (~100 ≤ *m/z* ≤ ~1000) with ultrahigh resolution mass spectrometry UHRMS (Q-Exactive Hybrid Quadrupole-Orbitrap Mass Spectrometer); -oxo-fatty acids, hydroxy fatty acids, dicarboxylic acids;-ozone uptake coefficient to seawater with flow tube reactor. Dissolved and atmospheric halogenated VSLS using on board purge and trap system, coupled to a gas chromatograph with mass spectrometric detection to measure discrete depth and underway samples for brominated, chlorinated and iodinated organic compounds (e.g., CH_3I, CH_2Cl_2, CH_2Br_2, $CHBr_3$, and CH_2I_2); canister samples for anthropogenic and natural trace gases; aerosol samples for bromine and vanadium and nickel. DOAS-measurements for BrO and halogen releases from *Sargassum*, stable isotope incubations for process rate determination. CTD with oxygen sensor, PAR, CDOM, ADCP (75kHz and 38kHz). Atmospheric profiling with radiosondes for temperature, wind, pressure and occasionally ozone. Specific optical properties (light absorption and scattering coefficients of dissolved and particulate matter), bio-optical parameters (pigments, POC, DOC) and radiometric measures (light intensity and reflectance) in the water column (euphotic zone: surface to 100 m), T, S, turbidity, light total attenuation, scattering and backscattering, light absorption, chlorophyll a-fluorescence, CDOM-fluorescence; phytopigment signatures and chemotaxonomic processing (HPLC-pigment analysis); microscopy of phytoplankton (enumeration); quantitative microscopy of planktonic protist after Utermöhl (1958); cell biovolume; biodiversity (including composition); Bray-Curtis dissimilarity. Particle and plankton distribution down to 6000m depth with an Underwater Vision Profiler, mounted on the CTD-Rosette; marine gel particles (TEP, CSP) abundance, size frequency distribution and C content. Discrete aerosol samples: total iron, DOC composition, EC. eDNA samples (tufa, CO1, 18SrRNA) from deep and surface waters for seaweed export. Dissolved DMS, incubation experiments to identify the influence of ship emissions on trace gas cycling. Measurements of NO_2, BrO, IO, HCHO, CHOCHO and SO_2 with a MAX-DOAS-System. Calculation of trace gas profiles in the marine troposphere, studying of horizontal inhomogeneities. In situ observations of ship emissions (NOx, SO_2, BC, CO), calculation of relative and absolute emission factors for NOx, BC and SO_2, calculation of the fuel sulfur content. Continuous PMD samples by filtration through a mesh-size of <1mm to collect PMD of >1mm for quantification and biofilm examination; biofilm and 16S rRNA amplicon sequencing; identify up to 7 different bacteria taxa in their spatial arrangement on PMD.

4 Narrative of the Cruise

With SO287-CONNECT, the research vessel SONNE set sail again for one of its most important areas of operation - the Pacific Ocean - after a long forced break due to the outbreak of the Corona pandemic, during which the vessel operated in the Atlantic Ocean and Mediterranean Sea, only.

Short-term visa and permissions, collaborative activities and mutual agreed rapid decisions between many actors enabled the successful conduct of SO287-CONNECT. The scientific team arrived to Las Palmas on the 8th and 9th of December. After embarkation on the 10th, an international team of 39 scientists from 11 different nations together with the 30 crewmembers of the research vessel SONNE set sail on the 11th of December 2021 to cross the Atlantic Ocean over Christmas. We took thousands of samples, made as many measurements and obtained millions of data points with continuous instrumentation in order to understand how marine biogeochemical processes during the transport from Africa across the Atlantic to the Sargasso Sea and all the way to the Caribbean are linked to climate change and other anthropogenic influences, such as ship traffic and plastic pollution. All arriving personnel were at least vaccinated twice against Covid-19. As all our PCR tests were negative, we were allowed to embark on the voyage and wore masks for a week until we were absolutely sure that no Corona

virus made it on board. We enjoyed the luxury of the virus free expedition, which gave us the opportunity to explore very fundamental questions in detail.

After the departure from Las Palmas on the 11th of December 2021, the underway program of SO287-CONNECT started immediately after 12nm with continuous underway measurements of temperature (T), salinity (S), and fluorescence. As soon as the equipment was set up, we started with the measurements of carbon cycle parameters (Dissolved and particulate organic carbon, nitrogen, phosphorus, carbohydrates, amino acids, gel-particles, lipids, cell abundance of bacteria, pico- and nano plankton, viruses, bacterial biomass production, fluorescence, primary production, enzyme activity), community characterization with 16S rRNA, 18S rRNA-sampling, phytoplankton fixation, chlorophyll and other pigments and flow cytometry from depth profiles. Trace gases (N2O, CH4, NO, halocarbons, DMS, oxygen) as well as nutrients, nitrate isotopes, iodide, iodate, total iodine, and ozone were sampled from the surface waters. Continuously NOx, SO2, CO, black carbon concentrations, and NO2, HCHO and SO2 integrated columns, as well as the ozone deposition velocity, water vapor and aerosol depth were measured in the atmosphere. The structure of the atmosphere was determined during 40 radiosonde and 7 ozone sonde launches, determining temperature, humidity, pressure, position and ozone up to 30 km height. Air samples were taken every 6 hours in stainless steel canisters, whereas aerosols were sampled on filters for 24 hours. The sunlight intensity as well as other optical properties such as photosynthetic active radiation (PAR), surface reflectance, the absorption coefficient of CDOM and particles (spectrally) were measured. The intensity and direction of ocean currents was measured with acoustic methods (ADCP 38 and 75 kHz) and the backscattered acoustic signal from marine organisms was determined with the echosounder EK60 (18, 38, 120, 200 kHz). Finally, plastic debris was sampled from the surface water regularly with a Neuston Cesuosnatamaran.

The regular routine of the expedition started on December 12 with the first station at noon soon after we reached international waters. We carried out 32 stations in the Atlantic, of which we carried out one around noon and one in the middle of the night in order to have a regular station distance during transit and also to be able to distinguish the light-dependent processes in the seawater. At noon, the ships' CTD was deployed down to 1000 m and an additional optical biological CTD from the project partner Hereon, equipped with a FastOcean ADP (Adapted Plus Dark) for photosynthetic parameters down to 100 m. Right at the beginning of the cruise, a sampling pump for in-situ sampling fell dry, burned out, and has since been unable to be used, putting strain on the water budget. As the water demand for sampling was very high, we included another cast down to 200 m of the ships CTD on every station. The working boat of RV SONNE was deployed to collect water from the sea surface microlayer with a Garret screen where the wind and wave situation made it possible. This was not the case in the first week of operation as the swell from northerly storms was too high. But on every noon station the sea surface microlayer was at least sampled from the ships deck, which was not possible during two stormy occasions. The Neuston Catamaran was deployed at every noon station, and several times during transit in the exclusive economic zones of the Caribbean islands along the ships route. Additionally, sun observations and special turns of RV SONNE to avoid air-and aerosol sample contamination were included on stations, which also allowed the start of the radiosondes at noon and at night. Four ozone sondes were started in the Atlantic after every third day. On our night stations across the Mid-Atlantic Ridge at the end of the first week of the cruise, the ocean floor was mapped before deployment of the CTD down to the bottom. The first *Sargassum* patches were encountered on 23rd of December (second week) on our way to the northern most station and the first samples of different morphotypes of this floating algae were collected from the boat and incubation work started. Besides the ongoing research program, we celebrated Christmas on December 24 and 25 with good food, singing, poems, presents and charades organized by the 11 nationalities on board. The last stations in the Atlantic worked

again smoothly and on December 29, we entered the first of six different exclusive economic zones (EEZ) in the Caribbean, starting with Puerto Rico.

In the Caribbean EEZs of Puerto Rico (29.12.), the Dominican Republic (29.-31.12.), Haiti (31.12.), Jamaica (31.12.-01.01.22), Columbia (01.-02.01.), Panama (02.-06.01.) and the Pacific side of Columbia (06.01.), the three-hourly-underway-sampling of trace gases and nutrients continued, as well as the acoustic identification of currents and organisms. Additionally, the Neuston Catamaran was deployed for the collection of plastic debris. As occasionally massive patches of *Sargassum* were encountered, the collection of the algae, stemming from the equatorial regions of the western Atlantic, was possible with the Catamaran and incubations continued. We could underline the international character of the cruise and short relaxations to the round-the-clock work on the expedition by toasting to the New Year for five times, starting with the Asian participants at 12 o'clock noon –ships time- on December 31 2021. During the cruise through the Caribbean Sea the incubations in the five incubators placed on the stern to perform nitrogen, halogen, sulfur, and volatile organic compound cycling incubation experiments where intensified. Turnover rate and trace gas production measurements were performed, while the influence of natural factors such as light and temperature and of anthropogenic stressors such as sulfuric waste water on the marine biogeochemical processes was investigated to understand potential coupling and feedback mechanisms between these processes. The incubations of *Sargassum*, sampled in the Sargasso Sea and the Caribbean, continued to identify its contribution to halogen cycles and the marine carbon budget. The data acquisition of the continuous measurements and regular sampling intervals were interrupted in the Panama Canal from January 33 2022, 10 am to January 5 2022, 2 am UTC. After passing through the Panama Canal, which was an impressive experience for all on board RV SONNE and doing four stations in the international waters of the tropical Pacific at 85.5 W, where we crossed the equator on January 7 2022 at 17:07 local time (22:07 UTC). We reached our destination port (the Ecuadorian city of Guayaquil) well protected from the navy after the pilot station on January 10, 2022 in the afternoon, where PCR-testing and container packing was due again.

5 Preliminary Results

5.0 Underway Hydroacoustics- Ecosystemic Acoustic Observation

(Patrice BREHMER[1], Ndague DIOGOUL[1])

[1]IRD, CRODT

Background

Underwater acoustics are increasingly used to acquire a wide variety of information on aquatic ecosystems. Acoustic methods make it possible to sample almost the entire water column by making waves penetrate the aquatic environment, using calibrated instruments (Demer *et al.*, 2015). This technology, based on the integration of echoes, offers many advantages including good bathymetric coverage, rapid production of results, and independence from commercial fishing data. Acoustic method has thus become a major tool in fisheries research and in many fields such as marine geosciences, research and exploitation of offshore petroleum resources but also in the field of physical oceanography (Bruneau and Hladky-Hennion, 2010).

In the field of fisheries, acoustics is used for the quantitative assessment of fish stocks, to study fish ecology, predator/prey relationships and individual or gregarious behavior in relation to the environment, etc. (Guillard and Lebourges-Dhaussy, 2014). Acoustic methods allow the acquisition of robust quantitative data on the locations, characteristics and densities of detected individuals, their distributions and movements, their size distributions, their biomasses, etc.

(Simmonds and MacLennan, 2005). It is a non-invasive ocean sampling technique that allows sampling the water column at high spatial and temporal frequency (Brehmer *et al*. 2006, 2019). However, zooplankton and micronektonic compartments remain relatively poorly understood in terms of their specific composition, their biomass and their spatial and temporal distribution, although they represent an intermediate level determining the pathways of energy transfer to the upper trophic links. These zooplanktonic and micronektonic organisms are routinely recorded with fish echotraces and appear as scattering layers on a scientific echogram. Scattering layers have long been considered a problem in fisheries acoustics. Considered as "noise" from which the fish schools must be extracted, the echoes of the scattering layers have long been ignored or filtered out (Remond, 2015). Nowadays, with the challenges linked to global change and the decrease in fishery resources, it is necessary for a better understanding of the functioning of ecosystems, to study the distribution of the organisms responsible for these layers in relation to their environment. Zooplankton and micronekton play an essential role in marine ecosystems. These organisms are the first two animal levels in the marine food web. The micronekton forms the prey of marine predators such as tunas, whose populations are heavily exploited by fisheries, or even birds and marine mammals. Given their distribution in all oceans and the amount of biomass they represent, these organisms, especially the micronekton, represent potential new resources for fisheries. The zooplankton and the micronekton share a singular behavior: nycthemeral migrations. In fact, the majority of zooplankton and micronekton organisms travel vertically for hundreds of meters, migrating from the mesopelagic domain where they reside during the day to the epipelagic zone where they spend the night. These resources are therefore major players in the exportation and sequestration of carbon due to these nycthemeral vertical migrations that they carry out every 24 hours. This very dynamic movement is observed in all the oceans of the planet (Bianchi *et al.*, 2013; Bianchi and Mislan, 2016). This vertical migratory behavior is explained as an escape from visual predation during the day, as the organisms feed on the surface at night (Haney, 1988; Bianchi *et al.*, 2013; Lehodey *et al.*, 2015). This active transport of organisms on the vertical and the associated metabolic activity (surface feeding at night and deep metabolization during the day) has significant consequences on the carbon cycle (Bianchi *et al.*, 2013). All these characteristics make zooplankton and micronectonic organisms a key compartment in the functioning of marine ecosystems.

Material and methods

The SO287 cruise was carried out along a transect from Las Palmas to Guayaquil crossing the North-East Atlantic, the Sargasso Sea, the Caribbean Sea and the Pacific. Hydroacoustic data were continuously recorded (day and night) along the transect using a Simrad EK60 echo sounder operating at four frequencies (18, 38, 120, and 200 kHz). The EK60 were set at 20 log R time- varied gain function (where R is the range in meters) and using a pulse length of 1.024 ms. Shift consisted in regular control of the acquisition and the absence of interferences, and report all abnormal event in the spatial organization of the biological component of the pelagic ecosystem (0 to a maximum excepted at 1800 m with the 18 kHz). A Simrad WBAT (Wide Band Acoustic Transceiver) with its 38 and 120 kHz transducers were also deployed concurrently with the shallow CTD probes (Figure 5.1) during the day stations.

Figure 5.1: WBAT mounted vertically on the CTD rosette.

The WBAT mission were pre-programmed and uploaded to the WBAT prior to each deployment (station). The deployment of the CTD were timed to correspond to the transmission times set in the mission plans, ensuring that data will be collected at the right times and that the WBAT will not transmit whilst out of water. WBAT were stopped at the depth(s) corresponding to the middle of the biological layers during 12 minutes acquisition per layer (to sampled correctly the biological layers). These 12 minutes are: 6 minutes for each frequency (38 and 120 kHz) (note that both basis do not transmit at the same time).

Preliminary results

Acoustic characterization of different zones

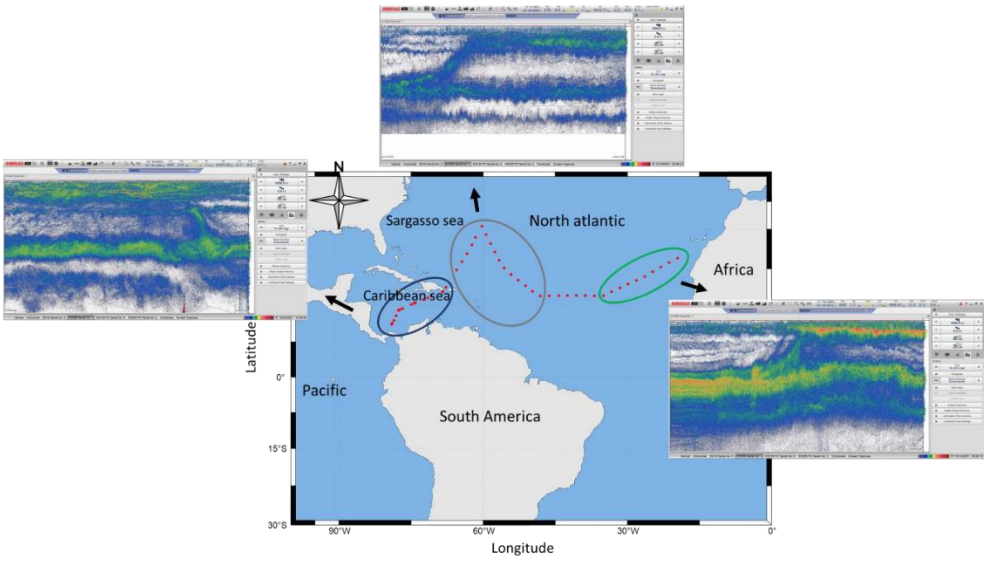

Figure 5.2: Cruise track (without the last 4 Pacific stations) combined with echograms showing characterizations of three main zones: The West African Atlantic area with a very high backscatter intensity in the SSL, the Eastern area in the Sargasso Sea with SSL showing low density, and the Caribbean area where the echogram shows again strong density in the SSL.

A first visualization of the echograms allows to characterize 3 different ecosystems (Figure 5. 2): The West African Atlantic area with a very high backscatter intensity in the SSL, the Eastern area in the Sargasso Sea with SSL showing low density, and the Caribbean area where the echogram show again strong density in the SSL.

Diel vertical migration (DVM)

DVM has been observed in all Atlantic areas where the small organisms migrate to surface waters at dusk and return to deeper waters at dawn. Indeed, the majority of macrozooplankton and micronecton organisms travel vertically tens or even hundreds of meters, migrating from deep areas where they reside during the day to surface waters where they spend the night.

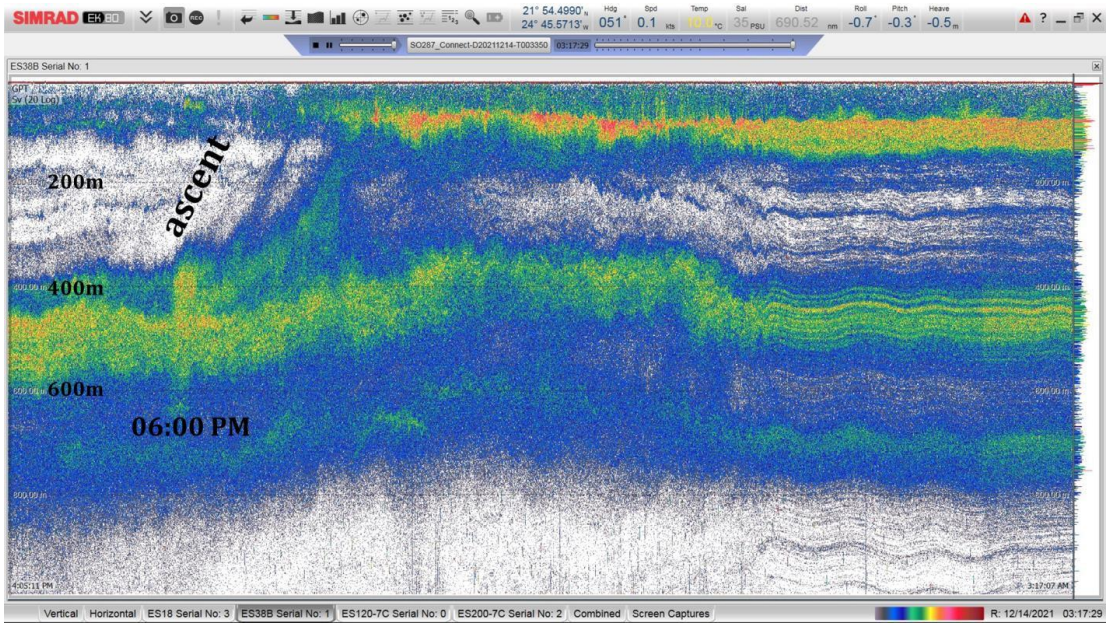

Figure 5.3: Echogram showing upward movement of the SSL migration.

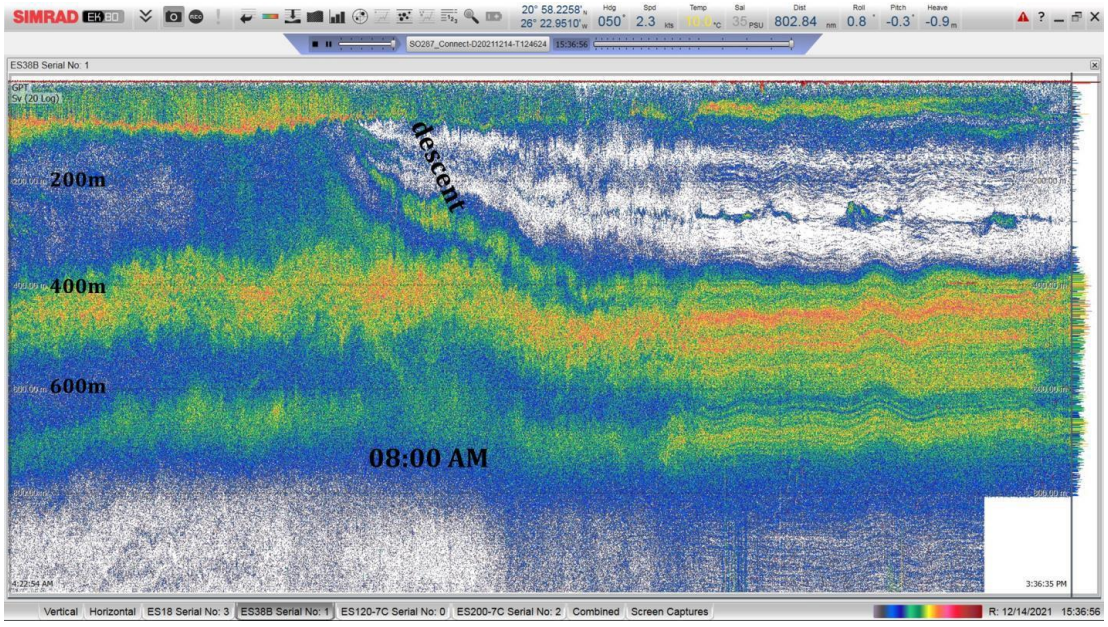

Figure 5.4: Echogram showing downward movement of the SSL migration

For example we see that during the day (Figure 5.3), the SSL is located below 400m depth; at 6pm, the upward movement begins and the SSL reaches the surface after two hours of migration. The SSL remains more or less stable at this depth for about 9 hours and begins the downward migration at 8am (Figure 5.4).

Future follow up studies data plans

Acoustic data treatment: For the processing of the acoustic data, an open source tool named "Matecho" (Perrot *et al.*, 2018) and developed by IRD will be used. The acoustic data will be corrected (e.g., by correcting bottom depths, removing empty pings, removing echogram interferences, and reducing background noise) then echo-integrated on elementary sampling units or ESU of 0.1 nmi per meter of depth. SSL extractions will be performed, then layer descriptors will be calculated for each ESU (Figure 5.5).

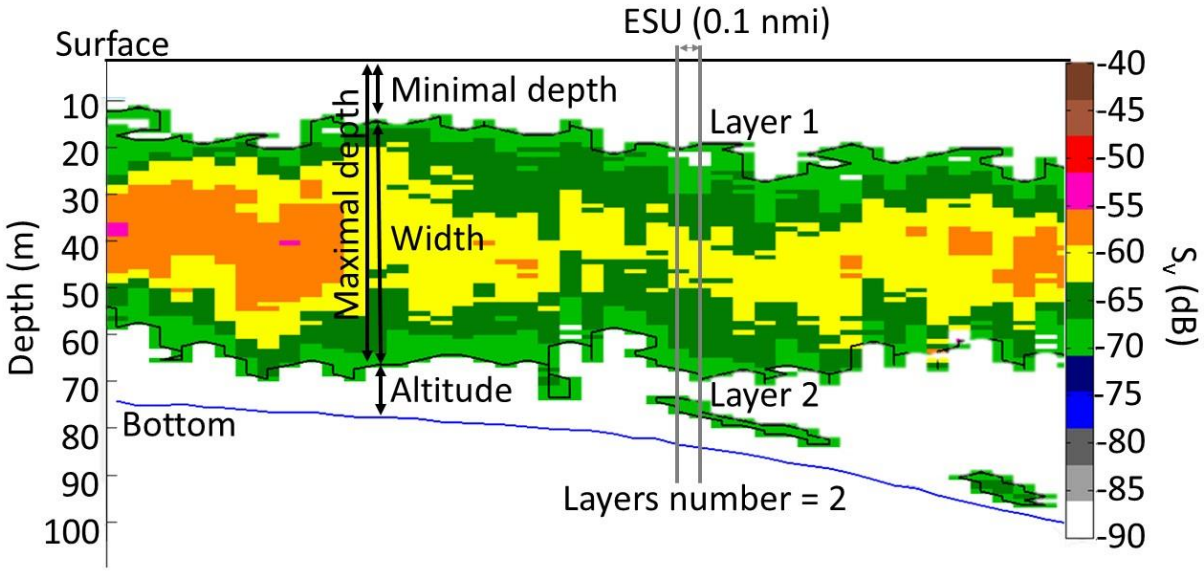

Figure 5.5: Schema showing typical sound scattering layers (SSLs) descriptors variables exported by Matecho software. Maximum depth of shallowest SSL (Layer 1), minimum depth of shallowest SSL, vertical width of shallowest SSL, altitude above the sea floor of shallowest SSL. Right axis depicts mean volume backscattering strength (S_V in dB) and left axis depicts local bottom depth. Sea surface is represented by a black bold line; bottom is represented by a blue line.

Acoustic vs. Environment

Previous studies showed that SSLs distribution are influenced by a variety of environmental factors (Dekshenieks et al., 2001; Marchal et al., 1993; Diogoul et al., 2020). Echogram and CTD profile Will be coupled and analyzed to determine the relation between environmental parameters and SSLs distribution. Models will be set to predict different SSL descriptors as a function of environmental parameters.

WBAT vs. UVP

The use of two frequencies 38 and 120 kHz from WBAT combined with UVP results will allow to discriminate macrozooplankton. Indeed, estimates of macrozooplankton abundances and sizes will be calculated with an inversion algorithm (Holliday, 1977) from the dual-frequency acoustic profiles and a scattering model. The results will be compared to UVP data collected at the same time.

5.1.1 Organic matter (carbon and nitrogen cycling)

(PI: Anja Engel, Responsible on board: Wanja Böhme, Quentin Devresse, Sandra Golde, Helmke Hepach, Tania Klüver, Tobias Müller, Jon Roa, Markus Schartau)

GEOMAR

Background

The quantity, composition and bioavailability of organic matter in the Western Tropical North Atlantic (WTNA) largely depends on processes in the Eastern Tropical North Atlantic (ETNA) itself and the transport from East to West along the North Equatorial Current (NEC). Investigating organic matter components along this gradient will provide information on the subsequent effects on productivity and excess carbon (C) accumulation in the WTNA and Sargasso Sea.

TEP formed from DOC contribute to the decoupling of C and nitrogen cycles under nitrogen deplete conditions (Engel et al., 2002). Most studies on organic matter transport and cycling have focused on either the ETNA or the WTNA region though organic matter dynamics in the WTNA may not be understood without knowing its history in the ETNA and the lateral transport to the WTNA. We suggest that C accumulation in the WTNA is linked to net community production of organic matter in the ETNA, becoming increasing resistant to microbial remineralization during transport to the west. The hypothesized slow-down of organic matter remineralization goes along with nutrient and trace metal deficiency becoming increasingly severe in the WTNA.

Material and methods

During the cruise SO287-CONNECT, the composition, quality and quantity of organic matter will be investigated by measuring particulate, dissolved and gel like organic matter components. To understand the fate of organic matter during the lateral transport from East to West more clearly, we measured the consumption (respiration and biomass production) and the production of organic matter from the Canary upwelling system to the oligotrophic waters of the North Atlantic Gyre.

Dissolved organic matter

Samples for dissolved organic matter components (Dissolved Organic Carbon (DOC), Dissolved Organic Nitrogen (DON), Dissolved Organic Phosphorous (DOP), Dissolved Hydrolysable Amino Acids (DHAA), Dissolved carbohydrates (DCCHO)) were taken in duplicates from all CTD stations from 6 to 7 depths each. For DOC and DON, 20 mL of seawater were filtered through 0.45 µm GMF filters into glass ampules, acidified using 20 µL of 30 % HCl and then stored at 4°C until analysis. For DOP, 50 mL of seawater were filtered through 0.45 µm GMF filters into flacon tubes and were then stored at -20°C until analysis. For DHAA, 4 mL of seawater were filtered through 0.45 µm Acrodisc filters into amber glass vials and stored at -20°C until analysis. Further 20 mL were filtered through Acrodisc filters into glass vials for analysis of DCCHO. DOC and DON will be measured back in the lab using High Temperature Catalytic Oxidation with a Shimadzu TOC-V, DOP will be analysed using photo-spectrometric methods, DHAA will be determined with HPLC (Agilent 1260 Infinity), and DCCHO will be measured applying Ion Exchange Chromatography with a Dionex ICS-6000.

Particulate organic matter (WP1/1, chapter: 5.1.1, WP2/3, chapter: 5.2.3)

Samples for particulate organic matter components (Particulate Organic Carbon (POC), Particulate Organic Nitrogen (PON), Particulate Organic Phosphate (POP) and Biogenic Silicate (BSi)) were filtered in duplicates from all CTD stations from 6 – 7 depths. For POC, PON and POP, about 1 L per sample were filtered through pre-combusted 0.7 µm GF/F filter.

For BSi, 0.5 L per sample were filtered through 0.8 µm cellulose acetate filters. POC and PON will be analysed in the lab using an elemental analyser. Both POP and BSi samples will be analysed in the lab using photo-spectrometry.

Lipids

Samples for lipids were taken at the three depths in the euphotic zone at every station in duplicates. About 1 L of seawater per sample were filtered through 0.22 µm PVDF membrane filters (47 mm) with a low constant vacuum (<0.2 mbar). Filters were rinsed with filtered seawater, packed into aluminium foil, shock-frozen in liquid nitrogen, and stored at -80°C. Back in the lab, filters will be analysed using reverse phase high performance liquid chromatography (HPLC) mass spectrometry (MS) coupled to a Thermo Q Exactive Orbitrap high resolution mass spectrometer.

Primary and secondary production, cell counts

Water samples for phytoplankton, bacterial, and viral cell counts were taken in duplicates from all CTD stations for 6 – 7 stations. 1.7 mL of water were fixed with 85 µL of glutardialdehyde (GDA, 25 %), gently mixed, incubated at room temperature for 15 min, shock frozen in liquid nitrogen, and finally stored at -80°C until analysis. Samples will be analysed back in the lab using a flow cytometer (FACSCalibur, Becton Dickinson, USA).

Samples for primary production were only taken during noon stations in the upper three depths. Samples were first filtered through a 200 µm net. Three times 312 mL were incubated with 100 to 200 µL of ^{14}C-bicarbonate (18 – 36 µCi). For standardization, 200 µL with 50 µL of 2N NaOH and added 4 mL cocktail were mixed and measured after about 2 h in the scintillation counter. Samples were incubated 24 h with a 12h light- and dark cycle under ambient temperatures and close to ambient light conditions.

Phytoplankton primary productivity was furthermore measured in-situ using a multi-wavelength Single Turnover Active Fluorometer (STAF) system (FastOcean APD (Ambient Plus Dark)) from Chelsea Technologies. The FastOcean APD was attached to the optical Hereon CTD rosette and deployed to 100 m at a speed of 0.1 m s-1 during the noon CTD stations. One sensor measured in the light at wavelengths of 450, 530 and 624 nm. The other sensor measured in-situ in the dark using an attached pump to pump water into a dark chamber to measure photosynthesis at 450, 530 and 624 nm. Data will be analysed at GEOMAR.

Secondary (bacterial biomass) production was measured by ^{3}H-Leucine incorporation. Samples were taken from each CTD station for 6 – 7 depths. Two times 1.5 mL of sample from each depth together with one poisoned control were incubated for 6 h with ^{3}H-Leucine (Hartmann Analytic, specific activity: 100 Ci mmol^{-1}) at a final concentration of 20 nmol L^{-1}. Samples were incubated at in-situ temperature and at +4°C. Incubations were terminated using trichloroacetic acid (TCA, Sigma Aldrich) at a final concentration of 5 % and processed by the centrifugation method according to Smith and Azam (1992). The incorporation of ^{3}H-Leucine into cells was measured using a scintillation counter.

Respiration

Respiration rates were measured within the euphotic layer from all CTD stations with two different approaches:

- Plankton community respiration was measured by monitoring the decrease in oxygen concentration after a 24 h dark bottle incubation. Dissolved oxygen concentration was measured by Winkler titration.
- Size-fractioned respiration was determined by the reduction of a tetrazolium salt by the cellular electron transport system (*in-vivo* ETS; Martínez-García et al., 2009) over 30-

90mn incubations. The method is based on the reduction of the 2-para (iodophenyl)-3(nitrophenyl)-5(phenyl) tetrazolium chloride (INT) salt inside the plankton cells and the subsequent quantitative spectrophotometric analysis of the reduced salt (formazan). This method allows for a size-class separation of the plankton community with the respiration of the <0.8 µm size class, considered to be predominantly bacteria.

Incubation temperatures were maintained at in situ values ± 1 °C inside a temperature controlled room.

Microbial composition and functioning

4 L of seawater were filtered for the upper four depths of all noon CTD stations. During day stations, seawater was prefiltered on 3 µm and then filtered onto 0.22 µm Millipore Sterivex filter units both for RNA and DNA for four depths. A second set of samples from these four depths was only filtered onto 0.22 µm Millipore Sterivex filter units without prefiltering. For night stations, 4 depths were prefiltered through 3 µm and then filtered onto 0.22 µm Millipore Sterivex filter units for DNA.

Preliminary results

Most of the data need to be analyzed in the lab at GEOMAR. First results for respiration measurements are shown below.

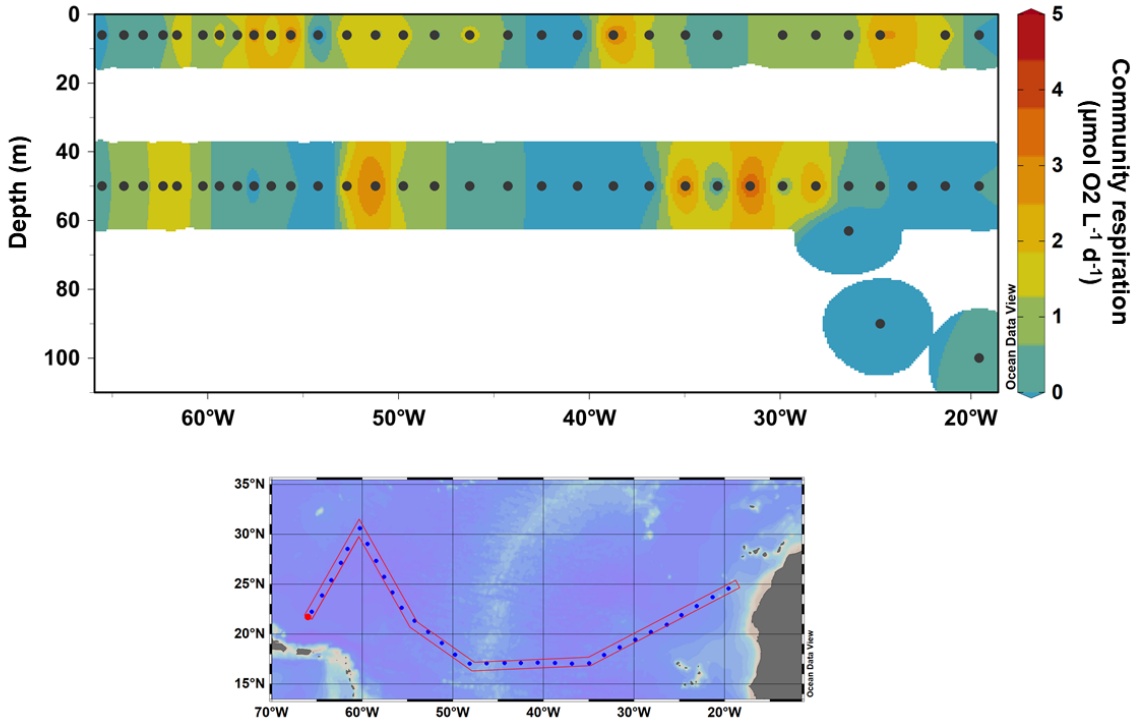

Figure 5.6: Plankton community respirations rates obtained from the Winkler titration method during SO287.

Preliminary results of the plankton community respiration obtained from the Winkler titration method show a high variability of respiration rates across the transect. This variability will be further investigated through currents, eddies and nutrients distribution. Respiration rates will also be compared to the quantity and quality of the DOM (carbohydrate and amino acids) and to plankton metabolic activities (enzymes, bacterial biomass production, and primary production).

Future follow up studies data plans

Most of the samples will be analysed at GEOMAR within 6 – 12 months. Further data analysis will then be carried out in comparison with metadata and data from other working groups from the cruise. We plan on writing three peer-reviewed publications. Two master theses (Wanja Böhme, Microbial Composition and Functioning; Tobias Müller, TEP and CSP) will be written with the data obtained during the cruise.

Table 5.1: Station list of WP1/1: Organic matter (carbon and nitrogen cycling).

Station	Date (UTC)	Lat (°N)	Lon (°W)	DOM	Lipids	Bact. product.	En-zymes	Flow cytometry	Autotro-phic produc-tion	POM	Gel particles	16S-RNA	UVP	Fast-Ocean APD
1	2021-12-12 14:12:23	24,5541	-19,5694	x	x	x	x	x	x	x	x	x		
2	2021-12-13 00:42:28	23,6944	-21,3384	x	x	x	x	x		x	x	x		
3	2021-12-13 13:56:32	22,7954	-23,0725	x	x	x	x	x	x	x	x	x	x	
4	2021-12-14 00:23:18	21,9078	-24,7597	x	x	x	x	x		x	x	x	x	
5	2021-12-14 12:36:54	20,9552	-26,3984	x	x	x	x	x	x	x	x	x	x	
6	2021-12-14 23:49:04	20,1999	-28,1330	x	x	x	x	x		x	x	x	x	
7	2021-12-15 11:51:53	19,4451	-29,8700	x	x	x	x	x	x	x	x	x	x	
8	2021-12-15 23:02:59	18,6661	-31,5816	x	x	x	x	x		x	x	x	x	
9	2021-12-16 11:30:55	17,8944	-33,2838	x	x	x	x	x	x	x	x	x	x	x
10	2021-12-17 00:23:50	17,0905	-34,9655	x	x	x	x	x		x	x	x	x	
11	2021-12-17 13:35:21	17,0582	-36,8634	x	x	x	x	x	x	x	x	x	x	x
12	2021-12-18 01:30:27	17,1115	-38,7327	x	x	x	x	x		x	x	x	x	
13	2021-12-18 15:22:01	17,1292	-40,6207	x	x	x	x	x	x	x	x	x	x	x
14	2021-12-19 02:46:53	17,1128	-42,5025	x	x	x	x	x		x	x	x	x	
15	2021-12-19 15:49:29	17,0972	-44,2672	x	x	x	x	x	x	x	x	x	x	x
16	2021-12-20 03:41:13	17,0752	-46,2643	x	x	x	x	x		x	x	x	x	
17	2021-12-20 15:19:26	17,0304	-48,1143	x	x	x	x	x	x	x	x	x	x	x
18	2021-12-21 02:56:49	17,9522	-49,7498	x	x	x	x	x		x	x	x	x	
19	2021-12-21 14:39:39	19,1015	-51,2052	x	x	x	x	x	x	x	x	x	x	x
20	2021-12-22 01:56:48	20,2320	-52,7119	x	x	x	x	x		x	x	x	x	
21	2021-12-22 13:59:31	21,3496	-54,2126	x	x	x	x	x	x	x	x	x	x	x
22	2021-12-23 01:40:31	22,6282	-55,6397	x	x	x	x	x		x	x	x	x	
23	2021-12-23 15:35:02	24,1522	-56,6691	x	x	x	x	x	x	x	x	x	x	x
24	2021-12-24 02:39:52	25,7393	-57,5788	x	x	x	x	x		x	x	x	x	
25	2021-12-24 15:16:48	27,3366	-58,4533	x	x	x	x	x	x	x	x	x	x	x
26	2021-12-25 02:48:51	29,0244	-59,3840	x	x	x	x	x		x	x	x	x	
27	2021-12-25 15:36:28	30,5839	-60,2585	x	x	x	x	x	x	x	x	x	x	x
28	2021-12-26 12:52:08	28,5187	-61,6064	x	x	x	x	x	x	x	x	x	x	x
29	2021-12-27 00:09:40	27,1144	-62,3463	x	x	x	x	x		x	x	x	x	
30	2021-12-27 15:14:05	25,3884	-63,3848	x	x	x	x	x	x	x	x	x	x	x
31	2021-12-28 02:38:41	23,8728	-64,4046	x	x	x	x	x		x	x	x	x	
32	2021-12-28 15:21:39	22,2433	-65,5400	x	x	x	x	x	x	x	x	x	x	x
33	2022-01-07 03:16:31	2,2640	-85,8331	x	x			x		x	x	x	x	
34	2022-01-08 16:08:47	0,4535	-85,8328	x	x			x		x	x	x	x	x
35	2022-01-08 04:38:20	-1,3396	-85,8334	x	x			x		x	x	x	x	
36	2022-01-08 16:25:24	-2,6664	-85,8316	x	x			x		x	x	x	x	x

5.1.2 Nutrient, O_2 and nitrogen cycle

(PI: Hermann Bange[1], Kirstin Dähnke[2], Damian Arevalo[1], responsible on board: Riel Ingeniero[1], Hanif Sulaiman[1], Kastriot Qelaj[1], Isabella Zehnder[1], Gesa Schulz[2])

[1]GEOMAR

[2]Hereon

5.1.2.1 Stable Isotopes (^{15}N & ^{18}O) of Nitrate (NO_3^-) in the Tropical Atlantic and Eastern Tropical North Pacific

Background

The tropical North Atlantic is known for its oligotrophic surface water. Major limiting nutrients such as nitrate and phosphate are scarce, making the area hardly productive. In the SO287 cruise, the tropical North Atlantic transect encompasses this oligotrophic region. Despite the generally low nutrient levels, elevated nitrate concentrations could still be observed in the eastern part of the transect. This is due to the Canary Current forming an eastern boundary current, causing upwelling in the northwest African Continental Margin. In the East Tropical North Pacific (ETNP), substantially higher nitrate concentrations are expected, due to it being in one of the world's major upwelling zones, which turned it into an oxygen-deficient zone (ODZ).

The different oceanographic settings between the Canary upwelling zone, oligotrophic tropical North Atlantic, and the ETNP gave rise to different biogeochemical processes. One of the prominent biogeochemical cycles in the ocean is the nitrogen cycle, a major limiting nutrient that partially controls atmospheric CO_2 removal through the biological carbon pump. Oxygen-deficient zones are also known to produce N_2O, a potent greenhouse gas that also plays a role in stratospheric ozone depletion. Therefore, a good understanding of biogeochemical processes and their interrelations between different oceanographic settings are vital to gain a solid view of the biogeochemical systems in the tropical North Atlantic and Pacific, especially in the face of climate change and increasing anthropogenic pressure.

Material and Methods

Stable isotopes of nitrate could be utilized as a way to delineate certain formation pathways of nitrogen species in the ocean. Enzymatic isotope fractionation could arise from differences in reaction rates containing heavy and light isotopes. Isotopic fractionation may result in differences in isotope ratios between the substrate and the product of a reaction. For example, enzymatic reaction products are commonly depleted in heavy isotopes due to the preferential entrainment of the lighter isotopes. On the contrary, the substrates would be enriched in the heavier isotopes.

Seawater samples for nitrate isotopes were taken from CTD casts during the SO287 cruise. Samples for nitrate isotopes were taken mostly during the night-time CTD, which went down until the bottom depth. The discrete depths of the CTD cast consist of the depths 3500, 2000, 200, 50, and 6 m, along with the near-bottom depth, oxygen minimum (OM) and the deep chlorophyll maximum (DCM). The samples for nitrate isotopes should eventually provide us with a comprehensive view of isotopic fractionations in the water column. In total, at least 96 seawater samples for nitrate isotopes were collected in 125 mL PET bottles from at least 16 stations.

The dual isotopes ($\delta^{15}N$ and $\delta^{18}O$) of nitrate (NO_3^-) are determined by the "chemical" method (McIlvin & Altabet, 2005). The sample NO_3^- is reduced to NO_2^- by cadmium (Cd) and then further reduced to N_2O by sodium azide (NaN_3) in an acetic acid buffer.

The $\delta^{15}N$ of ammonium (NH_4^+) is determined by oxidizing the NH_4^+ to NO_2^- by hypobromide reagent followed by azide conversion of NO_2^- to N_2O by sodium azide (NaN_3) in an acetic acid buffer (Zhang et al., 2007). For both analyses, preexisting NO_2^- is removed with sulphamic acid.

The produced N_2O is then extracted, purified and analysed using an automated purge-trap system (PT-CF-isotope ratio mass spectrometer (IRMS)). All isotopic parameters are calibrated against international standards and standard quality control practices will be adhered to. N and O isotopic ratios are expressed in per mil notation as:

$\delta^{15}N$ or $\delta^{18}O = ((R_{sample}/R_{reference})-1)*1000$

where $R = {}^{15}N/{}^{14}N$ or ${}^{18}O/{}^{16}O$ and references for N and O are AIR and VSMOW respectively.

Preliminary Results

The seawater samples taken from the CTD were safely labelled and contained in 125 mL bottles. Samples from each station were put in one plastic container/bag, before being stored and frozen at -20 °C. Eventually, the samples will be shipped as one of the frozen goods to GEOMAR Helmholtz Centre for Ocean Research Kiel, Germany. At GEOMAR, stable isotope analyses (^{15}N & ^{18}O) will be performed on the samples.

5.1.2.2 Nitric Oxide Measurement and Incubation Experiments

Background

NO is a short live intermediate of the nitrogen cycle – in the denitrification process from the conversion of NO_2^- to N_2O, in the nitrification process in the conversion of NH_3 or NH_2OH to NO_2^-, and in the anaerobic ammonium oxidation process in the conversion of NO_2^- to N_2. Moreover, NO in the ocean may come from various sources that may include atmospheric deposition, terrestrial inputs, and photochemical and biological production.

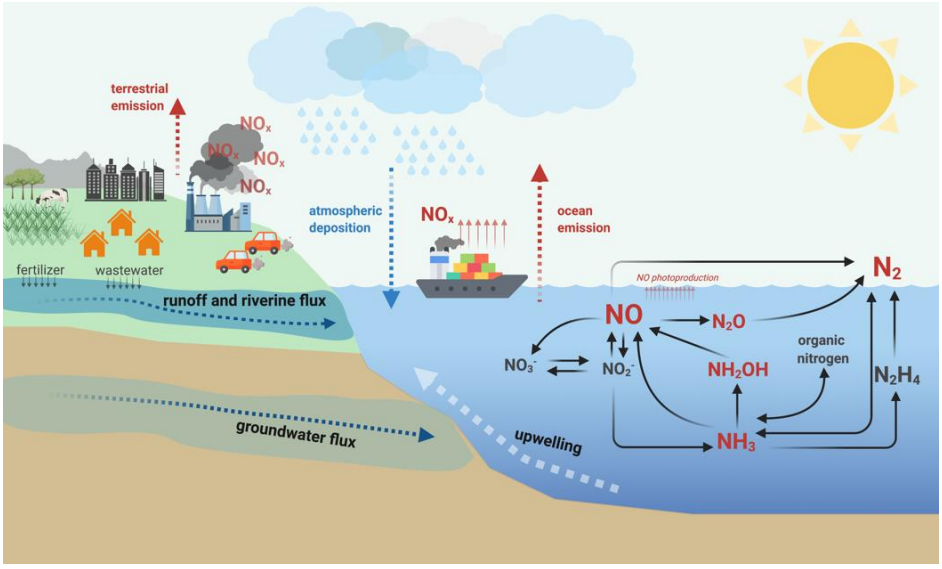

Figure 5.7: Nitric oxide is an intermediate in the marine nitrogen cycle (adapted from publications of Kuypers et al. (2018) and Zhang et al., 2020). Aside from anthropogenic emissions from fossil fuel combustion in transportation, industries, and ships, nitric oxide may be produced in the ocean through biological and photochemical processes. The molecules in red font are the nitrogen gases that may emitted or consumed during the different nitrogen cycle processes.

Several scientists have considerably focused on observing NO and pertinent biogeochemical processes in the soil and the atmosphere. Numerous studies have already been done to assess nitric oxide emissions on various terrestrial ecosystems such as deserts, grasslands, agricultural systems, and forests, including the effect of environmental factors such as fertilizer application, crop rotation, pH, temperature, soil type, and moisture (Pilegaard, 2013; Stehfest and Bouwman, 2006; Bouwman et al., 2002; Skiba et al., 1997; Delon et al., 2007; Ganzeveld et al., 2002). Because of the much available NO emission data from soils, scientists were able to estimate global NO emission from soils, which ranges from 9 -27 Tg N yr^{-1} (Oikawa et al., 2015).

Inevitably, there are only a few publications on observing nitric oxide in the ocean. Until today, little is known about the production and consumption mechanisms of NO in the ocean, the chemical processes and reactions of NO in seawater, and the global NO flux from the ocean to the atmosphere. Scranton (1983) in her review paper described NO as "a more exotic gaseous nitrogen species found in the ocean". Her paper highlighted the pioneering research of Zafiriou and colleagues who first attempted to measure NO in the ocean and observed the photolysis of NO_2^- to NO. Citing further research conducted by Ward and Zafiriou (1988), Bange (2008) mentioned that the formation process of NO in the upper boundary of the oxygen minimum zone (OMZ) remains uncertain. Moreover, Schreiber et al. (2012) commented that understanding NO formation may lead to advancing the knowledge on the mechanism in the release of nitrous oxide (N_2O), a potent greenhouse gas.

This research expedition provides us an opportunity to measure for the first time the concentration of dissolved nitric oxide in the Atlantic Ocean. Furthermore, in this research, we aim to further understand the processes involved in the production and consumption of nitric oxide by measuring the dissolved nitric oxide concentration in the ocean. We did this by collecting water samples daily through the underway pump and by performing a 48-hour light and dark incubation experiment of seawater samples collected from the North Atlantic Ocean, Sargasso Sea, and the Pacific Ocean.

Material and methods

Nitric Oxide Measurement

On the first days of the cruise, the NO analyzer system was setup and connected to the nitrogen generator (with minimum 99.999% purity). Shown in Figure 5.8 is the modified setup of the NO analyzer system based on the methods established by Lutterbeck and Bange (2015). After successful setup of the instrument, calibration checks were done to ensure that the instrument is ready. Bubble-free seawater samples in 50mL septum vials were collected from the underway system daily during the entire cruise.

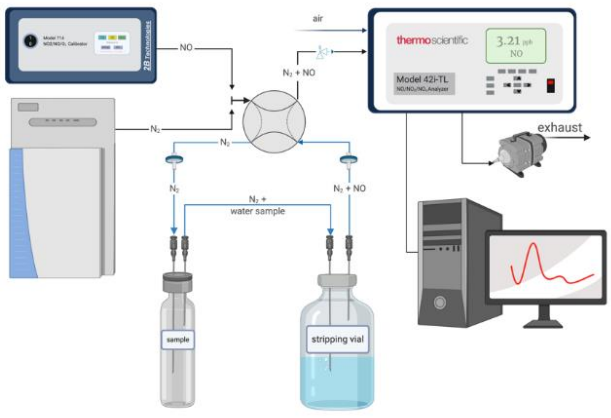

Figure 5.8 Schematic set-up of the NO measurement system that uses the Model 714 NO_2/NO/O_3 Calibrator and nitrogen gas generator. The design of the line connecting the sample and stripping vial now uses Luer Lock valves to ensure that no air may contaminate the sample bottles when transferring from one sample bottle to the next.

Incubation Experiment

We collected surface seawater samples through the underway pump from the North Atlantic Ocean, Sargasso Sea, and the Pacific Ocean. Simple incubation experiments were performed using these collected water samples. The collected samples will be transferred to an area exposed to ambient light conditions with constant flow of water (to minimize temperature fluctuations). Bottles were incubated in incubation vessels under conditions of light and dark to interrogate the impact of UV on photochemical pathways of NO.

Figure 5.9: Collection of seawater samples in 3.5 L Duran glass bottles for the 48-hour incubation experiment.

Simple incubation experiments were performed using these collected water samples. The collected samples were transferred to an area exposed to ambient light conditions with constant flow of ocean surface water. Bottles were incubated in incubation vessels under conditions of light and dark to interrogate the impact of UV on photochemical pathways of NO and CO. A further set of incubations were poisoned with sodium azide to prevent microbial production of nitric oxide. In all cases duplicate 3.5-Liter bottles were individually manipulated. An overview of the incubation setup is given below.

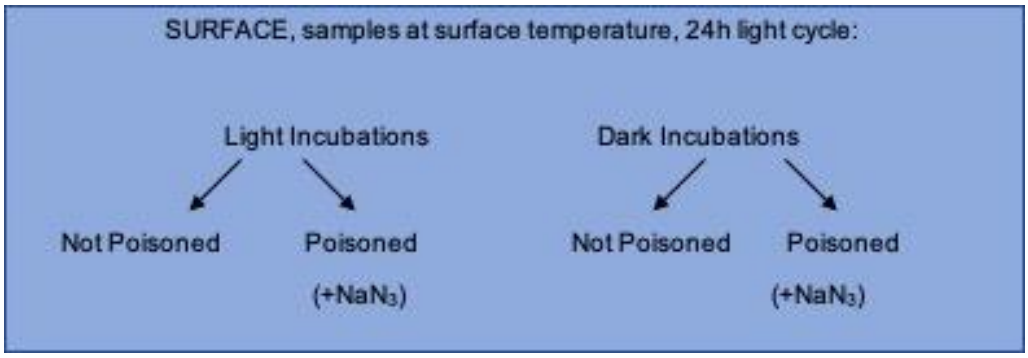

Figure 5.10: Schematic set-up of the incubations.

Aside from NO, ancillary parameters such as nutrient, O_2, marker pigments, CDOM, flow cytometry were also determined at least at the start and the end of the incubations (0, 24, 48 hours). Oxygen was measured using the Winkler method while nutrients and CDOM samples were stored in CCMAR's refrigerator until analysis. Water samples were filtered for marker pigments using standard filtration setup. These samples will be analyzed at GEOMAR at a later date. Meanwhile, samples for flow cytometry were preserved with 25% glutaraldehyde (EM Grade) and will be frozen in -80 °C freezer prior to shipment to GEOMAR's laboratory.

Preliminary results

In agreement with previous publication of Lutterbeck et al. (2018), initial results shows that NO concentration is close to or below the detection limit of the instrument in the surface layer of the Atlantic Ocean. Reports from colleague from IUP-Bremen indicated that NO concentration in the Atlantic Ocean is below 1 ppb. NO is a radical with unpaired electron, and is highly reactive with oxygen, superoxide, oxygen radicals, and transition metals. The estimated turnover time (lifetime) of dissolved NO in seawater reportedly ranges from 3 to 100 s. Shown below is a representative results from 14 December 2021 to 15 December 2022. Since data were logged with a freeware putty.exe and that Thermo Scientific 42i-TL doesn't have a built-in program for this type of analysis, more time is needed to process and analyse the data and arrive with a better conclusion.

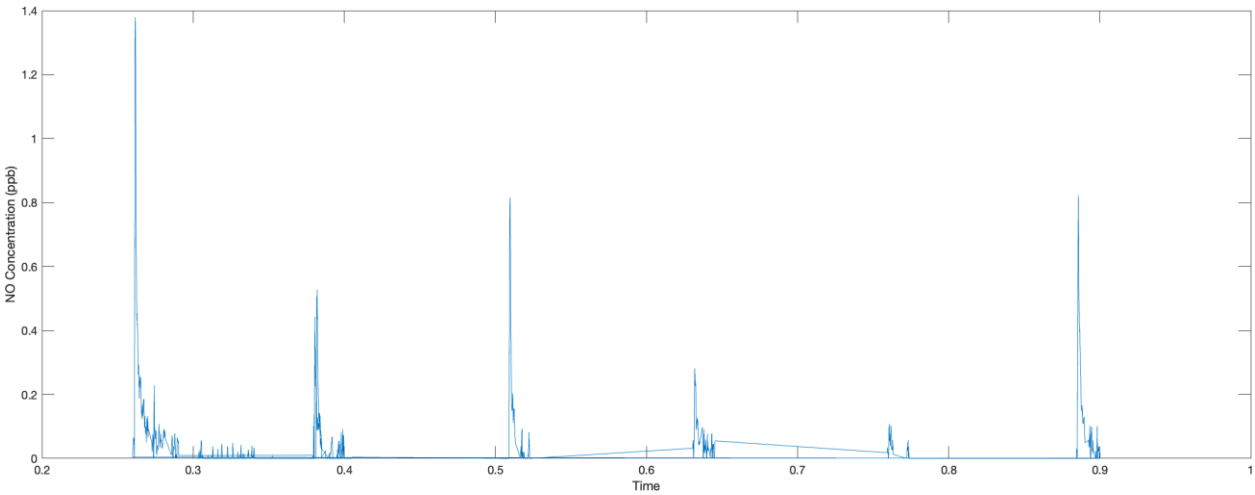

Figure 5.11: Signal peaks of the instrument during analysis on 14 December 2021 (09:00 UTC) to 15 December 2021 (10:00 UTC).

Future follow up studies data plans

We plan to publish results or part of the results of this research within a year or two once all laboratory analysis and data analysis at GEOMAR are finalized. The data generated from this research will provide valuable baseline data on nitric oxide concentration in the surface of the Atlantic Ocean, Sargasso Sea, and the Caribbean Sea, and the Pacific.

Datasets derived from the research project may be archived at the PANGAEA database. The nitrous oxide data concentrations from the incubation experiment may be published in the MEMENTO (Marine Methane and Nitrous Oxide) Database hosted by GEOMAR Helmholtz Centre for Ocean Research. Data may also be included as supplementary materials in published articles.

5.1.2.3 Water column nitrous oxide and methane concentration

Background

The ocean is a potential source for the long-lived climate relevant greenhouse gases nitrous oxide (N_2O) and methane (CH_4) (Rhee et al. 2009, Tian et al. 2020). Dissolved N_2O and CH_4 concentrations in the North Atlantic Ocean and eastern tropical South Pacific show characteristic variations in the vertical and horizontal distributions and can be explained by a combination of biological (productivity) and hydrographic (mixing/circulation) processes (Bange et al. 2019, Ji et al. 2019, Walter et al. 2006, Wilson et al. 2020). Therefore, it is timely to investigate their distribution, air-sea fluxes and production pathways.

Our main aim during the SO287-CONNECT cruise was to decipher the distributions of the trace gases, infer their main formation mechanism and investigate their air-sea dynamic. Further, we want to compare the results from different oceanic environments such the eastern and western Atlantic Ocean and the eastern tropical South Pacific. In conjunction with the other work packages, we hope to be able to provide an insight on the role of biology and ocean circulation on the production/consumption and overall budget of N_2O and CH_4 in the study area. We combined discrete and continuous measurements methods, which are described in the following together with first preliminary results.

Material and methods

At every sampling station, triplicate samples for N_2O and CH_4 were collected from CTD-Niskin bottles, which were fired at different depths. During the Day-CTD, six depths were sampled with the samples from 1000 m, the oxygen minimum zone, 200 m, the deep chlorophyll maximum, 50 m and 6 m. During the Night-CTD eight depths were samples: bottom water, 3500 m, 2000 m, the oxygen minimum zone, 200 m, the deep chlorophyll maximum, 50 m and 6 m.

For N_2O, triplicates were sampled bubble free into 20 mL brown glass vials. The sample vials were rinsed with about twice their volume and immediately sealed with butyl rubber stoppers and aluminum caps. To preserve the sample, 50 µL of oversaturated mercury chloride solution ($HgCl_2$) was added to each vial. Samples were stored upside down, in the dark at room temperature for later analysis.

For CH_4, water was collected air bubble free in triplicates into 50 mL glass vials after rinsing it with about twice their volume. The samples were sealed with butyl rubber stoppers and aluminium caps. For sample preservation, 125 mL of an oversaturated solution of mercury chloride ($HgCl_2$) was added to the samples. For later analysis, we stored the sampled upside down, in the dark at room temperature.

Continuous measurements of N_2O and CH_4 from surface water and atmosphere were done using a wavelength-scanned cavity ring-down spectroscopy (G2308 N_2O, CH_4 and H_2O Gas Concentration Analyser, Picarro, Inc.) coupled with a shower-head type equilibrator and a control unit (Figure 5.12). A submersible pump located at the moonpool provided the equilibrator with water from 6 m depth. In a closed loop, sample air was continuously pumped from the equilibrator headspace to the instrument and back to the equilibrator chamber. To prevent interferences from the water content, the sample air was dried before reaching the instrument using cooling traps and a Nafion dryer. The water temperature at the equilibrator was constantly monitored by means of a high accuracy thermometer (FLUKE 1523). Ambient air measurements were conducted every 6 hours for 30 min by drawing air into the system from the top deck of the ship. Every 12 hours, we conducted control measurements of three reference gases bracketing the expected range of seawater concentration of N_2O and CH_4. Discrete water samples (N_2O and CH_4) were taken once per day by sampling the water stream from the

submersible pump feeding the continuous system. The samples will be used as a cross-check for the continuous underway N_2O and CH_4 measurement. Sampling and preservation was the same as for the discrete sampling from the CTD rosette and is already described in detail above.

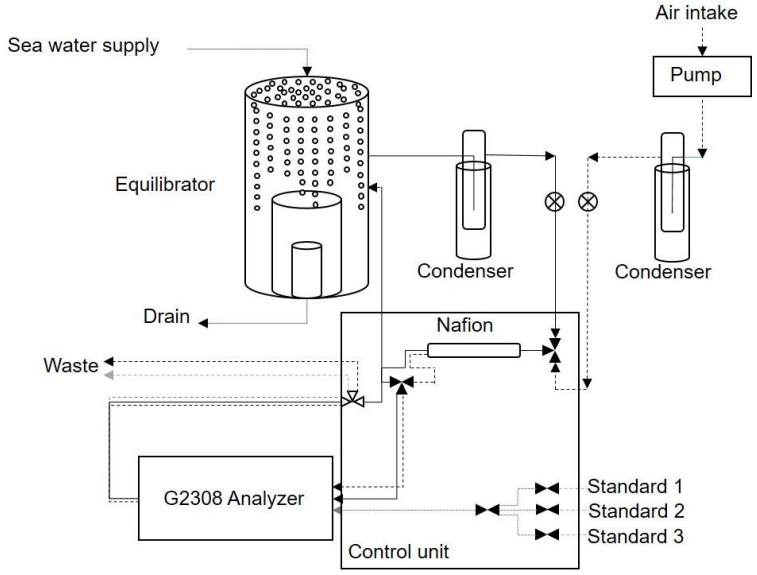

Figure 5.12: Schematic view of setup for the continuous measurements of N_2O and CH_4 in surface waters

Preliminary results

Preliminary results from continuous N_2O in the Northern Atlantic show dry mole fractions (Figure 5.13) and concentration (Figure 5.14) close to ambient conditions. N_2O dry mole fraction plotted over cruise time show a small gradient with slightly decreasing concentration in the Sargasso Sea. A similar trend is visible in the ambient air concentration (Figure 5.15). N_2O concentration in surface waters seems to be mostly influenced by mixing and equilibration processes.

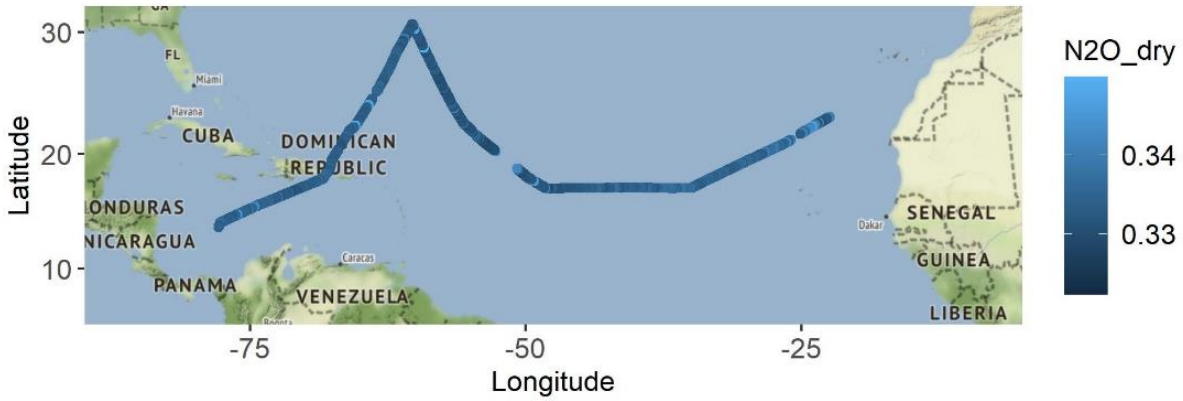

Figure 5.13: Preliminary along-track dry mole fraction of N_2O in ppm

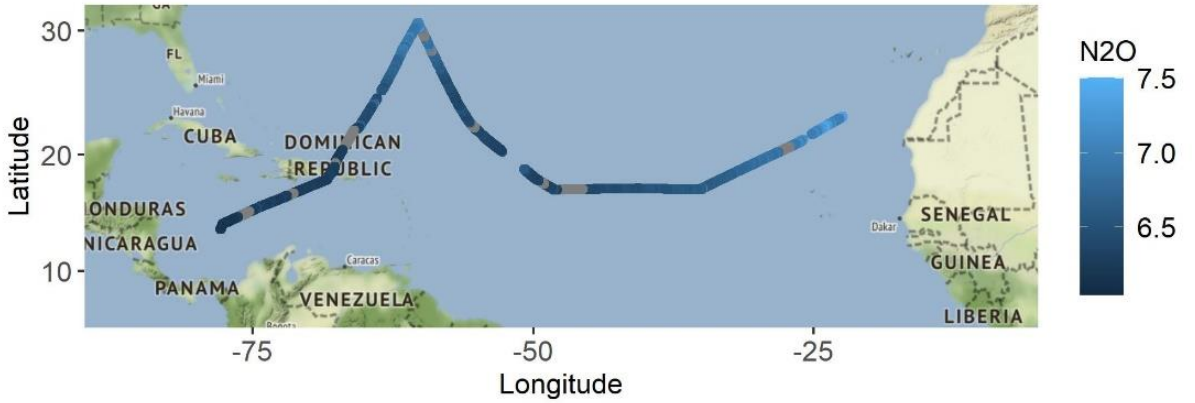

Figure 5.14: Preliminary along-track N_2O concentration in nmol L^{-1}

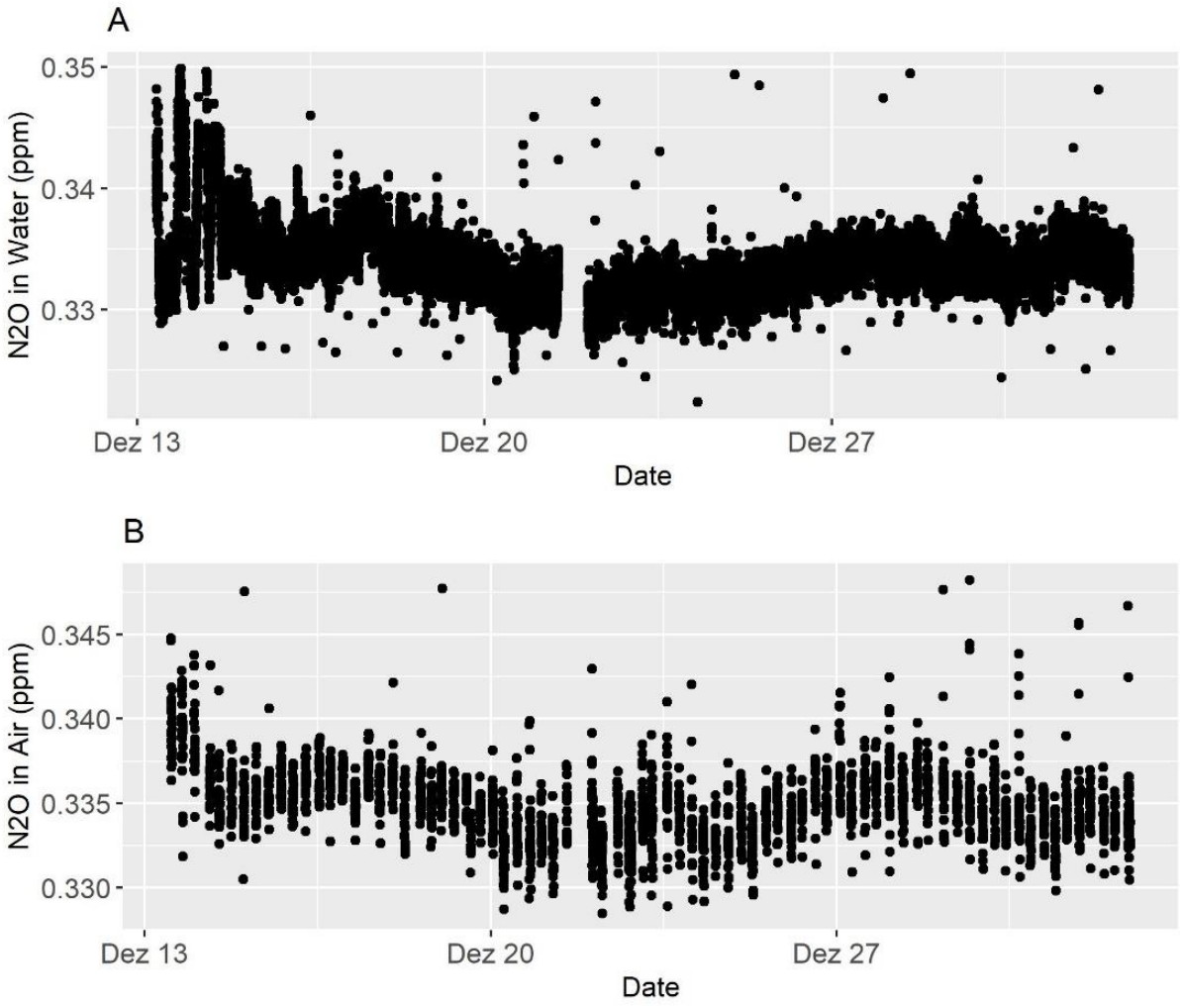

Figure 5.15: Dry mole fraction of N_2O in Water (A) and Air (B) over time during our cruise along the North Atlantic

Dry mole fraction of CH_4 in the North Atlantic (Figure 5.16) is close to ambient concentration. Mostly CH_4 concentration was influenced by mixing and equilibration processes. However, other processes might cause the gradient close to the Dominican Republic as the same increase was not visible in the ambient concentration.

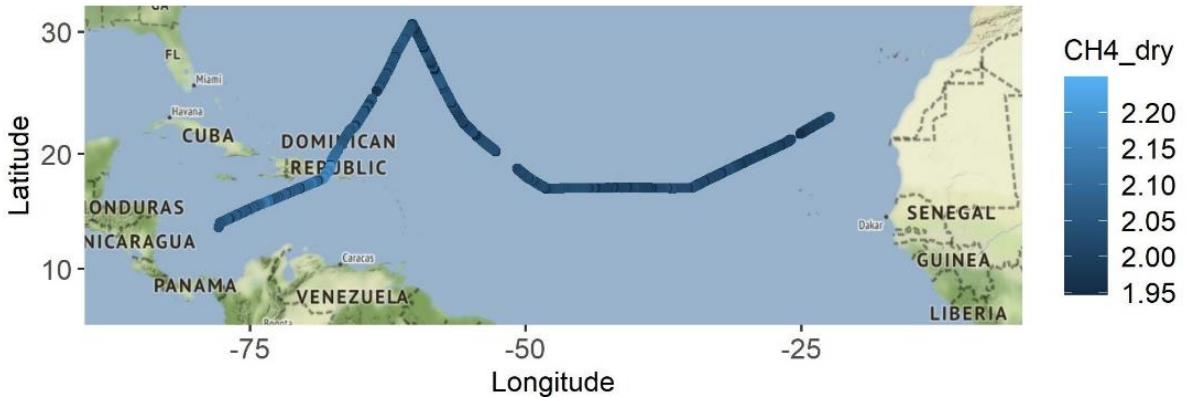

Figure 5.16: Along-track dry mole fraction of CH_4 in ppm

No preliminary results can be shown for the trace gases depth profiles from the CTD sampling, as the samples still need to be measured in the lab.

Future follow up studies data plans

Discrete water samples for N_2O and CH_4 need to be measured in the laboratory. For the continuous measurement of surface N_2O and CH_4 concentration, calculations for concentrations and fluxes, calibration and data quality control are needed to decipher final N_2O and CH_4 concentrations and quantify the air-sea exchange. Taking the results from the oxygen and nutrients measurements into account, we will study the main formation pathways of N_2O and CH_4. This tasks will be carried out during the following months.

5.1.2.4. Dissolved oxygen

Background

The dissolved oxygen measurements with Winkler-titration are mainly done for the calibration of the oxygen sensors of the CTD. There is a change in dissolved oxygen along the transect and in the different depths expected with very low concentrations at the last stations in the Pacific Ocean and in the OMZ. The link of dissolved oxygen concentration to NOx and N_2O is also part of the research question.

Material and methods

The sampling was done with a CTD which was placed into the water at 36 stations in total. In different depths the samples were taken during the day and during the night. At station 33 there were slight changes of the different depths (depths and number of depths). To get a good profile of the oxygen concentrations in the ocean, samples were taken at the surface, in the deep chlorophyll maximum, the middle part of the ocean, the oxygen minimum zone and in deeper parts of the ocean. At the day-station there were six different depths and the samples have been taken in triplicates. At the night-station there were eight different depths and only one sample for each depth was taken. During the sampling of the dissolved oxygen samples (100 ml bottles), it was important to ensure that they were taken bubble-free from the bottom of the bottle. About twice the volume of the bottle should overflow. Afterwards, the oxygen was fixed with 1 ml sodium iodide and manganese (II) chloride and then shaken for about 30 seconds. The samples were darkened with the help of a towel. In the lab, the oxygen measurements were done by Winkler titration (Figure 5.17).

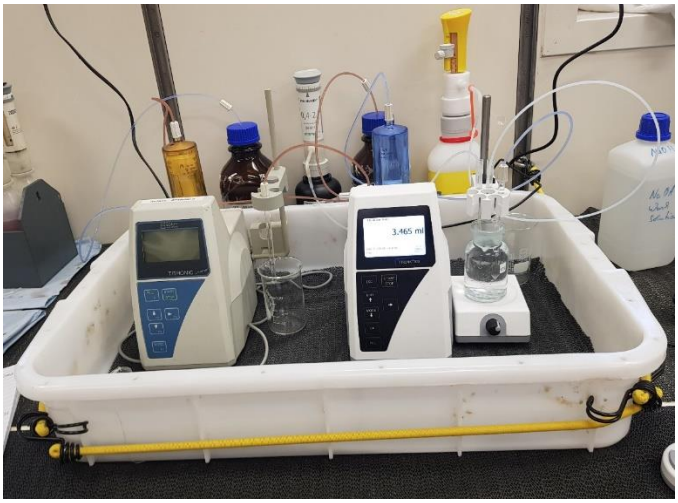

Figure 5.17: Winkler titration.

For this, 1 ml of 1:1 sulphuric acid had to be added to the sampling bottle and mixed until the precipitation has disappeared. The titration was done with a sodium thiosulfate solution that had to be added until the solution lost the dark yellow colour. Then a zinc iodide-starch solution was added what resulted in a blue colour. This colour had to be further removed by titration until the sample was fully colourless.

To check the solutions for their reliability, a standard (potassium hydrogen diiodate) was measured five times a day. For this approximately 50 ml Milli-Q water was used and the three solutions sulphuric acid, sodium iodide and manganese (II) chloride were added and mixed in the correct order. Afterwards, 10 ml of the standard was added and then directly titrated like the samples. The different solutions (the standard potassium hydrogen diiodate, the titration solution sodium thiosulfate, manganese (II) chloride and sodium iodide) had to be mixed from time to time at the beginning and when they were almost empty.

To get the µmol/L of dissolved oxygen, the titrated volume in ml, the bottle factor (different bottles have different volumes) and the factor of sodium thiosulfate had to be multiplied.

5.1.2.5 Nutrients

A total of 1610 samples were measured during the cruise. 222 samples were taken from 38 CTDs and analyzed as triplicates. 224 samples were taken from the underway system and determined as triplicates. Furthermore, 202 samples from incubation experiments were measured. The last 70 samples were *Sargassum* samples which were measured. The maximum sampling depth was different at each station and ranged from 5800 m to 1000 m, while the shallowest depth was 6 m below the surface. The 14-ml polyethylene sampling tubes and corresponding caps were rinsed at least three times with the sampling water before the last sample was collected. Samples were measured with a maximum delay of 10 hours or less after sampling. If the start of the measurement was delayed by more than one hour, the samples were stored in the refrigerator in the interim. In addition to the CTD samples, 33 bottles of Reference Material for Nutrients in Seawater (RMNS) from General Environmental Technos (KANSO) Co., Ltd. of Osaka, Japan (Batch CJ) were measured at least once daily in six replicates. Due to the high variability of maximum nutrient concentrations, 3 different calibrations were applied.

Table 5.2: Table of standards and deviations of nutrient standard measurements (TON is the sum of Nitrate and Nitrite.)

1. High Calibration:

Analyte	TON	PO4	NO2	SiO2
Highest	64	4	4	100
StdDev	0.129	0.013	0.002	1.311

2. Medium Calibration:

Analyte	TON	PO4	NO2	SiO2
Highest	32	2.5	2	50
StdDev	0.085	0.006	<0.001	0.123

3. Low Calibration:

Analyte	TON	PO4	NO2	SiO2
Highest	7	1	1	20
StdDev	0.048	0.003	<0.001	0.013

The underway samples and the Atlantic samples surface to 100m were measured with the low calibration. The Atlantic samples deeper 100m were measured with the medium calibration. The Pacific samples were measured with the high calibration.

5.1.3 Microbial connectivity of sinking particles and possible driving factors in the Atlantic Ocean and Pacific Ocean

(PI: Carolin Löscher, responsible on board: Peihang Xu)
University of Southern Denmark

Background

The sinking of organic particles generated through photosynthesis in the photic zone is a main source of carbon export into the deep ocean (Ducklow et al., 2001). The carbon particles that reach the dark ocean to a large extent depend on the activity of microbes attaching on them (Baltar et al., 2009). Studies have shown that composition of particle-associated microbial communities changes with depth (Bergauer et al., 2018; Roth Rosenberg et al., 2021). Sinking particles attached microbial assemblages could impact the dynamic of deeper bacterial communities or even supply immigrants continually to the dark ocean, e.g. some upper-layer taxa may thrive in a certain depth along the sinking. However, so far, it is not well understood whether sinking particles have a large contribution to immigrate upper-layer bacteria to deeper ocean or not. Only one recent study showed that the most abundant bacteria in the deep ocean occur in surface water, and larger size of particles shared higher taxonomic similarity across the water column (Mestre et al., 2018). Furthermore, other environmental phenomenon and factors change over spatial scales, such as currents, temperature, nutrients, could also affect the dispersion of particle-associated bacterial community structure (Milici et al., 2017; Roth Rosenberg et al., 2021). However, most studies do not emphasis microbial connectivity in the sinking particles. Understanding the connectivity of microbial community along the sinking particles could help to interpret the carbon transport route along the ocean, both in horizontal and vertical perspective.

This study focuses on exploring the microbial connectivity of sinking particles both in the Atlantic Ocean and Pacific Ocean, which are two totally different ocean statuses. Free-living microbial communities are also involved. Key environmental factors and phenomenon will be also investigated.

Materials and Methods

Samples were collected during a cruise from Dec. 11th, 2021 to Jan. 11th, 2022, on the German research vessel RV SONNE (SO287). The seawater was collected at depths between 6m and 1000m at daytime, between 6m and bottom at nighttime at 15 stations from the east to the west of the Atlantic Ocean. The samples were collected with a 12L Niskin bottle rosette water sampler, equipped with a conductivity-temperature-depth (CTD) sensor.

For DNA and RNA analysis, 1-2 L of seawater was collected and immediately filtered onto a 0.22µm MCE membrane filter (Merck Millipore Ltd., Ireland). Furthermore, for differentiating particle-associated and free-living microbial community, 2.4 – 5L of seawater was collected and immediately filtered onto 3 µm and 0.22µm MCE membrane filters subsequently using a peristaltic pump. All filters were stored at -80°C until further analysis. To extract the DNA and RNA, filters will be flash-frozen in liquid nitrogen and crushed. DNA and RNA will be extracted using the MasterPure Complete (MPC) DNA and RNA Purification Kit (Lucigen, USA), according to the manufacturer's protocol. Nucleic acids were quality checked on a spectrofluorometer (MySpec, VWR). cDNA will be generated from non-DNA contaminated RNA samples following the instructions of the QuantiTect Reverse Transcription Kit (Qiagen, Hilden, Germany). The preparation and platform of sequencing will be discussed and decided after checking the quality of DNA samples.

For carbon fixation rates, water samples from three depths (6m, DCM and 200m), were collected at daytime every second day in the Cruise. Water samples were filled bubble-free into 2.4 L glass bottles. Subsequently, 1 mL $H^{13}CO_3$ solution (1g per 50mL, Sigma-Aldrich, Saint Louis Missouri US) was added to each bottle through an air-tight septum and bottles were shaken to mix properly. Samples from 6m and DCM were incubated in an incubator covering with blue foil and flowing with local seawater, while samples from 200m were incubated in a fridge. After 24h of incubation time, samples were filtered through pre-combusted (450°C, 4-6 hours) 45 mm 0.7 GF/F Whatman filters and then stored at -80°C until further analysis. Filters will be acidified and dried before analysis on an Elemental Analyzer Flash EA 1112 series (Thermo Fisher) connected to an isotope ratio mass spectrometer (Finnigan Delta Plus XP, Thermo Fisher). Triplicate samples and a negative control were conducted and will be measured.

For the whole abundances of different phytoplankton and bacteria, 0.95 mL seawater samples were fixed with 4% formaldehyde. Abundances and sizes of Synechococcus, Prochlorococcus, picoeukaryotes and bacteria will be determined by flow cytometry using an XL-MCL cytometer.

For pH measurement, 15ml seawater samples were collected in 15ml falcon tubes and then stored in 4 °C. It will be measured by the PHM210 standard pH meter (Radiometer Analytical, Meterlab).

Preliminary Results

Sampling was turned out quite well except the first four stations. A lot of filters and cryotubes were stored. In total, 600 hundred of filters or seawater were stored in 2ml cryovials at -80°C and 110 seawater samples were stored in 15ml falcon tubes at 4°C.

Future follow up studies data plans

To extract the DNA and RNA, filters will be flash-frozen in liquid nitrogen and crushed. DNA and RNA will be extracted using the MasterPure Complete (MPC) DNA and RNA Purification Kit (Lucigen, USA), according to the manufacturer's protocol. Nucleic acids were quality checked on a spectrofluorometer (MySpec, VWR). cDNA will be generated from non-DNA contaminated RNA samples following the instructions of the QuantiTect Reverse Transcription

Kit (Qiagen, Hilden, Germany). The preparation and platform of sequencing will be discussed and decided after checking the quality of DNA samples. The above process will be conducted as soon as possible when the filters are sent back to SDU. The time of sequencing will last at least 1 or 2 months. Hopefully, we will conduct the sequencing data analysis in July and June 2022. Other measurements will be conducted as soon as possible when the samples are sent back to SDU. I hope to finish all other measurement within 1 or 2 months.

5.1.4.1 Ozone in the Troposphere

(PI: Lucy Carpenter, responsible on board: Lucy Brown, David Loades, Katherine Weddell)

University of York

Background

Ozone in the Troposphere

Ozone is an important atmospheric constituent, acting as a greenhouse gas, with a radiative forcing of 0.40 ± 0.20 W m^{-2} (Hartmann *et al.*, 2013). The consequences of short term ozone exposure to humans include harm to the respiratory and cardiovascular systems, while long term exposure is thought to contribute to respiratory mortality and new-onset asthma in children. In 2013, 16,000 premature deaths in EU-28 countries were attributed to ozone exposure (Nuvolone, 2018). Tropospheric ozone also causes risk to global food production due to its phytotoxic effects on crop plants, injuring the plant following uptake by stomata.

The tropospheric ozone burden (340 Tg) is controlled by a balance of influx from the stratosphere (550 Tg(O_3) yr^{-1}), chemical production (5100 Tg(O_3) yr^{-1}), chemical destruction (4650 Tg(O_3) yr^{-1}), and dry deposition (1000 Tg(O_3) yr^{-1}) to the Earth's surface (Stevenson *et al.*, 2006). The ocean surface has an effect on tropospheric ozone concentrations both by dry deposition of ozone, and by subsequent production of gaseous halogen species which destroy ozone by catalytic cycles. While oceanic dry deposition is considerably slower than deposition to crops and soil (Wesely and Hicks, 2000), the significant coverage of Earth by oceans renders its influence consequential in global atmospheric models. Dry deposition of ozone to the ocean surface contributes approximately a quarter of total loss from the atmosphere, and was the single largest total flux of ozone (361 Tg O_3 $Year^{-1}$) across 15 models (Hardacre, Wild and Emberson, 2015), however its mechanism and magnitude are not fully understood.

The Mechanism of Dry Deposition

To understand deposition of gas to solution, the process is often thought of analogously to electrical resistance. While gaseous deposition to solution is governed by a series of complex processes, the transfer is often simplified by separating the main processes into individual resistances. The total resistance (R_t) to deposition is therefore comprised of three terms (Eq 1):

$$\frac{1}{R_t} = \frac{1}{R_1 + R_2 + R_3} \quad (1)$$

Where R_1 is the aerodynamic resistance due to atmospheric turbulence. It is influenced by factors such as wind speed and aerodynamic roughness (Chang, Heikies and Lee, 2004). R_2 is the gas phase film resistance, or diffusion across the quasilaminar sub-layer directly above the surface (in laboratory experiments R_1 and R_2 are often combined into air resistance, R_a, which can be measured for a given set-up). R_3 is the surface resistance, which is significant when considering chemical controls on deposition of ozone, accounting for >90% of the total

observed resistance over marine waters (Lenschow, Pearson Jr. and Boba Stankov, 1982; Kawa and Pearson Jr., 1989).

Resistance to transfer across the liquid film can be separately defined by Equation 2, showing that the presence of ozone-reactive species lowers surface resistance, and increases the uptake coefficient (Garland, Elzerman and Penkett, 1980).

$$R_3 = \frac{H}{\sqrt{k_i[I^-]D}} \quad (2)$$

The dry deposition velocity (inverse of the total resistance, R_t) of ozone to the ocean has been measured by several authors, and is highly variable (Galbally and Roy, 1980; Garland, Elzerman and Penkett, 1980; Wesely, Cook and Williams, 1981; Lenschow, Pearson Jr. and Boba Stankov, 1982; Kawa and Pearson Jr., 1989; McKay, Stephens and Dollard, 1992; Heikies *et al.*, 1996; Gallagher, Beswick and Coe, 2001; Whitehead *et al.*, 2009; McVeigh, O'Dowd and Berresheim, 2010; Helmig *et al.*, 2012). Variation in oceanic deposition velocity is thought to be partly controlled by reaction with both iodide and dissolved organic matter (DOM) in the sea surface microlayer, and also influenced by sea surface temperature (Abdulkadir and Tsuchiya, 2008; Dittmar *et al.*, 2008; Oh *et al.*, 2008; Ganzeveld *et al.*, 2009; Helmig *et al.*, 2012; Sarwar *et al.*, 2016). Iodide concentration at the ocean surface is highly variable (from ≈1 nM to 700 nM) (Chance *et al.*, 2014), as is sea surface temperature, and DOM represents a large potential sink of ozone, with 685 x 10^{15} g of carbon being present in the oceans (Eder, 1995). However there is not yet enough understanding to accurately link parameters, such as iodide concentration, to deposition velocity. In lieu of accurate parameterisation methods, models typically apply a single deposition velocity of 0.05 cm s^{-1} globally, despite large variances in measured values (Ganzeveld *et al.*, 2009). Therefore, our research aboard the SO287-CONNECT cruise aims to improve understanding of the chemical controls behind ozone deposition in marine environments.

Material and methods

Sample Collection

During the days in which the ship carried out day-time stations, three surface seawater samples were taken: one from the ship's underway system, one from the hereon CTD and one sea surface microlayer (SML) sample collected using a Garrett screen. On all other days where sampling was permitted but there was no station, only an underway sample was taken. The SML sample was either collected via a crane over the side of the ship, or by hand by scientists on the Zodiac.

Dissolved Organic Matter Analysis

Solid Phase Extraction of Dissolved Organic Matter including Fatty Acids-

5 to 8 L volumes of the samples specified above were used for the solid phase extraction (SPE). Note that the method here was first developed by Dittmar *et al.* who used Bond Elut – PPL SPE cartridges to extract dissolved organic matter (DOM) out of seawater.(Dittmar *et al.*, 2008) The samples were first filtered through a GF/F filter and acidified with HCl (30-32%, Honeywell TraceSELECT) to pH 1.75-2.25. The PPL SPE cartridges were conditioned with three cartridge headspaces full of methanol (Ultra HPLC grade, JT Baker) prior to extraction. After conditioning, the samples were drawn through the cartridges to extract the organic matter present. For the station and non-station samples, 1 g and 500 mg sorbent cartridges were used respectively. Following extraction, the cartridges were washed with 3 cartridge headspaces of 0.01 M HCl and dried for 5 minutes with air. They were then eluted with 8 mL of methanol

(LC/MS Optimagrade, Promochem) into muffled 20 mL scintillation vials and stored at -20 °C until further analysis following the cruise.

Dissolved Organic Matter Analysis-

Half of the methanolic SPE extract will be used for non-targeted organic matter characterization by ultrahigh performance liquid chromatography-high resolution mass spectrometry (UHPLC-HR-MS). 4 mL of each extract will be evaporated to dryness and reconstituted in 5% acetonitrile-water (Fisher Optima LCMS Grade) prior to analysis. Samples will be analysed using a Dionex UltiMate 3000 (Thermo Scientific) chromatography system coupled to a Q-Exactive Orbitrap mass spectrometer (ThermoFisher Scientific) fitted with an electrospray (HESI-II) ion source. Chromatography will be reversed phase, with water and acetonitrile mobile phases (both Optima LCMS grade with 0.1% formic acid modifier) and an Accucore aQ column. Samples will be analysed in both positive and negative ionisation modes with an *m/z* range 85-1000; fragmentation spectra will be obtained for the most abundant ions. Data analysis will primarily take place in the open-source software MZmine2 (Pluskal *et al.*, 2010). Molecular formulae will be assigned to detected ions allowing semi-quantitative "fingerprinting" type analysis of SPE-DOM, and the calculation of bulk properties such as average double-bond equivalents. It may also be possible to conduct more quantitative investigation of specific compounds or groups of compounds of interest and/or high abundance.

FAME Conversion and Analysis-

The following FAME conversion method was first developed by Abdulkadir *et al*. but has been modified so that the conversion is acid catalysed using sulphuric acid (Eder, 1995; Abdulkadir and Tsuchiya, 2008). 4 mL of the methanol extract from the SPE step is acidified to form a 2.5% sulphuric acid mixture (puriss., 95-97%, Sigma-Aldrich) in a separate 20 mL scintillation vial. An internal standard of methyl nonadecanoic acid dissolved in acid was added to the extract followed by 4 mL of hexane (>= 95% HPLC grade, Fisher Chemical). The headspace of the vial was flushed with nitrogen and heated for 2 hours. The vial was allowed to cool for 30 minutes, after which, 1 mL of hexane and approximately 2 mL of water was added. The vial was shaken and the aqueous layer was removed. This process was repeated twice more. The hexane layer was removed, reduced to dryness with nitrogen and finally reconstituted in 100 µL of hexane which was analysed by GC-MS (Agilent Technologies 6850 GC and 5975C inert XL EI/CI MSD with Triple-Axis Detector).

Iodide

For each of the sample types mentioned above, 5 mL was taken after filtration through a GF/F filter and stored at -20 °C until further analysis. Samples will be measured for iodide (LOD = 0.2 nM, LOQ = 0.5 nM), quantified using LC-DAD (Diode Array Detection at 226 nm), with a Dionex IonPac AS23 column (4 x 250 mm) and NaCl (0.4 M) eluent at 0.64 ml/min. Injection volume 400 µl, run time 25 minutes. Iodate and total iodine may also be quantified.

Flow Reactor Deposition Studies

A flow reactor is used to measure deposition of ozone to the sea surface from a laminar flow of air. A schematic of the gas flow system is shown in Figure 5.18. Dry air is passed through a hydrocarbon trap, then enriched in ozone (to ~ 60 ppb) using a Penray UVP ozone generator. This gives a large total flow of ozone enriched air with a constant ozone concentration. The mass flow required by the experiment is diverted through the flow tube, or through the bypass line, while any excess is removed from the system through a back pressure regulator. After passing through the flow tube, the sample air is diluted to analytical requirements, and a constant flow is filtered and dried by Nafion prior to analysis of its ozone concentration by a

Therno 49i ozone monitor. Gas surplus to the sampling requirement is removed from the system by a second back pressure regulator.

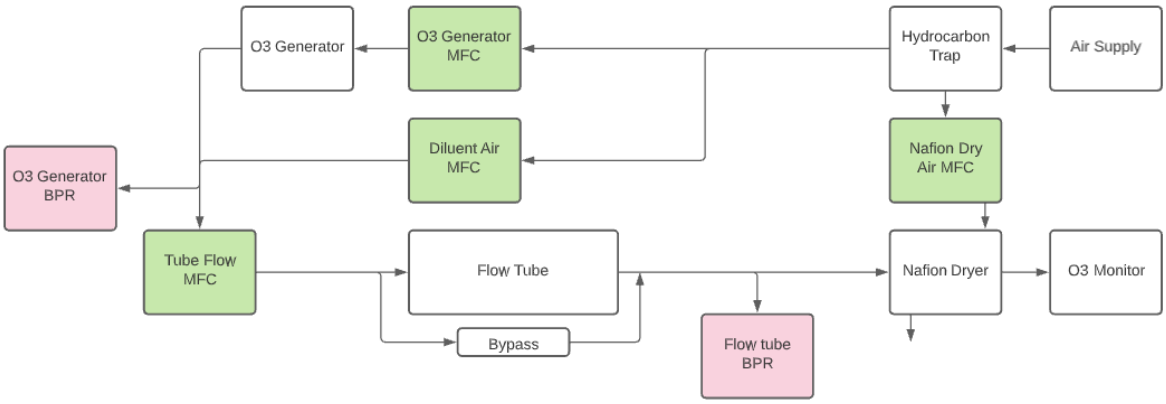

Figure 5.18: Schematic of gas flow in the ozone deposition flow reactor set-up. Green squares = mass flow controllers, red squares = back pressure regulators.

The experimental gas is a laminar flow of ozone enriched air which was flowed over the seawater, which was stirred to avoid the development of any vertical concentration gradients. By applying a stepped series of mass flow rates, a range of exposure times between ozone and the solution were achieved. Reaction time was calculated by the residence time of gas in the headspace, according to Equation 3.

$$reaction\ time\ (\text{minutes}) = \frac{headspace\ (cm^3)}{mass\ flow\ rate\ (cm^3\ min^{-1})} \quad (3)$$

With ozone being the limiting reagent, a plot of ln[O_3] against reaction time should show a linear relationship, assuming pseudo-first order conditions are achieved. The deposition velocity can then be calculated according to Equation 4, where m is the gradient of the slope, V is the volume of the headspace and A is the surface area of the sample.

$$v_d = \frac{-mV}{A} \quad (4)$$

Ozone flux measurements by eddy covariance

Eddy covariance is a measurement technique for determining the flux of some scalar via measurement of that scalar and the vertical wind at a high enough frequency to resolve small, high frequency eddies within the atmosphere. From such measurements, a deposition velocity can be obtained by dividing the molar flux by the molar concentration for comparison to the flow reactor studies (eq 5).

$$v_d = \frac{F}{C} \quad (5)$$

The ozone flux is calculated from the covariance between ozone concentration and vertical wind (w), hence the technique's name. 10 Hz wind measurements are measured using a Gill R3-50 sonic anemometer mounted at the top of the foremast, with an accompanying motion

pack to account for the movement of the ship. ~10 Hz ozone data are measured using a custom instrument from Air Quality Designs (AQD) that uses the principle of chemiluminescence. A 35 sccm supply no 10% NO (in Nitrogen) gas is supplied to react with all the ozone within the sample gas (which is drawn into the instrument at 1 SLPM). This forms NO_2 in an excited state, which release a photon upon relaxing. This emission is then detected by a photo-multiplier tube (PMT) which is cooled to -20°C to reduce the number of counts measured from thermal sources. The number of counts can then be calibrated against a slower, absolute ozone measurement – in this case a calibrated 2B model 205 dual beam ozone monitor.

Preliminary results

Surface resistance was measured using the heterogeneous flow reactor for samples from the underway pump, daytime CTD and surface microlayer sample. Prior to extensive analysis of all samples, example data from the 15th December is shown in Figure 5.19.

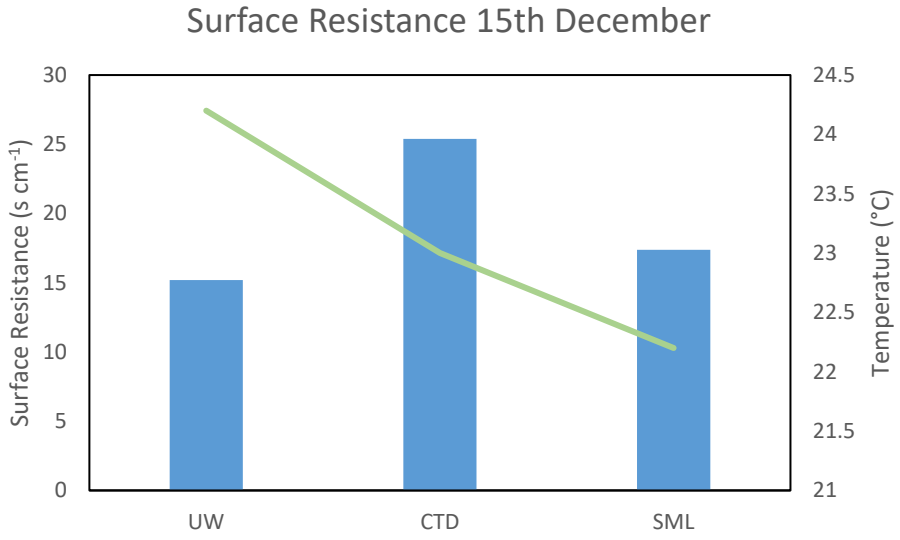

Figure 5.19: Surface resistance and temperature of 3 different samples on 15/12/2021. UW = underway, CTD = conductivity, temperature and depth sampler, SML = surface microlayer.

The SML sample has a lower surface resistance than the corresponding CTD sample, in correlation with the anticipated enhanced presence of DOC and surfactant materials. The underway sample displayed lower than anticipated surface resistance – according to depth alone, it could be expected this should be similar to the CTD resistance. This was taken approximately 3 hours prior to the CTD sample so is a different water– it could be enhanced in certain organics or iodide, or perhaps there is a temporal dependence in surface resistance. Further analysis of surface tension, DOC and iodine speciation may explain this difference.

The correlation coefficient between temperature and surface resistance is -0.31 – only weak. An increase in surface resistance is expected with increasing temperature due to the Henry's law, however the weak correlation displayed here indicates other factors, presumably chemical, are also affecting the surface resistance.

Future follow up studies data plans

Analysis of DOM speciation, iodide, iodate, total iodine, surface tension, surface resistances and fluxes from eddy covariance data shall be carried out at the University of York and communicated when available.

5.1.4.2 Gas phase iodine concentration over the open ocean

(PI: Dr Stephen Ball, responsible on board: Alice Offin)

University of Leicester

Background

The presence of iodine (I_2) in the atmosphere is known to affect the concentration of hydroxyl radicals, the partitioning of the HO_x and NO_x families and hence the oxidising capacity of the marine boundary layer. Additionally, I_2 can also partake in chain reactions leading to the production of cloud condensation nuclei increasing the volume of cloud in the atmosphere leading to a cooling effect on the climate (Saiz-Lopez et al., 2012).

Atmospheric I_2 is known to have two sources, abiotic (inorganic) and biotic. Abiotic production of I_2 stems from the heterogeneous reaction between tropospheric ozone and iodide at the air-sea interface – a schematic of this reaction is shown in Figure 5.20. Abiotic iodine production is believed to produce up to 80% of the iodine present in the troposphere and forms a considerable sink for tropospheric ozone with up to 20% of tropospheric ozone being lost to this deposition process (Carpenter et al. 2021). Whilst multiple laboratory experiments have been conducted to characterize this reaction (Tinel et al. 2020), there are no *in situ* measurements of iodine over the open ocean.

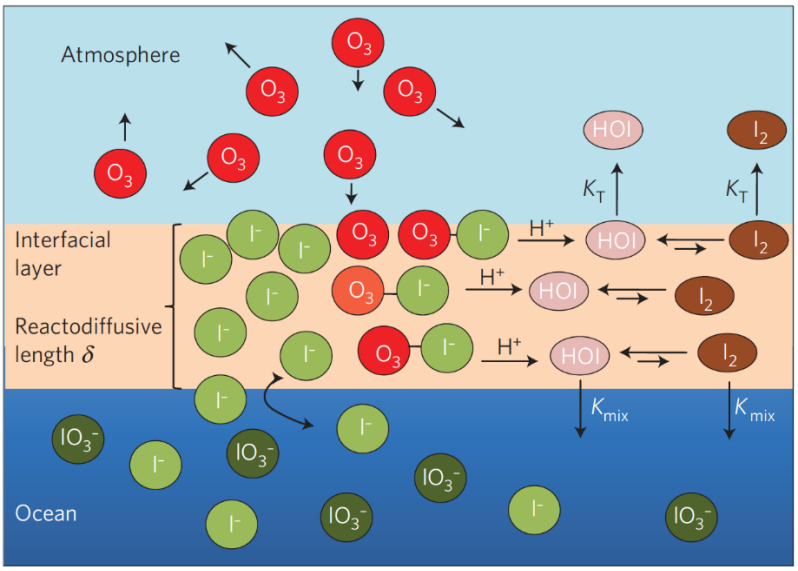

Figure 5.20: Schematic of I_2 and HOI production following the reaction of O_3 with I^- ions at the air-sea interface (taken from Carpenter et al. 2013).

The remaining 20% of iodine in the atmosphere is attributed to the biotic route, emissions from seaweeds under oxidative stress. To date the iodine emission from multiple seaweed species found in coastal regions have been characterized(Ball et al., 2010). However, the free-floating S*argassum* genus of seaweed has never been examined for I_2 production.

Material and methods

In situ measurements of inorganic iodine emissions

Iodine concentrations in ambient air were determined using broadband cavity enhanced absorption spectroscopy (BBCEAS). A schematic of the instrument used is shown in Figure 5.21.

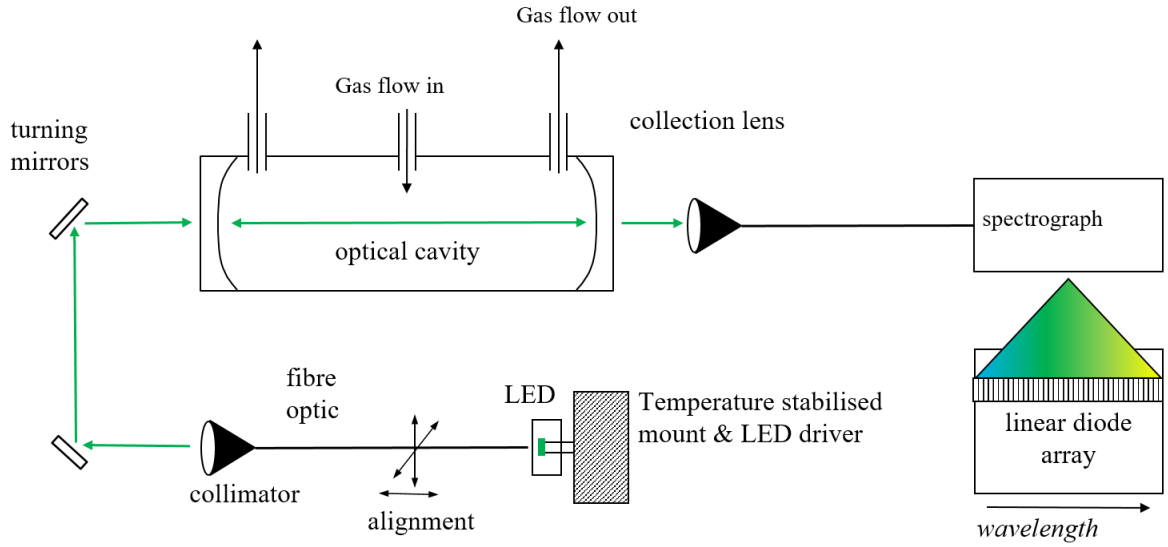

Figure 5.21: A schematic of the BBCEAS instrument used during SO287

A green LED (Intelligent LED solutions, ILH-GD01-TRGR-SC201) was mounted to a temperature controlled laser diode mount (ThorLabs), the temperature of the LED was maintained (Newport, Model 325) to ensure the emission spectrum of the LED was consistent between experiments. The LED was supplied with a controlled current of 1 A by a bench top power supply (Aim TTi, EL302RD). Light from the LED was coupled to a fibre (Ocean Insight, QP400-2-UV-BX; 400 µm fibre core, UV-visible, length = 2 m), Light leaving the fibre is passed through a collimating lens (Thorlabs) to focus the light beam. After reflection by two turning mirrors, the light was directed into the optical cavity formed by two highly reflective mirrors (Layertec, 111078). Each mirror was seated in a custom mirror mount affixed to a polytetrafluoroethylene (PTFE) tube (2.5 cm internal diameter) with a total mirror-mirror distance of 59 cm. Both mirror mounts contained bellows which allowed the mirror alignment to be changed as necessary to ensure maximum cavity reflectivity.

Light leaving the cavity was collected by a focussing lens (Thorlabs) and concentrated into a fibre (Ocean Insight, QP400-2-UV-BX) which fed the light into a USB spectrometer (OceanOptics, HR4000) and onto a 3648-element linear silicon CCD array detector. The spectrometer itself was situated within a custom-built Peltier cooled enclosure maintained at 12 °C to minimise any thermal drift in in the spectrometer's dark current. The cooled enclosure was also purged with a gas flow of approximately 1 slmp to prevent the build-up of condensation.

Ambient air was pulled through the cavity at a rate of 1 SLPM by a diaphragm pump connected downstream of the cavity gas outlets. Reference spectra, were obtained by flowing N_2 and O_2 through the cavity, in these cases the gas flow was entering the cavity was maintained at 1.4 SLPM using a mass flow controller (MKS, 1179A23CS1BV). The gas was pulled through the cavity by a diaphragm pump connected downstream of the cavity gas outlets with an approximate pull of 1.0 SLPM, excess gas flow left the cavity via an overflow exhaust line to prevent the system from becoming over pressurised.

Spectra were recorded on a desktop PC running the software package *OceanView* (OceanInsight) with an integration time of 100 ms, 50 spectra were averaged in *OceanView* before being saved to the PC giving a net acquisition time of 5 s. Spectra were averaged and analysed using a processing routine developed in *Mathcad Prime 3.0* (PTC). The data analysis process is known in the literature.

Determination of I_2 emissions from *Sargassum* seaweeds

For these experiments, samples of *Sargassum fluitans* seaweed in filtered seawater were collected and provided by P. Potin. Samples were placed in 20 L Nalgene carboys modified for the addition of a gas inlet/outlet to allow sampling of the headspace above the sample. Synthetic air was flow through the carboy inlet at a rate of 1.5 SLPM. The BBCEAS instrument was connected downstream of the carboy, pulling air from the carboy through the cavity at a rate of 1.0 SLPM. Excess air was vented before the carboy inlet to prevent the system from becoming over pressurised. The BBCEAS instrument and spectra recording settings were the same as used for the *in situ* measurements. Over the course of each experiment, the seaweed samples were drained of seawater and refilled to examine any changes in the iodine emissions, demonstrated by Figure 5.22.

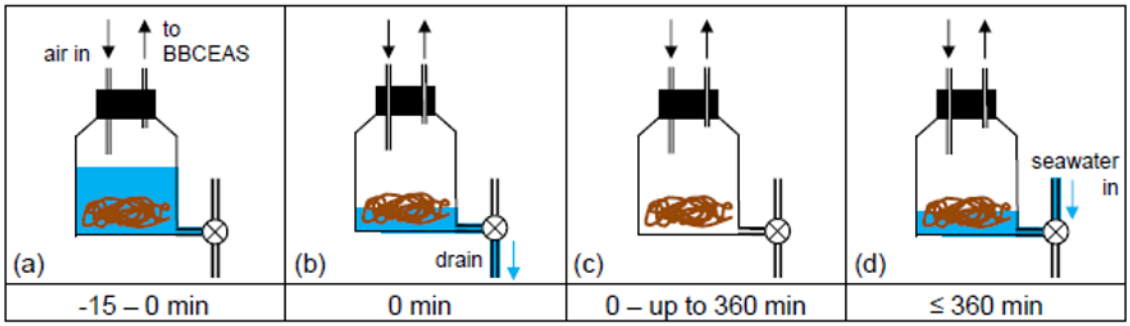

Figure 5.22: Schematic of the experimental procedure used to quantify iodine emissions from *Sargassum* seaweeds

Preliminary results

In situ measurements of inorganic iodine emissions

Overall close to 3 weeks of ambient data was recorded by the Leicester BBCEAS instrument over the course of the SO287 cruise. Figure 5.23 shows a nitrogen dioxide (NO_2) time series, each data point is formed from an average of 12 BBCEAS spectra. Five sharp peaks can be seen in this time series (20:38, 22:31, 02:09, 02:59 and 06:59) which have arised from either ship traffic or sampling the SONNE exhaust; definitive conclusions can be drawn once the time series has been matched with the SONNE's wind direction data.

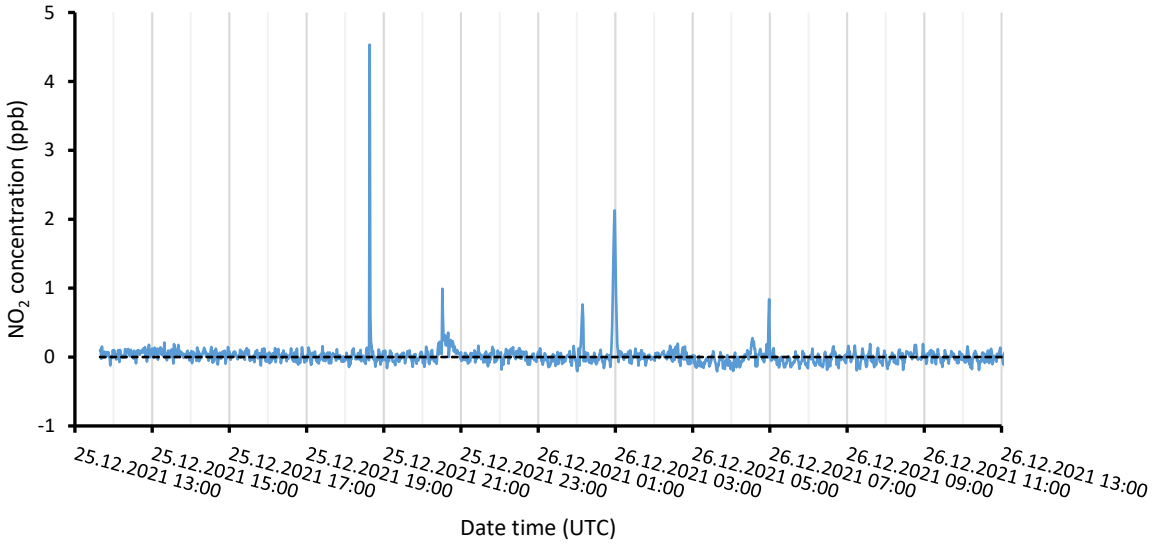

Figure 5.23: Nitrogen dioxide concentrations recorded from 25/12/2021 13:30 to 26/12/2021 13:00 (UTC).

Figure 5.24 shows an iodine time series recorded across the same timeframe and using the same data averaging as Figure 5.23. In this time series, there are a number of peaks in iodine concentration that match with peaks in nitrogen dioxide concentration – these peaks need to be filtered out as they are a result of inadequately removed nitrogen dioxide.

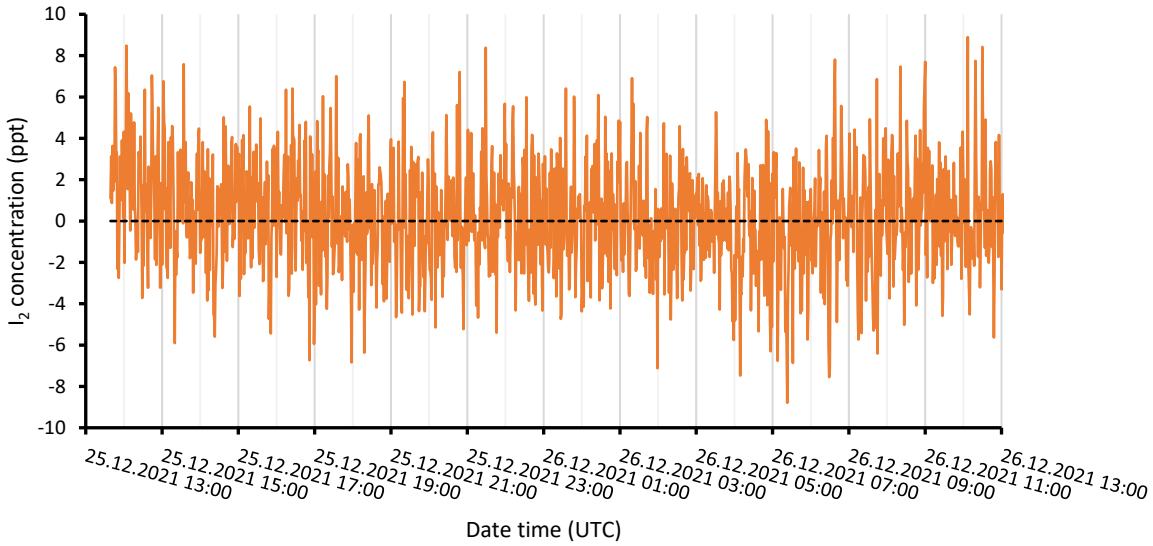

Figure 5.24: Iodine concentrations recorded from 25/12/2021 13:30 to 26/12/2021 13:00 (UTC).

There does appear to be an oscillation in the both the NO_2 and I_2 time series which correlates strongly with the temperature cycling of the laboratory due to the air conditioning system. These oscillations are affecting low concentration iodine retrieval; hence, iodine concentrations over the open ocean have yet to be measured.

Determination of I_2 emissions from *Sargassum* seaweeds

Figure 5.25 shows the results of the first three seaweed experiments conducted during SO287. Each point represents an I_2 concentration acquired from the average of 30 minutes of data where the sample carboy was left in the state shown. These preliminary results suggest that *Sargassum fluitans* does not emit iodine. However, more could be done to place the samples under a higher level of oxidative stress; for example, a low concentration of ozone could be flowed through the carboy.

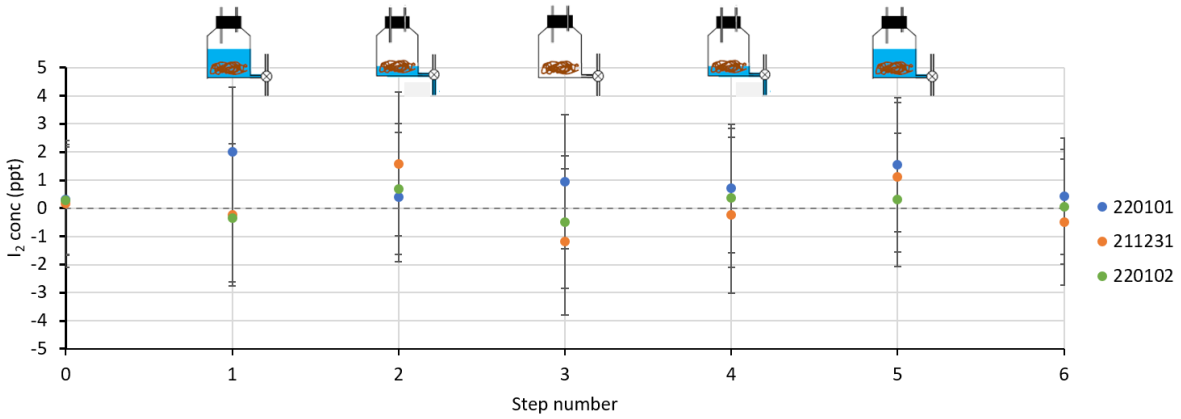

Figure 5.25: Iodine concentrations observed from 3 samples of *Sargassum fluitans* as they were drained of seawater and the seawater is reintroduced

Future follow up studies data plans

The plans for post-cruise processing are as follows:

- Filtering of peaks in nitrogen dioxide concentration ($[NO_2] > 0.5$ ppb)
- Determination of optimum averaging time period to remove time series oscillations and improve the instrument detection limit for molecular iodine

5.1.5.1. Brominated halocarbon production in sea water and influence on atmosphere

(PI: Birgit Quack[1] , Elliot Atlas[2], responsible on board: Josefine Karnatz[1], Hendrik Feil[1], Julia Mickenbecker[1])

[1]GEOMAR

[2]RSMAS

Background

The very short-lived substances (VSLS) bromoform ($CHBr_3$) and dibromomethane (CH_2Br_2) from marine sources provide a significant contribution to the stratospheric total bromine budget impacting ozone in the lower stratosphere (Keber et al., 2020). The distribution of brominated VSLS emissions is poorly constrained given the sparse observational database of their oceanic and atmospheric concentrations (Ziska et al., 2013). Bromine is considered a conservative element in seawater (814 µM), while enzymatic processes in seawater and organisms produce polybrominated methanes from organic compounds and seawater halides (Theiler et al., 1978). Studies on the bromination of dissolved organic matter (DOM) suggests that the composition of the two bromocarbons produced from the halogenation of DOM is highly substrate-dependent (Liu et al., 2015, Lin and Manley 2012). The ratio between $CHBr_3$ and CH_2Br_2

declines in the surface ocean towards the open ocean, with several potential processes involved. $CHBr_3$ may be lost faster from surface waters over time as it has a greater sea-air concentration gradient compared to CH_2Br_2 (Quack et al., 2007). The shift can also be due to a faster photolysis of $CHBr_3$ compared to CH_2Br_2 (Carpenter and Liss, 2000), a lower $CHBr_3$ to CH_2Br_2 production ratio in the open ocean, or a conversion of $CHBr_3$ to CH_2Br_2 via reductive hydrogenolysis (Vogel et al., 1987) and via microbial reduction (Kataoka et al., 2019). The laboratory studies indicate that the production of CH_2Br_2 from heterotrophic cycling of $CHBr_3$ is a widespread phenomenon in the marine environment. Recent cruise data from the Macaronesian Archipelagos of Cape Verde, the Canaries and Madeira revealed that anthropogenic sources increased oceanic $CHBr_3$ emissions significantly close to some islands, while most likely heterotrophic processes increased the flux of CH_2Br_2 from the sea to the atmosphere in the Cape Verde region. While CH_2Br_2 is less abundant than $CHBr_3$, it has a much longer atmospheric lifetime (120 compared to only 16 days) and can contribute even more to stratospheric ozone depletion than $CHBr_3$ (Tegtmeier et al., 2020). More CH_2Br_2 may be produced from increased heterotrophy in a warming, deoxygenated ocean, and could supply higher fractions of stratospheric bromine in the future, with yet unknown consequences for stratospheric ozone (Mehlmann e al., 2020). SO287 offered great opportunities to understand which processes dominate the source of CH_2Br_2 in the ocean, and how organic bromine compounds and seawater bromine in aerosols influence the atmosphere.

Material and methods

251 seawater samples from depth profiles and 112 surface seawater samples were analyzed for halogentated hydrocarbon using an onboard purge and trap system, coupled to a gas chromatograph with mass spectrometric detection In single ion mode the brominated, chlorinated and iodinated organic compounds (eg: CH_3I, CH_2Cl_2, $CHCl_3$, C_2HCl_3, C_2Cl_4, CH_2Br_2, $CHBr_3$, and CH_2I_2) were measured on board. 140 air canister samples for anthropogenic and natural trace gases were taken on the bow of the ship with a metal bellows pump and 30 aerosol samples for bromine and vanadium and nickel were taken daily on filters on the compass deck via aerosol samplers.

Figure 5.26: left: Purge and trap GC/MS–system (J. Karnatz) for the measurements of dissolved and atmospheric halogenated hydrocarbons, middle: intake line for the air sampling of volatiles in stainless steel canisters with a metal bellows pump, right: Norwich-sampler for the collection of size segregated aerosols.

Preliminary results

The concentrations of the dissolved halocarbon from natural origin were expectedly low in the lower picomolar range. Ratios and depth profiles were as expected and the analytical system has worked very well during the cruise. In the atmosphere the mixing ratios of the halocarbons were very variable from very low to moderately high and reflect sources and transport pattern (Figure 5.27).

Distinct source regions and transport regimes show low, respectively elevated mixing ratios.

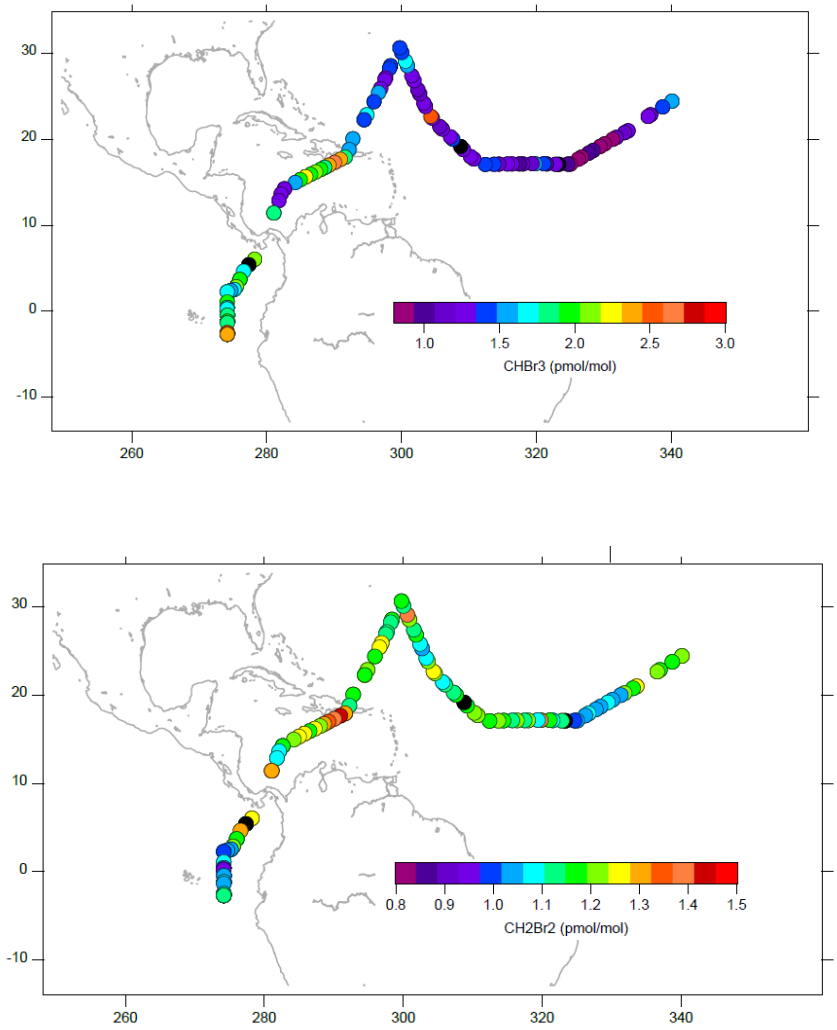

Figure 5.27: Bromoform ($CHBr_3$, left) dibromomethane (CH_2Br_2, right) mixing ratios in air along the cruise track (Elliot Atlas: preliminary data).

Future follow up studies data plans

Calculation of air-sea fluxes of halogenated hydrocarbons in the different regions of the cruise.

Determination and interpretation of the ratio between $CHBr_3$ and CH_2Br_2.

Correlation analysis of the ratio with biological parameters and the bacterial community try to determine the major process of CH_2B_2 generation in the area of the cruise.

Identify sources and transport pattern for the atmospheric mixing ratios.

How organic bromine compounds and seawater bromine in aerosols influence the atmosphere.

5.1.5.2 Incubations for Halogen Measurements

(PI and on board: Philippe Potin[1] , Josefine Karnatz[2], Birgit Quack[2], Hendrik Feil[2], Julia Mickenbecker[2], Alice Offin[3], Stephen Ball[3])

[1] CNRS

[2] GEOMAR

[3] University of Leicester

Background

$CHBr_3$ and CH_2Br_2 are released naturally from macroalgae and phytoplankton, with $CHBr_3$ as the dominant product (Lim et al., 2017 and references therein) up to nanomolar concentrations in the vicinity of macroalgal beds, as a possible result of stress and defense mechanisms in the algae (Carpenter and Liss, 2000, Quack et al., 2007). Nothing is known about the brominated halocarbon release of NA *Sargassum* and its contribution to atmospheric chemistry, which is of great environmental interest given the increasing golden tides comprising the same species. The extensive blooms of the holopelagic *Sargassum* spp. in the Atlantic raised the question of whether this brown seaweed may play an important role in the emissions of natural halogens in the Marine Boundary Layer.

A) Halocarbons in seawater

Few on halocarbon emissions from the *Sargassum* genus of seaweed (1,2). If holopelagic *Sargassum* are strong producers this would tell us about the seaweeds' contribution to the halogen cycle in the Sargasso Sea and the *Sargassum* Atlantic belt.

B) Iodine emitted to the air phase

No data (yet!) on iodine emissions from the *Sargassum* genus of seaweed. If *Sargassum* is found to emit I_2, this would tell us about the seaweeds' physiology and bioaccumulation of iodide.

Research questions

A) 1. How much halocarbon and which forms iodinated/brominated are contributed by the physiology of the seaweeds. In response to light and dark and nutrient enrichment.

2. Does the three different *Sargassum* morphotypes display different patterns of halocarbon emissions.

B) 1. How much of the observed I_2 in *Sargassum* Sea (and elsewhere) comes from:
Inorganic $O_3 + I^-_{(aq)}$ reaction at ocean surface? *versus*
Biogenic emissions from *Sargassum* seaweeds?
2. Do the blooming morphotypes display differences in I_2 emissions.

Material and methods

Seawater collection

Option 1 From the ship underway the system would provide a high flow to fill 140 liters for 12 full 10 liters bottles in a few times one time or twice a day. VERY EASY TO MANAGE.

Option 2 Collect waters using the large ship CTD at 6m depth. Limited for the beginning of the experiments until the CTD stopped on Dec. 28.

Seaweed collection

Option 1 From the ship use a Neuston net that could be immersed just below the surface using the catamaran and its launch winch. The less efficient procedure

Option 2 Use the zodiak to grab some seaweeds at the surface. The most efficient procedure

Seaweed storage on board

Option 1 Use of the two large buckets brought by Birgit to keep about 1 kg of seaweed per 10 liters.

Option 2 After Dec. 28, use the aquaria from Peihang/Riel incubations with circulating underway seawater to preserve about 5 kgs biomass per aquarium.

Algal samples

Sorting of the different morphotypes

After gathering, the thalli are sorted between the three distinct phenotypes following the characters defined by Parr (1939) cited by Schell et al 2015.

Figure 5.28: Undamaged and complete plants are selected whenever possible for experimental use.

Acclimatization

Before performing the incubation experiments, the seaweeds are kept with their epibionts to be representative of the holobiont.

All plants where acclimatized under the following conditions: temperature of 25-28°C, salinity of the sampled seawater 36-37 PSU, light: irradiance of 50 mmol photons, photoperiod 12:12 (light:dark) for 16 to 24 h in a container prior to the experiment.

Optimal conditions

Establish optimal incubation conditions by taking into account water temperature, nutrients (enriched seawater) and luminous intensity available on board and the ecology of the acquired strains. Water temperature: 20, 25 or 28°C, local salinity, light: 50, to 200 µmol photons m-2 s-1 photoperiod for long incubations: 12:12 (light:dark) and dark or light conditions for the measurements. For incubation systems, establish optimal incubation conditions between static culture and ventilation system (10 L). Analyse the physiological status of collected strains according to indoor incubation by photosynthesis measurements.

Photosynthesis measurements

The state of health of the seaweeds will be assessed prior to the experiment using a Junior Pulse Amplitude Modulator (PAM) Fluorometer (Heinz Walz GMBH) and after the incubation.

The change in Fv=Fm was calculated according to the following formula: Percentage decrease in Fv/Fm (%) = Fv/Fm before incubation - Fv/Fm after incubation /Fv=Fm before incubation x 100%:

The maximum quantum yield (Fv/Fm) indicates the stress level of the seaweeds prior to and post incubation. This was done by determining the ratio of the difference between the maximum (Fm) and minimum (Fv) fluorescence level to the maximum fluorescence emitted by the seaweed fronds after dark adaptation of seaweeds for at least 15 min using dark leaf clips (Walz, Germany).

Measurements of volatile emissions from selected seaweeds

All experiments have been conducted in 10 L polycarbonate carboys (Nalgene) with caps equipped with sampling tubing and filled with natural seawater. (500 mL or less fresh seaweeds in 10 liter of sea water).

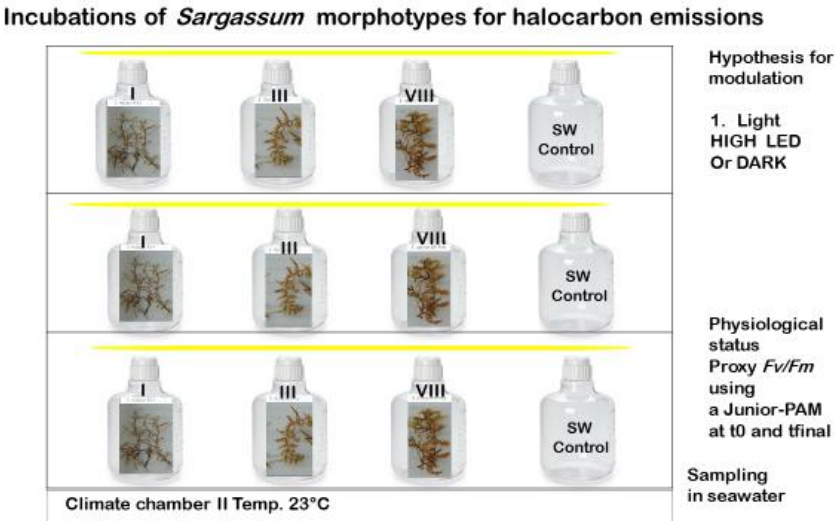

Figure 5.29: Three sample flasks (filtered seawater with seaweeds) and three control flasks (with only filtered seawater) have been used for each morphotype.

Seawater used throughout the experiment is collected simultaneously with the seaweed samples or at the start of the experiments from the ship underway. A set of three sample flasks (filtered seawater with seaweeds) and three control flasks (with only filtered seawater) have been used for each morphotype (Figure 5.30 and 5.31)

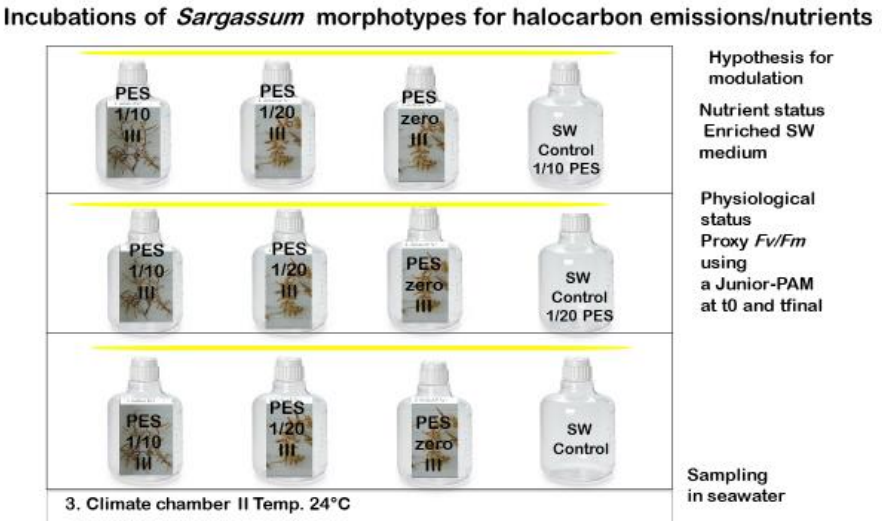

Figure 5.30: For nutrient incubation experiment, three replicates of PES 1/10, PES 1/20 and no PES were set up and the control seawater in accordance.

The difference between volatile concentrations observed between the control and treatment flasks will be assumed to be net emissions of the given compounds.

During the experiment, flasks have been incubated for four hours with three replicates for each experiment.

Iodine emissions from selected *Sargassum* morphotypes

The experiment: Measure I_2 emitted by seaweed samples during incubation experiments (online), Figure 5.31 and see work group report: 5.4.2.

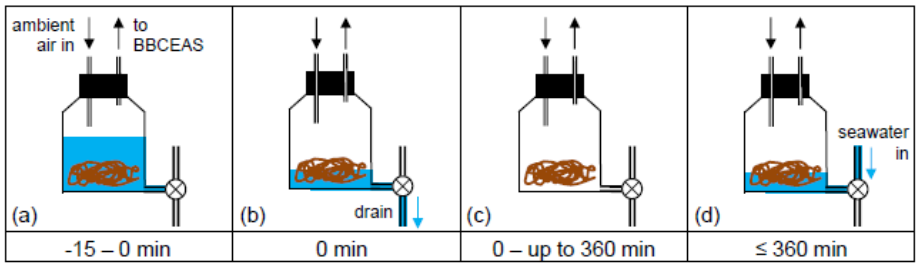

Figure 5.31: I_2 incubation experiment setup.

This experiment has been replicated 3 times using the 2 distinct morphotypes SnVIII and SfIII from the Caribbean. (500 mL volumes in 10 litre of seawater)

Biomass sampling and preservation after incubations for further analyses

All samples of biomass from each bottle incubated will be labelled and sun-dried or oven-dried at a maximum of 40°C. Dried biomass will be kept in Ziploc plastic bags and bring back to France for elemental analysis (I, Br, C, H, O, N, P, S) and other biochemical assays (phenolics,

total sugars, …). Three replicates of the three collected morphotypes will be also dried at each visited location.

Preliminary results

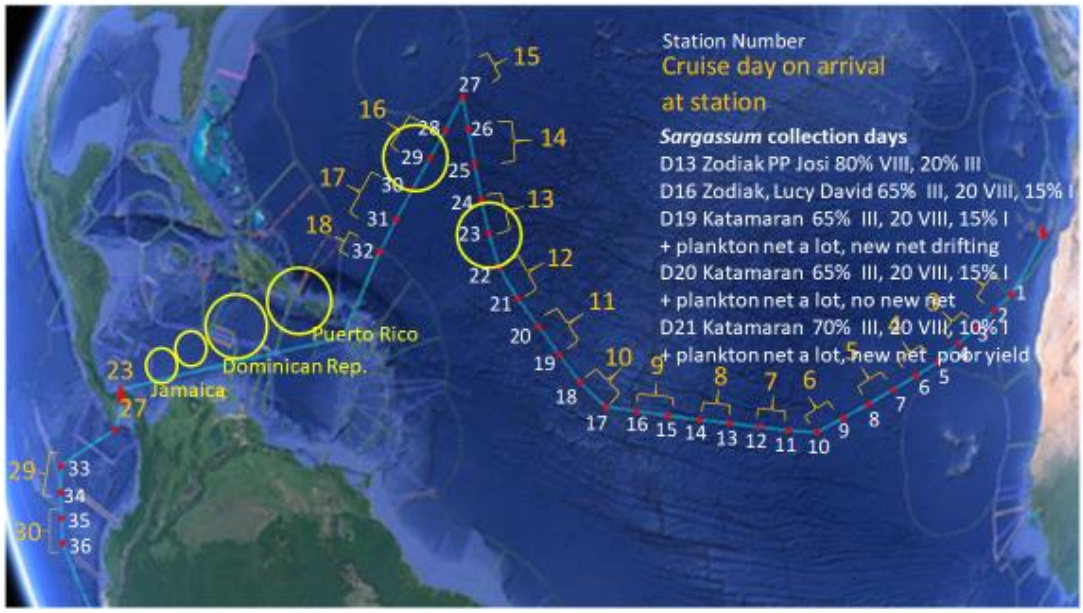

Figure 5.32: Overview of *Sargassum* collection days.

<u>*Sargassum* collection days</u>

- Day13 of the cruise: Zodiak PP Josi 80% morphotype S. natans VIII, 20% S. fluitans III, no S.n I
- D16 Zodiak, Lucy David 65% III, 20 VIII, 15% I
- D19 Katamaran 65% III, 20 VIII, 15% I + plankton net a lot, new net drifting
- D20 Katamaran 65% III, 20 VIII, 15% I + plankton net a lot, no new net
- D21 Katamaran 70% III, 20 VIII, 10% I + plankton net a lot, new net poor yield

Figure 5.33: Different morphotypes of *Sargassum*: left: *Sargassum* natans I (sampling day 26.12.2021), S. fluitans III (sampling day: 23.12.2021), S. natans VIII (sampling day 23.12.2021).

Future follow up studies data plans

- Dried weight acquisition for each sample analyzed by GC-MS or I2 BBCEAS.
- Elemental analysis (I, Br, As, Fe) by ICP-MS and(C, H, O, N, P, S)
- Biochemical assays (phenolics, total sugars, …).
- Haloperoxidase profiling from frozen samples of the 3 distinct morphotypes.
- DOC measurements for some incubations by Jon.
- Nutrient uptake and emission rates.

5.2.1.1 Meteo-oceanographic data

(Alexandra Rosa[1], Cláudio Cardoso[1], Jesus Reis[1],Birgit Quack[2])

[1]ARDITI

[2]GEOMAR

Background

The North Atlantic Subtropical Gyre is a coherent combination of ocean currents connecting the west coasts of Europe and Africa to the east coasts of Central and North America. Due to the low-intensity currents and winds, large patches of floating long-lived matter, such as *Sargassum* seaweed and human debris accumulate at the central gyre, a region known as the Sargasso Sea. Still, the impacts of the trans-Atlantic micro- and macro plastics to the biogeochemical cycles remain poorly understood. The biogeochemistry and ecology of the North Atlantic Subtropical Gyre is also highly influenced by the lateral transport of water and organic matter originating from the high productive Canary upwelling system. The Canary upwelling system, located along the northwestern African coast, is one of the four major Eastern boundary upwelling systems (Lovecchio et al., 2018), where its physical and biogeochemical dynamics are highly controlled by seasonal variations (Chavez and Messié, 2009). The Canary upwelling system forms the eastern boundary of the North Atlantic Subtropical and Tropical circulation (Mittelstaedt, 1991; Pelegrí and PeñaIzquierdo, 2015). The light and nutrient availability, and long residence time of the upwelled waters leads the Canary upwelling system to be the second most productive Eastern boundary upwelling system (Carr, 2001; Lachkar and Gruber, 2011). The northern region of the Canary upwelling system is dominated by the alongshore southward flow of the Canary Current (CC) and the Canary Upwelling Current (CUC; see Figure 1 from Bonino et al., 2021). In the Canary upwelling system, coastal instabilities, irregular topography, and also islands lead to intense mesoscale processes in this region (Garcìa-Muñoz et al., 2004; Sangrà et al., 2009). Mesoscale processes include the generation of upwelling filaments, causing upwelling of cold, nutrient-rich water in the coastal region, resulting in high productivity (Carr, 2002; Chavez and Messié, 2009), and eddies responsible for the transport of physical and biogeochemical properties to the open ocean (Stammer, 1998; Zhang et al., 2014; Amores et al., 2017). In the Eastern Tropical North Atlantic and in the Eastern Pacific minimal oxygen concentrations are usually found (e.g., Stramma et al., 2009 and Stramma et al., 2010, respectively), potentially associated with the enhanced biological productivity and an increased respiration related with settling particles in the water column (Wyrtki, 1962; Karstensen et al., 2008; Brandt et al., 2015), being stressful conditions to marine organisms (Stramma et al., 2010).

The SO287-CONNECT project aims to investigate the meteorological and oceanographic phenomenon that connect the two margins of the North Atlantic Ocean, focused on the biogeochemical and ecological processes and on the human activities that contribute to carbon increase in the atmosphere, in which the impacts are significant on the Earth’s climate. In addition, the project aims to identify the impact of human activities on the transport and accumulation of marine litter, as well as the influence of ship emissions on the marine ecosystem, associated with high ship traffic in this region. In this report, we show the preliminary results of CTD, and radiosonde data acquired during the SO287-CONNECT oceanographic campaign conducted in the Atlantic Ocean and part of the Pacific Ocean, to better understand the meteorological and oceanographic processes that prevailed during the cruise, including identification of eddies and water masses.

Material and methods

Cruise campaign

The SO287-CONNECT oceanographic campaign aimed to cross the North Atlantic Ocean from Las Palmas (Gran Canaria, Spain) to Guayaquil (Ecuador, in the Equatorial Pacific Ocean), during four weeks on board the German Research Vessel SONNE (between 11 December 2021 and 11 January 2022). In the first 16 days (between 12 and 28 December 2021), shallow (1000 m depth) and deep CTD casts (full depth) were performed at 32 stations in the North Atlantic Ocean (stations 1 to 32, red points in Figure 5.34). The shallow casts were performed at around the time of local zenith and the deep casts were performed at around local midnight, in order to contrast the sunlight with the dark. As can be seen in Figure 5.34, the most northern station was in the Sargasso Sea. At each station, GRAW radiosondes (https://www.graw.de/) were also launched to measure atmospheric parameters along the transect (red and blue points in Figure 5.34). In the Pacific Ocean, 4 CTD stations were also performed (stations 42 to 45, red points in Figure 5.34) between 7 and 8 January 2022.

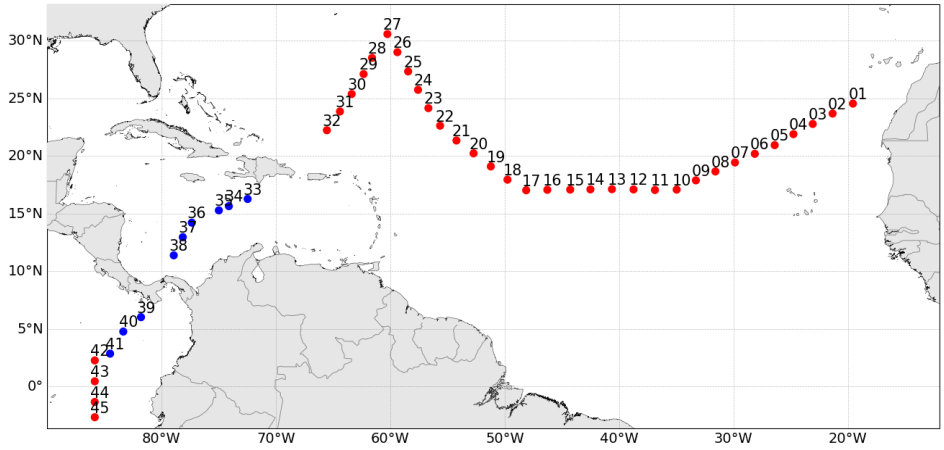

Figure 5.34: SO287 CONNECT cruise transect in the North Atlantic Ocean and part in the Pacific Ocean. Red points correspond to the stations where both CTD and radiosondes were deployed. Blue points correspond to the stations where only radiosondes were deployed.

Data acquisition and pre-processing procedures

CTD

The vertical profiles along the water column were performed using an SBE-911 plus. The SBE-911 plus measured 11 variables (temperature, pressure, conductivity, salinity, density, turbidity, dissolved oxygen, colored dissolved organic matter (CDOM), fluorescence ECO-AFL (chlorophyll-a), fluorescence wet star and irradiance\PAR) in each cast. The data acquisition was carried out using the Seaterm software, and the pre-processing included a set of SBE Data Processing routines (Sea-Bird Electronics). The recommended pre-processing procedures for the onboard probe model included: 1) the conversion of binary data file to a text ascii file (*.cnv); 2) filtration, that is, definition of the maximum and minimum limits for all variables; 3) Align CTD module, which decreases data transfer speed difference between the CTD, Deck Unit and PC, decreasing the spikes in the data; 4) the correction of the effect of thermal mass of the cell; and 5) Loop edit module, which decreases data noise. The data visualization was done using the Ocean Data View (ODV) software (version 4.7.10). It should be noted that some technical issues occurred with the optical sensors, which lead to extreme variations in the

datasets, in particular: i) the malfunction of the chlorophyll-a and turbidity (WET Labs ECO) sensor cable resulted in sometimes negative values in the first 10 stations, being then replaced by a new one (Figures 5.39 and 5.41, respectively); ii) the correction factor to obtain CDOM concentrations from fluorescence measurements was also corrected, due to negative values measured during the first 2 stations (Figure 5.40). As future work, an attempt should be made to recover/correct the negative values from the datasets.

Radiosonde

The acquisition of atmospheric data was performed through Graw DFM-17's radiosondes. The atmospheric radiosondes measured 45 vertical profiles of wind speed and direction, temperature, dew point temperature, virtual temperature, pressure, geopotential height, height and air density. The data acquisition was carried out using the GRAWMET software (version 5.16) and the data visualization of the vertical profiles was done using Python scripts.

Preliminary results

Preliminary results of oceanographic (**section a**) and meteorological data (**section b**) at the stations performed in the SO287 CONNECT cruise are shown and analyzed below.

Oceanographic data

Vertical variability of temperature, salinity, density, dissolved oxygen, chlorophyll-a, CDOM, and turbidity along the transects performed in the North Atlantic Ocean (stations 1-32) and in the Pacific Ocean (stations 42-45) are shown in Figures 5.35-41 and Figures 5.36-42, respectively. As supplementary information, the identification of mesoscale eddies in the Atlantic Ocean was performed using satellite-based altimetry data and the AMEDA algorithm (Le Vu et al., 2018) for the period between 12 and 29 December 2021. Eddy positions are represented in Figures 5.49-51, along with underway surface measurements of temperature, salinity and chlorophyll-a.

The vertical variability of the parameters clearly reflects the transport pathway of water from the upwelling zones off Africa into the Sargasso Sea, further to the Caribbean and also to the equatorial Pacific. The first two stations showed that the upper 150 m of the water column was well mixed, as suggested by homogeneous values of temperature (22 ºC; Figure 5.35), salinity (ca. 36.6; Figure 5.36) and density (ca. 25 kg m^{-3}; Figure 5.37). Filaments of high productivity waters originating from upwelling region are also visible in the vertical profiles. An increased chlorophyll-a concentration (> 0.5 mg m^{-3}; Figure 5.39) was observed at the second station, accompanied by high dissolved oxygen concentrations (> 200 µmol kg^{-1}; Figure 5.38), which reflects oxygen production by photosynthesis. At this station, deep chlorophyll-a maximum (DCM) was visible at around 100 m depth. Along with the increasing distance from Canary Islands, oligotrophic conditions are observed, as evidenced by low chlorophyll-a concentrations after station 3, along with the deepening of DCM (around 150 m depth; Figure 5.39). An interesting event was related with the detection of a cyclonic eddy at station 6, as suggested by the rise of the isopycnals (Figures 5.35-38) and by a shallow oxygen minimum zone (OMZ) just below the productive upper layers (around 180 m depth; Figures 5.38-39), indicating increased microbial respiration. The occurrence of this cyclonic eddy was also confirmed by the AMEDA eddy tracking algorithm (for details regarding the eddy tracking methodology, see Cardoso et al., 2020) applied for the Atlantic Ocean basin (Figures 5.49-51). Between stations 6 and 11, the thermocline remained relatively constant at around 180 m depth. After station 12, the thermocline started to decrease to 200 m depth (Figure 5.35. Here, temperature and salinity values increased (> 25ºC and > 37, respectively), associated with higher air temperatures at this lower latitude. In addition, after station 12, it is possible to observe an increase in dissolved oxygen concentrations, reflecting the termination of the shadow zone of the eastern tropical Atlantic Ocean. In the Sargasso Sea (around 60º W), the thermocline was shallower (ca. 150 m

depth), with a slight decrease of temperature (25 ºC; Figure 5.35) and salinity values (36.7; Figure 5.36).

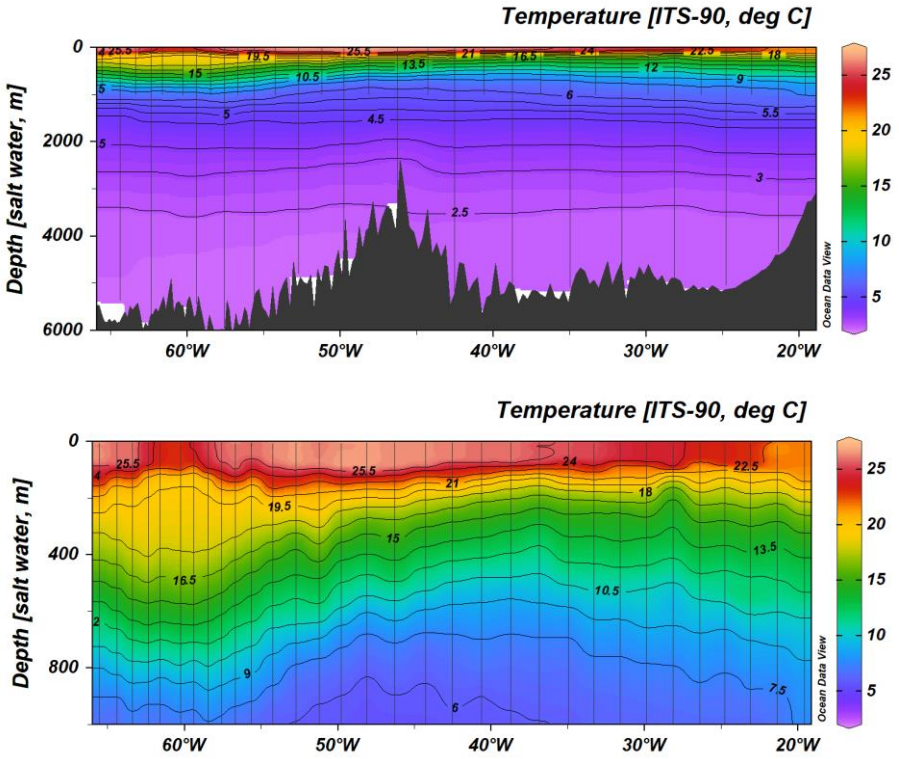

Figure 5.35: Vertical variability (6000 m and 1000 m depth) of temperature (ºC) along the North Atlantic Ocean transect. Vertical black lines represent the stations.

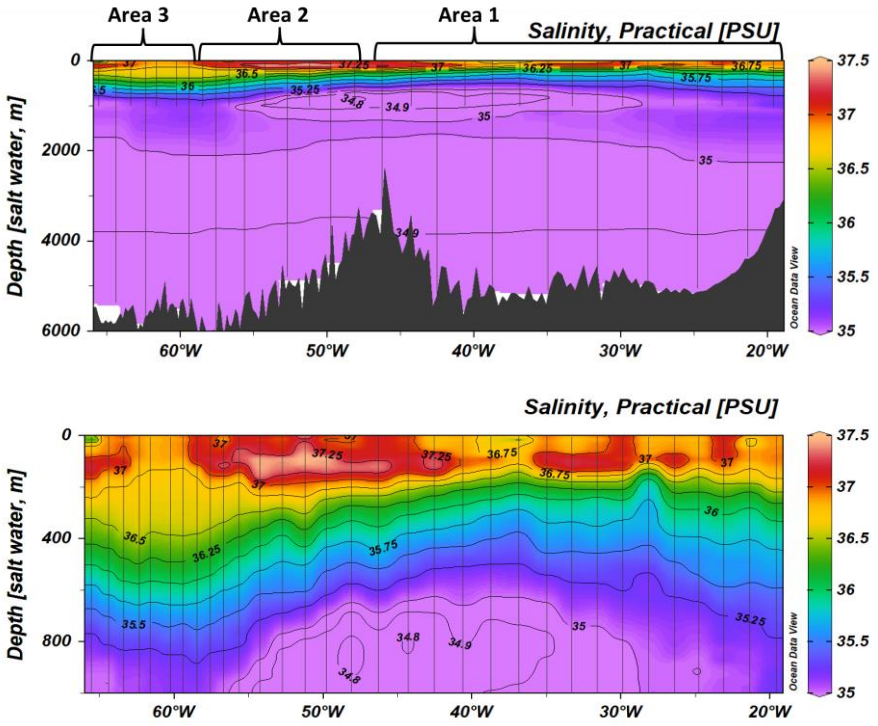

Figure 5.36: Vertical variability (6000 m and 1000 m depth) of salinity (PSU) along the North Atlantic Ocean transect. Vertical black lines represent the stations.

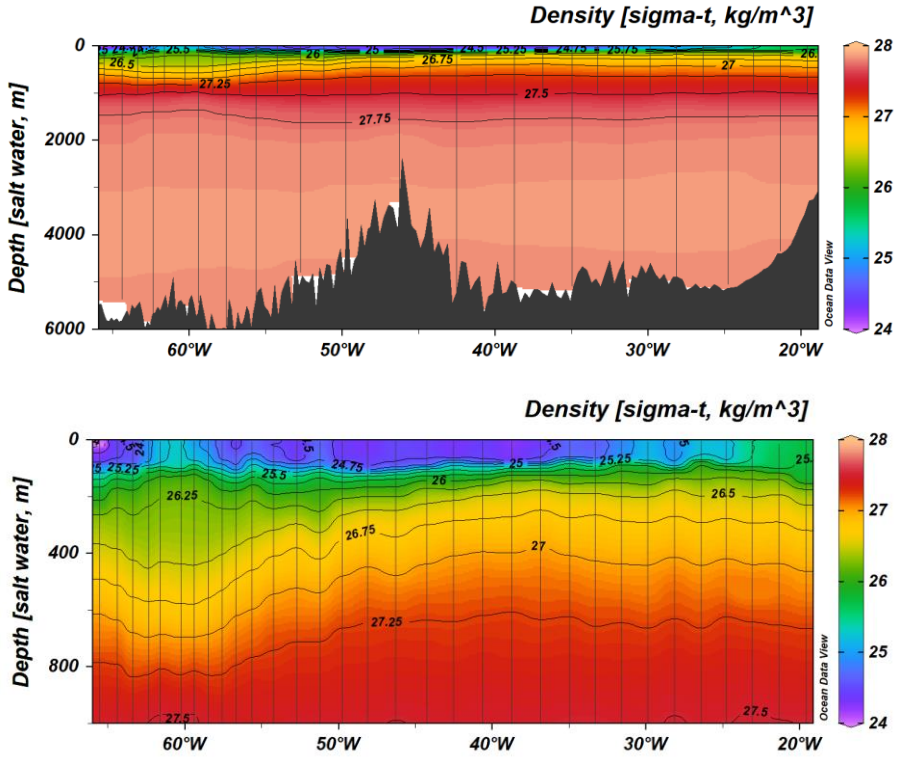

Figure 5.37: Vertical variability (6000 m and 1000 m depth) of density (kg m^{-3}) along the North Atlantic Ocean transect. Vertical black lines represent the stations.

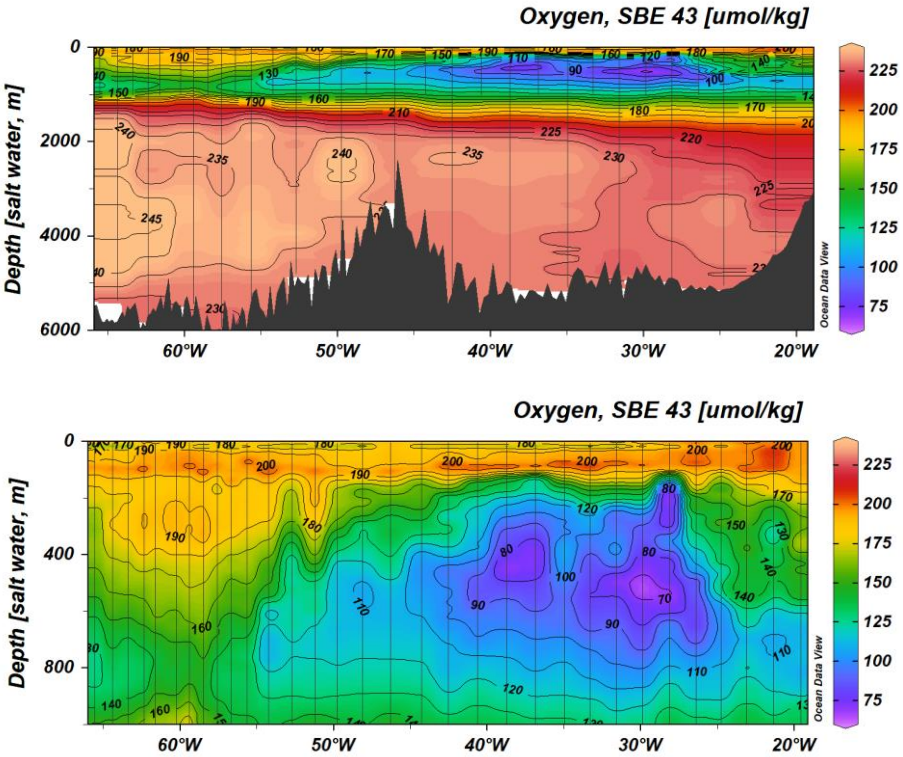

Figure 5.38: Vertical variability (6000 m and 1000 m depth) of dissolved oxygen (µmol Kg^{-1}) along the North Atlantic Ocean transect. Vertical black lines represent the stations.

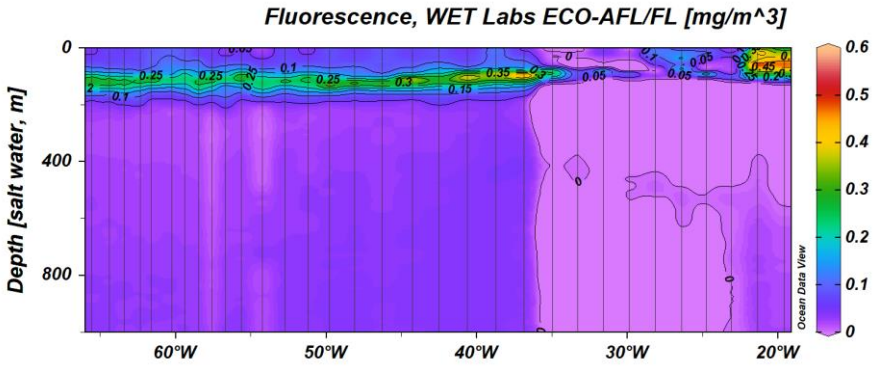

Figure 5.39: Vertical variability (1000 m depth) of chlorophyll-a (mg m^{-3}) along the North Atlantic Ocean transect. Vertical black lines represent the stations.

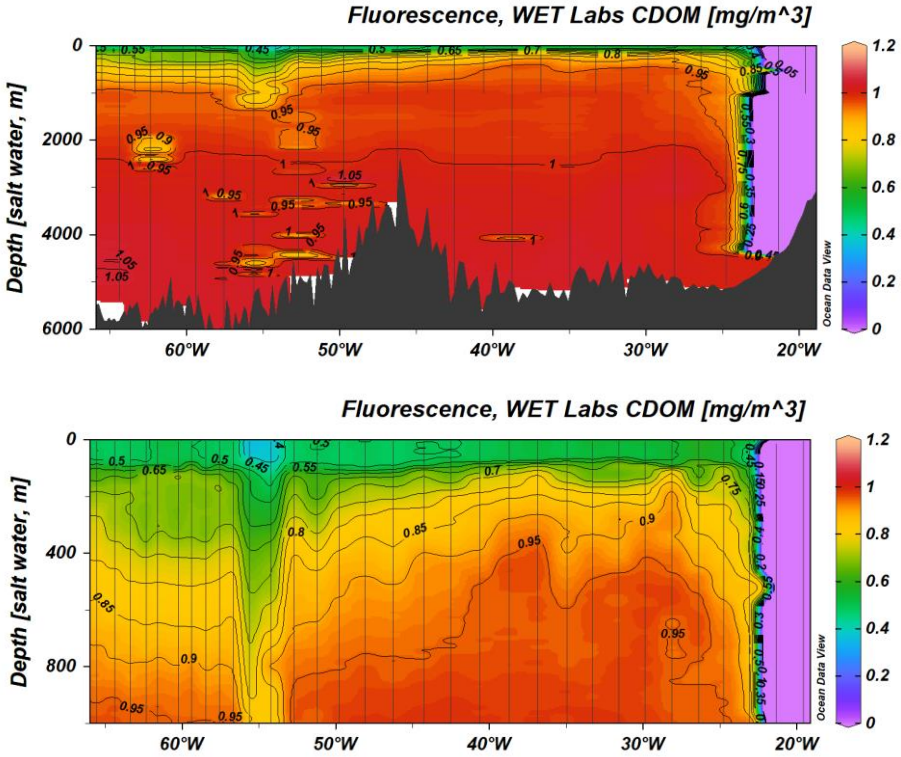

Figure 5.40: Vertical variability (6000 m and 1000 m depth) of colored dissolved organic matter (CDOM; mg m^{-3}) along the North Atlantic Ocean transect. Vertical black lines represent the stations.

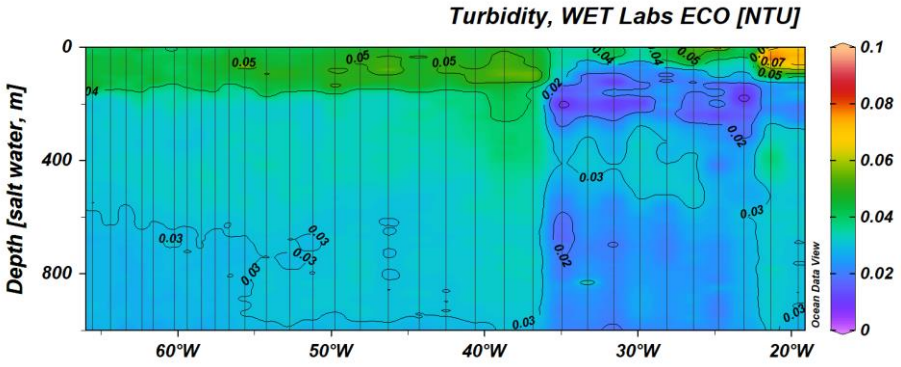

Figure 5.41: Vertical variability (1000 m depth) of turbidity (NTU) along the North Atlantic Ocean transect. Vertical black lines represent the stations.

The vertical variability of the parameters measured in the Pacific Ocean clearly show a distinct pattern of variability when compared to the Atlantic Ocean. The stations performed in the Pacific Ocean showed a shallower thermocline (around 50 m depth; Figure 5.42) and lower values of salinity (< 34; Figure 5.43) and density (< 23 kg m^{-3}; Figure 5.44) at the upper levels of the water column, when compared to the Atlantic Ocean. The low salinity values can be a result of heavy rainfall events that usually occur in this region. As we move southward (from 3º N to 3º S), salinity slightly increases from 33 to 34. Still, a shallow freshwater mass is trapped in the first 50 m depth of the water column, while higher salinity (ca. 35; Figure 5.43) and density (> 26 kg m^{-3}; Figure 5.44) persist below this depth. Such vertical salinity and density gradients implied strong stratification at the upper levels of the water column, which potentially retained nutrients and consequently favoured phytoplankton growth. Such speculation can be supported by high concentrations of chlorophyll-a (> 0.6 mg m^{-3}; Figure 5.46) and dissolved oxygen (> 200 µmol kg^{-1}; Figure 5.45) at the first 50 m depth. It is also important to note the shallower OMZ (between 350 and 400 m depth), characterized by low dissolved oxygen concentrations close to anoxic conditions (values close to 0 µmol kg^{-1}; Figure 5.45). The lower concentrations of dissolved oxygen can be associated with the fact that the waters in the Pacific Ocean are older than the Atlantic Ocean, leading to high removal of oxygen for respiration along the time.

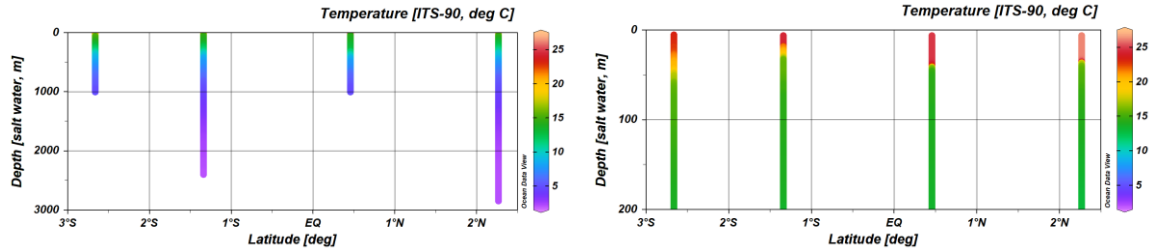

Figure 5.42: Vertical variability (3000 m and 200 m depth) of temperature (ºC) along the Pacific Ocean transect.

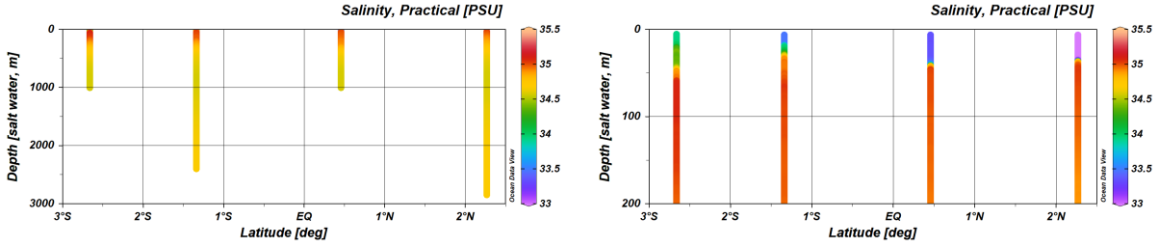

Figure 5.43: Vertical variability (3000 m and 200 m depth) of salinity (PSU) along the Pacific Ocean transect.

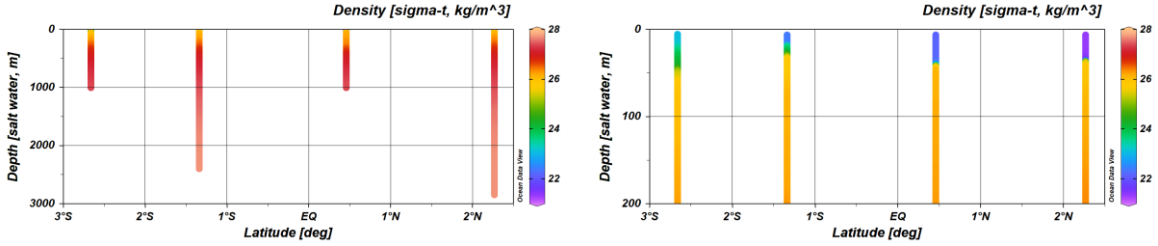

Figure 5.44: Vertical variability (3000 m and 200 m depth) of density (kg m^{-3}) along the Pacific Ocean transect.

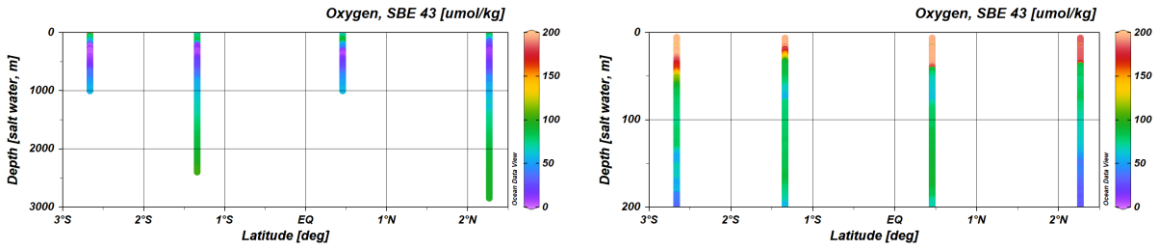

Figure 5.45: Vertical variability (3000 m and 200 m depth) of dissolved oxygen (µmol Kg^{-1}) along the Pacific Ocean transect.

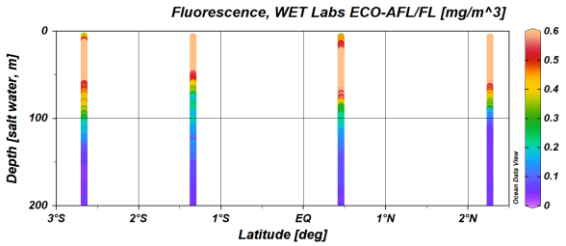

Figure 5.46: Vertical variability (200 m depth) of chlorophyll-a (mg m^{-3}) along the Pacific Ocean transect.

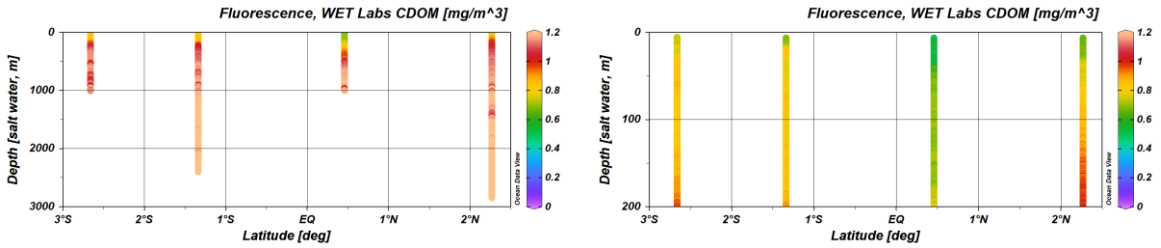

Figure 5.47: Vertical variability (3000 m and 1000 m depth) of colored dissolved organic matter (CDOM; mg m^{-3}) along the Pacific Ocean transect.

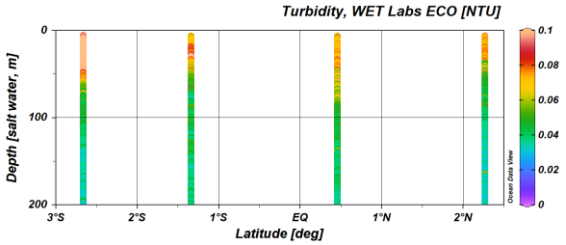

Figure 5.48: Vertical variability (200 m depth) of turbidity (NTU) along the Pacific Ocean transect.

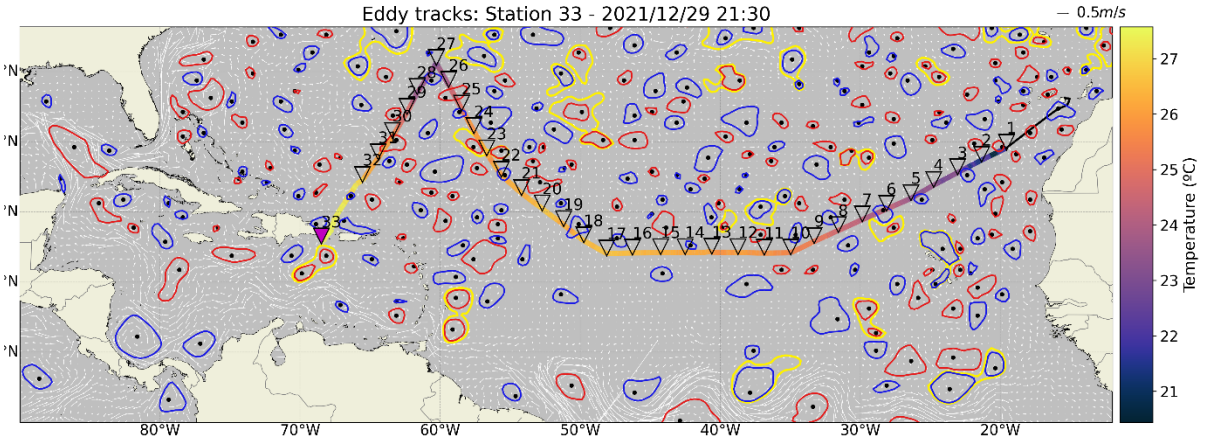

Figure 5.49: Eddy tracks from 12 to 29 December 2021, plotted against underway measurements of Sea Surface Temperature (ºC). The blue and red colors represent cyclonic and anticyclonic eddies, respectively.

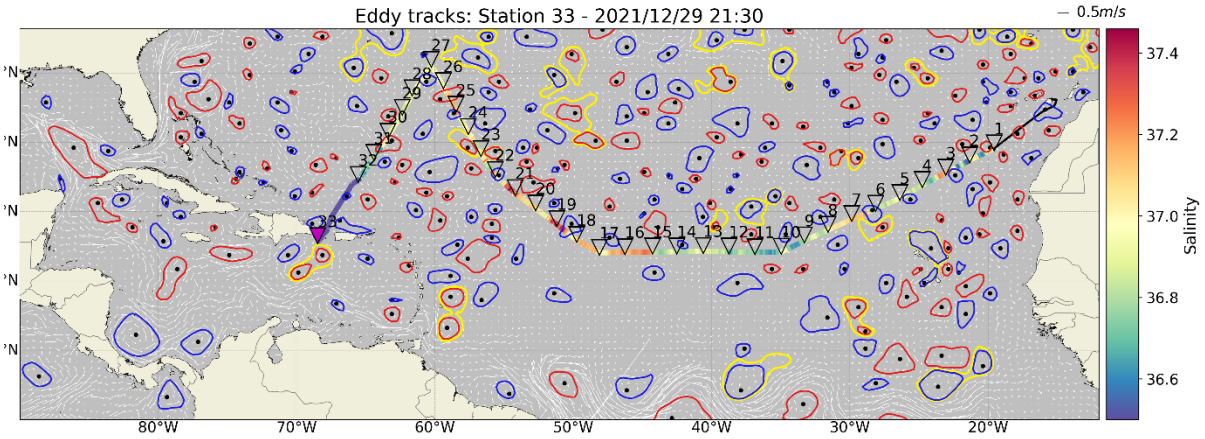

Figure 5.50: Eddy tracks from 12 to 29 December 2021, plotted against underway measurements of salinity. The blue and red colors represent cyclonic and anticyclonic eddies, respectively.

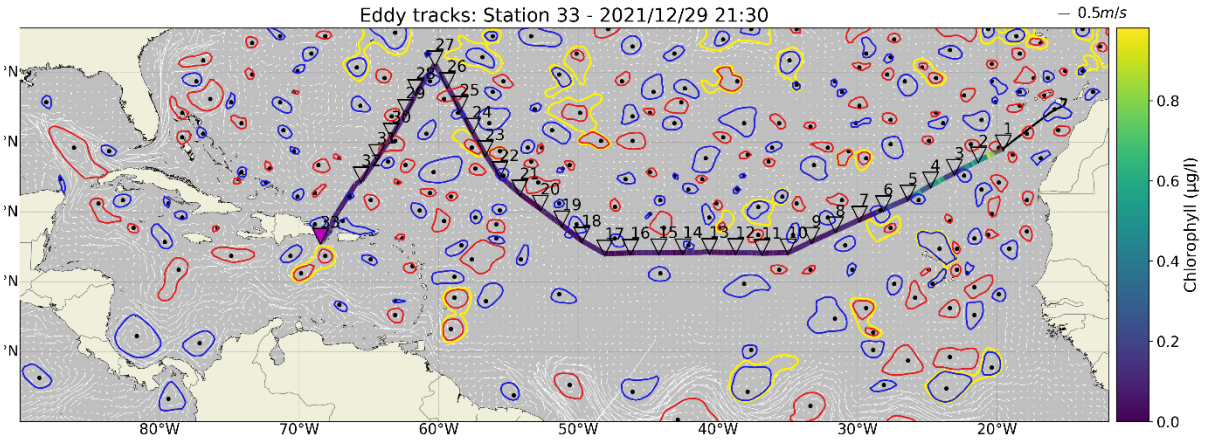

Figure 5.51: Eddy tracks from 12 to 29 December 2021, plotted against underway measurements of Chlorophyll-a concentrations (µg L^{-1}). The blue and red colors represent cyclonic and anticyclonic eddies, respectively.

Temperature-Salinity (T-S) diagrams were also performed to support the identification of the water masses in the Atlantic Ocean. With the preliminary analysis of the T-S diagrams (Figure 5.52), three different areas can be identified: the first area goes from station 1 to 15, the second from station 16 to 24 and the third from 25 to 32 (see Figure 5.36 for identification of the areas). The same water masses were found across all sampling stations, but from different sub-regions of formation.

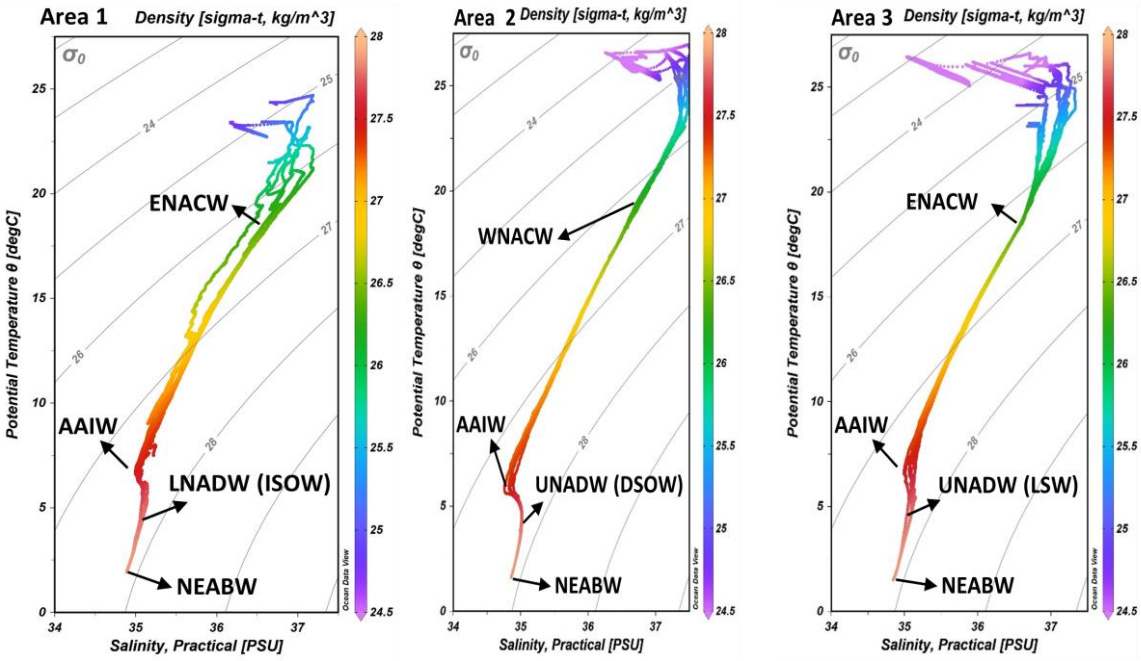

Figure 5.52: Temperature-Salinity diagrams of data acquired in area 1, area 2 and area 3 (see Figure 5.36 for identification of the areas).

The North Atlantic Central Water (NACW) is present at surface layers, being divided in two: the West North Atlantic Central Water (WNACW – area 2) and the East North Atlantic Central Water (ENACW – areas 1 and 3). The main difference is that WNACW has a significantly higher salinity (more 0.9 Units) than ENACW (Liu and Tanhua, 2021). Considering the intermediate layer in all the areas, we observed the presence of the Antarctic Intermediate Water (AAIW) created in the upper part of the Antarctic Circumpolar Current (Liu and Tanhua, 2021), which propagates in the North Atlantic towards the east, making area 1 slightly degraded and less saline than areas 2 and 3. The deep waters below the intermediate layer are also divided in two: the Lower North Atlantic Deep Water (LNADW) and the Upper North Atlantic Deep Water (UNADW). The LNADW is also known as Iceland-Scotland Overflow Water (ISOW) and is present only at the east side of the Mid-Atlantic Ridge (area 1). The UNADW is also divided in two: the Labrador Sea Water (LSW) and the Denmark Strait Overflow Water (DSOW). The LSW is near the Caribbean Sea (area 3) and has a slightly lower density compared to the DSOW, which is closer to the Mid-Atlantic Ridge (area 2; Ferreira and Kerr, 2017; Liu and Tanhua, 2021). The bottom layer, so far, was only identified as Northeast Atlantic Bottom Water (NEABW). As futures work, a similar methodology should be used to identify the water masses in the Pacific Ocean.

Atmospheric data

In this section, we only show the variability of the altitude of the Planetary boundary layer (PBL) along the CONNECT cruise transect (Figure 5.53), given the high number of vertical profiles measured by the radiosondes. The PBL was estimated following Aryee et al. (2020). The PBL is the lowest zone of the atmosphere, characterized for being directly influenced by exchanges between earth surface and atmosphere, including energy, momentum, moisture, and pollutants (Díaz et al., 2019; Aryee et al., 2020). From Figure 5.53, it is possible to observe that PBL altitude was mostly lower than 1500 m until station 13 (around 40º W). After that, PBL altitude started to increase, reaching maximum values (ca. 3000 m) at station 19 (around 50º W).

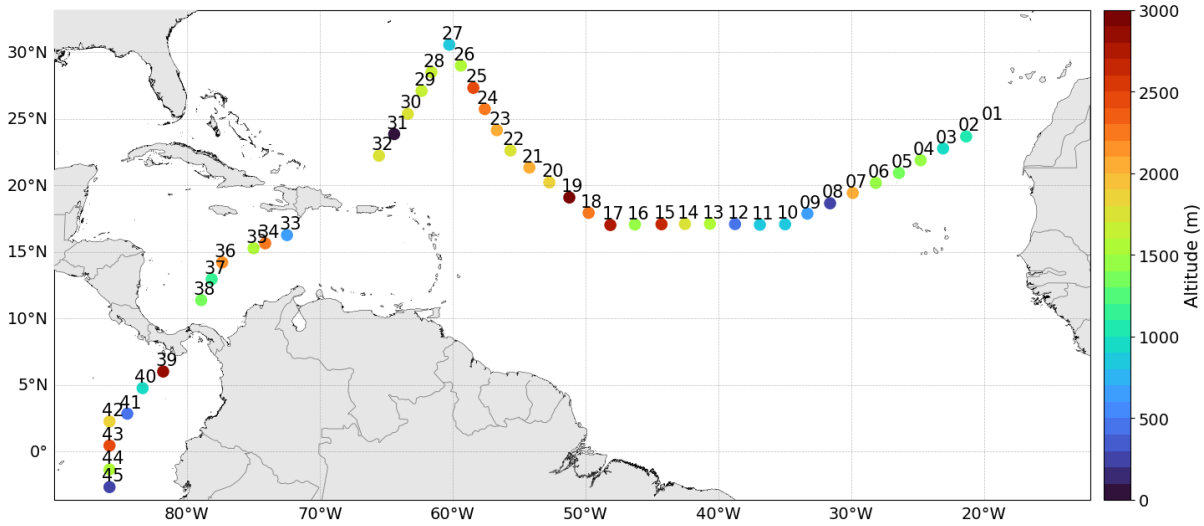

Figure 5.53: Altitude of the Planetary boundary layer at each station along the SO287 CONNECT cruise transect.

Future follow up studies data plans

Processing and analysis of CTD, radiosonde and ADCP data will be completed until December 2022, including scientific visualization and tabulation of all data. ARDITI's researchers will be also available to discuss results/analysis to support the identification of water masses, currents, long range and mesoscale transport processes, among others, particularly regarding the interpretation of the processed datasets. We are also available to collaborate in future peer-reviewed publications with other working groups from the cruise, in order to identify potential implications of the meteo-oceanographic processes on the biogeochemical and ecological realms. As supplementary information, we will perform compilation, processing, scientific visualization and analysis of remote sensing data of Chlorophyll-a concentrations and Sea Surface Temperature to support the interpretation of the oceanographic data acquired during the SO287-CONNECT cruise.

5.2.1.2 Ozone profiles of the atmosphere

(Sigrid Marie Vildskog Auganaes[3], Kirstin Krüger[3])

[3]University of Oslo, Oslo, Norway

Background

Ozone is a natural occurring gas in the atmosphere. Commonly it is associated with the ozone layer in the stratosphere, where it reaches its maximum due to a balance between sunlight that creates ozone and chemicals, as halogens, that destroy it. In the troposphere there are low values of ozone, created by chemical reactions between nitrogen oxide and organic compounds mostly from anthropogenic emissions. In the atmosphere, ozone plays an important role as the ozone layer shields the Earth surface from harmful UV radiation, but it also acts as a greenhouse gas.

Ozone profiles contain valuable information about the distribution of ozone in the troposphere and stratosphere. Less ozone profile measurements are conducted over the oceans. Recently, a minimum of ozone and OH values in the troposphere above the tropical West Pacific was detected, which impacts chemicals that originate from the surface and travels up through the troposphere into the stratosphere. Short-lived biogenic or anthropogenic chemical compounds can be affected by this. A molecule that reacts with and therefore breaks down these short-lived chemicals is radical hydroxide (OH). OH can therefore be considered a shield as it protects the stratosphere from these short-lived chemical compounds. The amount of OH in the troposphere is of interest not only because of its shielding properties, but also because of the atmospheric lifetime for several greenhouse gases. In clean tropospheric air, the main source for OH is a chemical reaction that requires ozone (O_3). One can therefor measure O_3 to find the OH levels in the troposphere. The paper of Rex et al (2014) on the tropical West Pacific tropospheric ozone and OH minimum and the relevance for the stratosphere is the main motivation behind this survey. These ozone sonde profile observations will be used as a basis to investigate if we find similar results over the tropical Atlantic Ocean.

Method

Ozone profiles of the atmosphere where obtained by launching 7 ozone sondes, scattered semi evenly along the cruise track. Figure 5.54 shows a simple visualization of the placement and timing of the launches, including nearby meteorological stations on land who also conduct ozone sondes.

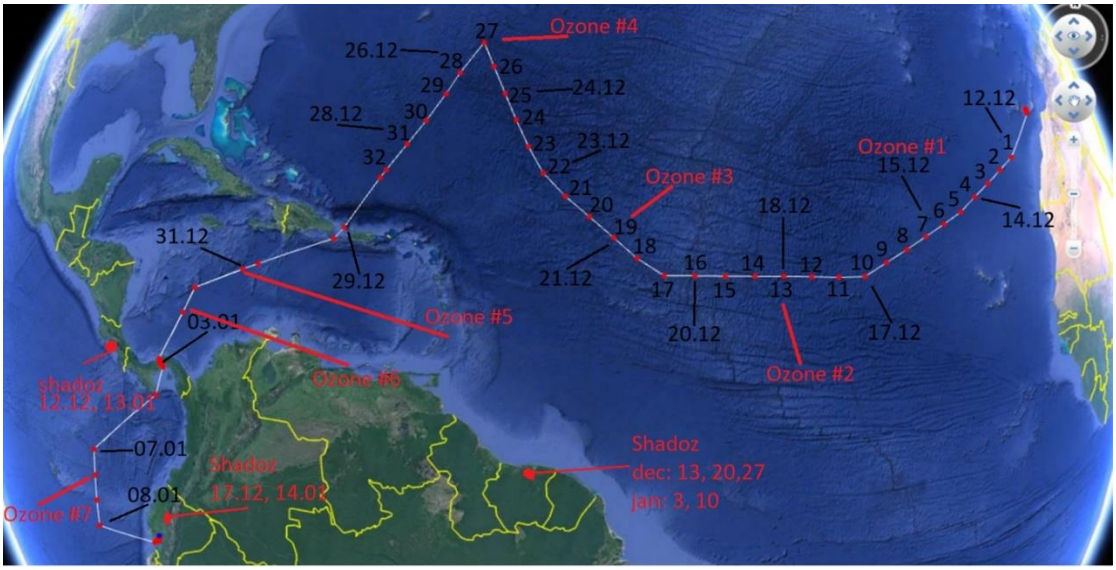

Figure 5.54: Overview of ozone launches and cruise track.

The 7 ozone sondes from the company En-Sci (https://www.en-sci.com/ecc-ozonesonde/), were coupled with a Graw radiosonde DFM 17 (https://www.graw.de/de/) and a ground station. The operator followed the preparations steps with chemical treatment, described in the 2019 Vaisala manual (https://www.vaisala.com/). Each Ozone sonde was prepared 2 times, and the first preparation was always between 3 and 7 days before launch. The second preparation was a few hours before launch, to retrieve values for the initialization of the radiosonde. Each ozone sonde was launched using a weather balloon filled with helium. The aim was to reach an ascend rate of 5 m/s, and an altitude of above 30km.

Preliminary results

Six ozone sonde launches could be conducted successfully (Figure 5.55), while one launch was disrupted by a sudden gust of wind which apparently affected the antenna and there with the signal of the sonde, so that the data were corrupted.

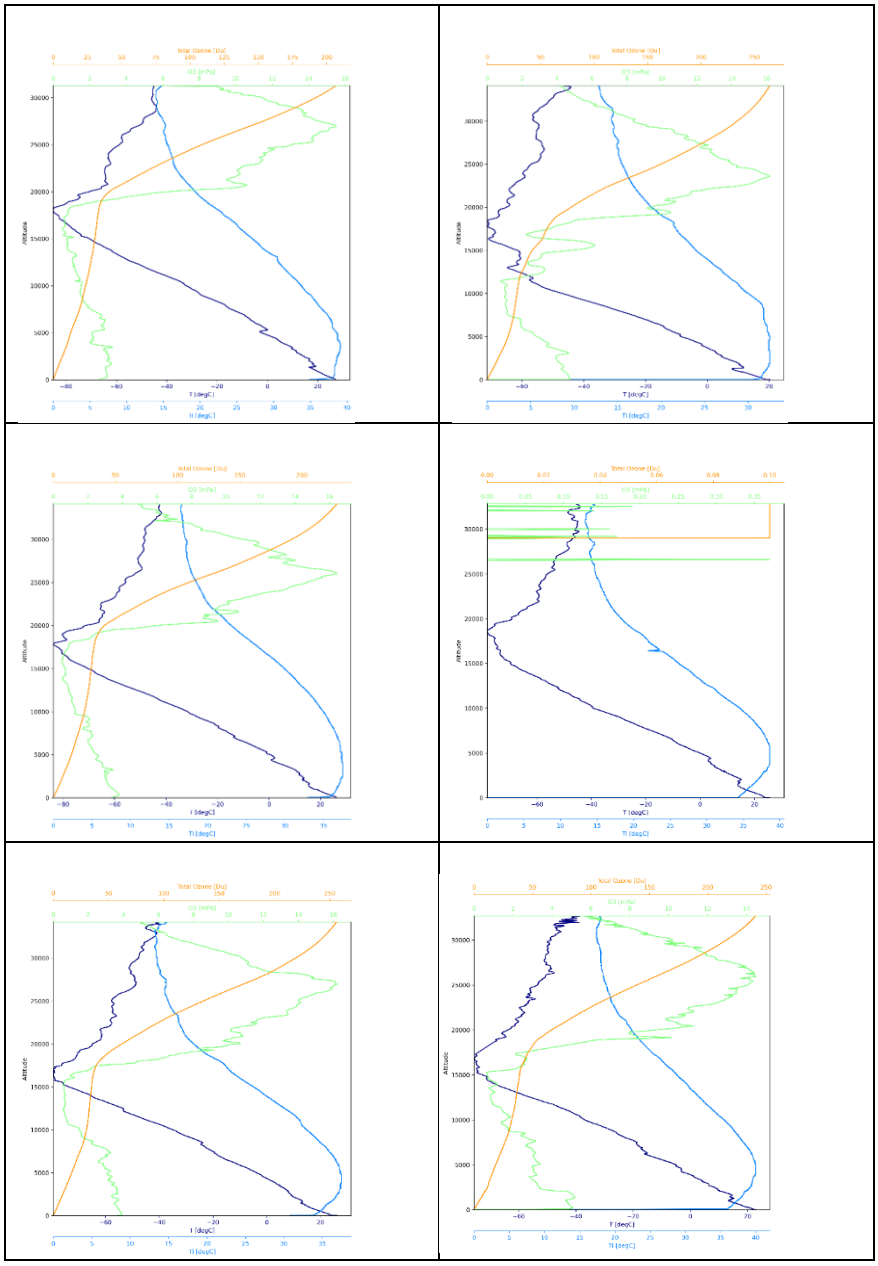

Figure 5.55: Temperature and ozone profiles of six ozone sonde launches on board SO287.

5.2.1.3 Sunphotometer measurements

(Sigrid Marie Vildskog Auganaes[3], Kirstin Krüger[3])

[3]University of Oslo, Oslo, Norway

Background

The MPI-M has since 2008 obtained calibrated instruments from the AERONET group at the NASA Goddard Space Flight Center. These instruments, consisting of a MICROTOPS sunphotometer and a GPS unit, is used to sample water vapor and aerosol properties on cruises with German research vessels. The data is used as references for remote sensing from satellites and global model simulations. The MICROTOPS sun photometer is a little handheld instrument and require direct sunlight without any disturbances from clouds. The device captures solar intensity in five pre-selected solar sub-spectral wavelength bands of 380, 440, 670, 870, and 940nm (Smirnov et al, 2009).

Method

During cloud free conditions one can sample aerosol and water vapor using the MICROTOPS and GPS device. The GPS is connected to the MICROTOPS and is ready for use after it has connected to several satellites. The sunphotometer is then pointed directly towards the sun. Every sampling a minimum of 5 samples were taken over a time interval of 5-10m minutes. Sampling occurred sporadically when conditions allowed. Data was downloaded from the instrument and sent to NASA for processing after a couple of samplings.

Preliminary results

Results can be found at https://aeronet.gsfc.nasa.gov/new_web/cruises_new/Sonne_21_1.html

Figure 5.56: Aerosol properties.

5.2.2 Optical properties and phytoplankton specification

(PI and on board: Rüdiger Röttgers, Martin Hieronymi, Kerstin Heymann & Henning Burmester)

Helmholtz-Zentrum Hereon, Institute of Carbon Cycles, Optical Oceanography

Background

Satellite remote sensing of ocean color provides global monitoring of the marine biomass and other water constituents in the upper ocean mixed layer. The cruise track of SO287 follows particular clear and oligotrophic waters, which is of strong contrast to generally more productive coastal or even inland waters. Not only many in situ sensors reach their detection limits in clear waters, also satellite data interpretation faces special challenges and reliable validation of ocean colour products of these remote regions is needed.

Objectives of this work package were to measure ocean colour at sea and to determine all ocean colour-relevant specific water properties in the upper 100 m layer to allow development and validation of satellite algorithms of the Hereon group, in particular for the European Sentinel-3 OLCI mission of ESA & EUMETSAT (Hieronymi et al., 2017). It was the goal to conduct precise measurements at sea and compare results with corresponding clear sky satellite matchups, i.e. validate the performance of atmospheric correction and the in-water retrieval, e.g. of chlorophyll-*a* concentration. Beyond Sentinel-3/OLCI, also other operational satellite sensors were of interest (Sentinel-2/MSI, Aqua/MODIS, VIIRS).

Moreover, special interest was on the chlorophyll-specific absorption and scattering properties of the dominant phytoplankton species *Synechococcus sp.* and *Prochlorococcus sp.* and its variation over the course of the cruise.

Material and Methods

Hereon-CTD. A 12-position water sampler frame was used for profiling the top 100 m at each day during noon at times of the highest sun zenith angle in parallel or in close timing to the radiometric measurements. The frame is equipped with eight 9l-sampling bottles, a CTD (that is additionally equipped with oxygen, chlorophyll fluorescence and turbidity sensors), several backscatter sensor (2x Eco-VSF and a HydroScat-6), an AC-S attenuation-absorption meter, a LISST-VSF scattering meter and a PAR irradiance sensor (additionally the frame carried a Chelsea FastOcean set from GEOMAR). Profiles were conducted at a low lowering speed of 0.1-0.3 m/s until a depth of 100 m. Water samples of 30-40 L were taken from about 50 m and 6 m water depths.

Radiometry. Ocean colour, i.e. remote-sensing reflectance Rrs, has been measured from the ship above water with ship and sensors orientated along the sun, preferably around local noontime. Hyperspectral (350 to 950 nm) Ramses sensors by TriOS GmbH (Germany) were used to measure: down-welling irradiance at the sea surface, sky radiance, and up-welling radiance from the sea surface. Remote-sensing reflectance is determined from these three quantities (Ruddick et al. 2019a+b). Moreover, Qmini sensors have been used to achieve higher spectral resolution and a hyperspectral (450 to 950 nm) camera by Cubert GmbH (Germany) was utilized to characterize the larger scale picture with upwelling radiance of water, whitecaps or *Sargassum*.

Filtration. Water samples taken from all surface depth (0-200 m) and regularly from the underway sampling have been filtered for phytoplankton pigment analysis by HPLC for later biomass and algal taxonomic group analysis. Samples from all stations and all depths and partly from the underway sampling have been taken for CDOM absorption measurements.

Occasionally POC and DOC sample were taken from the surface depth (Hereon CTD) for group analysis inter-comparison.

Onboard optical measurements. Total and particulate absorption of surface water samples (6 and 50 m) from the Hereon CTD was measured directly after sampling using a PSICAM (Röttgers et al., 2007) and QFT-ICAM (Röttgers et al., 2016) system. Absorption by dissolved matter (CDOM) was done using the PSICAM and a setup of three LWCC (liquid waveguide capillary cell) system of different path length (0.1, 0.5 and 2.5 m) using <0.22 µm-filtered sample water.

Preliminary results.

A number of match-ups have been achieved with diverse satellite missions. The measured optical parameters correspond to the expected very clear oceanic water; a typical example of remote-sensing reflectance of the Sargasso Sea is shown in Figure 5.58. Guided by satellite data, we found different patches of *Sargassum*, which is of particular challenge for satellite remote sensing algorithms; we were able to determine the remote-sensing reflectance of pure *Sargassum* and mixed water-*Sargassum* in the field of view.

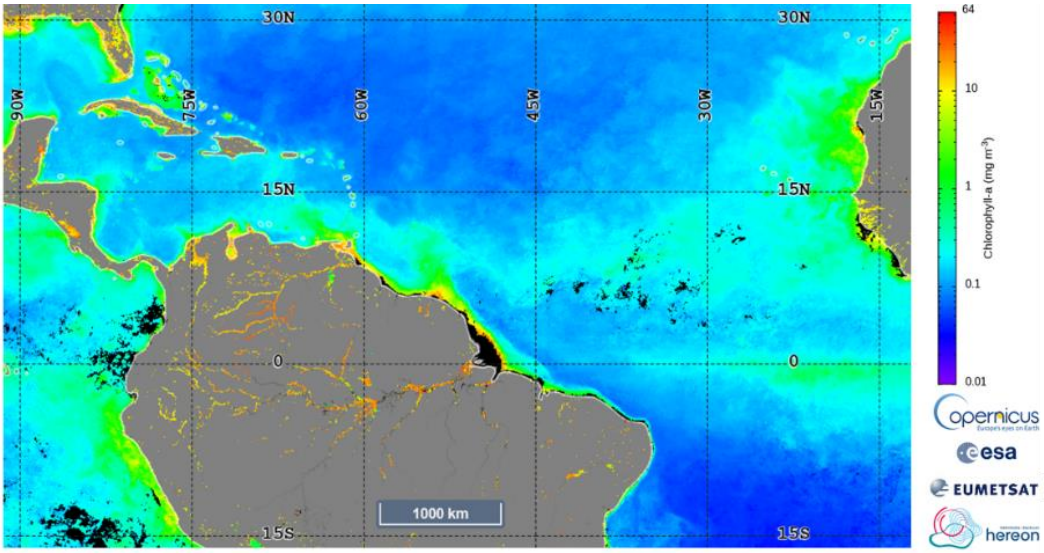

Figure 5.57: Monthly averaged chlorophyll a concentration for December 2021 and the SO287-CONNECT travel area derived from Sentinel-3 OLCI data.

The spectral absorption coefficient of CDOM was measured and preliminary analyzed onboard for the Atlantic section of the cruise and data of the coefficient at 350 nm are shown in the following graph. All other data have to be analyzed and processed at home.

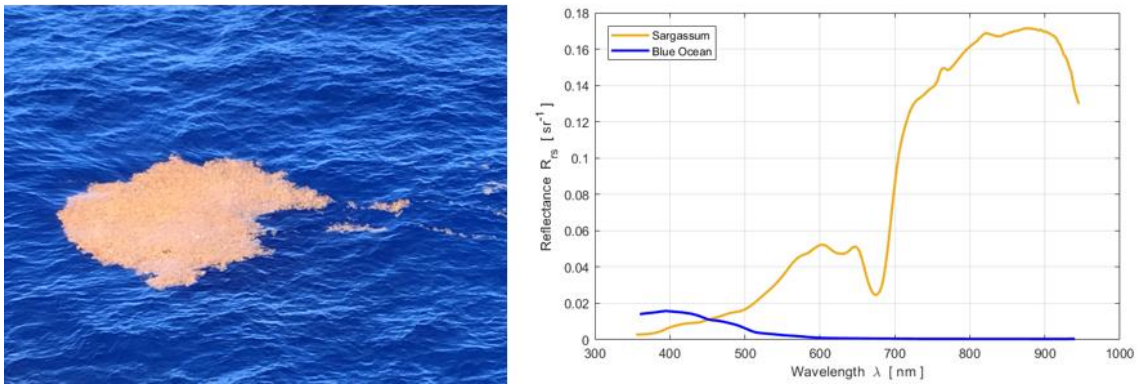

Figure 5.58: Left: Raft of *Sargassum* floating on oligotrophic waters of the Sargasso Sea. Right: Corresponding Ocean Colour of *Sargassum* and background water.

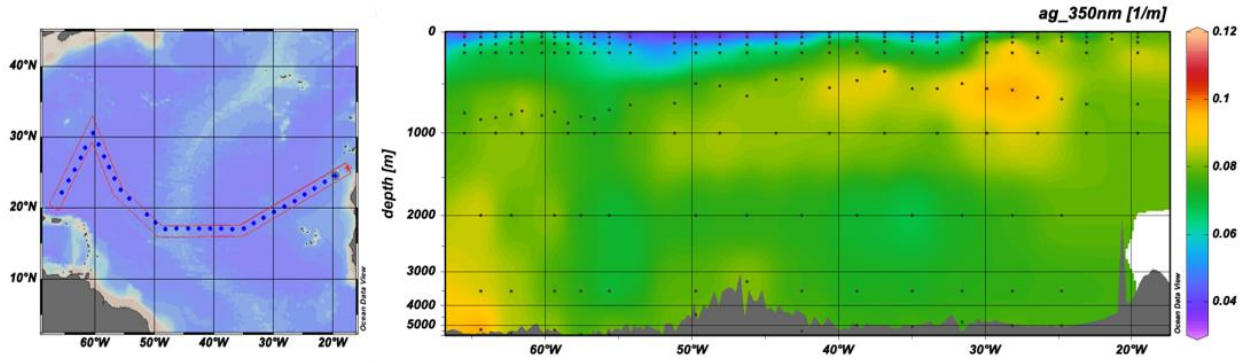

Figure 5.59: Absorption coefficient of CDOM at 350 nm along the cruise transect in the Atlantic Ocean.

5.2.3 Marine particle flux-Underwater Vision Pofiler

(PI: Anja Engel[1], Rainer Kiko[2], responsible on board: Jon Roa[1])

[1]GEOMAR

[2]LOV Villefranche-sur-Mer, France

Background

Many zooplankton and nekton organisms such as copepods, euphausiids and fish feed in the surface layer at night and migrate to depth during the day to avoid visual predation. Furthermore, these migrations and associated organic matter cycling lead to a net-downward transport of particulate and dissolved matter. Large particles formed through aggregation or faecal pellet production at all water depths compose the sinking fraction of the particle size spectrum. Their fragmentation and remineralisation along their path to the deep sea also contribute to the subsurface particle maximum, DOM, and nutrient pools.

Method

Data was obtained on particle and plankton distribution down to 6000 m depth to constrain particle flux to depth, and evaluate impacts of migration on particle fluxes. An Underwater Vision Profiler (UVP) from Hydroptic was attached to the CTD rosette to collect pictures of migrating zooplankton and large sinking particles. The UVP was deployed from station 3 on at every CTD station. Pictures are stored on a hard drive and will be analyzed back in the lab.

Confocal Laser Scanning Microscopy

For the investigation of TEP and CSP with the Confocal Laser Scanning Microscope (CLSM) a total of 144 filters were prepared. For each station seawater samples of two depths, the surface (6 m) and the DCM were filtered. Duplicates were prepared for every filtration of each depth. For the filtrations 100 mL were put through 0.2µm nucleopore filters and the filters were then conserved in petri dishes and frozen at -20°C.

Gel-like particles

For the abundance research of Transparent Exopolymeric Particles (TEP) and Coomassie Stainable Particles (CSP) a total of 932 filters were prepared. To achieve that a total of 560 litres of seawater were filtered.

At every of the 19 day stations six different depths were sampled and at every of the 17 night stations seven depth were sampled from the Niskin bottles attached to the CTD. The day station sampling went to a maximum depth of 1000 m while the night station sampling for TEP and CSP was at a maximum depth of 3500 m.

For each depth that was sampled, duplicates of TEP and CSP filtrations were prepared. The filtered volume varied for the different depths. The sampling volumes for the upper layers were mostly around 200 to 350 mL while the sampling volumes for the greater depths were around 400 to 500 mL.

The method used for the abundance research of TEP and CSP is colorimetric. The seawater samples were filtrated through 0.4 µm nucleopore filters and stained with Alcian Blue (for TEP) or Coomassie Brilliant Blue (for CSP). One millilitre of the staining solution was put on the filter after the water sample was filtered through. Alcian Blue was remained for five seconds on the filter before being removed via vacuum. The filter then was rinsed with miliQ water. Coomassie Brilliant Blue remained for 30 seconds on the filter before it was removed via vacuum and it was rinsed with MilliQ water. The filters then were stored on microscopy slides, closed and frozen at -20°C.

5.2.4 Aerosol particles: Iron (Fe), organic carbon (OC) and elemental carbon (EC)

(PI: Manuela van Pinxteren[1], responsible on board: Lucie Röttgers[2])

[1]TROPOS, [2]GEOMAR

Background

Aerosol particles over the ocean are a complex mixture of diverse sources. Elucidating their chemical composition enables a better understanding of ocean-atmosphere interactions.

Iron (Fe)

The cycling of trace metals, including their emissions, transport, and atmospheric deposition is still not well understood. Studies in remote marine areas have shown that trace metal concentrations in particulate matter are enriched above the ocean indicating that oceanic sources cannot be neglected (Fomba et al., 2013). Moreover, trace elements, especially Fe, serve as nutrients for the marine biota and as tracers for anthropogenic influences (Morel et al. 2003). The supply of trace metals in general, and Fe in particular, is therefore thought to control the structure and, possibly, the productivity of marine ecosystems thereby, regulating ocean processes and carbon cycling. The large-scale distribution of Fe is, however, poorly known. This represents a major barrier to understanding their biogeochemical role in the marine systems.

Organic carbon (OC) and elemental carbon (EC)

Organic carbon is a major component of (marine) aerosol particles and can constitute more than half of the aerosol mass (e.g. Quinn and Bates, 2011 and references therein). The enrichment of organic matter increases with particle size (O'Dowd et al., 2004), hence, the smaller the aerosol particles, the more organic matter they contain. OC may result from several sources, among them marine natural sources, where OC is transferred from the ocean to the atmosphere via bursting bubbles and forms aerosol particles. Furthermore, OC can derive from the continents, including biogenic and anthropogenic sources.

Elemental carbon (EC) is an often-used tracer for the determination of anthropogenic contamination, e.g. ship exhaust or pollution from land. EC concentrations in clean marine air are typically low with maxima of several tenth of ng m^{-3} (e.g. Cavalli et al., 2004;van Pinxteren et al., 2017).

Method

Aerosol particles (TSP = total suspended particles) were sampled with a filter sampler consisting of a filter holder equipped with a quartz fiber filter mounted to a pump. Sampling usually took place for 24 h with a flow rate between 5 and 10 L min^{-1}. Total volumes between 10 and 15 m^3 were sampled.

Measurements of total Fe will be performed with Total Reflection X-Ray Fluorescence (TXRF) S2 PICOFOX (Bruker AXS, Berlin, Germany) equipped with a Mo-X-ray source on polished quartz substrates (Fomba et al., 2014;Fomba et al., 2013). Organic carbon (OC) and elemental carbon (EC) determination will be carried out as described in van Pinxteren et al., (2017). In short, a thermal-optical method, applying the EUSAAR 2 temperature protocol is used from a filter piece with an area of 1.5 cm^2. Samples will be thermally desorbed from the filter medium under an inert He-atmosphere followed by an oxidizing O_2/He-atmosphere while applying carefully controlled heating ramps. A flame ionization detector is used to quantify methane following a catalytic methanation of CO_2. As a first step, nitrogen is employed to act as a carrier gas, kept at a temperature of 650°C, for the purpose of OC volatilization. Furthermore, as a second step, EC is combusted at a temperature of 650°C in an oxygen atmosphere.

Preliminary results:

24 aerosol filters were collected during the cruise. They will be transported to the TROPOS laboratories where the chemical analysis will be performed.

Future follow up studies data plans:

The aerosol data will be correlated with seawater measurements. It will be elucidated if biological activity in the ocean is connected to Fe concentration on the aerosol particles. Correlations between EC and OC can help to elucidate the origins of the OC; e.g. marine or combustion sources.

5.2.5 The lateral transport of continental seaweed

(PI: Florian Weinberger, responsible on board: Tobias Müller)

GEOMAR

Background

Macroalgae or ‘seaweeds’ are the dominant primary producers in coastal waters and form large expanses of underwater forest. Yet, their role in C sequestration has only been considered recently. Macroalgae-dominated ecosystems export considerable amounts of C (61-268 Tg C yr^{-1}) in dissolved and particulate form to the deep ocean and sediments (Krause-Jensen and Duarte, 2016). Despite that macroalgae are identified as producers of blue carbon, tracing and understanding the large C export flux from productive coastal habitats to the open ocean remains a challenge and is a major outstanding flaw in the global C budget (Krause-Jensen et al., 2018). During the cruise we address this challenge by identifying the abundance of laterally transported seaweed from coastal Africa and the abundance of *Sargassum* in deep waters of the Atlantic with eDNA as new method, applied during SO287.

Method

Water sampling for eDNA was conducted at every station, where different depths were sampled into a 250 ml sterile plastic device. 150m of the sample was evenly distributed in 10x50ml sterile centrifuge tubes and conserved with 35 ml of ethanol and acetate each. After the station work, the more than 1300 sample tubes were centrifuged in the Panama Canal because of the urge for a stable environment for the centrifuge.

Preliminary results

We have collected 140 samples. The samples were transported on dry ice to GEOMAR, where the DNA will now be extracted from the samples.

Future follow up studies data plans

eDNA-metabarcoding, targeting green algae (marker gene: tufA) brown algae and other eukaryotic plants and also animals with CO1 and 18SRNs gene-analysis.

Identification of coastal signatures and signatures from *Sargassum* and associated organisms in sea water samples.

5.3.1 DMS/P/O cycling in the surface ocean and the influence of ship emissions on trace gases (DMS)

(PI: Christa Marandino, Hermann Bange, Dennis Booge, Responsible on board: Inga Brockmann & Greta Wunderlich)

GEOMAR

Background

Despite the low concentrations of short-lived trace gases in the atmosphere, their impact on local and global climate is crucial. Dimethyl sulfide (DMS) is produced biogenically via dimethylsulfoniopropionate (DMSP) by a complex interplay of bacteria and phytoplankton in the surface ocean. It can undergo different microbial pathways or can be photochemically oxidized to dimethyl sulfoxide (DMSO) in the water column. These compounds are key players in the marine sulfur cycle and the microbial foodweb (Simó, 2001). Another main loss of DMS in the surface ocean is the loss to the atmosphere via air-sea gas exchange which accounts for 40% of the sulfur compounds in the atmosphere (Charlson et al., 1987). DMS, as a short-lived trace gas in the atmosphere, is an important precursors of cloud condensation nuclei in the remote marine boundary layer and therefore influences the radiation budget of the Earth.

Although the Atlantic is the second biggest ocean basin, anthropogenic pressure increases rapidly also in open ocean regions, especially in the North Atlantic. Shipping is the most widely used medium for transport of goods internationally and will continue to increase (Sardain et al. 2019). Although shipping is a carbon efficient transport medium, emissions of exhaust gases and particles into the marine boundary layer from ships contribute significantly to the total emissions from the transportation sector (Dalsoren et al. 2009). However, environmental consequences from pollutant emission from ship smoke stacks and liquid discharge (scrubber effluent) are poorly investigated. In a wet scrubber, the exhaust gas is treated using seawater in an open system or freshwater in a closed loop. The use of scrubbers is considered to be cheaper than using cleaner fuel, but the effects of scrubbers on seawater could potentially cause problems for marine ecosystems (Endres et al. 2018, Ytreberg et al. 2019), especially with respect to their influence on climate relevant biogenic trace gas production in the world's oceans.

The goal during this cruise is to better understand the biological pathways and interactions of DMS, DMSP and DMSO, as well as monitoring their concentrations in the surface waters of these contrasting regions (Atlantic Ocean, Caribbean Sea, East Pacific Ocean). Furthermore, we will investigate how the use of scrubbers impact the biogeochemistry in the surface ocean.

Material and methods

Surface water from the underway pump, located at about 6 m depth in the ship's moonpool, was sampled every 3 hours, in order to investigate the spatial distribution of DMS in the surface waters along the cruise track.

Besides surface measurements, discrete samples from different depths (6 m – 5900 m) were collected to resolve DMS concentration variations also in a vertical resolution. The water for the depth profiles were sampled using Niskin bottles attached to the CTD. During each CTD cast (one at daytime around noon and one during nighttime), 6 different depths were sampled. The noon CTD was shallow, going to ~1000 m deep. DMS samples were collected from the surface (6-10 m), the depth of the oxygen minimum, and the depth of the chlorophyll maximum, as well as three additional depths, in order to resolve the upper ocean DMS concentrations. During the night CTD, which was a deep profile to the ocean bottom, three additional sampling depths were distributed over the whole water column.

In addition to underway and CTD samplings, two incubation experiments were performed during the cruise. 36 1 L polycarbonate bottles were prepared by filling the bottles with surface water of the underway pump. 18 bottles were spiked with 1% and 2% of scrubber water at the beginning of the first and second experiment, respectively. The other 18 bottles were used as controls. The bottles were placed in a water bath at current ocean surface temperature and were exposed to a natural day/night light cycle to a maximum time of seven days. Triplicate sample bottles for each treatment (scrubber treatment and control) were taken once a day at the same time in order to be analyzed for following different parameters: DMS/DMSP/DMSO, nutrients, phytoplankton functional types, bacteria, chromophoric dissolved organic matter, trace metals, polycyclic aromatic hydrocarbons, and pH.

All DMS samples were directly measured on board, within two hours after sampling, using a purge and trap system coupled to a gas chromatograph attached with a flame photometric detector (P&T-GC-FPD; Figure 5.60). After the analysis, samples were prepared to bring them back to the GEOMAR lab for further analysis of DMSP and DMSO concentrations.

Figure 5.60: System set-up on board. P&T-System (left) and GC-FPD (right) used for DMS measurements.

Preliminary results (Underway and CTD)

In surface waters highest DMS concentrations (3-4 nmol L^{-1}) were detected in the Sargasso Sea (Figure 5.61), where a high biological productivity takes place. In the oligothrophic open ocean region between the coast of Africa and the Sargasso Sea, as well as in Caribbean waters, lower concentrations of DMS (1 nmol L^{-1} or less) were measured.

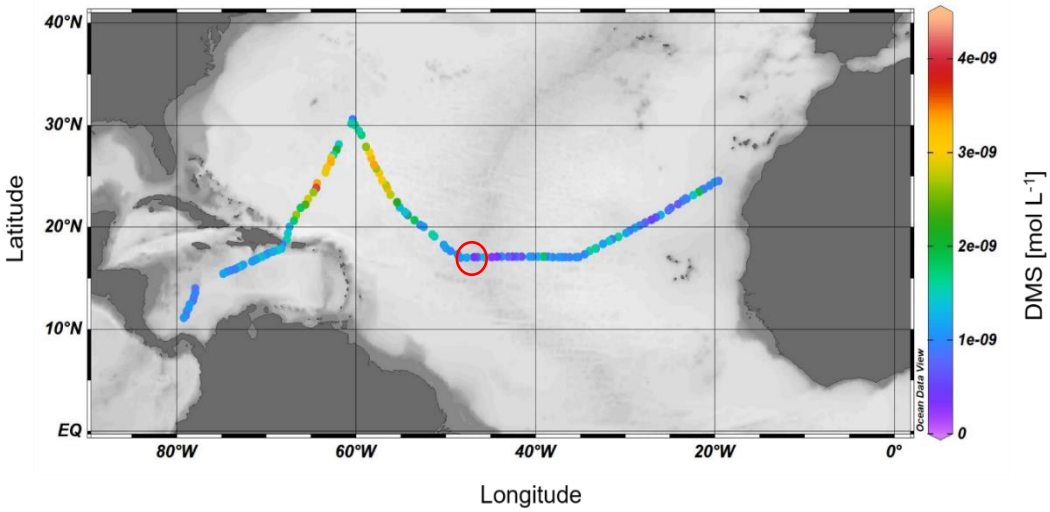

Figure 5.61: Spatial distribution of DMS in surface waters along the cruise track. The circle highlights station 17.

Figure 5.62 shows the vertical DMS distribution from an exemplary CTD profile in the mid-Atlantic from station 17 (location for station 17, please see Figure 5.61, red circle). The DMS profile is mainly following the chl-a profile (not shown) with higher concentrations in the mixed layer depth (MLD) until the depth of the chl-a maximum and a fast decrease with increasing depth below the MLD.

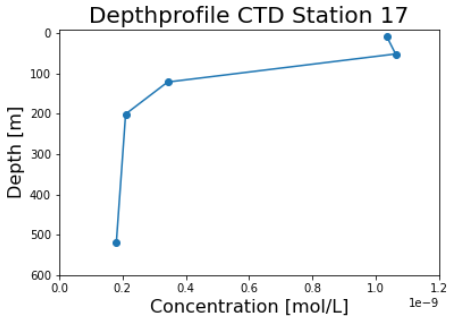

Figure 5.62: Depth profile of DMS at station 17.

Preliminary results (Incubation experiments)

Preliminary results from the first incubation experiment show a significant difference of DMS concentrations between the scrubber treatment and the controls over the whole time of the experiment (Figure 5.63). Interestingly, DMS concentrations in the scrubber treated water are already drastically reduced at time zero right at the start of the experiment. This result shows that there is an immediate effect (possibly pH related) of scrubber water addition on the actual DMS concentration in the incubation bottles. During the course of the experiment, DMS concentrations increase for the first three days, which is likely to be caused by biological production from a small algal bloom in the bottles. After four days (end of algal bloom, due to nutrient depletion), no biogenic production of DMSP and subsequent production of DMS takes

place anymore, and DMS concentrations sharply decrease due to further photooxidation to DMSO or due to microbial consumption.

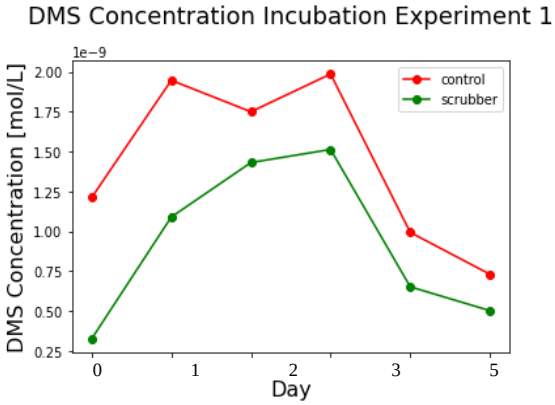

Figure 5.63: DMS concentrations in two different treatments during one incubation experiment.

Future follow up studies data plans

In addition to DMSP and DMSO samples from underway and CTD samplings, as well as from incubation experiments, ancillary parameters from incubation experiments (e.g. phytoplankton functional types, bacteria, trace metals, polycyclic aromatic hydrocarbons) will be analyzed after the cruise in GEOMAR labs within the next 3-6 months. It is planned to publish the results in scientific journals.

5.3.2 Measurements of Atmospheric Trace Gases

(PI: Folkard Wittrock, responsible on board: Tim Bösch, and Miriam Latsch)=

IUP Bremen

Background

Shipping plays an important role in the transport of goods internationally since it is the most often used medium with 80-90% of world trade being transported by ships (Krause et al., 2021). In the western part of the Atlantic, the ship traffic density is especially high. Studies by the International Maritime Organization (IMO) expect that ship emissions will increase by 90% to 130% of the 2008 emissions by 2050 (IMO, 2021). Most ships use combustion engines that emit various species as an unwanted side-effect: CO, CO_2, NOx, SO_2, Particulate matter, Black Carbon. These emissions lead to risks for human health, have an impact on ecosystems (e.g., acid rain), can interact with the Earth's energy budget (e.g., the reflection of sunlight), and have (in)direct effects on the weather (e.g., rain due to aerosols). Within the last decades, ship emissions have been regulated particularly concerning the sulphur and nitrogen content. However, the shipping emission regulations are not always followed. The aim of measurements of atmospheric pollutants during the cruise SO287 is to monitor the contribution of shipping emissions and long-range transport of anthropogenic pollution and biogenic emission on air quality and air chemistry in the marine troposphere over the remote Atlantic and the Eastern Pacific.

Material and methods

Observations of the atmospheric trace gases NO_2, Ozone and SO_2 were carried out using an Avantes spectrometer in MAX-DOAS configuration and a MAX-DOAS system (see e.g., Wittrock et al., 2004, Peters et al., 2012, Seyler et al., 2017, Seyler et al., 2019, Behrens et al., 2019). Trace gas profiles were calculated in the marine troposphere.

To better determine the impact of different sources (e.g., passing ships) in situ measurements of NOx (ThermoScientific MLU42i), SO_2 (ThermoScientific MLU43i-TLE), CO (MLU48i, Los Gatos Research Ultraportable Multi-gas carbon emission analyzer), and Black Carbon (Aethalometer AE33, Magee Scientific) were conducted (e.g., Kattner et al., 2015).

Preliminary results

In-situ measurements

Figure 5.64 shows the background-corrected in-situ time series of NO and SO_2 for the cruise SO287. Especially at the beginning of the cruise (until 14.12.), several peaks in both time series can be seen, indicating shipping emissions due to the absence of other emission sources south of the Canaries. As the cruise continues (14.12. – 29.12.), larger concentrations of NO and SO_2 are rare. Smaller peaks at the 15th, 17th, and 19th-20th of December might be attributed to a few encounters with other ships on the Atlantic Ocean. Here, the peaks are most likely smaller due to the larger distances between RV SONNE and the ships, and hence, the dispersion of the emitted plumes. From the 29th of December, extremely large concentrations can be seen for all in-situ instruments indicating either large emissions from the Dominican Republic or Puerto Rico while entering the Caribbean Sea or contamination of all in-situ instruments with water from condensation inside the inlet tubes and filters. This issue was solved on the 2nd of January which led to a decreased concentration of SO_2. Interestingly, NO concentrations remained on a high level, leaving it open if large concentrations or instrumental issues are responsible for the high values

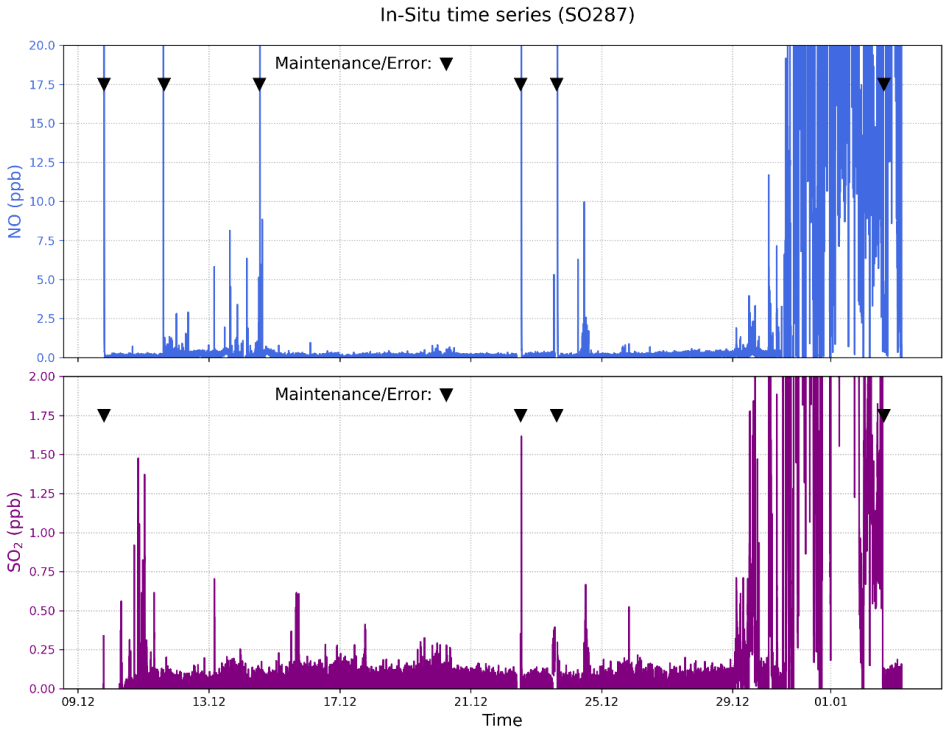

Figure 5.64: Background-corrected in-situ time series of NO and SO_2. Black triangles indicate times of maintenance work or errors of the instruments.

DOAS measurements

Measurements from the Avantes MAX-DOAS system need to be corrected for the pitch and roll angles of RV SONNE. This task will be done after the cruise as it needs DSHIP data and the adaption of two correction and analysis scripts.
Because of that, Figure 5.65 shows only a time series of the NO_2 differential slant column density (DSCD) from the 12th of December as it already indicates what can be expected from MAX-DOAS measurements of NO_2 during the whole cruise.
The beginning of this day (until 12 UTC) was dominated by broken clouds and bad viewing conditions which can be seen as unsteady and rough elevations scan peaks.
From 12 to 13 UTC, increasing peaks sizes with smooth peak shapes indicate a close emission source such as a large ship. The increase in time with an abrupt drop in signal is representative for a passing ship.
Later in the afternoon (after 13 UTC), measurements are dominated by low signals and/or thick clouds. The afternoon results can be expected throughout the full cruise unless plumes from ships or emissions sources ashore will be encountered.
The small increase of the time series in the evening (after 17 UTC) represents the change in light path due to the lower sun and the larger contribution of stratospheric nitrogen dioxide when the sun is low.
The creation of NO vertical column density (VCD) time series and vertical concentration profiles from the inversion algorithm BOREAS will be performed after the cruise and might shed more light on the question of what kind of source might be responsible for larger peaks in NO_2 columns.

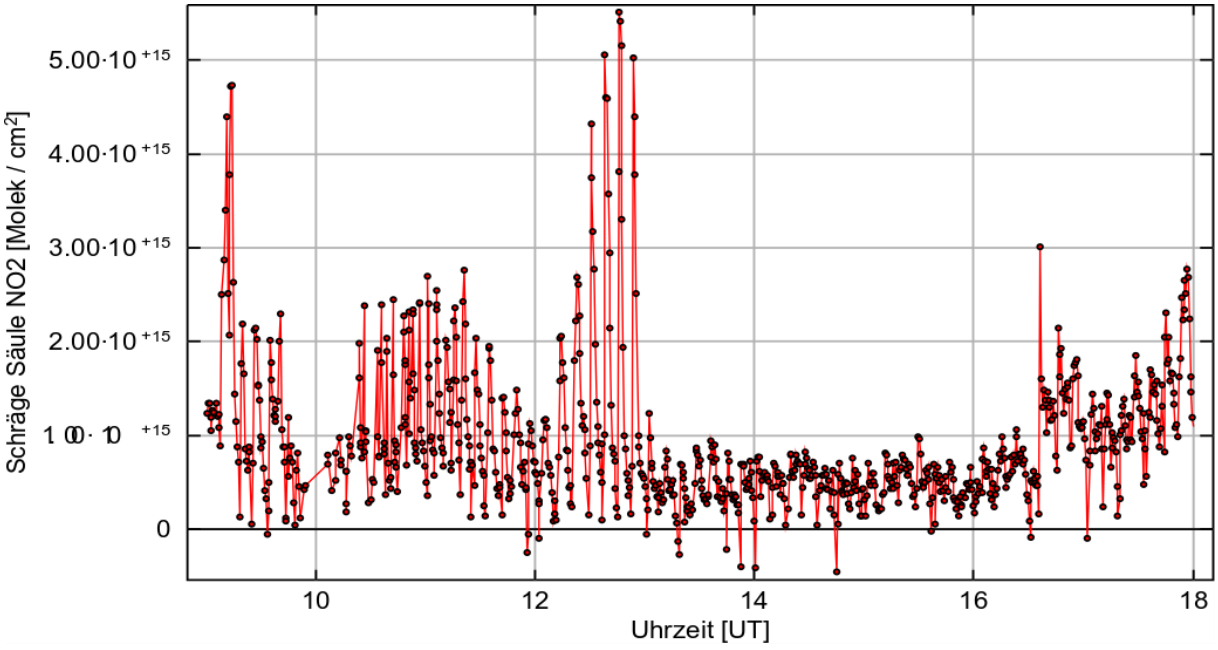

Figure 5.65: Uncorrected DSCD of NO_2 from the 12th of December measured by the Avantes MAX-DOAS instrument.

Future follow up studies data plans

After the cruise, the measurements will be compared with satellite and model data, which enables us to assess the air pollution of ships on a larger scale. In this way, the impact of shipping emissions as an additional source of anthropogenic pollution for the Caribbean Sea littoral states can be better estimated.
Furthermore, long-range transport of trace gases from continental outflow will be constrained geographically by using back-trajectory models.

5.3.3 Marine Plastics Debris

(PI: Anja Engel/ Cathleen Schlundt; responsible on board: Lindsay Scheidemann)

GEOMAR

Background

Plastic Marine Debris (PMD) is the most common and exponentially increasing pollutant in the ocean (Jambeck et al., 2015). Microplastics is known to have detrimental effects on marine biota (see review by Galloway et al., 2017, see review by Wang et al., 2019) and to cause enormous economic costs like damage of ship propellers, motors, and fishing equipment, beach cleaning or decline in tourism due to soiled marine landscapes (Newman et al., 2015). Another important aspect of PMD are the effects on the microscale level. PMD can act as a new habitat and a vector for harmful algae, pathogenic bacteria and viruses but the effects of this are still poorly understood. It is clear that microbes immediately settle on plastic upon its entrance to the aquatic environment, having multiple effects on the fate of PMD (Rummel et al., 2017). However, the magnitude and impact of microbes on PMD distributed in the world oceans and their invasion to remote ecosystems is still poorly understood and needs urgent investigation.

Material and methods

- Catamaran tows of up to 20 minutes and additional sample sorting for identification of relatively large particles of suspected plastics and removal of some naturally occurring biomass, such as *Sargassum* and fish larvae. Remaining biology will be degraded using a standard procedure and remaining plastics will be quantified in the lab.

- Underway sampling: continuous sequential filtration of underway water over stainless steel sieves of 1mm, and 300µm (and 50µm) over elongated periods of time during transit. Biology will be degraded using a standard procedure and remaining plastics will be quantified in the lab.

- Incubation experiment: HDPE, LDPE, PS and Mater-bi fragments obtained from commercial sources were incubated in changing seawater across the transect for 14 days to assess microbial colonization of plastics. Samples were taken for 16s RNA analysis and clasi-FISH analysis.

- Samples for clasi-FISH: large Microplastics pieces have been treated with paraformaldehyde and were rinsed with Ethanol. These will be stained for up too seven bacterial taxa using in-situ hybridization in combination with advanced microscopy techniques

- 16s RNA: Samples were stored in RNA-later buffer. The RNA will be extracted using an RNA extraction kit and then used to identify bacterial taxa

- Combi-staining: plastics will be stained in Nile Red and additionally samples will be co-stained for TEP and CSP to observe for beginning of aggregation on the plastic surface

Preliminary results

First preliminary observations from Catamaran samples suggest, that plastic abundance changes with regional factors. While abundances of suspected plastic particles seemed to be increasing in the presence of *Sargassum* in the open Atlantic Ocean, in the Caribbean Sea observed abundances of suspected plastics were low in the *Sargassum* rich east and increased towards the west. The first samples from the Pacific Ocean show comparatively high abundances, which could be connected to the high input of terrestrial particles, which could be inferred from the presence of dead insects in the sample.

Table 5.3: Plastic underway surface water samples.

Sample name	Status	Date	Time (UTC)	Latitude	Longitude	Comments
Pl-UW 1/2	Underway start	20.12.2021	18:30			first sample taken, sieves mostly empty before this one
	Underway end	21.12.2021	09:30			1-300µm, 2-50µm
Pl-UW 3	Duration 7:30	26.12.2021				Test Sinuspumpe (Schiff), 300 µm
Pl-UW 5	Underway start	29.12.2021	23:32	17° 39,788' N	68° 58,321' W	
	Underway end	30.12.2021	11:30	16° 58,828' N	70° 42,134' W	300µm
Pl-UW 6	Underway start	31.12.2021	23:00	15° 19,983' N	74° 51,885' W	
	Underway end	01.01.2022	12:00	14° 33,977' N	76° 35,062' W	300µm
Pl-UW 7	Underway start	02.01.2021	22:00	11° 02,876' N	79° 06,835' W	
	Underway end	03.01.2021	10:00	9° 51,039' N	79° 44,885' W	
Pl-UW 8	Underway start	05.01.2022	00:00			
	Underway end	06.01.2022	15:08	03° 17,677' N	84° 13,540' W	forgotten, ran over morningstation
Pl-UW 9	Underway start	06.01.2022	00:00	2° 32,283' N	84° 47,809' W	
	Underway end	07.01.2022	02:25	2° 16,247' N	85° 49,320'W	
Pl-UW 10	Underway start	07.01.2022	06:07	2° 15,682' N	85° 20,257' W	
	Underway end	07.01.2022	15:29	00° 27,465' N	85° 49,990' W	
Pl-UW 11	Underway start	07.01.2022	22:18	00° 02,427' S	85° 49,886' W	
	Underway end	08.01.2022	02:00	00° 55,346'S	85° 47,254' W	
Pl-UW 12	Underway start	08.01.2022	07:20	01° 22,875' S	85° 49,876' W	
	Underway end	08.01.2022	12:44	02° 39,146'S	85° 49,913' W	

Future follow up studies data plans:

First, the samples for clasi-FISH, 16s-RNA and combi-staining will be analysed and evaluated until the end of 2022. Then follow up studies on the aggregation of Microplastic with TEP and CSP may follow.

Table 5.1: Station list of Catamaran surface water samples of plastic.

Sample Name	Date	Time	Lat	Lon
Pl-Net 1 (Station 1)	12.12.2021	16:06	24° 33,252' N	19° 34,131' W
Pl-Net 2 (Station 3)	13.12.2021	15:53	22° 47,746' N	23° 04,283' W
Pl-Net 3 (Station 5)	14.12.2021	15:08	20° 57,430' N	26° 23,789' W
Pl-Net 4 (Station 7)	15.12.2021	14:31	19° 26,733' N	29° 52,137' W
Pl-Net 5 (Station 9)	16.12.2021	14:32	17° 53,668' N	33° 16,950' W
Pl-Net 6 (Station 11)	17.12.2021	16:04	17° 03,51' N	36° 51,667' W
Pl-Net 7 (Station 13)	18.12.2021	17:28	17° 07,809' N	40° 37,077' W
Pl-Net 8 (Station 15)	19.12.2021	17:55	17° 05,858' N	44° 15,984' W
Pl-Net 9 (Station 17)	20.12.2021	17:51	17° 01,839' N	48° 06,805' W
Pl-Net 10 (Station 19)	21.12.2021	17:13	19° 06,091' N	51° 12,262' W
Pl-Net 11 (Station 21)	22.12.2021	16:51	21° 20,689' N	54° 12,597' W
Pl-Net 12 (Station 23)	23.12.2021	18:12	24° 08,963' N	56° 40,130' W
Pl-Net 13 (Station 25)	24.12.2021	17:47	27° 20,238' N	58° 27,314' W
PL-Net 14 (Station 27)	25.12.2021	18:03	30° 35,074' N	60° 16,534' W
Pl-Net 15 (Station 28)	26.12.2021	15:51	28° 31,124' N	61° 36,421' W
Pl-Net 16 (Station 30)	27.12.2021	17:40	25° 23,350' N	65° 32,420' W
Pl-Net 17 (Station 32)	28.12.2021	18:03	22° 14,756' N	65° 32,420' W
Pl-Net 18 (Station 33)	29.12.2021	12:05	18° 46,938' N	67° 44,449' W
Pl-Net 19 (Station 35)	29.12.2021	19:28	17° 51,780' N	68° 28,349' W
Pl-Net 20 (Station 36)	30.12.2021	12:00	16° 58,336' N	70° 44,571' W
Pl-Net 21 (Station 37)	30.12.2021	19:31	16° 38,687' N	71° 32,118' W
Pl-Net 22 (Station 39)	31.12.2021	12:00	15° 54,337' N	73° 24,450' W
Pl-Net 23 (Station 41)	31.12.2021	19:28	15° 32,752' N	74° 23,160' W
Pl-Net 24 (Station 43)	01.01.2022	13:58	14° 28,245' N	76° 47,840' W
Pl-Net 25 (Station 45)	01.01.2022	20:26	14° 05,288' N	77° 39,294' W
Pl-Net 26 (Station 47)	02.01.2022	13:00	12° 00,134' N	78° 36,496' W
Pl-Net 27 (Station 49)	02.01.2022	20:26	11° 10,607' N	79° 01,952' W
Pl-Net 28 (Station 50)	05.01.2022	13:00	06° 34,239' N	81° 00,940' W
Pl-Net 29 (Station 52)	05.01.2022	20:29	05° 46,390' N	82° 07,866' W
Pl-Net 30 (Station 54)	06.01.2022	12:59	03° 34,886' N	84° 03,078' W
Pl-Net 31 (Station 56)	06.01.2022	20:27	02° 33,455' N	84° 45,016' W
Pl-Net 32 (Station 58)	07.01.2022	19:45	00° 27,109' N	85° 50,058' W
Pl-Net 33 (Station 60)	08.01.2022	19:44	02° 40,043' S	85° 49,915' W

6 Ship's Meteorological Station

Not available. Meteorological measurements have been performed with radiosondes (refer to chapter 5.2) and meteorological data have been obtained from the ships sensors, and can be obtained from http://dship.bsh.de/.

7 Station List SO287

7.1 Overall Station List

- Hereon-CTD: A 12-position water sampler frame with eight 9L-sampling bottles, a CTD (equipped with oxygen, chlorophyll fluorescence and turbidity sensors), several backscatter sensor (2x Eco-VSF and a HydroScat-6), an AC-S attenuation-absorption meter, a LISST-VSF scattering meter and a PAR irradiance sensor
- CTD: A 24 bottle rosette-sampler, with CTD, SBE-911, and sensors for temperature, pressure, conductivity, salinity, density, turbidity, dissolved oxygen, colored dissolved organic matter (CDOM), fluorescence ECO-AFL (chlorophyll-a), fluorescence wet star and irradiance\PAR
- Radiosonde: GRAW-DFM-17 Radiosonde, Sensors: temperature, humidity, pressure, wind
- Ozone sonde: EnSCi-ECC-2Z-V7 Ozone sonde
- ISP: Insitu pump
- Garretscreen: Collection of sea surface microlayer from stern
- Catamaran: Surface deployment for 20 min, collecting neuston from sea surface
- WBAT (attached to CTD): Wide band scientific echo sounder, SIMRAD-EK80
- Zodiak: The ships rubber boatt was used to deploy the Garretscreen from the sea surface.

Activity No.	Station on position	Date	Gear	Time (UTC)	Latitude	Longitude	Ocean Depth [m]	Deployment Depth [m]
SO287_1-1	1	12.12.2021	Hereon-CTD	12:47	24° 33,25' N	019° 34,17' W		70
SO287_1-2	1	12.12.2021	CTD	09:33	24° 33,21' N	019° 34,19' W		200
SO287_1-3	1	12.12.2021	CTD	10:48	24° 33,25' N	019° 34,17' W	3352	200
SO287_1-4	1	12.12.2021	Hereon-CTD	12:47	24° 33,25' N	019° 34,17' W	3352	80
SO287_1-5	1	12.12.2021	Radio sonde	12:59	24° 33,25' N	019° 34,16' W	3352	
SO287_1-6	1	12.12.2021	Garretscreen	13:00	24° 33,25' N	019° 34,16' W	3353	
SO287_1-7	1	12.12.2021	CTD (WBAT)	13:33	24° 33,25' N	019° 34,17' W	3355	1000
SO287_1-8	1	12.12.2021	ISP	14:53	24° 33,24' N	019° 34,16' W	3352	104
SO287_1-9	1	12.12.2021	Catamaran	16:04	24° 33,24' N	019° 34,16' W	3353	
SO287_2-1	2	13.12.2021	CTD	00:30	23° 41,68' N	021° 20,31' W	4411	200
SO287_2-2	2	13.12.2021	CTD	01:08	23° 41,66' N	021° 20,30' W	4411	4350
SO287_2-3	2	13.12.2021	Radio sonde	01:36	23° 41,65' N	021° 20,30' W	4410	
SO287_3-1	3	13.12.2021	Garretscreen	12:48	22° 47,71' N	023° 04,35' W	4870	
SO287_3-2	3	13.12.2021	Radio sonde	12:52	22° 47,72' N	023° 04,35' W	4870	
SO287_3-3	3	13.12.2021	Hereon-CTD	13:00	22° 47,72' N	023° 04,35' W	4870	100
SO287_3-4	3	13.12.2021	CTD (WBAT)	13:40	22° 47,72' N	023° 04,35' W	4870	200
SO287_3-5	3	13.12.2021	CTD (WBAT)	14:12	22° 47,72' N	023° 04,35' W	4870	1000
SO287_3-6	3	13.12.2021	Catamaran	15:50	22° 47,71' N	023° 04,34' W	4871	
SO287_4-1	4	14.12.2021	CTD	00:10	21° 54,47' N	024° 45,58' W	5102	200
SO287_4-2	4	14.12.2021	CTD	00:37	21° 54,48' N	024° 45,59' W	5100	5050
SO287_4-3	4	14.12.2021	Radio sonde	00:51	21° 54,48' N	024° 45,59' W	5100	
SO287_5-1	5	14.12.2021	CTD (WBAT)	12:24	20° 57,31' N	026° 23,90' W	5049	200
SO287_5-2	5	14.12.2021	Garretscreen	12:28	20° 57,31' N	026° 23,90' W	5300	
SO287_5-3	5	14.12.2021	Hereon-CTD	13:00	20° 57,32' N	026° 23,91' W	5299	100
SO287_5-4	5	14.12.2021	Radio sonde	13:34	20° 57,32' N	026° 23,90' W	5301	
SO287_5-5	5	14.12.2021	CTD (WBAT)	13:40	20° 57,31' N	026° 23,91' W	5048	1000
SO287_5-6	5	14.12.2021	Catamaran	14:59	20° 57,32' N	026° 23,91' W	5299	
SO287_6-1	6	14.12.2021	CTD	23:38	20° 11,98' N	028° 07,99' W	4954	200

SO287_6-2	6	15.12.2021	CTD	00:12	20° 12,00' N	028° 07,98' W	4955	4900
SO287_6-3	6	15.12.2021	Radio sonde	00:37	20° 12,01' N	028° 07,98' W	4955	
SO287_7-1	7	15.12.2021	Sun observ.	11:21	19° 26,72' N	029° 52,20' W	5071	
SO287_7-2	7	15.12.2021	CTD (WBAT)	11:42	19° 26,70' N	029° 52,20' W	4773	200
SO287_7-3	7	15.12.2021	Garretscreen	11:43	19° 26,70' N	029° 52,20' W	4784	
SO287_7-4	7	15.12.2021	CTD (WBAT)	12:22	19° 26,71' N	029° 52,21' W	4783	1000
SO287_7-5	7	15.12.2021	Ozone sonde	13:08	19° 26,70' N	029° 52,20' W	4789	
SO287_7-6	7	15.12.2021	Hereon-CTD	13:44	19° 26,71' N	029° 52,21' W	4777	100
SO287_7-7	7	15.12.2021	Catamaran	14:26	19° 26,71' N	029° 52,20' W	4786	
SO287_8-1	8	15.12.2021	CTD	22:52	18° 39,95' N	031° 34,92' W	4860	200
SO287_8-2	8	15.12.2021	CTD	23:29	18° 40,01' N	031° 34,85' W	4876	
SO287_8-3	8	15.12.2021	Radio sonde	23:46	18° 39,99' N	031° 34,84' W	4870	
SO287_9-1	9	16.12.2021	Sun observ.	10:48	17° 53,69' N	033° 16,96' W	4987	
SO287_9-2	9	16.12.2021	Zodiac	11:16	17° 53,65' N	033° 16,98' W	4976	
SO287_9-3	9	16.12.2021	CTD (WBAT)	11:22	17° 53,66' N	033° 17,00' W	4981	200
SO287_9-4	9	16.12.2021	CTD (WBAT)	12:01	17° 53,66' N	033° 17,02' W	4983	1000
SO287_9-5	9	16.12.2021	Radio sonde	13:03	17° 53,67' N	033° 17,02' W	5303	
SO287_9-6	9	16.12.2021	Zodiac	13:29	17° 53,67' N	033° 17,02' W	4989	
SO287_9-7	9	16.12.2021	Hereon-CTD	13:38	17° 53,67' N	033° 17,02' W	4994	100
SO287_9-8	9	16.12.2021	Catamaran	14:29	17° 53,67' N	033° 17,01' W	4998	
SO287_9-9	9	16.12.2021	Sun observ.	15:00	17° 54,15' N	033° 15,86' W	5081	
SO287_10-1	10	17.12.2021	CTD	00:13	17° 05,43' N	034° 57,93' W	5429	
SO287_10-2	10	17.12.2021	CTD	00:45	17° 05,44' N	034° 57,94' W	5181	5100
SO287_10-3	10	17.12.2021	Radio sonde	01:10	17° 05,43' N	034° 57,93' W	5179	
SO287_11-1	11	17.12.2021	Sun observ.	13:02	17° 03,62' N	036° 51,38' W	4760	
SO287_11-2	11	17.12.2021	CTD (WBAT)	13:25	17° 03,49' N	036° 51,81' W	5035	200
SO287_11-3	11	17.12.2021	Garretscreen	13:26	17° 03,49' N	036° 51,81' W	5040	
SO287_11-4	11	17.12.2021	Hereon-CTD	13:55	17° 03,49' N	036° 51,81' W	5053	100
SO287_11-5	11	17.12.2021	Radio sonde	14:32	17° 03,49' N	036° 51,81' W	5046	
SO287_11-6	11	17.12.2021	CTD (WBAT)	14:36	17° 03,49' N	036° 51,81' W	5045	1000
SO287_11-7	11	17.12.2021	Catamaran	15:59	17° 03,49' N	036° 51,80' W	5047	
SO287_12-1	12	18.12.2021	CTD	01:18	17° 06,69' N	038° 43,95' W	5190	200
SO287_12-2	12	18.12.2021	CTD	01:46	17° 06,70' N	038° 43,95' W	5188	5000
SO287_12-3	12	18.12.2021	Radio sonde	02:10	17° 06,68' N	038° 43,95' W	5185	
SO287_13-1	13	18.12.2021	Sun observ.	14:06	17° 07,73' N	040° 36,84' W	5032	
SO287_13-2	13	18.12.2021	Garretscreen	14:28	17° 07,75' N	040° 37,25' W	5222	
SO287_13-3	13	18.12.2021	Hereon-CTD	14:30	17° 07,75' N	040° 37,24' W	4953	100
SO287_13-4	13	18.12.2021	Ozone sonde	14:42	17° 07,74' N	040° 37,24' W	4946	
SO287_13-5	13	18.12.2021	CTD (WBAT)	15:05	17° 07,76' N	040° 37,24' W	4952	200
SO287_13-6	13	18.12.2021	CTD (WBAT)	15:35	17° 07,74' N	040° 37,24' W	4952	1000
SO287_13-7	13	18.12.2021	Catamaran	17:24	17° 07,76' N	040° 37,19' W	4971	
SO287_14-1	14	19.12.2021	CTD	02:35	17° 06,76' N	042° 30,14' W	5555	200
SO287_14-2	14	19.12.2021	CTD	03:01	17° 06,77' N	042° 30,15' W	5562	5530
SO287_14-3	14	19.12.2021	Radio sonde	03:24	17° 06,77' N	042° 30,14' W	5558	
SO287_15-1	15	19.12.2021	Hereon-CTD	14:53	17° 05,84' N	044° 16,04' W	4113	100
SO287_15-2	15	19.12.2021	Radio sonde	15:18	17° 05,82' N	044° 16,03' W	4118	
SO287_15-3	15	19.12.2021	CTD (WBAT)	15:33	17° 05,83' N	044° 16,03' W	4117	200
SO287_15-4	15	19.12.2021	Garretscreen	15:51	17° 05,83' N	044° 16,04' W	4119	
SO287_15-5	15	19.12.2021	CTD (WBAT)	16:01	17° 05,83' N	044° 16,04' W	4105	1000
SO287_15-6	15	19.12.2021	Catamaran	17:55	17° 05,85' N	044° 15,99' W	4133	
SO287_16-1	16	20.12.2021	CTD	03:33	17° 04,51' N	046° 15,86' W	4122	200
SO287_16-2	16	20.12.2021	CTD	03:59	17° 04,52' N	046° 15,86' W	3283	3248
SO287_16-3	16	20.12.2021	Radio sonde	04:20	17° 04,52' N	046° 15,86' W	3283	
SO287_17-1	17	20.12.2021	Sun observ.	14:29	17° 01,89' N	048° 06,53' W	3284	
SO287_17-2	17	20.12.2021	CTD (WBAT)	14:46	17° 01,82' N	048° 06,87' W	3997	200
SO287_17-3	17	20.12.2021	Hereon-CTD	15:37	17° 01,82' N	048° 06,86' W	4064	100
SO287_17-4	17	20.12.2021	Radio sonde	15:57	17° 01,83' N	048° 06,86' W	4058	
SO287_17-5	17	20.12.2021	CTD (WBAT)	16:19	17° 01,83' N	048° 06,88' W	4073	1000
SO287_17-6	17	20.12.2021	Garretscreen	16:37	17° 01,83' N	048° 06,86' W	4066	
SO287_17-7	17	20.12.2021	Catamaran	17:46	17° 01,84' N	048° 06,87' W	4053	
SO287_18-1	18	21.12.2021	CTD	02:43	17° 57,14' N	049° 44,99' W	4062	200
SO287_18-2	18	21.12.2021	CTD	03:09	17° 57,14' N	049° 44,99' W	4591	4400
SO287_18-3	18	21.12.2021	Radio sonde	03:27	17° 57,13' N	049° 44,98' W	4599	
SO287_19-1	18	21.12.2021	Sun observ.	14:07	19° 05,73' N	051° 11,73' W	4576	
SO287_19-2	19	21.12.2021	CTD (WBAT)	14:29	19° 06,09' N	051° 12,28' W	4287	200

SO287_19-3	19	21.12.2021	Garretscreen	14:39	19° 06,09' N	051° 12,31' W	4251	
SO287_19-4	19	21.12.2021	Hereon-CTD	15:02	19° 06,10' N	051° 12,31' W	4266	100
SO287_19-5	19	21.12.2021	Ozone sonde	15:33	19° 06,10' N	051° 12,31' W	4304	
SO287_19-6	19	21.12.2021	CTD (WBAT)	15:44	19° 06,09' N	051° 12,31' W	4312	1000
SO287_19-7	19	21.12.2021	Catamaran	17:10	19° 06,10' N	051° 12,30' W	4319	
SO287_20-1	20	22.12.2021	CTD	01:46	20° 13,91' N	052° 42,75' W	4348	200
SO287_20-2	20	22.12.2021	CTD	02:23	20° 13,92' N	052° 42,70' W	4943	4800
SO287_20-3	20	22.12.2021	Radio sonde	02:44	20° 13,92' N	052° 42,70' W	4986	
SO287_21-1	21	22.12.2021	Sun observ.	13:28	21° 20,82' N	054° 12,60' W	4996	
SO287_21-2	21	22.12.2021	Zodiac	13:28	21° 20,82' N	054° 12,60' W	5035	
SO287_21-3	21	22.12.2021	CTD (WBAT)	13:50	21° 20,98' N	054° 12,76' W	5047	200
SO287_21-4	21	22.12.2021	Heron-CTD	14:22	21° 20,98' N	054° 12,76' W	5057	100
SO287_21-5	21	22.12.2021	Radio sonde	14:52	21° 20,98' N	054° 12,76' W	5069	
SO287_21-6	21	22.12.2021	CTD (WBAT)	15:05	21° 20,97' N	054° 12,76' W	5060	1000
SO287_21-7	21	22.12.2021	Catamaran	16:51	21° 20,87' N	054° 12,60' W	5061	
SO287_22-1	22	23.12.2021	CTD	01:30	22° 37,69' N	055° 38,39' W	5048	200
SO287_22-2	22	23.12.2021	CTD	02:02	22° 37,69' N	055° 38,39' W	6238	5910
SO287_22-3	22	23.12.2021	Radio sonde	02:18	22° 37,69' N	055° 38,39' W	6008	
SO287_23-1	23	23.12.2021	Sun observ.	15:00	24° 09,10' N	056° 40,12' W		
SO287_23-2	23	23.12.2021	Zodiac	15:08	24° 09,13' N	056° 40,16' W	5757	
SO287_23-3	23	23.12.2021	CTD (WBAT)	15:25	24° 09,13' N	056° 40,15' W	5776	200
SO287_23-4	23	23.12.2021	Hereon-CTD	15:47	24° 09,13' N	056° 40,14' W	5765	100
SO287_23-5	23	23.12.2021	Radio sonde	16:03	24° 09,13' N	056° 40,14' W	5753	
SO287_23-6	23	23.12.2021	CTD (WBAT)	16:27	24° 09,13' N	056° 40,14' W	5768	
SO287_23-7	23	23.12.2021	Catamaran	18:07	24° 09,11' N	056° 40,13' W	5763	
SO287_24-1	24	24.12.2021	CTD	02:30	25° 44,37' N	057° 34,73' W	6307	200
SO287_24-2	24	24.12.2021	CTD	02:54	25° 44,36' N	057° 34,72' W	6300	
SO287_24-3	24	24.12.2021	Radio sonde	03:32	25° 44,36' N	057° 34,73' W	6300	5950
SO287_25-1	25	24.12.2021	Sun observ.	14:45	27° 20,10' N	058° 27,23' W	6479	
SO287_25-2	25	24.12.2021	CTD (WBAT)	15:06	27° 20,19' N	058° 27,19' W	6484	200
SO287_25-3	25	24.12.2021	Garretscreen	15:13	27° 20,19' N	058° 27,20' W	6487	
SO287_25-4	25	24.12.2021	Hereon-CTD	15:30	27° 20,20' N	058° 27,20' W	6485	100
SO287_25-5	25	24.12.2021	CTD (WBAT)	16:09	27° 20,20' N	058° 27,19' W	6484	1000
SO287_25-6	25	24.12.2021	Radio sonde	16:11	27° 20,20' N	058° 27,19' W	6485	
SO287_25-7	25	24.12.2021	Catamaran	17:43	27° 20,20' N	058° 27,22' W	6488	
SO287_26-1	26	25.12.2021	CTD	02:39	29° 01,44' N	059° 23,02' W	6483	200
SO287_26-2	26	25.12.2021	CTD	03:01	29° 01,51' N	059° 23,06' W	6493	5450
SO287_26-3	26	25.12.2021	Radio sonde	03:27	29° 01,51' N	059° 23,06' W	5531	
SO287_27-1	27	25.12.2021	Sun observ.	15:06	30° 34,80' N	060° 15,39' W	5536	
SO287_27-2	27	25.12.2021	CTD (WBAT)	15:26	30° 35,03' N	060° 15,51' W	5549	200
SO287_27-3	27	25.12.2021	Garretscreen	15:43	30° 35,03' N	060° 15,51' W	5538	
SO287_27-4	27	25.12.2021	Hereon-CTD	15:49	30° 35,04' N	060° 15,51' W	5492	100
SO287_27-5	27	25.12.2021	CTD (WBAT)	16:30	30° 35,03' N	060° 15,50' W	5506	1000
SO287_27-6	27	25.12.2021	Ozone sonde	16:44	30° 35,03' N	060° 15,51' W	5518	
SO287_27-7	27	25.12.2021	Catamaran	17:59	30° 35,03' N	060° 15,50' W	5513	
SO287_28-1	28	26.12.2021	CTD	12:40	28° 31,12' N	061° 36,38' W	5512	200
SO287_28-2	28	26.12.2021	CTD	13:28	28° 31,12' N	061° 36,37' W	5482	1000
SO287_28-3	28	26.12.2021	Garretscreen	13:38	28° 31,12' N	061° 36,39' W	5371	
SO287_28-4	28	26.12.2021	Hereon-CTD	15:09	28° 31,13' N	061° 36,38' W	5372	100
SO287_28-5	28	26.12.2021	Radio sonde	15:13	28° 31,13' N	061° 36,38' W	5382	
SO287_28-6	28	26.12.2021	Catamaran	15:47	28° 31,12' N	061° 36,38' W	5371	
SO287_29-1	29	27.12.2021	CTD	00:00	27° 06,85' N	062° 20,77' W	5371	200
SO287_29-2	29	27.12.2021	CTD	00:39	27° 06,86' N	062° 20,77' W	5368	5750
SO287_29-3	29	27.12.2021	Radio sonde	00:55	27° 06,85' N	062° 20,78' W	6090	
SO287_30-1	30	27.12.2021	Sun observ.	14:48	25° 23,30' N	063° 23,08' W	5836	
SO287_30-2	30	27.12.2021	CTD (WBAT)	15:02	25° 23,30' N	063° 23,08' W	5836	200
SO287_30-3	30	27.12.2021	Garretscreen	15:10	25° 23,30' N	063° 23,08' W	5714	
SO287_30-4	30	27.12.2021	Hereon-CTD	15:27	25° 23,31' N	063° 23,08' W	5718	100
SO287_30-5	30	27.12.2021	Radio sonde	15:50	25° 23,31' N	063° 23,08' W	5738	
SO287_30-6	30	27.12.2021	CTD (WBAT)	16:06	25° 23,31' N	063° 23,09' W	5718	1000
SO287_30-7	30	27.12.2021	Catamaran	17:35	25° 23,30' N	063° 23,08' W	5714	
SO287_31-1	31	28.12.2021	CTD	02:28	23° 52,37' N	064° 24,28' W	5713	200
SO287_31-2	31	28.12.2021	CTD	02:52	23° 52,37' N	064° 24,28' W	5717	5370
SO287_31-3	31	28.12.2021	Radio sonde	03:13	23° 52,37' N	064° 24,27' W	5844	
SO287_32-1	32	28.12.2021	Sun observ.	15:00	22° 14,60' N	065° 32,42' W	5465	

SO287_32-2	32	28.12.2021	Zodiac	15:07	22° 14,60' N	065° 32,40' W	5445	
SO287_32-3	32	28.12.2021	CTD (WBAT)	15:12	22° 14,60' N	065° 32,40' W	5811	200
SO287_32-4	32	28.12.2021	Hereon-CTD	15:45	22° 14,60' N	065° 32,40' W	5814	100
SO287_32-5	32	28.12.2021	CTD (WBAT)	16:26	22° 14,60' N	065° 32,40' W	5811	1000
SO287_32-6	32	28.12.2021	Radio sonde	16:48	22° 14,60' N	065° 32,34' W	6064	
SO287_32-7	32	28.12.2021	Catamaran	17:51	22° 14,61' N	065° 32,40' W	6067	
SO287_33-1	transit	29.12.2021	Catamaran	12:00	18° 47,01' N	067° 44,63' W		
SO287_34-1	transit	29.12.2021	Catamaran	17:14	17° 53,95' N	068° 21,62' W		
SO287_35-1	transit	29.12.2021	Catamaran	19:26	17° 51,78' N	068° 28,38' W		
SO287_36-1	transit	30.12.2021	Catamaran	12:00	16° 58,33' N	070° 44,58' W		
SO287_37-1	transit	30.12.2021	Catamaran	19:29	16° 38,86' N	071° 32,17' W		
SO287_37-2	transit	30.12.2021	Catamaran	19:45	16° 38,93' N	071° 31,78' W		
SO287_38-1	transit	31.12.2021	Radio sonde	04:03	16° 16,78' N	072° 27,33' W		
SO287_39-1	transit	31.12.2021	Catamaran	11:59	15° 54,34' N	073° 27,49' W		
SO287_40-1	transit	31.12.2021	Ozone sonde	16:59	15° 39,76' N	074° 05,92' W		
SO287_41-1	transit	31.12.2021	Catamaran	19:27	15° 32,81' N	074° 23,07' W		
SO287_42-1	transit	01.01.2022	Radio sonde	00:23	15° 17,47' N	074° 58,48' W		
SO287_43-1	transit	01.01.2022	Catamaran	13:57	14° 28,29' N	076° 47,77' W		
SO287_44-1	transit	01.01.2022	Radio sonde	17:55	14° 13,87' N	077° 20,09' W		
SO287_45-1	transit	01.01.2022	Catamaran	20:24	14° 05,35' N	077° 39,14' W		
SO287_46-1	transit	02.01.2022	Radio sonde	05:12	12° 58,04' N	078° 07,53' W		
SO287_47-1	transit	02.01.2022	Catamaran	12:58	12° 00,22' N	078° 36,40' W		
SO287_48-1	transit	02.01.2022	Ozone sonde	17:55	11° 24,96' N	078° 54,92' W		
SO287_49-1	transit	02.01.2022	Catamaran	20:19	11° 10,99' N	079° 01,68' W		
SO287_50-1	transit	05.01.2022	Catamaran	13:00	06° 34,25' N	081° 00,94' W		
SO287_51-1	transit	05.01.2022	Radio sonde	18:01	06° 01,86' N	081° 46,43' W		
SO287_52-1	transit	05.01.2022	Catamaran	20:25	05° 46,53' N	082° 07,63' W		
SO287_53-1	transit	06.01.2022	Radio sonde	05:15	04° 45,88' N	083° 20,09' W		
SO287_54-1	transit	06.01.2022	Catamaran	12:57	03° 34,93' N	084° 03,06' W		
SO287_55-1	transit	06.01.2022	Radio sonde	17:59	02° 52,12' N	084° 28,90' W		
SO287_56-1	transit	06.01.2022	Catamaran	20:22	02° 33,60' N	084° 44,85' W	2989	
SO287_57-1	33	07.01.2022	Hereon-CTD	02:35	02° 15,80' N	085° 49,89' W	2907	100
SO287_57-2	33	07.01.2022	CTD	02:59	02° 15,83' N	085° 49,97' W	2901	400
SO287_57-3	33	07.01.2022	CTD	03:54	02° 15,84' N	085° 49,99' W	2904	2850
SO287_57-4	33	07.01.2022	Radio sonde	04:24	02° 15,84' N	085° 49,99' W	2905	
SO287_58-1	34	07.01.2022	Sun observ.	15:37	00° 27,20' N	085° 49,96' W	2795	
SO287_58-2	34	07.01.2022	CTD (WBAT)	15:58	00° 27,21' N	085° 49,97' W	2802	200
SO287_58-3	34	07.01.2022	Garretscreen	16:58	00° 27,21' N	085° 49,97' W	2804	
SO287_58-4	34	07.01.2022	Heron-CTD	17:29	00° 27,21' N	085° 49,97' W	2807	100
SO287_58-5	34	07.01.2022	Ozone sonde	17:31	00° 27,20' N	085° 49,97' W	2802	
SO287_58-6	34	07.01.2022	CTD (WBAT)	18:07	00° 27,21' N	085° 49,98' W	2803	1000
SO287_58-7	34	07.01.2022	Catamaran	19:41	00° 27,19' N	085° 49,99' W	2800	
SO287_59-1	35	08.01.2022	Hereon-CTD	04:00	01° 20,38' S	085° 50,00' W	2458	100
SO287_59-2	35	08.01.2022	CTD	04:20	01° 20,38' S	085° 49,99' W	2456	400
SO287_59-3	35	08.01.2022	CTD	04:57	01° 20,38' S	085° 50,00' W	2456	2400
SO287_59-4	35	08.01.2022	Radio sonde	05:41	01° 20,38' S	085° 49,99' W	2460	
SO287_60-1	36	08.01.2022	CTD (WBAT)	16:14	02° 39,99' S	085° 49,90' W	3156	200
SO287_60-2	36	08.01.2022	Zodiac	16:59	02° 39,99' S	085° 49,90' W	3153	
SO287_60-3	36	08.01.2022	Radio sonde	17:13	02° 39,99' S	085° 49,89' W	3155	
SO287_60-4	36	08.01.2022	Hereon-CTD	17:31	02° 39,98' S	085° 49,89' W	3156	100
SO287_60-5	36	08.01.2022	CTD (WBAT)	18:03	02° 39,98' S	085° 49,90' W	3157	1000
SO287_60-6	36	08.01.2022	Catamaran	19:42	02° 39,99' S	085° 49,90' W	3154	

Table 7.1: Overview of the station work during SO287-CONNECT.

7.2 Profile Station List (CTD stations)

The following table covers all sampled parameters oft he CTD profiles during SO287 (the station name is in the first column indicated with SO287_XX-X). The numbers represent the following parameters:

1 – Oxygen (O_2), nutrients, halocarbons
2 – Nitrous oxide (N_2O), methane (CH_4), nitrate isotopes
3 – Nitrogen oxide (NO)
4 – Dimethylsulfide (DMS) and derivates

5 – eDNA (environmental DNA)
6 – Respiration measurements
7 – Components of dissolved organic matter (DOC – dissolved organic carbon, TDN – total dissolved nitrogen, DHAA – dissolved hydrolysable amino acids, DCCHO – dissolved organic hydrocarbons, DOP – dissolved organic phosphate)
8 – Lipids
9 – Secondary production (bacterial biomass production, BBP), extracellular enzyme activity
10 – Flow cytometry
11 – Autotrophic production (primary production, PP) including dissolved inorganic carbon (DIC), total alkalinity (TA), pH
12 – Components of dissolved organic matter (POC – particulate organic carbon, PON – particulate organic nitrogen, POP – particulate organic phosphate, BSi – biogenic silicate)
13 – Gel-like particles (TEP – transparent exopolymer particles, CSP – Coosmassie stainable particles)
14 – Confocal laser scanning microscopy (CLM)
15 – Colored dissolved organic matter (CDOM)
16 – Pigments
17 – Metagenomics
18 – Bacterial community composition (16SRNA)
19 – Microscopic phytoplankton speciation (Lugol)
20 – Ozone / dissolved organic matter

SO287 –	Bottle depth (m)	Date (UTC)	Lat (°N)	Lon (°E)	1	2	3	4	5	6	7	8	9	10	11	12	13	14	15	16	17	18	19	20
1-7	998,9	2021-12-12 14:12:23	24,55	-19,57	x	x		x			x		x	x		x	x		x		x			
1-7	699,8	2021-12-12 14:19:58	24,55	-19,57	x	x		x			x		x	x		x			x		x			
1-7	200,9	2021-12-12 14:30:46	24,55	-19,57	x	x		x	x		x		x	x		x	x		x	x	x	x		
1-7	101,6	2021-12-12 14:34:46	24,55	-19,57	x	x		x		x	x	x	x	x	x	x	x	x	x	x	x	x		
1-7	51,6	2021-12-12 14:38:15	24,55	-19,57	x	x		x	x	x	x	x	x	x	x	x	x		x				x	
1-7	8,5	2021-12-12 14:41:26	24,55	-19,57	x	x		x	x	x	x	x	x	x	x	x	x	x	x				x	
2-1	201,1	2021-12-13 00:42:28	23,69	-21,34																		x		
2-1	71,0	2021-12-13 00:47:34	23,69	-21,34																	x	x		
2-1	51,6	2021-12-13 00:49:33	23,69	-21,34																		x		
2-2	7,3	2021-12-13 00:52:46	23,69	-21,34																		x		
2-2	4341,2	2021-12-13 02:47:56	23,69	-21,34	x	x		x	x							x	x		x		x			
2-2	3494,6	2021-12-13 03:05:00	23,69	-21,34	x	x			x		x		x	x		x	x		x		x			
2-2	1998,4	2021-12-13 03:33:45	23,69	-21,34	x	x		x			x		x	x		x	x		x		x			
2-2	702,3	2021-12-13 03:57:44	23,69	-21,34	x	x					x		x	x			x		x					
2-2	203,0	2021-12-13 04:07:35	23,69	-21,34	x	x		x	x		x		x	x		x	x		x	x				
2-2	73,4	2021-12-13 04:11:22	23,69	-21,34	x	x		x		x	x	x	x	x		x	x	x	x	x				
2-2	53,6	2021-12-13 04:13:25	23,69	-21,34	x	x		x	x	x	x	x	x	x		x	x		x	x				
2-2	9,3	2021-12-13 04:16:20	23,69	-21,34	x	x		x	x	x	x	x	x	x		x	x	x	x	x				
3-4	201,2	2021-12-13 13:56:32	22,80	-23,07																	x	x		
3-4	96,4	2021-12-13 14:02:21	22,80	-23,07																	x	x		
3-4	51,2	2021-12-13 14:05:20	22,80	-23,07																	x	x		
3-4	7,7	2021-12-13 14:08:09	22,80	-23,07																	x	x		
3-5	998,6	2021-12-13 15:15:46	22,80	-23,07	x	x		x			x		x	x		x	x		x					
3-5	699,3	2021-12-13 15:23:05	22,80	-23,07	x	x		x			x		x	x		x	x		x					
3-5	201,5	2021-12-13 15:33:38	22,80	-23,07	x	x		x	x		x		x	x		x	x		x	x				

3-5	101,9	2021-12-13 15:37:01	22,80	-23,07	x	x		x		x	x	x	x	x	x	x	x	x	x	x			x	
3-5	52,0	2021-12-13 15:40:08	22,80	-23,07	x	x		x	x	x	x	x	x	x	x	x	x		x				x	
4-1	200,9	2021-12-14 00:23:18	21,91	-24,76																		x		
4-1	91,7	2021-12-14 00:28:35	21,91	-24,76																		x		
4-1	51,7	2021-12-14 00:31:51	21,91	-24,76																		x		
4-1	8,9	2021-12-14 00:34:31	21,91	-24,76																		x		
4-2	5039,9	2021-12-14 02:24:18	21,91	-24,76	x	x		x	x						x			x						
4-2	3495,1	2021-12-14 02:53:36	21,91	-24,76	x	x			x		x		x	x		x	x		x					
4-2	1998,0	2021-12-14 03:21:26	21,91	-24,76	x	x		x			x		x	x		x	x		x					
4-2	651,5	2021-12-14 03:46:40	21,91	-24,76	x	x					x		x	x			x		x					
4-2	203,4	2021-12-14 03:56:02	21,91	-24,76	x	x		x	x		x		x	x		x	x		x	x				
4-2	93,0	2021-12-14 03:59:50	21,91	-24,76	x	x		x		x	x	x	x	x		x	x	x	x	x				
4-2	53,5	2021-12-14 04:02:12	21,91	-24,76	x	x		x	x	x	x	x	x	x		x	x		x	x				
4-2	10,0	2021-12-14 04:04:43	21,91	-24,76	x	x		x	x	x	x	x	x	x		x	x	x	x	x				
5-1	201,3	2021-12-14 12:36:54	20,96	-26,40																		x		
5-1	72,5	2021-12-14 12:43:51	20,96	-26,40																		x	x	
5-1	52,4	2021-12-14 12:45:54	20,96	-26,40																		x	x	
5-1	8,2	2021-12-14 12:48:47	20,96	-26,40																		x	x	
5-5	998,7	2021-12-14 14:04:55	20,96	-26,40	x	x		x			x		x	x		x	x		x		x			
5-5	639,4	2021-12-14 14:14:00	20,96	-26,40	x	x		x			x		x	x		x	x		x		x			
5-5	200,9	2021-12-14 14:43:09	20,96	-26,40	x	x		x	x		x		x	x		x	x		x	x				
5-5	64,6	2021-12-14 14:49:54	20,96	-26,40	x	x		x		x	x	x	x	x	x	x	x	x	x	x	x			
5-5	51,7	2021-12-14 14:52:25	20,96	-26,40	x	x		x	x	x	x	x	x	x	x	x	x		x					
5-5	7,2	2021-12-14 14:55:43	20,96	-26,40	x	x		x	x	x	x	x	x	x	x	x	x	x						
6-1	200,4	2021-12-14 23:49:04	20,20	-28,13																		x		
6-1	100,9	2021-12-14 23:52:39	20,20	-28,13																		x		
6-1	51,0	2021-12-14 23:55:25	20,20	-28,13																		x		
6-1	7,9	2021-12-14 23:58:41	20,20	-28,13																		x		
6-2	4891,3	2021-12-15 01:44:10	20,20	-28,13	x	x		x	x									x						
6-2	3495,0	2021-12-15 02:11:10	20,20	-28,13	x	x					x		x	x		x	x		x					
6-2	1999,3	2021-12-15 02:38:14	20,20	-28,13	x	x		x			x		x	x		x	x		x					
6-2	562,7	2021-12-15 03:05:09	20,20	-28,13	x	x					x		x	x			x		x					
6-2	203,9	2021-12-15 03:13:05	20,20	-28,13	x	x		x	x		x		x	x		x	x		x	x				
6-2	104,0	2021-12-15 03:16:36	20,20	-28,13	x	x		x		x	x	x	x	x		x	x	x	x	x				
6-2	54,4	2021-12-15 03:19:39	20,20	-28,13	x	x		x	x	x	x	x	x	x		x	x		x	x				
6-2	10,5	2021-12-15 03:22:24	20,20	-28,13	x	x		x	x	x	x	x	x	x		x	x	x	x	x				
7-2	204,3	2021-12-15 11:51:53	19,45	-29,87																		x		
7-2	99,5	2021-12-15 11:55:28	19,45	-29,87																		x	x	
7-2	54,8	2021-12-15 11:58:13	19,45	-29,87																		x	x	
7-2	10,6	2021-12-15 12:01:09	19,45	-29,87																		x	x	
7-4	998,8	2021-12-15 12:46:45	19,45	-29,87	x	x		x			x		x	x		x	x		x		x			
7-4	550,8	2021-12-15 12:56:48	19,45	-29,87	x	x		x			x		x	x		x	x		x					
7-4	201,8	2021-12-15 13:28:31	19,45	-29,87	x	x		x	x		x		x	x		x	x		x	x				
7-4	96,9	2021-12-15 13:31:34	19,45	-29,87	x	x		x		x	x	x	x	x	x	x	x	x		x				
7-4	52,5	2021-12-15 13:34:18	19,45	-29,87	x	x		x	x	x	x	x	x	x	x	x	x		x					
7-4	8,1	2021-12-15 13:36:54	19,45	-29,87	x	x		x	x	x	x	x	x	x	x	x	x	x	x					
8-1	201,8	2021-12-15 23:02:59	18,67	-31,58																		x		
8-1	82,0	2021-12-15 23:07:12	18,67	-31,58																		x		
8-1	51,9	2021-12-15 23:09:25	18,67	-31,58																		x		

8-1	8,1	2021-12-15 23:12:16	18,67	-31,58																	x		
8-1	4789,0	2021-12-16 00:57:35	18,67	-31,58	x	x		x	x									x					
8-2	3492,4	2021-12-16 01:22:29	18,67	-31,58	x	x			x		x		x	x		x	x		x					
8-2	1997,3	2021-12-16 01:51:41	18,67	-31,58	x	x		x			x		x	x		x	x		x					
8-2	501,0	2021-12-16 02:19:33	18,67	-31,58	x	x					x		x	x		x	x		x					
8-2	202,1	2021-12-16 02:26:33	18,67	-31,58	x	x		x	x		x		x	x		x	x		x	x				
8-2	82,5	2021-12-16 02:30:26	18,67	-31,58	x	x		x		x	x	x	x	x		x	x	x	x	x				
8-2	52,3	2021-12-16 02:33:05	18,67	-31,58	x	x		x	x	x	x	x	x	x		x	x		x	x				
8-2	9,3	2021-12-16 02:36:17	18,67	-31,58	x	x		x	x	x	x	x	x	x		x	x	x	x	x				
9-3	201,6	2021-12-16 11:30:55	17,89	-33,28																	x	x		
9-3	101,9	2021-12-16 11:34:34	17,89	-33,28																	x	x	x	
9-3	52,6	2021-12-16 11:37:26	17,89	-33,28																		x	x	
9-3	8,4	2021-12-16 11:40:06	17,89	-33,28																	x	x		
9-4	999,9	2021-12-16 12:27:09	17,89	-33,28	x	x		x			x		x	x		x	x		x		x			
9-4	551,8	2021-12-16 12:39:03	17,89	-33,28	x	x		x			x		x	x		x	x		x		x			
9-4	202,3	2021-12-16 13:12:06	17,89	-33,28	x	x		x	x		x		x	x		x	x		x	x				
9-4	102,6	2021-12-16 13:15:19	17,89	-33,28	x	x		x		x	x	x	x	x	x	x	x	x	x	x				
9-4	53,0	2021-12-16 13:18:42	17,89	-33,28	x	x		x	x	x	x	x	x	x	x	x	x		x					
9-4	9,3	2021-12-16 13:21:37	17,89	-33,28	x	x		x	x	x	x	x	x	x	x	x	x	x	x					
10-1	201,7	2021-12-17 00:23:50	17,09	-34,97																		x		
10-1	92,0	2021-12-17 00:27:27	17,09	-34,97																		x		
10-1	52,4	2021-12-17 00:29:51	17,09	-34,97																		x		
10-1	8,2	2021-12-17 00:32:27	17,09	-34,97																		x		
10-2	5089,5	2021-12-17 02:21:40	17,09	-34,97	x	x		x	x						x			x		x				
10-2	3493,8	2021-12-17 02:51:20	17,09	-34,97	x	x			x		x		x	x		x	x		x					
10-2	1997,8	2021-12-17 03:20:27	17,09	-34,97	x	x		x			x		x	x		x	x		x		x			
10-2	551,3	2021-12-17 03:47:44	17,09	-34,97	x	x					x		x	x		x	x		x		x			
10-2	202,1	2021-12-17 03:55:31	17,09	-34,97	x	x		x	x		x		x	x		x	x		x	x	x			
10-2	92,5	2021-12-17 03:58:56	17,09	-34,97	x	x		x		x	x	x	x	x		x	x	x	x	x	x			
10-2	52,9	2021-12-17 04:01:28	17,09	-34,97	x	x		x	x	x	x	x	x	x		x	x		x	x				
10-2	9,4	2021-12-17 04:04:04	17,09	-34,97	x	x		x	x	x	x	x	x	x		x								
11-2	201,6	2021-12-17 13:35:21	17,06	-36,86																		x		
11-2	81,6	2021-12-17 13:39:30	17,06	-36,86																		x	x	
11-2	51,9	2021-12-17 13:41:54	17,06	-36,86																		x	x	
11-2	7,5	2021-12-17 13:44:36	17,06	-36,86																		x	x	
11-6	998,8	2021-12-17 15:02:19	17,06	-36,86	x	x		x			x		x	x		x	x		x					
11-6	380,4	2021-12-17 15:39:55	17,06	-36,86		x		x			x		x	x		x	x		x					
11-6	200,9	2021-12-17 15:44:40	17,06	-36,86	x	x		x	x		x		x	x		x	x		x	x				
11-6	96,5	2021-12-17 15:48:21	17,06	-36,86	x	x		x		x	x	x	x	x	x	x	x	x	x	x				
11-6	51,8	2021-12-17 15:51:45	17,06	-36,86	x	x		x	x	x	x	x	x	x	x	x	x		x					
11-6	7,7	2021-12-17 15:54:58	17,06	-36,86	x	x		x	x	x	x	x	x	x	x	x	x	x	x					
12-1	201,2	2021-12-18 01:30:27	17,11	-38,73																		x		
12-1	96,2	2021-12-18 01:37:53	17,11	-38,73																		x		
12-1	51,9	2021-12-18 01:40:29	17,11	-38,73																		x		
12-1	8,0	2021-12-18 01:43:01	17,11	-38,73																		x		
12-2	4989,8	2021-12-18 03:27:56	17,11	-38,73	x	x		x	x						x			x						
12-2	3494,1	2021-12-18 03:56:18	17,11	-38,73	x	x			x		x		x	x		x	x							
12-2	1997,7	2021-12-18 04:24:40	17,11	-38,73	x	x		x			x		x	x		x	x		x					
12-2	471,9	2021-12-18 04:53:57	17,11	-38,73	x	x					x		x	x		x	x		x					

12-2	203,2	2021-12-18 04:59:30	17,11	-38,73	x	x		x	x		x		x	x		x	x		x	x				
12-2	93,2	2021-12-18 05:02:34	17,11	-38,73	x	x		x		x	x	x	x	x		x	x	x	x	x				
12-2	53,0	2021-12-18 05:05:48	17,11	-38,73	x	x		x	x	x	x	x	x	x		x	x		x	x				
12-2	9,5	2021-12-18 05:08:30	17,11	-38,73	x	x		x	x	x	x	x	x	x		x	x	x	x	x				
13-5	201,8	2021-12-18 15:22:01	17,13	-40,62																	x	x		
13-5	91,3	2021-12-18 15:26:19	17,13	-40,62																	x	x	x	
13-5	51,7	2021-12-18 15:29:15	17,13	-40,62																		x	x	
13-5	6,4	2021-12-18 15:32:17	17,13	-40,62																	x	x	x	
13-6	997,9	2021-12-18 16:17:28	17,13	-40,62	x	x		x			x		x	x		x	x		x		x			
13-6	538,1	2021-12-18 16:29:42	17,13	-40,62	x	x		x			x		x	x		x	x		x		x			
13-6	200,2	2021-12-18 17:01:57	17,13	-40,62	x	x		x	x		x		x	x		x	x		x	x				
13-6	105,7	2021-12-18 17:08:36	17,13	-40,62	x	x		x		x	x	x	x	x	x	x	x	x	x	x				
13-6	51,7	2021-12-18 17:12:35	17,13	-40,62	x	x		x	x	x	x	x	x	x	x	x	x		x					
13-6	7,6	2021-12-18 17:16:05	17,13	-40,62	x	x		x	x	x	x	x	x	x	x	x	x	x	x					
14-1	201,0	2021-12-19 02:46:53	17,11	-42,50																		x		
14-1	101,0	2021-12-19 02:51:10	17,11	-42,50																		x		
14-1	51,6	2021-12-19 02:54:18	17,11	-42,50																		x		
14-1	6,6	2021-12-19 02:57:22	17,11	-42,50																		x		
14-2	5518,1	2021-12-19 05:00:21	17,11	-42,50	x	x		x	x							x			x		x			
14-2	3492,3	2021-12-19 05:39:11	17,11	-42,50	x	x			x		x		x	x		x	x		x		x			
14-2	1997,9	2021-12-19 06:08:10	17,11	-42,50	x	x		x			x		x	x		x	x		x		x			
14-2	457,8	2021-12-19 06:40:16	17,11	-42,50	x	x					x		x	x		x	x		x		x			
14-2	203,1	2021-12-19 06:46:31	17,11	-42,50	x	x		x	x		x		x	x		x	x		x	x	x			
14-2	113,7	2021-12-19 06:52:30	17,11	-42,50	x	x		x		x	x	x	x	x		x	x	x	x	x	x			
14-2	53,1	2021-12-19 06:55:55	17,11	-42,50	x	x		x	x	x	x	x	x	x		x	x		x	x				
14-2	9,5	2021-12-19 06:58:34	17,11	-42,50	x	x		x	x	x	x	x	x	x		x	x	x	x	x	x			
15-3	200,0	2021-12-19 15:49:29	17,10	-44,27																		x		
15-3	100,8	2021-12-19 15:53:11	17,10	-44,27																		x	x	
15-3	50,6	2021-12-19 15:56:07	17,10	-44,27																		x	x	
15-3	7,4	2021-12-19 15:58:50	17,10	-44,27																		x	x	
15-5	998,4	2021-12-19 16:54:28	17,10	-44,27	x	x		x			x		x	x		x	x		x					
15-5	460,7	2021-12-19 17:06:39	17,10	-44,27	x	x		x			x		x	x		x	x		x					
15-5	200,8	2021-12-19 17:13:19	17,10	-44,27	x	x		x	x		x		x	x		x	x		x	x				
15-5	111,2	2021-12-19 17:39:11	17,10	-44,27	x	x		x		x	x	x	x	x	x	x	x	x	x	x				
15-5	52,7	2021-12-19 17:43:39	17,10	-44,27	x	x		x	x	x	x	x	x	x	x	x	x		x					
15-5	8,1	2021-12-19 17:46:12	17,10	-44,27	x	x		x	x	x		x	x	x	x	x	x	x	x					
16-1	202,3	2021-12-20 03:41:13	17,08	-46,26																		x		
16-1	111,5	2021-12-20 03:50:29	17,08	-46,26																		x		
16-1	53,6	2021-12-20 03:54:09	17,08	-46,26																		x		
16-1	9,2	2021-12-20 03:56:44	17,08	-46,26																		x		
16-2	3242,6	2021-12-20 05:18:56	17,08	-46,26	x	x		x	x		x		x	x		x	x		x					
16-2	1997,2	2021-12-20 05:42:47	17,08	-46,26	x	x		x			x		x	x		x	x							
16-2	621,7	2021-12-20 06:09:07	17,08	-46,26	x	x					x		x	x		x	x		x					
16-2	202,5	2021-12-20 06:17:56	17,08	-46,26	x	x		x	x		x		x	x		x	x		x	x				
16-2	127,2	2021-12-20 06:21:19	17,08	-46,26	x	x		x		x	x	x	x	x		x	x	x	x	x				
16-2	53,1	2021-12-20 06:24:34	17,08	-46,26	x	x		x	x	x	x	x	x	x		x	x		x	x				
16-2	8,9	2021-12-20 06:27:12	17,08	-46,26	x	x		x	x	x	x	x	x	x		x	x	x	x	x				
17-2	200,6	2021-12-20 15:19:26	17,03	-48,11																	x	x		
17-2	115,2	2021-12-20 15:24:58	17,03	-48,11																	x	x	x	

17-2	51,5	2021-12-20 15:28:42	17,03	-48,11																	x	x	
17-2	7,9	2021-12-20 15:32:10	17,03	-48,11																x	x	x	
17-5	997,5	2021-12-20 16:48:33	17,03	-48,11	x	x		x			x		x	x		x	x		x		x			
17-5	519,9	2021-12-20 16:59:00	17,03	-48,11	x	x		x			x		x	x		x	x		x		x			
17-5	200,5	2021-12-20 17:07:10	17,03	-48,11	x	x		x	x		x		x	x		x	x		x	x				
17-5	121,2	2021-12-20 17:35:27	17,03	-48,11	x	x		x		x	x	x	x	x	x	x	x	x	x	x				
17-5	50,8	2021-12-20 17:39:38	17,03	-48,11	x	x		x	x	x	x	x	x	x	x	x		x						
17-5	7,0	2021-12-20 17:42:51	17,03	-48,11	x	x		x	x	x	x	x	x	x	x	x	x	x						
18-1	199,9	2021-12-21 02:56:49	17,95	-49,75																	x			
18-1	124,7	2021-12-21 03:01:09	17,95	-49,75																	x			
18-1	51,0	2021-12-21 03:04:28	17,95	-49,75																	x			
18-1	7,2	2021-12-21 03:07:09	17,95	-49,75																	x			
18-2	4390,7	2021-12-21 04:41:03	17,95	-49,75	x	x		x	x						x			x		x				
18-2	3494,9	2021-12-21 04:59:19	17,95	-49,75	x	x			x		x		x	x		x	x		x		x			
18-2	1998,0	2021-12-21 05:28:08	17,95	-49,75	x	x		x			x		x	x		x	x		x		x			
18-2	502,2	2021-12-21 05:56:24	17,95	-49,75	x	x					x		x	x		x	x		x		x			
18-2	203,4	2021-12-21 06:03:37	17,95	-49,75	x	x		x	x	x	x		x	x		x	x		x	x				
18-2	123,9	2021-12-21 06:09:23	17,95	-49,75	x	x		x	x	x	x	x	x	x		x	x	x	x	x				
18-2	54,6	2021-12-21 06:13:13	17,95	-49,75	x	x		x	x	x	x	x	x	x		x	x		x	x				
18-2	9,8	2021-12-21 06:16:32	17,95	-49,75	x	x		x	x	x	x	x	x	x		x	x	x	x	x	x			
19-2	200,9	2021-12-21 14:39:39	19,10	-51,21																	x			
19-2	115,6	2021-12-21 14:42:59	19,10	-51,21																	x	x		
19-2	50,5	2021-12-21 14:46:47	19,10	-51,21																	x	x		
19-2	7,5	2021-12-21 14:49:43	19,10	-51,21																	x	x		
19-6	998,5	2021-12-21 16:09:08	19,10	-51,21	x	x		x			x		x	x		x	x		x					
19-6	693,8	2021-12-21 16:17:18	19,10	-51,21	x	x		x			x		x	x		x	x		x					
19-6	200,7	2021-12-21 16:41:42	19,10	-51,21	x	x		x	x		x		x	x		x	x		x	x				
19-6	110,8	2021-12-21 16:59:15	19,10	-51,21	x	x		x		x	x	x	x	x	x	x	x	x	x	x				
19-6	51,0	2021-12-21 17:03:27	19,10	-51,21	x	x		x	x	x	x	x	x	x	x	x	x		x					
19-6	7,8	2021-12-21 17:07:10	19,10	-51,21	x	x		x	x	x	x	x	x	x	x	x	x	x	x					
20-1	201,6	2021-12-22 01:56:48	20,23	-52,71																	x			
20-1	121,7	2021-12-22 02:00:44	20,23	-52,71																	x			
20-1	51,6	2021-12-22 02:04:23	20,23	-52,71																	x			
20-1	8,1	2021-12-22 02:07:18	20,23	-52,71																	x			
20-2	4790,0	2021-12-22 03:57:39	20,23	-52,71	x	x		x	x						x			x						
20-2	3493,2	2021-12-22 04:22:37	20,23	-52,71	x	x			x		x		x	x		x	x		x					
20-2	1997,7	2021-12-22 04:51:52	20,23	-52,71	x	x		x			x		x	x		x	x		x					
20-2	731,6	2021-12-22 05:17:05	20,23	-52,71	x	x					x		x	x		x	x		x					
20-2	203,0	2021-12-22 05:28:08	20,23	-52,71	x	x		x	x		x		x	x		x	x		x	x				
20-2	118,7	2021-12-22 05:33:07	20,23	-52,71	x	x		x		x	x	x	x	x		x	x	x	x	x				
20-2	53,2	2021-12-22 05:37:26	20,23	-52,71	x	x		x	x	x	x	x	x	x		x	x		x	x				
20-2	9,9	2021-12-22 05:40:07	20,23	-52,71	x	x		x	x	x	x	x	x	x		x	x	x	x	x				
21-3	201,9	2021-12-22 13:59:31	21,35	-54,21																x	x			
21-3	126,8	2021-12-22 14:03:00	21,35	-54,21																x	x	x		
21-3	52,2	2021-12-22 14:06:56	21,35	-54,21																	x	x		
21-3	8,2	2021-12-22 14:09:45	21,35	-54,21																x	x	x		
21-6	999,0	2021-12-22 15:35:12	21,35	-54,21	x	x		x			x		x	x		x	x		x		x			
21-6	709,1	2021-12-22 15:42:43	21,35	-54,21	x	x		x			x		x	x		x	x		x		x			
21-6	201,2	2021-12-22 16:06:33	21,35	-54,21	x	x		x	x		x		x	x		x	x		x	x				

21-6	136,4	2021-12-22 16:23:35	21,35	-54,21	x	x		x		x	x	x	x	x	x	x	x	x	x	x				
21-6	51,8	2021-12-22 16:27:33	21,35	-54,21	x	x		x	x	x	x	x	x	x	x	x	x		x					
21-6	8,4	2021-12-22 16:30:47	21,35	-54,21	x	x		x	x	x	x	x	x	x	x	x	x	x	x					
22-1	199,9	2021-12-23 01:40:31	22,63	-55,64																		x		
22-1	105,3	2021-12-23 01:45:28	22,63	-55,64																		x		
22-1	50,5	2021-12-23 01:48:26	22,63	-55,64																		x		
22-1	6,7	2021-12-23 01:51:31	22,63	-55,64																		x		
22-2	5898,6	2021-12-23 03:55:02	22,63	-55,64	x	x		x	x						x			x		x				
22-2	3495,5	2021-12-23 04:41:12	22,63	-55,64	x	x			x		x		x	x		x	x		x		x				
22-2	1999,4	2021-12-23 05:10:15	22,63	-55,64	x	x		x			x		x	x		x	x		x		x				
22-2	762,5	2021-12-23 05:33:35	22,63	-55,64	x	x					x		x	x		x	x		x		x				
22-2	204,5	2021-12-23 05:45:06	22,63	-55,64	x	x		x	x		x		x	x		x	x		x	x	x				
22-2	110,4	2021-12-23 05:49:40	22,63	-55,64	x	x		x		x	x	x	x	x		x	x	x	x	x	x				
22-2	55,1	2021-12-23 05:52:37	22,63	-55,64	x	x		x	x	x	x	x	x	x		x	x		x	x					
22-2	11,5	2021-12-23 05:55:31	22,63	-55,64	x	x		x	x	x	x	x	x	x		x	x	x	x	x	x				
23-3	201,0	2021-12-23 15:35:02	24,15	-56,67																		x		
23-3	116,1	2021-12-23 15:38:17	24,15	-56,67																		x	x	
23-3	51,5	2021-12-23 15:42:09	24,15	-56,67																		x	x	
23-3	7,9	2021-12-23 15:45:04	24,15	-56,67																		x	x	
23-6	998,6	2021-12-23 17:00:52	24,15	-56,67	x	x		x			x		x	x		x	x		x					
23-6	849,0	2021-12-23 17:06:15	24,15	-56,67	x	x		x			x		x	x		x	x		x					
23-6	201,0	2021-12-23 17:32:35	24,15	-56,67	x	x		x	x		x		x	x		x	x		x	x				
23-6	116,5	2021-12-23 17:46:23	24,15	-56,67	x	x		x		x	x	x	x	x	x	x	x	x	x	x				
23-6	51,9	2021-12-23 17:50:33	24,15	-56,67	x	x		x	x	x	x	x	x	x	x	x	x		x					
23-6	8,0	2021-12-23 17:53:33	24,15	-56,67	x	x		x	x	x	x	x	x	x	x	x	x	x	x					
24-1	201,0	2021-12-24 02:39:52	25,74	-57,58																		x		
24-1	119,5	2021-12-24 02:45:17	25,74	-57,58																		x		
24-1	51,9	2021-12-24 02:49:06	25,74	-57,58																		x		
24-1	8,2	2021-12-24 02:52:09	25,74	-57,58																		x		
24-2	5937,0	2021-12-24 04:55:43	25,74	-57,58	x	x		x	x						x			x							
24-2	3494,8	2021-12-24 05:41:34	25,74	-57,58	x	x		x			x		x	x		x	x								
24-2	1998,2	2021-12-24 06:11:13	25,74	-57,58	x	x		x			x		x	x		x	x		x						
24-2	831,2	2021-12-24 06:34:08	25,74	-57,58	x	x					x		x	x		x	x		x						
24-2	203,5	2021-12-24 06:46:43	25,74	-57,58	x	x		x	x		x		x	x		x	x		x	x					
24-2	114,5	2021-12-24 06:51:14	25,74	-57,58	x	x		x		x	x	x	x	x		x	x	x	x	x					
24-2	54,8	2021-12-24 06:54:27	25,74	-57,58	x	x		x	x	x	x	x	x	x		x	x		x						
24-2	10,4	2021-12-24 06:57:42	25,74	-57,58	x	x		x	x	x	x	x	x	x		x	x	x	x	x					
25-2	201,6	2021-12-24 15:16:48	27,34	-58,45																	x	x			
25-2	121,0	2021-12-24 15:20:36	27,34	-58,45															x		x	x	x		
25-2	52,4	2021-12-24 15:25:13	27,34	-58,45																		x	x		
25-2	8,0	2021-12-24 15:27:54	27,34	-58,45																	x	x	x		
25-5	998,2	2021-12-24 16:44:32	27,34	-58,45	x	x		x			x		x	x		x	x		x		x				
25-5	898,3	2021-12-24 16:48:34	27,34	-58,45	x	x		x			x		x	x		x	x		x		x				
25-5	201,4	2021-12-24 17:15:44	27,34	-58,45	x	x		x	x		x		x	x		x	x		x	x					
25-5	113,3	2021-12-24 17:31:08	27,34	-58,45	x	x		x		x	x	x	x	x	x	x	x	x	x	x					
25-5	51,6	2021-12-24 17:35:18	27,34	-58,45	x	x		x	x	x	x	x	x	x	x	x	x		x						
25-5	7,7	2021-12-24 17:38:21	27,34	-58,45	x	x		x	x	x	x	x	x	x	x	x	x	x	x						
26-1	201,3	2021-12-25 02:48:51	29,02	-59,38																		x		
26-1	112,3	2021-12-25 02:52:44	29,02	-59,38																		x		

26-1	51,6	2021-12-25 02:56:34	29,02	-59,38																		x		
26-1	7,9	2021-12-25 02:59:22	29,03	-59,38																		x		
26-2	5437,6	2021-12-25 04:53:42	29,03	-59,38	x	x		x	x						x			x						
26-2	3495,3	2021-12-25 05:30:41	29,03	-59,38	x	x			x		x		x	x		x	x		x						
26-2	1997,7	2021-12-25 05:58:35	29,03	-59,38	x	x		x			x		x	x		x	x		x		x				
26-2	780,7	2021-12-25 06:21:33	29,03	-59,38	x	x					x		x	x		x	x		x		x				
26-2	203,7	2021-12-25 06:32:50	29,03	-59,38	x	x		x	x		x		x	x		x	x		x	x					
26-2	113,3	2021-12-25 06:36:21	29,03	-59,38	x	x		x		x	x	x	x	x		x	x	x	x	x	x				
26-2	53,9	2021-12-25 06:39:46	29,03	-59,38	x	x		x	x	x	x	x	x	x		x	x		x	x					
26-2	9,8	2021-12-25 06:42:20	29,03	-59,38	x	x		x	x	x	x	x	x	x		x	x	x	x	x	x				
27-2	200,2	2021-12-25 15:36:28	30,58	-60,26																		x		
27-2	106,5	2021-12-25 15:40:37	30,58	-60,26																		x	x	
27-2	51,0	2021-12-25 15:43:42	30,58	-60,26																		x	x	
27-2	7,2	2021-12-25 15:46:26	30,58	-60,26																		x	x	
27-5	998,0	2021-12-25 17:01:17	30,58	-60,26	x	x		x			x		x	x		x	x		x						
27-5	819,7	2021-12-25 17:06:39	30,58	-60,26	x	x		x			x		x	x		x	x		x						
27-5	201,8	2021-12-25 17:42:40	30,58	-60,26	x	x		x	x		x		x	x		x	x		x	x					
27-5	106,3	2021-12-25 17:48:48	30,58	-60,26	x	x		x		x	x	x	x	x	x	x	x	x	x	x					
27-5	51,7	2021-12-25 17:52:26	30,58	-60,26	x	x		x	x	x	x	x	x	x	x	x	x		x						
27-5	8,2	2021-12-25 17:56:31	30,58	-60,26	x	x		x	x	x	x	x	x	x	x	x	x	x	x						
28-1	201,1	2021-12-26 12:52:08	28,52	-61,61																	x	x			
28-1	106,8	2021-12-26 12:56:30	28,52	-61,61																	x	x	x		
28-1	51,5	2021-12-26 12:59:45	28,52	-61,61																		x	x		
28-1	7,6	2021-12-26 13:02:49	28,52	-61,61																	x	x	x		
28-2	999,0	2021-12-26 13:53:52	28,52	-61,61	x	x		x			x		x	x		x	x		x		x				
28-2	769,7	2021-12-26 14:00:59	28,52	-61,61	x	x		x			x		x	x		x	x		x		x				
28-2	201,1	2021-12-26 14:25:33	28,52	-61,61	x	x		x	x		x		x	x		x	x		x	x					
28-2	102,2	2021-12-26 14:40:41	28,52	-61,61	x	x		x		x	x	x	x	x	x	x	x	x	x	x					
28-2	52,9	2021-12-26 14:44:44	28,52	-61,61	x	x		x	x	x	x	x	x	x	x	x	x		x						
28-2	8,6	2021-12-26 14:48:45	28,52	-61,61	x	x		x	x	x	x	x	x	x	x	x	x	x	x						
29-1	201,5	2021-12-27 00:09:40	27,11	-62,35																		x		
29-1	114,4	2021-12-27 00:15:51	27,11	-62,35																		x		
29-1	52,1	2021-12-27 00:19:19	27,11	-62,35																		x		
29-1	8,0	2021-12-27 00:22:11	27,11	-62,35																		x		
29-2	5737,6	2021-12-27 02:26:23	27,11	-62,35	x	x		x	x						x			x		x				
29-2	3493,2	2021-12-27 03:11:21	27,11	-62,35	x	x			x		x		x	x		x	x		x		x				
29-2	1998,2	2021-12-27 03:41:15	27,11	-62,35	x	x		x			x		x	x		x	x		x		x				
29-2	811,6	2021-12-27 04:04:41	27,11	-62,35	x	x					x		x	x		x	x		x		x				
29-2	203,7	2021-12-27 04:17:02	27,11	-62,35	x	x		x	x		x		x	x		x	x		x	x	x				
29-2	111,7	2021-12-27 04:20:48	27,11	-62,35	x	x		x		x	x	x	x	x		x	x	x	x	x	x				
29-2	54,2	2021-12-27 04:24:18	27,11	-62,35	x	x		x	x	x	x	x	x	x		x	x		x	x					
29-2	9,5	2021-12-27 04:26:59	27,11	-62,35	x	x		x	x	x	x	x	x	x		x	x	x	x	x	x				
30-2	200,5	2021-12-27 15:14:05	25,39	-63,38																		x		
30-2	111,1	2021-12-27 15:18:10	25,39	-63,38																	x	x	x		
30-2	51,8	2021-12-27 15:21:49	25,39	-63,38																		x	x		
30-2	7,8	2021-12-27 15:24:59	25,39	-63,38																		x	x		
30-6	998,9	2021-12-27 16:38:35	25,39	-63,38	x	x		x			x		x	x		x	x		x						
30-6	838,5	2021-12-27 16:43:36	25,39	-63,38	x	x		x			x		x	x		x	x		x						
30-6	201,3	2021-12-27 17:20:30	25,39	-63,38	x	x		x	x		x		x	x		x	x		x	x					

30-6	121,5	2021-12-27 17:25:28	25,39	-63,38	x	x		x		x	x	x	x	x	x	x	x	x	x				
30-6	51,4	2021-12-27 17:29:49	25,39	-63,38	x	x		x	x	x	x	x	x	x	x	x		x					
30-6	8,1	2021-12-27 17:33:12	25,39	-63,38	x	x		x	x	x	x	x	x	x	x	x	x	x					
31-1	202,5	2021-12-28 02:38:41	23,87	-64,40																	x		
31-1	122,9	2021-12-28 02:42:04	23,87	-64,40																	x		
31-1	52,7	2021-12-28 02:45:48	23,87	-64,40																	x		
31-1	9,4	2021-12-28 02:49:19	23,87	-64,40																	x		x
31-2	5357,9	2021-12-28 04:46:20	23,87	-64,40	x	x		x	x						x			x					
31-2	3492,6	2021-12-28 05:21:09	23,87	-64,40	x	x			x		x		x	x		x	x		x				
31-2	1997,7	2021-12-28 05:49:16	23,87	-64,40	x	x		x			x		x	x		x	x		x				
31-2	860,5	2021-12-28 06:11:43	23,87	-64,40	x	x					x		x	x		x	x		x				
31-2	203,3	2021-12-28 06:24:39	23,87	-64,40	x	x		x	x		x		x	x		x	x		x	x			
31-2	124,0	2021-12-28 06:29:11	23,87	-64,40	x	x		x		x	x	x	x	x		x	x	x	x	x			
31-2	53,5	2021-12-28 06:32:42	23,87	-64,40	x	x		x	x	x	x	x	x	x		x	x		x	x			
31-2	10,1	2021-12-28 06:35:35	23,87	-64,40	x	x		x	x	x	x	x	x	x		x	x	x	x	x			
32-3	200,1	2021-12-28 15:21:39	22,24	-65,54																	x	x		
32-3	115,3	2021-12-28 15:25:37	22,24	-65,54																	x	x	x	
32-3	50,7	2021-12-28 15:30:10	22,24	-65,54																		x	x	
32-3	7,4	2021-12-28 15:33:10	22,24	-65,54																	x	x	x	
32-5	998,7	2021-12-28 16:52:55	22,24	-65,54	x	x		x			x		x	x		x	x		x		x			
32-5	793,0	2021-12-28 16:59:09	22,24	-65,54	x	x		x			x		x	x		x	x		x		x			
32-5	201,2	2021-12-28 17:35:37	22,24	-65,54	x	x		x	x		x		x	x		x	x		x	x				
32-5	126,9	2021-12-28 17:41:19	22,24	-65,54	x	x		x		x	x	x	x	x	x	x	x	x	x	x				
32-5	51,7	2021-12-28 17:45:12	22,24	-65,54	x	x		x	x	x	x	x	x	x	x	x	x		x					
32-5	8,1	2021-12-28 17:48:35	22,24	-65,54	x	x		x	x	x	x	x	x	x	x	x	x	x	x					
57-2	350,1	2022-01-07 03:16:31	2,26	-85,83														x						
57-2	350,8	2022-01-07 03:16:40	2,26	-85,83																	x	x		
57-2	201,1	2022-01-07 03:21:05	2,26	-85,83																	x	x		
57-2	50,8	2022-01-07 03:35:56	2,26	-85,83																	x	x		
57-2	35,1	2022-01-07 03:28:35	2,26	-85,83																	x	x		
57-2	8,0	2022-01-07 03:31:00	2,26	-85,83																	x	x	x	
57-3	2845,9	2022-01-07 04:51:25	2,26	-85,83	x	x	x	x							x			x		x				
57-3	1997,5	2022-01-07 05:08:57	2,26	-85,83	x	x	x	x			x			x		x	x		x		x			
57-3	999,9	2022-01-07 05:28:25	2,26	-85,83	x	x	x	x			x			x		x	x		x					
57-3	502,2	2022-01-07 05:39:15	2,26	-85,83	x															x				
57-3	351,9	2022-01-07 05:43:21	2,26	-85,83	x	x	x				x			x		x	x		x		x			
57-3	203,0	2022-01-07 05:47:32	2,26	-85,83	x	x	x	x			x			x		x	x		x	x	x			
57-3	52,9	2022-01-07 05:52:04	2,26	-85,83	x	x	x	x			x	x		x		x	x		x	x	x			
57-3	35,8	2022-01-07 05:56:13	2,26	-85,83	x	x	x	x			x	x		x		x	x		x	x	x			
57-3	10,2	2022-01-07 05:58:25	2,26	-85,83	x	x	x	x			´	x		x		x	x		x	x	x			
58-2	201,6	2022-01-07 16:08:47	0,45	-85,83																x	x	x		
58-2	71,9	2022-01-07 16:14:29	0,45	-85,83																x	x	x		
58-2	52,7	2022-01-07 16:16:45	0,45	-85,83																x	x	x		
58-2	8,5	2022-01-07 16:19:52	0,45	-85,83																x	x	x		
58-6	998,1	2022-01-07 18:32:25	0,45	-85,83	x	x	x	x			x			x		x	x		x		x			
58-6	400,4	2022-01-07 18:45:21	0,45	-85,83	x	x	x	x			x			x		x	x		x		x		x	
58-6	201,5	2022-01-07 19:02:44	0,45	-85,83	x	x	x	x	x		x			x		x	x		x	x				
58-6	70,2	2022-01-07 19:12:24	0,45	-85,83	x	x	x	x			x	x		x		x	x		x	x				
58-6	51,1	2022-01-07 19:15:11	0,45	-85,83	x	x	x	x	x		x	x		x		x	x		x					

58-6	8,0	2022-01-07 19:31:03	0,45	-85,83	x	x	x	x	x		x	x		x		x	x		x					
59-2	350,9	2022-01-08 04:38:20	-1,34	-85,83															x			x	x	
59-2	201,8	2022-01-08 04:43:16	-1,34	-85,83																		x	x	
59-2	52,0	2022-01-08 04:48:40	-1,34	-85,83																		x	x	
59-2	29,9	2022-01-08 04:52:16	-1,34	-85,83																		x	x	
59-2	8,3	2022-01-08 04:54:37	-1,34	-85,83																		x	x	
59-3	2395,0	2022-01-08 06:04:10	-1,34	-85,83	x	x	x	x	x							x			x		x			
59-3	1996,0	2022-01-08 06:12:42	-1,34	-85,83	x	x	x	x			x			x		x			x		x			
59-3	998,8	2022-01-08 06:32:28	-1,34	-85,83	x	x	x		x		x			x		x			x					
59-3	500,7	2022-01-08 06:42:30	-1,34	-85,83	x																x			
59-3	331,3	2022-01-08 06:46:56	-1,34	-85,83	x	x	x				x			x		x			x		x			
59-3	201,7	2022-01-08 06:50:30	-1,34	-85,83	x	x	x	x	x		x			x		x			x	x	x			
59-3	52,2	2022-01-08 06:55:01	-1,34	-85,83	x	x	x	x	x		x	x		x		x			x	x	x			
59-3	30,5	2022-01-08 06:58:27	-1,34	-85,83	x	x	x	x			x	x		x		x			x	x	x			
59-3	8,5	2022-01-08 07:01:07	-1,34	-85,83	x	x	x	x	x		x	x		x		x			x	x	x			
60-1	201,0	2022-01-08 16:25:24	-2,67	-85,83																		x	x	
60-1	50,7	2022-01-08 16:30:05	-2,67	-85,83																		x	x	
60-1	23,0	2022-01-08 16:34:19	-2,67	-85,83																		x	x	
60-1	7,9	2022-01-08 16:36:32	-2,67	-85,83																		x	x	
60-5	998,1	2022-01-08 18:37:03	-2,67	-85,83	x	x	x	x			x			x		x	x		x		x			
60-5	365,6	2022-01-08 18:53:31	-2,67	-85,83	x	x	x	x			x			x		x	x		x		x		x	
60-5	199,9	2022-01-08 19:11:19	-2,67	-85,83	x	x	x	x			x			x		x	x		x	x	x			
60-5	51,3	2022-01-08 19:17:01	-2,67	-85,83	x	x	x	x			x	x		x		x	x		x	x	x			
60-5	33,5	2022-01-08 19:32:06	-2,67	-85,83	x	x	x	x			x	x		x		x	x		x		x			
60-5	7,5	2022-01-08 19:34:41	-2,67	-85,83	x	x	x	x	x		x	x		x		x	x		x		x			

7.3 Sample Station List (underway samples)

The following table gives an overview of samples taken from the ships' moonpool (underway samples).

Date	Hours	Sample ID	Lat	Lon	DMS	Hal.	N2O/CH4	Nuts	eDNA	Air	O_2	Pig.	NO	Ozone/DOM
UTC	UTC		°N	°E										
11.12.2021	18	28700003	26,92	-16,47		x								
12.12.2021	0	28700005	26,01	-17,67		x								
12.12.2021	6	28700007	25,08	-18,88		x								x
12.12.2021	9	28700008	24,61	-19,50	x									
12.12.2021	12	28700009	24,55	-19,57		x								
12.12.2021	15	28700010	24,55	-19,57	x									
12.12.2021	18	28700011	24,41	-19,86	x	x				x				
12.12.2021	21	28700012	24,07	-20,56	x									
13.12.2021	0	28700013	23,73	-21,26	x	x		x		x				
13.12.2021	3	28700014	23,69	-21,34	x			x						
13.12.2021	6	28700015	23,52	-21,67	x	x		x		x			x	x
13.12.2021	9	28700016	23,17	-22,35	x		x	x						
13.12.2021	12	28700017	22,81	-23,04	x	x		x		x			x	
13.12.2021	15	28700018	22,80	-23,07	x		x	x			x			
13.12.2021	18	28700019	22,61	-23,41	x	x		x		x			x	
13.12.2021	21	28700020	22,26	-24,08	x			x						
14.12.2021	0	28700021	21,91	-24,75	x	x		x		x				
14.12.2021	3	28700022	21,91	-24,76	x			x					x	
14.12.2021	6	28700023	21,70	-25,12	x	x		x		x			x	x

14.12.2021	9	28700024	21,31	-25,79	x			x				x	x	
14.12.2021	12	28700025	20,96	-26,40	x	x	x	x		x			x	
14.12.2021	15	28700026	20,96	-26,40	x			x				x	x	
14.12.2021	18	28700027	20,74	-26,90	x	x		x		x		x	x	
14.12.2021	21	28700028	20,45	-27,57	x			x				x		
15.12.2021	0	28700029	20,20	-28,13	x			x		x				
15.12.2021	3	28700030	20,20	-28,13	x			x				x	x	
15.12.2021	6	28700031	19,98	-28,65	x	x		x		x		x	x	x
15.12.2021	9	28700032	19,67	-29,34	x			x					x	
15.12.2021	12	28700033	19,45	-29,87	x	x		x		x			x	
15.12.2021	15	28700034	19,46	-29,85	x		x	x					x	
15.12.2021	18	28700035	19,15	-30,53	x	x		x		x		x	x	
15.12.2021	21	28700036	18,84	-31,21	x			x						
16.12.2021	0	28700037	18,67	-31,58		x		x		x				
16.12.2021	3	28700038	18,68	-31,60	x								x	
16.12.2021	6	28700039	18,35	-32,27	x	x		x		x		x	x	x
16.12.2021	9	28700040	18,05	-32,94	x			x					x	
16.12.2021	12	28700041	17,89	-33,28	x			x		x			x	
16.12.2021	15	28700042	17,90	-33,26	x	x	x	x				x	x	
16.12.2021	18	28700043	17,66	-33,77	x	x		x		x		x	x	
16.12.2021	21	28700044	17,38	-34,36	x			x						
17.12.2021	0	28700045	17,10	-34,94	x	x		x		x				
17.12.2021	3	28700046	17,09	-34,97	x			x				x	x	
17.12.2021	6	28700047	17,09	-35,32	x	x		x		x		x	x	x
17.12.2021	9	28700048	17,07	-35,99	x	x		x					x	
17.12.2021	12	28700049	17,06	-36,65	x	x		x		x			x	
17.12.2021	15	28700050	17,06	-36,86	x		x	x				x	x	
17.12.2021	18	28700051	17,07	-37,15	x	x		x		x		x	x	
17.12.2021	21	28700052	17,09	-37,82	x			x						
18.12.2021	0	28700053	17,10	-38,47	x	x		x		x				
18.12.2021	3	28700054	17,11	-38,73	x			x				x		
18.12.2021	6	28700055	17,12	-38,86	x	x		x		x		x	x	x
18.12.2021	9	28700056	17,12	-39,53	x			x					x	
18.12.2021	12	28700057	17,13	-40,18	x	x		x		x				
18.12.2021	15	28700058	17,13	-40,62	x		x	x				x		
18.12.2021	18	28700059	17,15	-40,60	x	x		x		x		x	x	
18.12.2021	21	28700060	17,12	-41,29	x			x				x	x	
19.12.2021	0	28700061	17,12	-41,99	x	x		x		x				
19.12.2021	3	28700062	17,11	-42,50	x			x						
19.12.2021	6	28700063	17,11	-42,50	x	x		x		x		x	x	x
19.12.2021	9	28700064	17,11	-42,90	x			x				x	x	
19.12.2021	12	28700065	17,10	-43,61	x	x		x		x			x	
19.12.2021	15	28700066	17,10	-44,27			x	x						
19.12.2021	18	28700067	17,10	-44,26	x	x		x		x				
19.12.2021	21	28700068	17,09	-44,83	x			x				x		
20.12.2021	0	28700069	17,08	-45,54	x	x		x		x				
20.12.2021	3	28700070	17,08	-46,24	x			x						
20.12.2021	6	28700071	17,08	-46,26	x	x		x		x		x		x
20.12.2021	9	28700072	17,06	-46,83	x			x				x	x	
20.12.2021	12	28700073	17,04	-47,55	x	x		x		x			x	
20.12.2021	15	28700074	17,03	-48,11	x			x					x	
20.12.2021	18	28700075	17,03	-48,11	x	x	x	x		x		x		
20.12.2021	21	28700076	17,33	-48,64	x			x				x		
21.12.2021	0	28700077	17,68	-49,27	x	x		x		x				
21.12.2021	3	28700078	17,95	-49,75	x			x						
21.12.2021	6	28700079	17,95	-49,75	x	x		x		x		x		x
21.12.2021	9	28700080	18,32	-50,22				x				x	x	
21.12.2021	12	28700081	18,78	-50,80	x	x		x		x			x	
21.12.2021	15	28700082	19,10	-51,21	x		x	x					x	
21.12.2021	18	28700083	19,13	-51,20	x	x		x		x				

21.12.2021	21	28700084	19,55	-51,80	x			x				x	x	
22.12.2021	0	28700085	19,99	-52,39	x	x		x		x				
22.12.2021	3	28700086	20,23	-52,71				x				x		
22.12.2021	6	28700087	20,25	-52,72	x	x		x		x		x	x	x
22.12.2021	9	28700088	20,69	-53,32	x			x				x	x	
22.12.2021	12	28700089	21,15	-53,95	x	x		x		x			x	
22.12.2021	15	28700090	21,35	-54,21	x		x	x				x	x	
22.12.2021	18	28700091	21,43	-54,30	x	x		x		x		x	x	
22.12.2021	21	28700092	21,92	-54,86	x			x				x	x	
23.12.2021	0	28700093	22,42	-55,40	x	x		x		x				
23.12.2021	3	28700094	22,63	-55,64				x						
23.12.2021	6	28700095	22,63	-55,64	x	x		x		x		x	x	x
23.12.2021	9	28700096	23,18	-56,01	x			x				x	x	
23.12.2021	12	28700097	23,78	-56,42	x	x		x		x			x	
23.12.2021	15	28700098	24,15	-56,67			x	x					x	
23.12.2021	18	28700099	24,15	-56,67	x	x		x		x		x	x	
23.12.2021	21	28700100	24,59	-56,92	x			x				x	x	
24.12.2021	0	28700101	25,23	-57,29	x	x		x		x				
24.12.2021	3	28700102	25,74	-57,58	x			x						
24.12.2021	6	28700103	25,74	-57,58	x	x		x		x		x	x	x
24.12.2021	9	28700104	26,11	-57,78	x			x				x	x	
24.12.2021	12	28700105	26,77	-58,14	x	x		x		x			x	
24.12.2021	15	28700106	27,34	-58,45			x	x					x	
24.12.2021	18	28700107	27,34	-58,46	x	x		x		x		x		
24.12.2021	21	28700108	27,91	-58,77				x						
25.12.2021	0	28700109	28,52	-59,11	x	x				x				
25.12.2021	3	28700110	29,03	-59,38	x			x						
25.12.2021	6	28700111	29,03	-59,38	x	x		x		x		x		x
25.12.2021	9	28700112	29,45	-59,62	x			x				x	x	
25.12.2021	12	28700113	30,03	-59,95	x	x		x		x			x	
25.12.2021	15	28700114	30,57	-60,25	x		x	x				x	x	
25.12.2021	18	28700115	30,58	-60,26	x	x		x		x		x		
25.12.2021	21	28700116	30,19	-60,51				x						
26.12.2021	0	28700117	29,69	-60,85						x				
26.12.2021	6	28700119	28,71	-61,48		x				x			x	x
26.12.2021	9	28700120	28,52	-61,61	x								x	
26.12.2021	12	28700121	28,52	-61,61		x		x		x			x	
26.12.2021	15	28700122	28,52	-61,61	x		x						x	
26.12.2021	18	28700123	28,20	-61,78		x		x		x		x	x	
26.12.2021	21	28700124	27,65	-62,06	x								x	
27.12.2021	0	28700125	27,11	-62,35	x	x		x		x				
27.12.2021	3	28700126	27,11	-62,35	x			x				x		
27.12.2021	6	28700127	26,88	-62,49	x	x		x		x			x	x
27.12.2021	9	28700128	26,39	-62,79	x			x					x	
27.12.2021	12	28700129	25,86	-63,11	x	x		x		x			x	
27.12.2021	15	28700130	25,39	-63,38			x	x				x	x	
27.12.2021	18	28700131	25,40	-63,40		x		x		x				
27.12.2021	21	28700132	24,85	-63,75	x							x	x	
28.12.2021	0	28700133	24,35	-64,09	x	x		x		x				
28.12.2021	3	28700134	23,87	-64,40	x									
28.12.2021	6	28700135	23,87	-64,40	x	x				x		x	x	x
28.12.2021	9	28700136	23,43	-64,71	x							x	x	
28.12.2021	12	28700137	22,82	-65,14	x					x			x	
28.12.2021	15	28700138	22,24	-65,54	x		x	x						
28.12.2021	18	28700139	22,24	-65,54	x	x				x		x		
28.12.2021	21	28700140	21,91	-66,02	x			x					x	
29.12.2021	0	28700141	21,29	-66,41	x			x		x				
29.12.2021	3	28700142	20,67	-66,81	x			x						
29.12.2021	6	28700143	20,04	-67,20	x	x		x		x			x	x
29.12.2021	9	28700144	19,42	-67,57	x			x				x	x	

29.12.2021	12	28700145	18,78	-67,74	x	x		x		x		x	x	
29.12.2021	15	28700146	18,33	-68,11	x		x	x				x		
29.12.2021	18	28700147	17,90	-68,35	x	x		x	x	x		x		
29.12.2021	21	28700148	17,81	-68,60	x			x				x		
30.12.2021	0	28700149	17,64	-69,04	x	x		x		x				
30.12.2021	3	28700150	17,47	-69,47	x			x						
30.12.2021	6	28700151	17,30	-69,90	x	x		x	x	x				x
30.12.2021	9	28700152	17,12	-70,34	x			x				x	x	
30.12.2021	12	28700153	16,97	-70,74	x	x		x		x		x	x	
30.12.2021	15	28700154	16,83	-71,07	x		x	x				x		
30.12.2021	18	28700155	16,71	-71,38	x	x		x	x	x		x		
30.12.2021	21	28700156	16,65	-71,52	x			x				x	x	
31.12.2021	0	28700157	16,49	-71,95	x	x		x		x				
31.12.2021	3	28700158	16,34	-72,32	x			x						
31.12.2021	6	28700159	16,18	-72,72	x	x		x	x	x				x
31.12.2021	9	28700160	16,04	-73,09	x			x				x	x	
31.12.2021	12	28700161	15,91	-73,46	x	x		x		x		x	x	
31.12.2021	15	28700162	15,77	-73,82	x		x	x				x	x	
31.12.2021	18	28700163	15,63	-74,19	x	x		x	x	x		x	x	
31.12.2021	21	28700164	15,46	-74,58				x						
1.1.2022	0	28700165	15,29	-74,98		x				x				
1.1.2022	3	28700166	15,14	-75,31										
1.1.2022	6	28700167	14,95	-75,73		x			x	x				x
1.1.2022	9	28700168	14,76	-76,15								x	x	
1.1.2022	12	28700169	14,57	-76,57	x	x				x		x	x	
1.1.2022	15	28700170	14,42	-76,92			x	x				x	x	
1.1.2022	18	28700171	14,23	-77,34	x			x	x	x		x	x	
1.1.2022	21	28700172	14,06	-77,70	x			x				x		
2.1.2022	0	28700173	13,63	-77,85	x	x		x		x				
2.1.2022	3	28700174	13,26	-78,01	x			x						
2.1.2022	6	28700175	12,86	-78,17	x	x		x	x	x				x
2.1.2022	9	28700176	12,45	-78,36	x			x						
2.1.2022	12	28700177	12,10	-78,55	x	x		x		x		x		
2.1.2022	15	28700178	11,76	-78,73	x		x	x				x	x	
2.1.2022	18	28700179	11,41	-78,92	x	x		x	x	x				
2.1.2022	21	28700180	11,14	-79,06	x			x						
3.1.2022	0	28700181	10,87	-79,21	x	x		x						
3.1.2022	3	28700182	10,59	-79,35	x			x						
3.1.2022	6	28700183	10,28	-79,52	x	x		x	x					x
3.1.2022	9	28700184	9,96	-79,69				x						
4.1.2022	6	28700191	8,87	-79,53										x
5.1.2022	0	28700197	8,88	-79,52	x								x	
5.1.2022	3	28700198	8,24	-79,46	x			x						
5.1.2022	6	28700199	7,55	-79,66	x			x						x
5.1.2022	9	28700200	6,99	-80,22	x			x						
5.1.2022	12	28700201	6,69	-80,87	x	x		x				x	x	
5.1.2022	15	28700202	6,39	-81,28	x		x	x				x	x	
5.1.2022	18	28700203	6,03	-81,77	x	x		x	x	x		x	x	
5.1.2022	21	28700204	5,75	-82,17	x			x				x	x	
6.1.2022	0	28700205	5,41	-82,63	x	x		x		x				
6.1.2022	3	28700206	5,08	-83,09	x	x		x						
6.1.2022	6	28700207	4,65	-83,40		x		x	x	x				x
6.1.2022	9	28700208	4,18	-83,69	x	x							x	
6.1.2022	12	28700209	3,71	-83,98	x	x		x		x		x	x	
6.1.2022	15	28700210	3,32	-84,21	x	x	x	x				x	x	
6.1.2022	18	28700211	2,87	-84,48	x	x		x		x			x	
6.1.2022	21	28700212	2,54	-84,80	x	x		x		x				
7.1.2022	0	28700213	2,41	-85,30	x	x		x		x				
7.1.2022	3	28700214	2,26	-85,83		x		x					x	
7.1.2022	6	28700215	2,26	-85,83	x	x				x				x

7.1.2022	9	28700216	1,69	-85,83	x			x					
7.1.2022	12	28700217	1,10	-85,83	x	x		x		x		x	
7.1.2022	15	28700218	0,54	-85,83	x			x				x	
7.1.2022	18	28700219	0,45	-85,83	x	x		x		x	x		
7.1.2022	21	28700220	0,26	-85,84	x	x		x		x			
8.1.2022	0	28700221	-0,44	-85,81	x	x		x		x		x	
8.1.2022	3	28700222	-1,16	-85,81	x	x		x		x			
8.1.2022	6	28700223	-1,34	-85,83	x	x		x		x			
8.1.2022	9	28700224	-1,77	-85,83	x	x		x					
8.1.2022	12	28700225	-2,48	-85,83	x	x		x		x		x	
8.1.2022	15	28700226	-2,67	-85,83	x	x		x		x		x	
8.1.2022	18	28700227	-2,67	-85,83		x		x		x			
8.1.2022	21	28700228	-2,68	-85,84		x							
9.1.2022	0	28700229	-2,76	-85,53		x							

Table 7.3: Samples taken from the ships' moonpool. The following abbreviations were used: Hal. – Halocarbons, Nuts – Nutrients, Air – air canister samples (taken from the ships' bow), Pig. – pigments. See description in 7.2 for the remaining abbreviations.

8 Data and Sample Storage and Availability

The following Table summarizes the data taken on board and its' storage and availability.

Table 8.1 Overview of data availability

Type	Database	Available	Free Access	Contact
DOC/TDN Data (CTD and incubation experiments)	OSIS --> PANGAEA	06/2023	06/2024	Anja Engel, aengel@geomar.de
DCCHO/DHAA/DOP data (CTD only)	OSIS --> PANGAEA	06/2023	06/2024	Anja Engel, aengel@geomar.de
CLSM data (CTD only)	OSIS --> PANGAEA	06/2023	06/2024	Anja Engel, aengel@geomar.de
Lipid data (CTD only)	OSIS --> PANGAEA	06/2023	06/2024	Kevin Becker, kbecker@geomar.de
POC/PON/Bsi/POP data (CTD only)	OSIS --> PANGAEA	06/2023	06/2024	Anja Engel, aengel@geomar.de
TEP/CSP data (CTD only)	OSIS --> PANGAEA	06/2023	06/2024	Anja Engel, aengel@geomar.de
Flow cytometry data (CTD only)	OSIS --> PANGAEA	06/2023	06/2024	Anja Engel, aengel@geomar.de
Bacterial biomass production data (CTD only)	OSIS --> PANGAEA	06/2023	06/2024	Anja Engel, aengel@geomar.de
Photosynthesis activity (continuous CTD profiles)	OSIS --> PANGAEA	06/2023	06/2024	Anja Engel, aengel@geomar.de
Autotrophic production data (CTD only)	OSIS --> PANGAEA	06/2023	06/2024	Anja Engel, aengel@geomar.de
Extracellular enzyme acitvity	OSIS --> PANGAEA	06/2023	06/2024	Anja Engel, aengel@geomar.de
Microbial respiration data (CTD only)	OSIS --> PANGAEA	06/2023	06/2024	Anja Engel, aengel@geomar.de
Bacterial community composition (CTD only)	OSIS --> PANGAEA	06/2023	06/2024	Anja Engel, aengel@geomar.de
Microscopic phytoplankton speciation (CTD only)	OSIS --> PANGAEA	06/2023	06/2024	Birte Matthiessen, bmatthiessen@geomar.de
CDOM data (continuous CTD profiles)	OSIS --> PANGAEA	06/2023	06/2024	Anja Engel, aengel@geomar.de
NO, N2O, CH4 (discrete CTD, underway)	OSIS --> PANGAEA	06/2023	06/2024	Hermann Bange, hbange@geomar.de

NO (discrete data incubation experiments)	OSIS --> PANGAEA	06/2023	06/2024	Hermann Bange, hbange@geomar.de
Oxygen data (discrete CTD, underway, incubatiun	OSIS --> PANGAEA	06/2023	06/2024	Hermann Bange, hbange@geomar.de
Nutrient data (CTD, underway, incubatiun experiments)	OSIS --> PANGAEA	06/2023	06/2024	Hermann Bange, hbange@geomar.de
Nitrate isotope data (CTD only)	OSIS --> PANGAEA	06/2023	06/2024	Hermann Bange, hbange@geomar.de
Metagenomics data (CTD and incubation exoeriments)	OSIS --> PANGAEA	06/2023	06/2024	Carolin Löscher, cloescher@biology.sdu.dk
Iodine speciation/DOC/ozone uptake coefficient data (CTD,	OSIS --> PANGAEA	06/2023	06/2024	Lucy Carpenter, lucy.carpenter@york.ac.uk
Surface tension/-activity/water soluble DOM (CTD, SML)	OSIS --> PANGAEA	06/2023	06/2024	Lucy Carpenter, lucy.carpenter@york.ac.uk
Atmospheric ozone contration and fluxes data (continuous)	OSIS --> PANGAEA	06/2023	06/2024	Lucy Carpenter, lucy.carpenter@york.ac.uk
Gas phase molecular iodine/photolysis rates of	OSIS --> PANGAEA	06/2023	06/2024	Stephen Ball, sb263@leicester.ac.uk
Halocarbons (CTD, underway, incubation experiments)	OSIS --> PANGAEA	06/2023	06/2024	Birgit Quack, bquack@geomar.de
Halocarbons (discrete atmospheric measurements)	OSIS --> PANGAEA	06/2023	06/2024	Elliot Atlas, e.atlas@miami.edu
Sargassum experimental data (incubation experiments)	OSIS --> PANGAEA	06/2023	06/2024	Philippe Potin, potin@sb-roscoff.fr
Aerosol data (discrete atmospheric measurements)	OSIS --> PANGAEA	06/2023	06/2024	Alex Baker, alex.baker@uea.ac.uk
Underway continuous salinity/temperature/fluorescence	OSIS --> PANGAEA	06/2023	06/2024	Birgit Quack, bquack@geomar.de
CTD temperature/salinity data	OSIS --> PANGAEA	06/2023	06/2024	Birgit Quack, bquack@geomar.de
ADCP data	OSIS --> PANGAEA	06/2023	06/2024	Birgit Quack, bquack@geomar.de
EK60/WBAT data	OSIS --> PANGAEA	06/2023	06/2024	Patrice Brehmer, patrice.brehmer@ird.fr
Ozone sondes (tropospheric and stratospheric data)	OSIS --> PANGAEA	06/2023	06/2024	Kirstin Krüger, kirstin.kruger@geo.uio.no
Radio sondes (tropospheric and stratospheric data)	OSIS --> PANGAEA	06/2023	06/2024	Birgit Quack, bquack@geomar.de
Phytooptical measurements (CTD only)	OSIS --> PANGAEA	06/2023	06/2024	Rüdiger Röttgers, ruediger.roettgers@hereon.de
Phytoplankton pigment measurements (CTD, underway)	OSIS --> PANGAEA	06/2023	06/2024	Rüdiger Röttgers, ruediger.roettgers@hereon.de
Radiometric measurements (atmosphere)	OSIS --> PANGAEA	06/2023	06/2024	Rüdiger Röttgers, ruediger.roettgers@hereon.de
CDOM data (discrete CTD and underway)	OSIS --> PANGAEA	06/2023	06/2024	Rüdiger Röttgers, ruediger.roettgers@hereon.de
Underwater vision profiler (continuous CTD profiles)	OSIS --> PANGAEA	06/2023	06/2024	Rainer Kiko, rainer.kiko@obs-vlfr.fr
Iron aerosol data (discrete artmospheric)	OSIS --> PANGAEA	06/2023	06/2024	Manuela van Pinxteren, manuela.vanpinxteren@tropos.de
eDNA data (CTD, underway)	OSIS --> PANGAEA	06/2023	06/2024	Florian Weinberger (fweinberger@geomar.de)
DMS/derivates (CTD, underway, incubation	OSIS --> PANGAEA	06/2023	06/2024	Christa Marandino, cmarandino@geomar.de
Ship emissions/atmospheric trace gases (continuous	OSIS --> PANGAEA	06/2023	06/2024	Folkard Wittrock, folkard@iup.physik.uni-
Plastics concentration (catamaran, underway)	OSIS --> PANGAEA	06/2023	06/2024	Anja Engel, aengel@geomar.de

9 Acknowledgements

Our sincere thanks goes to many people who supported the success of SO287-CONNECT in many ways. The expedition was created on short-notice and needed rapid actions, flexibility and indomitable endurance of all involved to make the cruise possible and successful under these exceptional COVID-19 conditions. Captain Tilo Birnbaum and his crew are honored for their everlasting support during the cruise and some last-minute rescues, which helped to avoid failures and delays. Marcel Deeke, who represented the generous and reliable shipping company Briese on board, is memorized for his outstanding support to enable the stay of our Senegalese researcher for the entire cruise. Special thanks to the German Research Fleet Coordination Centre at the Universität Hamburg (LDF) for their general support and especially for their tireless and persistent efforts in obtaining all seven diplomatic clearances from the Ministries of Foreign Affairs of Spain, Puerto Rico, the Dominican Republic, Haiti, Jamaica, Columbia and Panama to conduct research in the economic exclusive zones of these countries. A great thank you to the employees in the German consulates of these countries, including Washington, who were involved in the Puerto Rico notification and to the German Ministry of Foreign Affairs. A great thank you also to the authorities in the respective countries who were involved in issuing the permissions. The German Federal Ministry of Education and Research (BMBF), the Review Panel German Research Vessels (GPF) and the 'Projektträger Jülich' at the Jülich Research Centre GmbH (PtJ) put a lot of effort in reviewing and promoting the different proposals for SO287-CONNECT. A special thanks also to the administrative and technical personnel of GEOMAR, who reacted rapidly on many different requests, related to funding, purchase of equipment, traveling, legislation and logistics. Thanks to GEOMAR for supporting the immediate necessities and over hours for the technical personnel on board via the ships fond. Appreciation and recognition also to the young scientific crew on board, of whom a quarter have been on a research vessel for the first time, while they worked very hard to achieve the goals of the expedition. While logistical problems were solved frequently from many involved, e.g .LPL Projects + Logistics GmbH, our special thanks goes to Eric Achterberg and his crew of SO289, who delayed their departure and packed hundreds of kilos of frozen samples, which then luckily reached the storage rooms in our home labs, where they are now waiting for analysis.

10 References

Abdulkadir, S., Tsuchiya, M., 2008. One-step method for quantitative and qualitative analysis of fatty acids in marine animal samples. J. Exp. Mar. Bio. Ecol. 354, 1–8. Doi: https://doi.org/10.1016/j.jembe.2007.08.024.

Amores, A., Melnichenko, O., Maximenko, N., 2017. Coherent mesoscale eddies in the North Atlantic subtropical gyre: 3-D structure and transport with application to the salinity maximum. J. Geophys. Res.-Oceans 122, 23–41. Doi: https://doi.org/10.1002/2016JC012256.

Aryee, J. N. A., Amekudzi, L. K., Preko, K., Atiah, W. A., Danuor, S. K., 2020. Estimation of planetary boundary layer height from radiosonde profiles over West Africa during the

AMMA field campaign: Intercomparison of different methods. Scientific African, 7, e00228. Doi: https://doi.org/10.1016/j.sciaf.2019.e00228.

Ball, S. M., Hollingsworth, A. M., Humbles, J., Leblanc, C., Potin, P., McFiggans, G., 2010. Spectroscopic studies of molecular iodine emitted into the gas phase by seaweed. Atmos. Chem. Phys. 10, 6237-6254.

Baltar, F., Arístegui, J., Gasol, J. M., Sintes, E., Herndl, G. J., 2009. Evidence of prokaryotic metabolism on suspended paerticulate organic matter in the darf waters of the subtropical North Atlantic. Limnol. Oceanogr. 54, 182-193, Doi: 10.4319/lo.2009.54.1.0182.

Bange, H. W., 2008. Gaseous Nitrogen Compounds (NO, N2O, N2, NH3) in the Ocean. In: Capone, D. G., Bronk, D. A., Mulholland, M. R., Carpenter, E. J. Nitrogen in the Marine Environment. 2nd edition. Acadamic Press, Elsevier, 51–94. Doi: https://doi.org/10.1016/b978-0-12-372522-6.00002-5.

Bange, H. W., Arévalo-Martínez, D. L., de la Paz, M., Farías, L., Kaiser, J., Kock, A., Law, C. S., Rees, A. P., Rehder, G., Tortell, P. D., Upstill-Goddard, R. C., Wilson, S. T., 2019. A harmonized nitrous oxide (N2O) ocean observation network for the 21st century. Frontiers in Marine Science 6. Doi: https://doi.org/10.3389/fmars.2019.00157.

Behrens, L. K., Hilboll, A., Richter, A., Peters, E., Alvarado, L. M. A., Kalisz Hedegaard, A. B., Wittrock, F., Burrows, J. P., Vrekoussis, M., 2019. Detection of outflow of formaldehyde and glyoxal from the African continent to the Atlantic Ocean with a MAX-DOAS instrument. Atmos. Chem. Phys. 19, 10257–10278. Doi: https://doi.org/10.5194/acp-19-10257-2019.

Bergauer, K., Fernandez-Guerra, A., Garcia, J. A. L., Sprenger, R. R., Stepanauskas, R., Pachiadaki, M. G., Jensen, O. N., Herndl, G. J., 2018. Organic matter processing by microbial communities throughout the Atlantic water column as revealed by metaproteomics. Proc. Natl. Acad. Sci. 115, E400-E408. Doi: 10.1073/pnas.1708779115.

Bianchi, D., Mislan, K. A. S., 2016. Global patterns of diel vertical migration times and velocities from acoustic data. Limnology and Oceanography 61(1), 353–364. Doi: 10.1002/lno.10219.

Bianchi, D., Stock, C., Galbraith, E. D., Sarmiento, J. L., 2013. Diel vertical migration: Ecological controls and impacts on the biological pump in a one-dimensional ocean model. Global Biogeochemical Cycles 27(2), 478–491. Doi: 10.1002/gbc.20031.

Bonino, G., Lovecchio, E., Gruber, N., Münnich, M., Masina, S., Iovino, D., 2021. Drivers and impact of the seasonal variability of the organic carbon offshore transport in the Canary upwelling system. Biogeosciences,18(8), 2429-2448. Doi: https://doi.org/10.5194/bg-18-2429-2021.

Bouwman, A., Boumans, L., Batjes, N., 2002. Modeling global annual N2O and NO emissions from fertilized fields. Global Biogeochemical Cycles 16(4). 28-1-28–9. Doi: https://doi.org/10.1029/2001gb001812.

Brandt, P., Bange, H. W., Banyte, D., Dengler, M., Didwischus, S.-H., Fischer, T., Greatbatch, R. J., Hahn, J., Kanzow, T., Karstensen, J., Körtzinger, A., Krahmann, G., Schmidtko, S., Stramma, L., Tanhua, T., and Visbeck, M., 2015. On the role of circulation and mixing in the ventilation of oxygen minimum zones with a focus on the eastern tropical North Atlantic. Biogeosciences 12, 489–512. Doi: https://doi.org/10.5194/bg-12-489-2015

Brehmer, P. A. J.-P., 2006. Fisheries Acoustics: Theory and Practice. In: Simmonds, E. J., MacLennan, D. N. (Eds.), Fish and Fisheries. 2nd ed, Blackwell Publishing, Oxford, 7(3). pp. 227–228. Doi: 10.1111/j.1467-2979.2006.00220.x.

Brehmer, P. A. J.-P., Sarré, A., Guennégan, Y., Guillard, J., 2019. Vessel Avoidance Response: A Complex Tradeoff Between Fish Multisensory Integration and Environmental Variables. Reviews in Fisheries Science & Aquaculture 27(3), 380–391. Doi: 10.1080/23308249.2019.1601157.

Browning, T. J., Achterberg, E. P., Yong, J. C., Rapp, I., Utermann, C., Engel, A., Moore, C. M., 2017. ron limitation of microbial phosphorus acquisition in the tropical North Atlantic. Nat Commun 8, 1546. Doi: https://doi.org/10.1038/ncomms15465.

Bruneau, M., Hladky-Hennion, A. C., 2010. MEMS acoustiques. In: SFA (Eds.), Livre blanc de l'acoustique en France en 2010. Société Française d'Acoustique, p. 80. Available at: https://hal.archives-ouvertes.fr/hal-00800615 (Accessed: 9 July 2020).

Bucciarelli, E., Ridame, C., Sunda, W. G., Dimier-Hugheney, C., Cheize, M., Belviso, S. 2013. Increased intracellular concentrations of DMSP and DMSO in iron-limited oceanic phytoplankton Thalassiosira oceanica and Trichodesmium erythraeum. Limnology and Oceanography 58(5), 1667-1679. Doi: https://doi.org/10.4319/lo.2013.58.5.1667.

Cardoso, C., Caldeira, R. M., Relvas, P., Stegner, A., 2020. Islands as eddy transformation and generation hotspots: Cabo Verde case study. Progress in Oceanography 184, 102271. Doi: https://doi.org/10.1016/j.pocean.2020.102271.

Carpenter, E. J., Romans, K., 1991. Major Role of the Cyanobacterium Trichodesmium in Nutrient Cycling in the North Atlantic Ocean. Science 254 (5036), 1356-1358.

Carpenter, L. J., Liss, P. S., 2000. On temperate sources of bromoform and other reactive organic bromine gases. Journal of Geophysical Research Atmospheres 105(D16), 20539-20547, Doi: https://doi.org/10.1029/2000JD900242.

Carpenter, L. J., MacDonald, S. M., Shaw, M. D., Kumar, R., Saunders, R. W., Parthipan, R., Wilson, J., Plane, J. M. C., 2013. Atmospheric iodine levels influenced by sea surface emissions of inorganic iodine. Nat. Geosci., 2013, 6, 108-111. Doi: https://doi.org/10.1038/ngeo1687.

Carpenter, L. J., Chance, R. J., Sherwen, T., Adams, T. J., Ball, S. M., Evans, M. J., Hepach, H., Hollis, L. D. J., Hughes, C., Jickells, T. D., Mahajan, A., Stevens, D. P., Tinel, L., Wadley, M. R., 2021. Marine Iodine Emissions in a Changing World. Proceedings of the Royal Society A: Mathematical, Physical and Engineering Sciences, 477 (2247). Doi: 10.1098/rspa.2020.0824.

Carr, M.-E., 2001. Estimation of potential productivity in Eastern Boundary Currents using remote sensing. Deep-Sea Res. Pt. II 49, 59–80. Doi: https://doi.org/10.1016/S0967-0645(01)00094-7.

Carr, M.-E., 2002. Estimation of potential productivity in the Eastern Boundary Currents using remote sensing. Deep-Sea Res. Pt. II 49, 59–80. Doi: https://doi.org/10.1016/S0967-0645(01)00094-7, 2002.

Cavalli, F., Facchini, M. C., Decesari, S., Mircea, M., Emblico, L., Fuzzi, S., Ceburnis, D., Yoon, Y. J., O'Dowd, C. D., Putaud, J. P., Dell'Acqua, A., 2004. Advances in characterization of size-resolved organic matter in marine aerosol over the North Atlantic, Journal of Geophysical Research - Atmospheres 109, D24215, Doi: 10.1029/2004jd005137.

Chance, R., Baker, A. R., Kupper, F., Hughes, C., Kloareg, B., Malin, G., 2009. Release and transformations of inorganic iodine by marine macroalgae. Estuarine coastal and shelf science 82(3), 406-414. Doi: https://doi.org/10.1016/j.ecss.2009.02.004.

Chance, R., Baker, A. R., Carpenter, L. J., Jickells, T. D., 2014. The distribution of iodide at the sea surface. Environ. Sci. Process. Impacts 16, 1841–1859. Doi: 10.1039/c4em00139g.

Chang, W., Heikies, B. G., Lee, M., 2004. Ozone deposition to the sea surface: chemical enhancement and wind speed dependence. Atmospheric Environment 38, 1053–1059. Doi: https://doi.org/10.1016/j.atmosenv.2003.10.050.

Charlson, R.J., Lovelock, J.E., Andreae, M.O., Warren, S.G., 1987. Oceanic phytoplankton, atmospheric sulphur, cloud albedo and climate. Nature 326, 655-661.

Chavez, F. P., Messié, M., 2009. A comparison of Eastern Boundary Upwelling Ecosystems. Prog. Oceanogr. 83, 80–96. Doi: https://doi.org/10.1016/j.pocean.2009.07.032.

Dalsoren, S. B., Eide, M. S., Endresen, O., Mjelde, A., Gravir, G., Isaksen, I. S. A., 2009. Update on emissions and environmental impacts from the international fleet of ships: the contribution from major ship types and ports. Atmospheric Chemistry and Physics 9(6), 2171-2194. Doi: 10.5194/acp-9-2171-2009.

Díaz, J. P., Expósito, F. J., Pérez, J. C., González, A., Wang, Y., Haimberger, L., Wang, J., 2019. Long-term trends in marine boundary layer properties over the Atlantic ocean. Journal of Climate 32(10), 2991-3004. Doi: https://doi.org/10.1175/JCLI-D-18-0219.1.

Dekshenieks, M. M., Donaghay, P. L., Sullivan, J. M., Rines, J. E. B., Osborn, T. R., Twardowski, M. S., 2001. Temporal and spatial occurrence of thin phytoplankton layers in relation to physical processes. Marine Ecology Progress Series (223), 61–71. Doi: 10.3354/meps223061.

Delon, C., Serça, D., Boissard, C., Dupont, R., Dutot, A., Laville, P., De Rosnay, P., Delmas, R., 2007. Soil NO emissions modelling using artificial neural network. Tellus B 59(3). Doi: https://doi.org/10.3402/tellusb.v59i3.17025.

Demer, D. A., Berger, L., Bernasconi, M., Bethke, E., Boswell, K., Chu, D., Domokos, R., Dunford, A., Fassler, S., Gauthier, S., Hufnagle, L. T., Jech, J. M., Bouffant, N., Lebourges-Dhaussy, A., Lurton, X., Macauly, G. J., Perrot, Y., Ryan, T., Parker-Stetter, S., Stienessen, S., Weber, T., Williamson, N., 2015. Calibration of acoustic instruments. ICES Cooperative Research Report (326), p. 133.

Diogoul, N., Brehmer, P. A. J.-P., Perrot, Y., Tiedemann, M., Thiam, A., El Ayoubi, S., Mouget, A., Migayrou, C., Sadio, O., Sarré, A., 2020. Fine-scale vertical structure of sound-scattering layers over an east border upwelling system and its relationship to pelagic habitat characteristics. Ocean Science 16(1), 65–81. Doi: https://doi.org/10.5194/os-16-65-2020.

Dittmar, T., Koch, B., Hertkorn, N., Kattner, G., 2008. A simple and efficient method for the solid-phase extraction of dissolved organic matter (SPE-DOM) from seawater. Limnol. Oceanogr. Methods 6, 230–235. Doi: https://doi.org/10.4319/lom.2008.6.230.

Ducklow, H. W., Steinberg, D. K., Buesseler, K. O., 2001. Upper ocean carbon export and the biological pump. Oceanography 14, 50-58. Doi: 10.5670/oceanog.2001.06.

Eder, K., 1995. Gas chromatographic analysis of fatty acid methyl esters. J. Chromatogr. B Biomed. Sci. Appl. 671, 113–131. Doi: https://doi.org/10.1016/0378-4347(95)00142-6.

Endres, S., Maes, F., Hopkins, F., Houghton, K., Martensson, E. M., Oeffner, J., Quack, B., Singh, P., Turner, D., 2018. A New Perspective at the Ship-Air-Sea-Interface: The Environmental Impacts of Exhaust Gas Scrubber Discharge. Frontiers in Marine Science 5. DOI: 10.3389/fmars.2018.00139.

Engel, A., Goldthwait, S., Passow, U., Alldredge, A., 2002. Temporal decoupling of carbon and nitrogen dynamics in a mesocosm diatom bloom. Limnology and Oceanography 3. Doi: 10.4319/lo.2002.47.3.0753.

Engel, A., Händel, N., Wohlers, J., Lunau, M., Grossart, H. P., Sommer, U., Riebesell, U., 2011. Effects of sea surface warming on the production and composition of dissolved organic matter during phytoplankton blooms: results from a mesocosm study. Journal of Plankton Research 33 (3), 357-372. Doi: 10.1093/plankt/fbq122.

Fawcett, S. E., Johnson, K. S., Riser, S. C., van Oostende, N., Sigman, D. M., 2018. Low-nutrient organic matter in the Sargasso Sea thermocline: A hypothesis for its role, identity, and carbon cycle implications. Marine Chemistry 207, 108-123. Doi: https://doi.org/10.1016/j.marchem.2018.10.008.

Ferreira, M. L. D. C., Kerr, R. (2017). Source water distribution and quantification of North Atlantic deep water and Antarctic bottom water in the Atlantic Ocean. Progress in Oceanography,153, 66-83. Doi: https://doi.org/10.1016/j.pocean.2017.04.003.

Fomba, K. W., Müller, K., van Pinxteren, D., Herrmann, H., 2013. Aerosol size-resolved trace metal composition in remote northern tropical Atlantic marine environment: case study Cape Verde islands. Atmospheric Chemistry and Physics 13, 4801-4814. Doi: 10.5194/acp-13-4801-2013.

Fomba, K. W., Mueller, K., van Pinxteren, D., Poulain, L., van Pinxteren, M., Herrmann, H., 2014. Long-term chemical characterization of tropical and marine aerosols at the Cape Verde Atmospheric Observatory (CVAO) from 2007 to 2011. Atmospheric Chemistry and Physics 14, 8883-8904. Doi: 10.5194/acp-14-8883-2014.

Galbally, I. E., Roy, C. R., 1980. Destruction of ozone at the earth's surface. Q. J. R. Meteorol. Soc. 106, 599–620. Doi: https://doi.org/10.1002/qj.49710644915.

Gallagher, M. W., Beswick, K. M., Coe, H., 2001. Ozone deposition to coastal waters. Q. J. R. Meteorol. Soc. 127, 539–558. Doi: https://doi.org/10.1002/qj.49712757215.

Galloway, T., Cole, M., Lewis, C., 2017. Interactions of microplastic debris throughout the marine ecosystem. Nat Ecol Evol 1, 0116. Doi: https://doi.org/10.1038/s41559-017-0116, 2017.

Ganzeveld, L., Lelieveld, J., Dentener, F., Krol, M., Bouwman, A., Roelofs, G., 2002. Global soil-biogenic NOx emissions and the role of canopy processes. Journal of Geophysical Research: Atmospheres (1984–2012) 107(D16). Doi: https://doi.org/10.1029/2001jd001289.

Ganzeveld, L., Helmig, D., Fairall, C., Hare, J. E., Pozzer, A., 2009. Atmosphere-ocean ozone exchange: A global modeling study of biogeochemical, atmospheric, and waterside turbulence dependencies. Global Biogeochem. Cycles 23, 1–16. Doi: 10.1029/2008GB003301.

Garcìa-Muñoz, M., Arístegui, J., Montero, M. F., Barton, E. D., 2004. Distribution and transport of organic matter along a filament-eddy system in the Canaries – NW Africa coastal transition zone region. Prog. Oceanogr. 62, 115–129. Doi: https://doi.org/10.1016/j.pocean.2004.07.005.

Garland, J. A., Elzerman, A. W., Penkett, S. A., 1980. The Mechanism for Dry Deposition of Ozone to Seawater Surfaces. J. Geophys. Res. 85, 7488–7492, Doi: 10.1029/JC085iC12p07488.

Guillard, J., Lebourges-Dhaussy, A., 2014. A l'écoute des bancs de poisons. Pour la Science 436, 38–45.

Haney, J. F., 1988. Diel Patterns of Zooplankton Behavior. Bulletin of Marine Science 43(3), 583–603.

Hardacre, C., Wild, O., Emberson, L., 2015. An evaluation of ozone dry deposition in global scale chemistry climate models. Atmos. Chem. Phys. 15, 6419–6436. Doi: https://doi.org/10.5194/acp-15-6419-2015.

Hartmann, D. L., Klein Tank, A. M. G., Rusticucci, M., Alexander, L. V., Brönnimann, S., Charabi, Y., Dentener, F. J., Dlugokencky, E. J., Easterling, D. R., Kaplan, A., Soden, B. J., Thorne, P.W., Wild, M., Zhai, P. M., 2013. Observations: Atmosphere and Surface. In: Stocker, T. F., Qin, D., Plattner, G.-K., Tignor, M., Allen, S. K., Boschung, J., Nauels, A., Xia, Y., Bex, V., Midgley, P. M. (eds). Climate Change 2013: The Physical Science Basis. Contribution of Working Group I to the Fifth Assessment Report of the Intergovernmental Panel on Climate Change. Cambridge University Press, Cambridge, United Kingdom and New York, NY, USA.

Heikies, B. G., Lee, M., Jacob, D., Talbot, R., Bradshaw, J., Singh, H., Blake, D., Anderson, B., Fuelberg, H., Thompson, A. M., 1996. Ozone, hydroperoxides, oxides of nitrogen, and hydrocarbon budgets in the marine boundary layer over the South Atlantic. J. Geophys. Res. 101, 24221–24234. Doi: https://doi.org/10.1029/95JD03631.

Held, N. A., Webb, E. A., McIlvin, M. M., Hutchins, D. A., Cohen, N. R., Moran, D. M., Kunde, K., Lohan, M. C., Mahaffey, C., Woodward, E. M. S., Saito, M. A., 2020. Co-occurrence of Fe and P stress in natural populations of the marine diazotroph Trichodesmium. Biogeosciences 17, 2537–2551. Doi: https://doi.org/10.5194/bg-17-2537-2020.

Helmig, D., Boylan, P., Johnson, B., Oltmans, S., Fairall, C., Staebler, R., Weinheimer, A., Orlando, J., Knapp, D. J., Montzka, D. D., Flocke, F., Frieó, U., Sihler, H., Shepson, P. B., 2012. Ozone dynamics and snow-atmosphere exchanges during ozone depletion events at Barrow, Alaska. J. Geophys. Res. Atmos. 117, 1–15. Doi: http://dx.doi.org/10.1029/2012JD017531.

Hepach, H., Hughes, C., Hogg, K., Collings, S., Chance, R., 2020. Senescence as the main driver of iodide release from a diverse range of marine phytoplankton. Biogeosciences 17, 2453–2471. Doi: https://doi.org/10.5194/bg-17-2453-2020.

Hieronymi, M., Müller, D., Doerffer, R., 2017. The OLCI Neural Network Swarm (ONNS): a bio-geo-optical algorithm for open ocean and coastal waters. Frontiers in Marine Science, 4, 140.

Holliday, D. V., 1977. Extracting bio-physical information from the acoustic signature of marine organisms. Oceanic sound scattering prediction, 619–624.

Holthusen, L., 2017. Die Verteilung von Lachgas (N2O) entlang des 86°W-Schnittes im tropischen Ostpazifik. BSc, Kiel University, Kiel, 33 pp.

International Maritime Organization (IMO): Fourth IMO Greenhouse Gas Study 2020. Report, 2021.

Jambeck, J. R., Geyer, R., Wilcox, C., Siegler, T. R., Perryman, M., Andrady, A., Narayan, R., Law, K. L., 2015. Plastic waste inputs from land into the ocean. Science 347(6223), 768-771. Doi: 10.1126/science.1260352.

Ji, Q., Altabet, M. A., Bange, H. W., Graco, M. I., Ma, X., Arévalo-Martínez, D. L., Grundle, D. S., 2019. Investigating the effect of El Niño on nitrous oxide distribution in the eastern tropical South Pacific. Biogeosciences 16, 2079-2093. Doi: https://doi.org/10.5194/bg-16-2079-2019.

Karstensen, J., Stramma, L., Visbeck, M., 2008. Oxygen minimum zones in the eastern tropical Atlantic and Pacific oceans. Prog. Oceanogr. 77, 331–350. Doi: https://doi.org/10.1016/j.pocean.2007.05.009.

Kataoka, T., Ooki, A., Nomura, D., 2019. Production of Dibromomethane and Changes in the Bacterial Community in Bromoform-Enriched Seawater. Microbes Environ. 34(2), 215–218. Doi: 10.1264/jsme2.ME18027

Kattner, L., Mathieu-Üffing, B., Burrows, J. P., Richter, A., Schmolke, S., Seyler, A., Wittrock, F., 2015. Monitoring compliance with sulfur content regulations of shipping fuel by in situ measurements of ship emissions. Atmos. Chem. Phys. 15, 10087-10092. Doi:10.5194/acp-15-10087-2015, 2015.

Kawa, S. R., Pearson Jr., R., 1989. Ozone Budgets From the Dynamics and Chemistry of Marine Stratocumulus Experiment. J. Geophys. Res. 94, 9809–9817. Doi: 10.1029/JD094iD07p09809.

Keber, T., Bönisch, H., Hartick, C., Hauck, M., Lefrancois, F., Obersteiner, F., Ringsdorf, A., Schohl, N., Schuck, T., Hossaini, R., Graf, P., Jöckel, P., Engel, A. 2020. Bromine from short-lived source gases in the extratropical northern hemispheric upper troposphere and lower stratosphere (UTLS). Atmos. Chem. Phys. 20, 4105–4132, https://doi.org/10.5194/acp-20-4105-2020.

Krause, K., Wittrock, F., Richter, A., Schmitt, S., Pöhler, D., Weigelt, A., Burrows, J. P., 2021. Estimation of ship emission rates at a major shipping lane by long-path DOAS measurements. Atmos. Meas. Tech. 14, 5791–5807. Doi: https://doi.org/10.5194/amt-14-5791-2021.

Kuypers, M. M. M., Marchant, H. K., Kartal, B., 2018. The microbial nitrogen-cycling network. Nature Reviews Microbiology 16(5), 263–276. Doi: https://doi.org/10.1038/nrmicro.2018.9.

Lachkar, Z., Gruber, N., 2011. What controls biological production in coastal upwelling systems? Insights from a comparative modeling study. Biogeosciences 8, 2961–2976. Doi: https://doi.org/10.5194/bg-8-2961-2011.

Lathuilière, C., Echevin, V., Lévy, M., Madec, G., 2010. On the role of the mesoscale circulation on an idealized coastal upwelling ecosystem. Journal of Geophysical Research: Oceans 115(C9). Doi: https://doi.org/10.1029/2009JC005827.

Lehodey, P., Conchon, A., Senina, I., Domokos, R., Calmettes, B., Jouanno, J., Hernandez, O., Kloser, R., 2015. Optimization of a micronekton model with acoustic data. ICES Journal of Marine Science 72(5), 1399–1412. Doi: 10.1093/icesjms/fsu233.

Lenschow, D. H., Pearson Jr., R., Boba Stankov, B., 1982. Measurement of Ozone Vertical Flux to Ocean and Forest. J. Geophys. Res. 87, 8833–8837. Doi: 10.1029/JC087iC11p08833.

Le Vu, B., Stegner, A., Arsouze, T., 2018. Angular Momentum Eddy Detection and Tracking Algorithm (AMEDA) and Its Application to Coastal Eddy Formation. Journal of Atmospheric and Oceanic Technology 35(4), 739–762. Doi: https://doi.org/10.1175/JTECH-D-17-0010.1.

Lim, Y.-K., Phang, S.-M., Abdul Rahman, N., Sturges, W. T., Malin, G., 2017. Halocarbon emissions from marine phytoplankton and climate change. Int. J. Environ. Sci. Technol. 14, 1355–1370. Doi: https://doi.org/10.1007/s13762-016-1219-5.

Lin, C. Y., Manley, S. L., 2012. Bromoform production from seawater treated with bromoperoxidase. Limnology and Oceanography 57(6), 1857-1866. Doi: 10.4319/lo.2012.57.6.1857.

Liu, Y., Thornton, D. C. O., Bianchi, T. S., Arnold, W. A., Shields, M. R., Chen, J., Yvon-Lewis, S. A., 2015. Dissolved organic matter composition drives the marine production of brominated very short-lived substances. Environ. Sci. Technol. 49, 3366–3374. Doi:10.1021/es505464k.

Liu, M., Tanhua, T., 2021. Water masses in the Atlantic Ocean: characteristics and distributions. Ocean Science 17(2), 463-486. Doi: https://doi.org/10.5194/os-17-463-2021.

Lovecchio, E., Gruber, N., Münnich, M., 2018. Mesoscale contribution to the long-range offshore transport of organic carbon from the Canary Upwelling System to the open North Atlantic. Biogeosciences 15, 5061–5091. Doi: https://doi.org/10.5194/bg-15-5061-2018.

Lutterbeck, H. E., Bange, H. W., 2015. An improved method for the determination of dissolved nitric oxide (NO) in seawater samples. Ocean Science 11(6), 937–946. Doi: https://doi.org/10.5194/os-11-937-2015.

Lutterbeck, H. E., Arévalo-Martínez, D. L., Löscher, C. R., Bange, H. W., 2018. Nitric oxide (NO) in the oxygen minimum zone off Peru. Deep Sea Research Part II: Topical Studies in Oceanography 156, 148–154. Doi: https://doi.org/10.1016/j.dsr2.2017.12.023.

Marchal, E, Gerlotto, F., Stéquert, B., 1993. On the relationship between scattering layer, thermal structure and tuna abundance in the Eastern Atlantic equatorial current system. Oceanologica Acta 16(3), 261–272.

McIlvin, M. R., M. A. Altabet, 2005. Chemical conversion of nitrate and nitrite to nitrous oxide for nitrogen and oxygen isotopic analysis in freshwater and seawater. Anal. Chem. 77:5589–5595.

McKay, W. A., Stephens, B. A., Dollard, G. J., 1992. Laboratory measurements of ozone deposition to sea water and other saline solutions. Atmos. Environ. Part A, Gen. Top. 26, 3105–3110. Doi: https://doi.org/10.1016/0960-1686(92)90467-Y.

McVeigh, P., O'Dowd, C., Berresheim, H., 2010. Eddy Correlation Measurements of Ozone Fluxes over Coastal Waters West of Ireland. Adv. Meteorol., 1–7. Doi: https://doi.org/10.1155/2010/754941.

Mehlmann, M., Quack, B., Atlas, E., Hepach, H., Tegtmeier, S., 2020. Natural and anthropogenic sources of bromoform and dibromomethane in the oceanographic and biogeochemical regime of the subtropical North East Atlantic. Environmental Science: Processes & Impacts 22 (3), 679-707. Doi: 10.1039/C9EM00599D.

Mestre, M., Ruiz-González, C., Logares, R., Duarte, C. M., Gasol, J. M., Sala, M. M., 2018. Sinking particles promote vertical connectivity in the ocean microbiome. Proc. Natl. Acad. Sci. 115, E6799-E6807. Doi: 10.1073/pnas.1802470115.

Milici, M., Vital, M., Tomasch, J., Badewien, T. H., Giebel, H. A., Plumeier, I., Wang, H., Pieper, D. H., Wagner-Döbler, I., Simon, M., 2017. Diversity and community composition of particle-associated and free-living bacteria in mesopelagic and bathypelagic Southern Ocean water masses: Evidence of dispersal limitation in the Bransfield Strait. Limnol. Oceanogr. 62, 1080–1095. Doi:10.1002/lno.10487.

Mithoo-Singh, P. K., Keng, F. S.-L., Phang, S.-M-, Leedham Elvidge, E. C., Sturges, W. T., Malin, G., Abd Rahman, N., 2017. Halocarbon emissions by selected tropical seaweeds: species-specific and compound specific responses under changing pH. PeerJ 5:e2918, Doi: 10.7717/peerj.2918.

Mittelstaedt, E., 1991. The ocean boundary along the northwest African coast: Circulation and oceanographic properties at the sea surface. Prog. Oceanogr. 26, 307–355. Doi: https://doi.org/10.1016/0079-6611(91)90011-A.

Newman, S., Watkins, E., Farmer, A., Brink, P.., Schweitzer, J. P., 2015. The Economics of Marine Litter. In: Bergmann M., Gutow L., Klages M. (eds) Marine Anthropogenic Litter. Springer, Cham. Doi: https://doi.org/10.1007/978-3-319-16510-3_14.

Nuvolone, D., Petri, D., Voller, F., 2018. The effects of ozone on human health. Environ. Sci. Pollut. Res. 25, 8074–8088. Doi: https://doi.org/10.1007/s11356-017-9239-3.

O'Dowd, C. D., Facchini, M. C., Cavalli, F., Ceburnis, D., Mircea, M., Decesari, S., Fuzzi, S., Yoon, Y. J., Putaud, J. P., 2004. Biogenically driven organic contribution to marine aerosol. Nature 431, 676-680. Doi 10.1038/Nature02959.

Oh, I., Byun, D. W., Kim, H., Kim, S., Cameron, B., 2008. Modeling the effect of iodide distribution on ozone deposition to seawater surface. Atmos. Environ. 42, 4453–4466. Doi: 10.1016/j.atmosenv.2008.02.022.

Oikawa, P., Eberwein, J., Liang, L., Allsman, L., Grantz, D., Jenerette, G., 2015. Unusually high soil nitrogen oxide emissions influence air quality in a high-temperature agricultural region. Nature Communications, 6(1), 8753. Doi: https://doi.org/10.1038/ncomms9753.

Pelegrí, J. L., Peña-Izquierdo, J., 2015. Eastern Boudary Currents off Northwest Africa. In: Váldes, L., Déniz-González, I. (eds). Oeanographic and biological features in the Canary Current Large Marine Ecosystem. IOC-UNESCO Technical Series 115, Intergovernmental Oceanographic Commission.

Perrot, Y., Brehmer, P., Habasque, J., Roudat, G., Behagle, N., Sarré, A., Lebourges-Dhaussy, A., 2018. Matecho: An Open-Source Tool for Processing Fisheries Acoustics Data. Acoustics Australia 46(2), 241–248. Doi: 10.1007/s40857-018-0135-x.

Peters, E., Wittrock, F., Großmann, K., Frieß, U., Richter, A., Burrows, J. P., 2012. Formaldehyde and nitrogen dioxide over the remote western Pacific Ocean: SCIAMACHY and GOME-2 validation using ship-based MAX-DOAS observations. Atmos. Chem. Phys. 12, 11179-11197. Doi:10.5194/acp-12-11179-2012.

Pilegaard, K., 2013. Processes regulating nitric oxide emissions from soils. Philosophical Transactions of the Royal Society B: Biological Sciences 368(1621), 20130126. Doi: https://doi.org/10.1098/rstb.2013.0126.

Pluskal, T., Castillo, S., Villar-Briones, A., Orešič, M., 2010. MZmine 2: Modular framework for processing, visualizing, and analyzing mass spectrometry-based molecular profile data. BMC Bioinformatics. DOI:10.1186/1471-2105-11-395.

Polimene, L., Archer, S. D., Burtenschön, M., Allen, J. I., 2011. A mechanistic explanation of the Sargasso Sea DMS “summer paradox”. Biogeochemistry 110, 243-255.

Polovina, J. J., Howell, E. A., Abecassis, M., 2008. Ocean's least productive waters are expanding. Geophysical Research Letters 35(3). Doi: https://doi.org/10.1029/2007GL031745.

Quack, B., Peeken, I., Petrick, G., Nachtigall, K., 2007. Oceanic distribution and sources of bromoform and dibromomethane in the Mauritanian upwelling. Journal of Geophysical Research: Oceans 112(C10). Doi: https://doi.org/10.1029/2006JC003803.

Quinn, P. K., Bates, T. S., 2011. The case against climate regulation via oceanic phytoplankton sulphur emissions. Nature 480, 51-56. Doi: 10.1038/nature10580.

Remond, B., 2015. Les couches diffusantes du golfe de Gascogne: caractérisation acoustique, composition spécifique et distribution spatiale. Thèse de doctorat, Université Pierre et Marie Curie.

Rex, M., Wohltmann, I., Ridder, T., Lehmann, R., Rosenlof, K., Wennberg, P., Weisenstein, D., Notholt, J., Krüger, K., Mohr, V., Tegtmeier, S. 2014. A tropical West Pacific OH minimum and implications for stratospheric composition. Atmos. Chem. Phys. 14, 4827–4841. Doi: https://doi.org/10.5194/acp-14-4827-2014.

Rhee, T. S., Kettle, A. J., Andreae, M. O., 2009. Methane and nitrous oxide emissions from the ocean: A reassessment using basin-wide observations in the Atlantic. Journal of Geophysical Research 114, D12304.

Roth Rosenberg, D., Haber, M., Goldford, J., Lalzar, M., Aharonovich, D., Al-Ashhab, A., Lehahn, Y., Segrè, D., Steindler, L., Sher, D., 2021. Particle-associated and free-living bacterial communities in an oligotrophic sea are affected by different environmental factors. Environ. Microbiol. 23, 4295–4308. doi:10.1111/1462-2920.15611.

Röttgers, R., C. Häse, R. Doerffer, 2007. Determination of the particulate absorption of microalgae using a point-source integrating-cavity absorption meter: verification with a photometric technique, improvements for pigment bleaching and correction for chlorophyll fluorescence. Limnol. Oceanogr. Methods 5: 1–12.

Röttgers, R., D. Doxaran, C. Dupouy, 2016. Quantitative filter technique measurements of spectral light absorption by aquatic particles using a portable integrating cavity absorption meter (QFT-ICAM). Opt. Express 24: A1.

Ruddick, K. G., Voss, K., Boss, E., Castagna, A., Frouin, R., Gilerson, A., Hieronymi, M., Johnson, B. C., Kuusk, J., Lee, Z., Ondrusek, M., Vabson, V., Vendt, R., 2019. A review of protocols for fiducial reference measurements of water-leaving radiance for validation of satellite remote-sensing data over water. Remote Sensing 11(19), 2198.

Ruddick, K. G., Voss, K., Banks, A. C., Boss, E., Castagna, A., Frouin, R., Hieronymi, M., Jamet, C., Johnson, B. C., Kuusk, J., Lee, Z., Ondrusek, M., Vabson, V., Vendt, R., 2019. A review of protocols for fiducial reference measurements of downwelling irradiance for the validation of satellite remote sensing data over water. Remote Sensing, 11(15), 1742.

Rummel, C. D., Jahnke, A., Gorokhova, E., Kühnel, D., Schmitt-Jansen, M., 2017. Impacts of biofilm formation on the fate and potential effects of microplastic in the aquatic environment. Environmental Science & Technology Letters, 4 (7), 258-267, DOI: 10.1021/acs.estlett.7b00164.

Saiz-Lopez, A., Plane, J. M. C., Baker, A. R., Carpenter, L. J., von Glasow, R., Martin, J. C. G., McFiggans, G., Saunders, R. W., 2012. Atmospheric Chemistry of Iodine. Chem. Rev. 112, 1773-1804. Doi: 10.1021/cr200029u.

Sangrà, P., Pascual, A., Rodríguez-Santana, Á., Machín, F., Mason, E., McWilliams, J., Pelegrí, J., Dong, C., Rubio, A., Arístegui, J., Marrero-Díaz, Á., Hernández-Guerra, A., Martínez-Marrero, A., Auladell, M., 2009. The Canary Eddy Corridor: A major pathway for long-lived eddies in the subtropical North Atlantic. Deep-Sea Res. Pt. I 56, 2100–2114. Doi: https://doi.org/10.1016/j.dsr.2009.08.008.

Sardain, A., Sardain, E., Leung, B., 2019. Global forecasts of shipping traffic and biological invasions to 2050. Nature Sustainability 2(4), 274-282, DOI: 10.1038/s41893-019-0245-y.

Sarwar, G., Kang, D., Foley, K., Schwede, D., Gantt, B., Mathur, R., 2016. Technical note: Examining ozone deposition over seawater. Atmos. Environ. 141, 255–262. Doi: 10.1016/j.atmosenv.2016.06.072.

Scranton, M. I., 1983. Nitrogen in the Marine Environment. I: Distributions, 37–64. Doi: https://doi.org/10.1016/b978-0-12-160280-2.50010-9.

Seyler, A., Wittrock, F., Kattner, L., Mathieu-Üffing, B., Peters, E., Richter, A., Schmolke, S., Burrows, J. P., 2017. Monitoring shipping emissions in the German Bight using MAX-DOAS measurements. Atmos. Chem. Phys. 17, 10997-11023. Doi: https://doi.org/10.5194/acp-17-10997-2017.

Seyler, A., Meier, A. C., Wittrock, F., Kattner, L., Mathieu-Üffing, B., Peters, E., Richter, A., Ruhtz, T., Schönhardt, A., Schmolke, S., Burrows, J. P., 2019. Studies of the horizontal inhomogeneities in NO2 concentrations above a shipping lane using ground-based multi-axis differential optical absorption spectroscopy (MAX-DOAS) measurements and validation with airborne imaging DOAS measurements. Atmos. Meas. Tech. 12, 5959–5977. Doi: https://doi.org/10.5194/amt-12-5959-2019.

Simmonds, J., MacLennan, D. N., (Eds), 2006. Fisheries Acoustics: Theory and Practice. 2nd ed, Blackwell Publishing, Oxford. Doi: 10.1002/9780470995303.fmatter.

Simó, R., 2001. Production of atmospheric sulfur by oceanic plankton: biogeochemical, ecological and evolutionary links. TRENDS in Ecology & Evolution 16, 287-293.

Skiba, U., Fowler, D., Smith, K., 1997. Nitric oxide emissions from agricultural soils in temperate and tropical climates: sources, controls and mitigation options. Nutrient Cycling in Agroecosystems 48(1–2), 139–153. Doi: https://doi.org/10.1023/a:1009734514983.

Smirnov, A., B. N. Holben, I. Slutsker, D. M. Giles, C. R. McClain, T. F. Eck, S. M. Sakerin, A. Macke, P. Croot, G. Zibordi, P. K. Quinn, J. Sciare, S. Kinne, M. Harvey, T. J. Smyth, S. Piketh, T. Zielinski, A. Proshutinsky, J. I. Goes, N. B. Nelson, P. Larouche, V. F. Radionov, P. Goloub, K. Krishna Moorthy, R. Matarrese, E. J. Robertson, F. Jourdin, 2009. Maritime Aerosol Network as a component of Aerosol Robotic Network. Journal of Geophysical Research: Atmospheres 114(D6). Doi: https://doi.org/10.1029/2008JD011257.

Smith, D. C., Azam, F., 1992. A simple, economical method for measuring bacterial protein synthesis rates in seawater using 3H-leucine. Marine Microbial Food Webs, 107–114.

Stammer, D., 1998. On Eddy Characteristics, Eddy Transports, and Mean Flow Properties. J. Phys. Oceanogr. 28, 727–739. Doi: https://doi.org/10.1175/1520-0485(1998)028<0727:OECETA>2.0.CO;2.

Stehfest, E., Bouwman, L., 2006. N2O and NO emission from agricultural fields and soils under natural vegetation: summarizing available measurement data and modeling of global annual emissions. Nutrient Cycling in Agroecosystems 74(3), 207–228. Doi: https://doi.org/10.1007/s10705-006-9000-7.

Stevenson, D. S., Dentener, F. J. , Schultz, M. G., Ellingsen, K., van Noije, T. P. C., Wild, O., Zeng, G., Amann, M., Atherton, C. S., Bell, N., Bergmann, D. J., Bey, I., Butler, T., Cofala, J., Collins, W. J., Derwent, R. G., Doherty, R. M., Drevet, J., Eskes, H. J., Fiore, A. M., Gauss, M., Hauglustaine, D. A., Horowitz, L. W., Isaksen, I. S. A., Krol, M. C., Lamarque, J. F., Lawrence, M. G., Montanaro, V., Müller, J. F., Pitari, G., Prather, M. J., Pyle, J. A., Rast, S., Rodriquez, J. M., Sanderson, M. G., Savage, N. H., Shindell, D. T., Strahan, S. E.,

Sudo, K., Szopa, S., 2006. Multimodel ensemble simulations of present-day and near-future tropospheric ozone. J. Geophys. Res. Atmos. 111 (D8). Doi:10.1029/2005JD006338.

Stramma, L., Visbeck, M., Brandt, P., Tanhua, T., Wallace, D., 2009. Decreasing oxygen in the oxygen minimum zone of the eastern tropical North Atlantic. Geochim. Cosmochim. Ac.,73, A1281– A1281.

Stramma, L., Schmidtko, S., Levin, L. A., Johnson, G. C., 2010. Ocean oxygen minima expansions and their biological impacts. Deep Sea Research Part I: Oceanographic Research Papers 57(4), 587-595. Doi: https://doi.org/10.1016/j.dsr.2010.01.005.

Tegtmeier, S., Atlas, E., Quack, B., Ziska, F., Krüger, K., 2020. Variability and past long-term changes of brominated very short-lived substances at the tropical tropopause. Atmos. Chem. Phys. 20, 7103–7123. Doi: https://doi.org/10.5194/acp-20-7103-2020.

Thamdrup, B., 2012. New Pathways and Processes in the Global Nitrogen Cycle. Annual Review of Ecology, Evolution, and Systematics 43(1), 407–428. Doi: https://doi.org/10.1146/annurev-ecolsys-102710-145048.

Theiler, R., Cook, J. C., Hager, L. P., 1978. Halohydrocarbon synthesis by bromoperoxidase, Science 202, 1094-1096. Doi: 10.1126/science.202.4372.1094.

Tian, H., Rongting, X., Canadell, J. G., Thompson, R. L., Winiwarter, W., Suntharalingam, P., Davidson, E. A., Ciais, P., Jackson, R. P., Janssens-Maenhout, G., Prather, M. J., Regnier, P., Pan, N., Pan, S., Peters, G. P., Shi, H., Tubiello, F. N., Zaehle, S., Zhou, F., Arneth, A., Battaglia, G., Berthet, S., Bopp, L., Bouwmann, A. F., Buitenhuis, E. T., Chang, J., Chipperfield, M. P., Dangal, S. R. S., Dlugokencky, E., Elkins, J. W., Eyre, B. D., Fu, B., Hall, B., Ito, A., Joos, F., Krummel, P. B., Landolfi, A., Laruelle, G. G., Lauerwald, R., Li, W., Lienert, S., Maavara, T., MacLeaod, M., Millet, D. B., Olin, S., Patra, P. K., Prinn, R. G., Raymond, P. A., Ruiz, D. J., van der Werf, G. R., Vuichard, N., Wang, J. Weiss, R. F., Wells, K. C., Wilson, C., Yang, J., Yao, Y., 2020. A comprehensive quantification of global nitrous oxide sources and sinks. Nature 586, 248-256. Doi: https://doi.org/10.1038/s41586-020-2780-0.

Tinel, L., Adams, T. J., Hollis, L. D. J., Bridger, A. J. M., Chance, R. J., Ward, M. W., Ball, S. M., Carpenter, L. J., 2020. Influence of the Sea Surface Microlayer on Oceanic Iodine Emissions. Environ. Sci. Technol. 54, 13228-13237. Doi: 10.1021/acs.est.0c02736.

van Pinxteren, M., Barthel, S., Fomba, K., Müller, K., von Tümpling, W., Herrmann, H., 2017. The influence of environmental drivers on the enrichment of organic carbon in the sea surface microlayer and in submicron aerosol particles – measurements from the Atlantic Ocean. Elem Sci Anth 5. Doi: https://doi.org/10.1525/elementa.225.

Vogel, T. M., Criddle, C. S., McCarty, P. L., 1987. Es critical reviews: Transformations of halogenated aliphatic compounds. Environ. Sci. Technol. 21, 722-736. Doi: 10.1021/es00162a001.

Wadley, M. R., Stevens, D. P., Jickells, T., Hughes, C., Chance, R., Hepach, H., Tinel, L., Carpenter, L. J., 2020. *A Global Model for Iodine Speciation in the Upper Ocean.* Global Biogeochemical Cycles 34 (9), e2019GB006467. Doi: 10.1029/2019GB006467.

Walter, S., Bange, H. W., Breitenbach, U., Wallace, D. W. R., 2006. Nitrous oxide in the North Atlantic Ocean. Biogeosciences 3, 607-619. Doi: https://doi.org/10.5194/bg-3-607-2006.

Wang, W., Gao, H., Jin, S., Li, R., Na, G, 2019. The ecotoxicological effects of microplastics on aquatic food web, from primary producer to human: A review. Ecotoxicol Environ Saf. 173, 110-117. Doi: 10.1016/j.ecoenv.2019.01.113.

Wesely, M. L., Cook, D. R., Williams, R. M., 1981. Field Measurement of Small Ozone Fluxes to Snow, Wet Bare Soil, and Lake Water. Boundary-Layer Meteorol. 20, 459–471.

Wesely, M. L., Hicks, B. B., 2000. A review of the current status of knowledge on dry deposition. Atmospheric Environment 34, 2261–2282. Doi: https://doi.org/10.1016/S1352-2310(99)00467-7.

Whitehead, J. D., Mcfiggans, G. B., Gallagher, M. W., Flynn, M. J., 2009. Direct linkage between tidally driven coastal ozone deposition fluxes, particle emission fluxes, and subsequent CCN formation. Geophys. Res. Lett. 36, 1–5. Doi: 10.1029/2008GL035969.

Wilson, S. T., Al-Haj, A. N., Bourbonnais, A., Frey, C., Fulweiler, R. W., Kessler, J. D., Marchant, H. K., Milucka, J., Ray, N. E., Suntharalingam, P., Thornton, B. F., Upstill-Goddard, R. C., Weber, T. S., Arévalo-Martínez, D. L., Bange, H. W., Benway, H. M., Bianchi, D., Borges, A. V., Chang, B. X., Crill, P. M., del Valle, D. A., Farías, Joye, S. B., Kock, A., Labidi, J., Manning, C. C., Pohlmann, J. W., Rehder, G., Sparrow, K. J., Tortell, P. D., Treude, T., Valentine, D. L., Ward, B. B., Yang, S., Yurganov, L. N., 2020. Ideas and perspectives: A strategic assessment of methane and nitrous oxide measurements in the marine environment. Biogeosciences 17, 5809-5828. Doi: https://doi.org/10.5194/bg-17-5809-2020.

Wittrock, F., H. Oetjen, A. Richter, S. Fietkau, T. Medeke, A. Rozanov, J. P. Burrows, 2004. MAX-DOAS measurements of atmospheric trace gases in Ny-Ålesund - Radiative transfer studies and their application. Atmos. Chem. Phys. 4, 955-966. Doi: https://doi.org/10.5194/acp-4-955-2004.

Wyrtki, K., 1962. The oxygen minima in relation to ocean circulation. Deep-Sea Res. 9, 11–23. https://doi.org/10.1016/0011-7471(62)90243-7.

Ytreberg, E., Hassellöv, I.-M., Nylund, A., T., Hedblom, M., Al-Handal, A. Y., Wulff, A. 2019. Effects of scrubber washwater discharge on microplankton in the Baltic Sea. Marine Pollution Bulletin 145, 316-324. Doi: 10.1016/j.marpolbul.2019.05.023.

Zhang, L., M. A. Altabet, T.Wu, O. Hadas, 2007. Sensitive measurement of NH4+ 15N/14N (d15NH4+) at natural abundance levels in fresh and saltwaters. Anal. Chem. 79, 5297–5303.

Zhang, Z., Wang, W., Qiu, B., 2014. Oceanic mass transport by mesoscale eddies. Science, 345, 322–324. Doi: https://doi.org/10.1126/science.1252418.

Zindler, C., Peeken, I., Marandino, C. A., Bange, H. W., 2012. Environmental control on the variability of DMS and DMSP in the Mauritanian upwelling region. Biogeosciences 9, 1041–1051. Doi: https://doi.org/10.5194/bg-9-1041-2012.

Zindler, C., Marandino, C. A., Bange, H. W., Schütte, F., Saltzman, E. S., 2014. Nutrient availability determines dimethyl sulfide and isoprene distribution in the eastern Atlantic Ocean. Geophysical Research Letters 41(9), 3181-3188. Doi: https://doi.org/10.1002/2014GL059547.

Ziska, F., Quack, B., Abrahamsson, K., Archer, S. D., Atlas, E., Bell, T., Butler, J. H., Carpenter, L. J., Jones, C. E., Harris, N. R. P., Hepach, H., Heumann, K. G., Hughes, C., Kuss, J., Krüger, K., Liss, P., Moore, R. M., Orlikowska, A., Raimund, S., Reeves, C. E., Reifenhäuser, W., Robinson, A. D., Schall, C., Tanhua, T., Tegtmeier, S., Turner, S., Wang, L., Wallace, D., Williams, J., Yamamoto, H., Yvon-Lewis, S., Yokouchi, Y., 2013. Global sea-to-air flux climatology for bromoform, dibromomethane and methyl iodide. Atmos. Chem. Phys. 13, 8915–8934. Doi: https://doi.org/10.5194/acp-13-8915-2013.

11 Abbreviations

ADCP	= Acoustic Doppler Current Profiler
APA	= Alkaline phosphatase
BrO	= Bromine Oxide
CanC	= Canary Current
dCCHO	= dissolved Combined Carbohydrates
CDOM	= Chromophoric Dissolved Organic Matter
CRM	= Certified Reference Material
CSP	= Coomassie Stainable Particles
CTD	= Conductivity Temperature Depth Rosette
dAA	= dissolve Amino Acids
DIP	= Dissolved Inorganic Phosphorus
DOAS	= Differential optical absorption spectroscopy
DOC	= Dissolved Organic Carbon
DON	= Dissolved Organic Nitrogen
DOM	= Dissolved Organic Matter
DOP	= Dissolved Organic Phosphorus
DVM	= Diel vertical migration
EBUS	= Eastern Boundary Upwelling Systems
EEZ	= Exclusive Economic Zone
ETNA	= Eastern Tropical North Atlantic
FDOM	= Fluorenscent Dissolved Organic Matter
GC	= Gas Chromatography
HPLC	= High performance liquid chromatography
MS	= Mass spectrometry
NA	= North Atlantic
NEC	= North Equatorial Current
PMD	= Plastic Marine Debris
POC	= Particulate Organic Carbon
POM	= Particulate Organic Matter
SD	= Standard Deviation
SSL	= Sound scattering layer
TON	= Total Dissolved Nitrogen
TEP	= Transparent Exopolymeric Particles
TSG	= Thermosalinograph
UVP	= Underwater Vision Profiler
WBAT	= Wide Band Acoustic Transceiver
WTNA	= Western Tropical North Atlantic

.